

# RENEWABLE FURAN- DERIVED EPOXY THERMOSETS AND NANOCOMPOSITES FOR COATING APPLICATIONS

Angela Marotta

PH.D. IN INDUSTRIAL PRODUCT AND PROCESS ENGINEERING (XXXI CYCLE)

*Department of Chemical, Materials and Production Engineering (DICMaPI)*

Ph.D. Tutor:

Prof. Veronica Ambrogi, Prof. Alice Mija

Ph.D. Co-Tutor:

Dott. Pierfrancesco Cerruti, Dott. Gennaro Gentile



DI  
C  
Ma  
PI

Dipartimento  
di Ingegneria Chimica,  
dei Materiali e della  
Produzione Industriale  
Università degli Studi  
di Napoli Federico II





---

# Abstract

---

Research on bio-based polymers is rapidly increasing in last years, pushed by growing environmental and economic concerns, as well as by the uncertainty about future availability of finite petrochemical resources. Sustainability is a keyword in this process. In this frame, products that are respectful towards the environment, including eco-compatible building blocks and additives, are now researched to replace petroleum-based polymers with those derived from naturally occurring feedstocks.

Epoxy resins are very versatile thermosetting polymers, extremely resistant to corrosion, moisture and chemicals, with good adhesive strength toward most materials (wettability) and low shrinkage upon curing. Due to their high glass transition temperatures and excellent mechanical strength, epoxy resins are widely employed in a broad range of applications, such as electronics, structural adhesives, aerospace composites and protective coatings.

More than two-thirds of epoxy resins nowadays are based on diglycidyl ether of bisphenol A. In this industry the trend to replace petrol-derived materials with bio-based ones is related also to the necessity to substitute the Bisphenol A (BPA), a controversial building block recognized as an endocrine disrupter and reprotoxic substance. In particular in application as coating, the use of BPA results in hazard for customers of food and beverage products packed into containers treated with epoxy resins. The effects of human body contamination caused by BPA are diabetes, cardiovascular diseases, altered liver

enzymes and reproductive apparatus damages. For these reasons, this molecule has been banned in many countries for the manufacturing of child products, and in France and Canada from all the materials in direct contact with food. The necessity to develop new epoxy resins results therefore urgent.

Bio-derived molecules since now developed show the most various chemical structure, each of them producing different properties of final polymers. Peculiar characteristic shown by epoxy resins are related to the aromatic structure of its components. Aromatic molecules present in natural feedstock are mainly derived from lignin, one of the principal constituents of natural cell walls. However, to extract aromatic moieties from lignin, difficult and energy consuming processes are required. A valuable replacement of aromatic molecules, easily recoverable from glucose, are furanic molecules; their validity has been supported by several studies.

In the light of the above, the work here presented is focused on production of furanic bio-based epoxy resins as potential substitute of DGEBA in can coating industry. The complete cycle of the material has been studied: the synthesis of furanic epoxy monomers and epoxy thermosets, the characterization of their chemical and physical properties (study of curing kinetics, mechanical and thermal properties). Furthermore, the application of bio-based epoxy thermosets as cans internal lining has been evaluated. Experimental results demonstrated that the obtained resins have good potential to be proposed as good alternatives to the traditional BPA-containing epoxy resins.







# Table of contents

---

<i>List of figures</i> .....	7
<i>List of Tables</i> .....	19
<i>List of abbreviations</i> .....	23
<b>Chapter 1.</b> ....	27
<i>Introduction and objectives</i> .....	27
<b>1.1. General overview on bio-based polymers</b> .....	29
<b>1.2. Epoxy resins</b> .....	32
1.2.1. Crosslinking process of epoxy resins.....	36
1.2.2. BPA issue .....	36
<b>1.3. Bio-based epoxy resins</b> .....	39
1.3.1. Epoxides derived from vegetable oils .....	39
1.3.2. Epoxides derived from lignocellulosic compounds .....	40
1.3.3. Epoxides derived from polysaccharides .....	40
1.3.4. Bio-based curing agents .....	41
<b>1.4. Coatings</b> .....	42
<b>1.5. Objectives</b> .....	43
<b>1.6. Bibliography</b> .....	44
<b>Chapter 2.</b> .....	53
<i>Synthesis of furan-based epoxy monomers</i> .....	53
<b>2.1. Introduction</b> .....	55
<b>2.2. Experimental section</b> .....	55
2.2.1. Materials.....	55

<b>2.2.2. Synthesis of bis(oxiran-2-yl-methyl)furan-2,5-dicarboxylate (BOFD).....</b>	<b>55</b>
<i>Glycidylation of FDCA with ECH .....</i>	<i>55</i>
<i>Transesterification of DM-FDCA and glycidol .....</i>	<i>56</i>
<b>2.2.3. Synthesis of 2,5-bis[(oxiran-2-ylmethoxy)methyl]furan (BOMF) .....</b>	<b>56</b>
<b>2.2.4. Methods.....</b>	<b>56</b>
<i>Epoxy equivalent weight (EEW) evaluation .....</i>	<i>57</i>
<b>2.3. Results and discussion.....</b>	<b>58</b>
<b>2.3.1. Synthesis and characterization of bis(oxiran-2-yl-methyl)furan-2,5-dicarboxylate (BOFD) .....</b>	<b>58</b>
<i>Glycidylation of FDCA with ECH .....</i>	<i>58</i>
<i>Transesterification of dimethyl 2,5-furandicarboxylate and glycidol.....</i>	<i>70</i>
<b>2.3.2. Synthesis and characterization of 2,5-bis[(oxiran-2-ylmethoxy)methyl]furan (BOMF) .....</b>	<b>77</b>
<b>2.4. Conclusions .....</b>	<b>86</b>
<b>2.5. Bibliography .....</b>	<b>88</b>
<b>Chapter 3.....</b>	<b>95</b>
<b>3.1. Introduction.....</b>	<b>97</b>
<b>3.2. Experimental section .....</b>	<b>99</b>
<b>3.2.1. Materials.....</b>	<b>99</b>
<b>3.2.2. Preparation of epoxy/anhydride thermosets.....</b>	<b>100</b>
<b>3.2.3. Methods.....</b>	<b>101</b>
<b>3.2.4. Kinetic models.....</b>	<b>103</b>
<i>Calorimetric models.....</i>	<i>103</i>
<i>Kinetic analysis by FT-IR .....</i>	<i>104</i>
<b>3.3. Results and discussion.....</b>	<b>106</b>
<b>3.3.1. Optimization of curing formulations .....</b>	<b>106</b>

<b>3.3.2. Thermokinetics study of crosslinking .....</b>	<b>114</b>
DSC analysis .....	114
FT-IR analysis.....	128
Rheological analysis.....	135
<b>3.3.3. Study of cured epoxies.....</b>	<b>144</b>
Thermogravimetric (TGA) analysis .....	145
Swelling measurements .....	150
Mechanical tests .....	151
<b>3.4. Conclusions .....</b>	<b>157</b>
<b>3.5. Bibliography .....</b>	<b>159</b>
<b>Chapter 4.....</b>	<b>169</b>
<b><i>Furan-based bio-epoxy resins and nanocomposites as tinfoil coatings .....</i></b>	<b>169</b>
<b>4.1. Introduction.....</b>	<b>171</b>
<b>4.2. Experimental section .....</b>	<b>172</b>
<b>4.2.1. Materials.....</b>	<b>172</b>
<b>4.2.2. Tinfoil treatment .....</b>	<b>173</b>
<b>4.2.3. Preparation of coatings.....</b>	<b>173</b>
<b>4.2.4. Methods.....</b>	<b>174</b>
i.Kinetic analysis by FTIR-ATR spectroscopy .....	177
<b>4.3. Results and discussion.....</b>	<b>178</b>
<b>4.3.1. Characterization of bulk epoxy resins and nanocomposites .....</b>	<b>178</b>
ii.Thermal analysis of epoxy resins and nanocomposites .....	179
iii.Chemo-rheological analysis of epoxy resins and nanocomposites .....	183

iv. Thermal and mechanical properties of epoxy resins and nanocomposites	193
<b>4.3.2. Optimization of the coating process</b>	<b>198</b>
<b>4.3.3. Evaluation of coating properties</b>	<b>203</b>
v. Contact angle	203
vi. Chemical resistance	205
vii. Pencil hardness of coatings.	211
viii. Adhesion tests	212
<b>4.4. Conclusions</b>	<b>214</b>
<b>4.5. Bibliography</b>	<b>216</b>

# List of figures

---

<b>Figure 1.1</b> – Number of papers published about “bio-based polymers” from 1988 .....	30
<b>Figure 1.2</b> – Epoxide ring structure. ....	32
<b>Figure 1.3</b> – Chemical structures of (a) BPA and (b) DGEBA.....	37
<b>Figure 2.1</b> – General formula of oligomeric epoxy resins based on BOFD.....	57
<b>Figure 2.2</b> – <sup>1</sup> H-NMR spectra for the crude product of FDCA glycidylation (red line) and .....	61
<b>Figure 2.3</b> – FTIR spectra of FDCA and BOFD .....	62
<b>Figure 2.4</b> – <sup>1</sup> H-NMR spectra of BOFD obtained by FDCA glycidylation .....	64
<b>Figure 2.5</b> – <sup>13</sup> C-NMR spectra of BOFD obtained by glycidylation.....	65
<b>Figure 2.6</b> – DEPT 90 (blue line) and DEPT 135 (red line) NMR analysis for BOFD obtained by glycidylation .....	66
<b>Figure 2.7</b> – COSY analysis of BOFD obtained by glycidylation .....	68
<b>Figure 2.8</b> – HSQC analysis of BOFD obtained by glycidylation .....	68
<b>Figure 2.9</b> – HMBC analysis of BOFD obtained by glycidylation.....	69
<b>Figure 2.10</b> – <sup>1</sup> H-NMR spectra for the crude product of transesterification (red line) and DM-FDCA (blue line) .....	72
<b>Figure 2.11</b> – FTIR spectra for DM-FDCA and BOFD obtained by transesterification .....	73

<b>Figure 2.12</b> – $^1\text{H}$ -NMR spectra of BOFD obtained by transesterification of DM-FDCA .....	74
<b>Figure 2.13</b> – $^{13}\text{C}$ -NMR spectra of BOFD obtained by transesterification of DM-FDCA .....	75
<b>Figure 2.14</b> –TGA analysis (10 °C/min, under nitrogen) of BOFD obtained by transesterification.....	76
<b>Figure 2.15</b> – Dynamic DSC analysis (heating – cooling cycle) of BOFD obtained by transesterification.....	77
<b>Figure 2.16</b> – FTIR spectra of BOMF and BHMF.....	80
<b>Figure 2.17</b> – $^1\text{H}$ -NMR spectrum of BOMF .....	81
<b>Figure 2.18</b> – $^{13}\text{C}$ -NMR spectrum of BOMF .....	81
<b>Figure 2.19</b> – DEPT 90 (blue line) and DEPT 135 (red line) NMR analysis for BOMF .....	82
<b>Figure 2.20</b> – COSY analysis of BOMF .....	83
<b>Figure 2.21</b> – HSQC analysis of BOMF.....	84
<b>Figure 2.22</b> – HSQC analysis of BOMF .....	85
<b>Figure 2.23</b> – (a) Weight percent and (b) derivative weight percent of BOMF .	86
<b>Figure 3.1</b> – DSC Dynamic heating scan curves at 10 °C/min heating rate of BOMF/MNA-BDMA <sub>0.5</sub> , BOMF/MNA-1-MI <sub>0.5</sub> and BOMF/MNA-2-MI <sub>0.5</sub> mixtures .....	110
<b>Figure 3.2</b> – DSC isothermal curves at T = 130 °C of BOMF/MNA-BDMA <sub>0.5</sub> , BOMF/MNA-1-MI <sub>0.5</sub> and BOMF/MNA-2-MI <sub>0.5</sub> mixtures.....	111



<b>Figure 3.3</b> – (a) DSC heating scan at 10 °C/min heating rate and (b) Isothermal curves at T = 130 °C of samples containing different percentages of 2-MI.....	112
<b>Figure 3.4</b> – DSC heating scan curves at different heating rates of BOMF/MNA-2-MI <sub>0.5</sub> .....	115
<b>Figure 3.5</b> – DSC heating scan curves at different heating rates of 1BOMF/0.8MNA-2-MI <sub>0.5</sub> .....	115
<b>Figure 3.6</b> – DSC thermograms in dynamic mode at different heating rates of 0.8BOMF/1MNA-2-MI <sub>0.5</sub> .....	116
<b>Figure 3.7</b> – DSC dynamic heating scan curves at 10 °C/min up to 300 °C of 1BOMF/0.8MNA-2-MI <sub>0.5</sub> .....	118
<b>Figure 3.8</b> – Comparison of T <sub>g</sub> of 1BOMF/0.8MNA-2-MI <sub>0.5</sub> after being heated up to 200 °C (solid curve) and up to 300 °C (dashed curve).....	118
<b>Figure 3.9</b> – Isothermal curves obtained at different temperatures for BOMF/MNA-2-MI <sub>0.5</sub> .....	119
<b>Figure 3.10</b> – Isothermal curves obtained at different temperatures for 1BOMF/0.8MNA-2-MI <sub>0.5</sub> .....	120
<b>Figure 3.11</b> – Isothermal curves obtained at different temperatures for 0.8BOMF/1MNA-2-MI <sub>0.5</sub> .....	120
<b>Figure 3.12</b> – T <sub>g</sub> of BOMF/MNA-2-MI <sub>0.5</sub> cured for 2 h in isothermal method.....	121
<b>Figure 3.13</b> – T <sub>g</sub> of 1BOMF/0.8MNA-2-MI <sub>0.5</sub> cured for 2 h in isothermal method.....	121
<b>Figure 3.14</b> – T <sub>g</sub> of 0.8BOMF/1MNA-2-MI <sub>0.5</sub> cured for 2 h in isothermal method.....	122

<b>Figure 3.15</b> – Degree of conversion ( $\alpha$ ) in function of time for BOMF/MNA-2-MI0.5 .....	123
<b>Figure 3.16</b> – Degree of conversion ( $\alpha$ ) in function of time for 1BOMF/0.8MNA-2- MI0.5.....	123
<b>Figure 3.17</b> – Degree of conversion ( $\alpha$ ) in function of time for 0.8BOMF/1MNA-2- MI0.5.....	124
<b>Figure 3.18</b> – Isothermal conversion rate at different temperatures as a function of the conversion degree. Open symbols are the experimental values and black line represents the fitting according to Equation 3.11 for BOMF/MNA-2-MI0.5	125
<b>Figure 3.19</b> – Isothermal conversion rate at different temperatures as a function of the conversion degree. Open symbols are the experimental values and black line represents the fitting according to Equation 3.11 for 1BOMF/0.8MNA-2-MI0.5 .....	126
<b>Figure 3.20</b> – Isothermal conversion rate at different temperatures as a function of the conversion degree. Open symbols are the experimental values and black line represents the fitting according to Equation 3.11 for 0.8BOMF/1MNA-2-MI0.5 .....	126
<b>Figure 3.21</b> – ATR FT-IR spectra of the epoxy monomer (BOMF) and curing agent (MNA) .....	129
<b>Figure 3.22</b> – ATR FT-IR spectra of BOMF/MNA-2-MI0.5.....	129
<b>Figure 3.23</b> – 3D plot of spectra collected upon heating during rheological measurements on BOMF/MNA-2-MI0.5.....	131
<b>Figure 3.24</b> – Time evolution of ATR FT-IR spectra of BOMF/MNA-2-MI0.5 reacting system in the wavenumber region between 1900 – 1650 $\text{cm}^{-1}$ .....	131

**Figure 3.25** – Time evolution of ATR FT-IR spectra of BOMF/MNA-2-MI<sub>0.5</sub> reacting system in the wavenumber region between 1150 – 750 cm<sup>-1</sup> ..... 132

**Figure 3.26** – Absolute conversion of characteristic groups, evaluated from ATR FT-IR spectra collected during the rheological measurements at 1.5 °C/min heating rate on BOMF/MNA-2-MI<sub>0.5</sub>. ..... 133

**Figure 3.27** – Absolute conversion of characteristic groups, evaluated from ATR FT-IR spectra collected during the rheological measurements at 1.5 °C/min heating rate on 1BOMF/0.8MNA-2-MI<sub>0.5</sub>. ..... 133

**Figure 3.28** – Absolute conversion of characteristic groups, evaluated from ATR FT-IR spectra collected during the rheological measurements at 1.5 °C/min heating rate on 0.8BOMF/1MNA-2MI-0.5. .... 134

**Figure 3.29** – Absolute conversion of ester groups for BOMF/MNA-2-MI<sub>0.5</sub>, 1BOMF/0.8MNA-2-MI-0.5 AND 0.8BOMF/1MNA-2-MI<sub>0.5</sub> ..... 135

**Figure 3.33** – Elastic modulus ( $G'$ ), viscous modulus ( $G''$ ) and complex viscosity ( $|\eta^*|$ ) compared with ester conversion of BOMF/MNA-2-MI<sub>0.5</sub> heated at 1.5 °C/min. .... 136

**Figure 3.34** – Elastic modulus ( $G'$ ), viscous modulus ( $G''$ ) and complex viscosity ( $|\eta^*|$ ) compared with ester conversion of 1BOMF/0.8MNA-2-MI<sub>0.5</sub> heated at 1.5 °C/min. .... 136

**Figure 3.35** – Elastic modulus ( $G'$ ), viscous modulus ( $G''$ ) and complex viscosity ( $|\eta^*|$ ) compared with ester conversion of 0.8BOMF/1MNA-2-MI<sub>0.5</sub> heated at 1.5 °C/min. .... 137

**Figure 3.36** – Comparison of (a) elastic moduli ( $G'$ ) and (b) complex viscosity ( $\eta^*$ ) of BOMF/MNA-2-MI0.5, 1BOMF/0.8MNA-2-MI0.5, and 0.8BOMF/1MNA-2-MI0.5 heated at 1.5 °C/min..... 137

**Figure 3.37** – Absolute conversion ( $C_0\alpha$ ) evaluated from ATR FT-IR spectra collected during the rheological measurements at 110 °C on BOMF/MNA-2-MI0.5. .... 139

**Figure 3.38** – Absolute conversion ( $C_0\alpha$ ) evaluated from ATR FT-IR spectra collected during the rheological measurements at 110 °C on 1BOMF/0.8MNA-2-MI0.5..... 139

**Figure 3.39** – Absolute conversion ( $C_0 \alpha$ ) evaluated from ATR FT-IR spectra collected during the rheological measurements at 110 °C on 0.8BOMF/1MNA-2-MI 0.5. .... 140

**Figure 3.40** – Comparison between absolute conversions of ester groups for BOMF/MNA-2-MI0.5, 1 BOMF/0.8MNA-2-MI0.5 and 0.8 BOMF/1MNA-2-MI0.5 . 141

**Figure 3.53** – Elastic modulus ( $G'$ ), viscous modulus ( $G''$ ) and complex viscosity ( $|\eta^*|$ ) compared with ester conversion of BOMF/MNA-2-MI0.5 at 110 °C, in time ..... 142

**Figure 3.54** – Elastic modulus ( $G'$ ), viscous modulus ( $G''$ ) and complex viscosity ( $|\eta^*|$ ) compared with ester conversion of 1BOMF/0.8MNA-2-MI0.5 at 110 °C, in time ..... 142

**Figure 3.55** – Elastic modulus ( $G'$ ), viscous modulus ( $G''$ ) and complex viscosity ( $|\eta^*|$ ) compared with ester conversion of 0.8BOMF/1MNA-2-MI0.5 at 110 °C, in time ..... 143

**Figure 3.56** – Comparison between (a) elastic moduli ( $G'$ ) and (b) complex viscosity ( $|\eta^*|$ ) of selected samples at 110 °C..... 143

**Figure 3.57** – (a) Weight loss and (b) derivative weight loss in nitrogen atmosphere for samples cured at 180 °C..... 145

**Figure 3.58** – (a) Weight loss and (b) derivative weight loss in air atmosphere for samples cured at 180 °C ..... 146

**Figure 3.59** – (a) Weight loss and (b) derivative weight loss in nitrogen atmosphere for samples cured at 230 °C..... 146

**Figure 3.60** – (a) Weight loss and (b) derivative weight loss in air atmosphere for samples cured at 230 °C ..... 146

**Figure 3.61** – Weight loss of (a) BOMF/MNA-2-MI0.5-pc180 and (b) BOMF/MNA-2-MI0.5-pc230 under inert (nitrogen) and oxidative (air) atmosphere ..... 148

**Figure 3.62** – Weight loss of (a) 1BOMF/0.8MNA-2-MI0.5-pc180 and (b) 1BOMF/0.8MNA-2-MI0.5-pc230 under inert (nitrogen) and oxidative (air) atmosphere ..... 149

**Figure 3.63** – Weight loss of (a) 0.8BOMF/1MNA-2-MI0.5-pc180 and (b) 0.8BOMF/1MNA-2-MI0.5-pc230 in inert (Nitrogen) and oxidative (Air) atmosphere ..... 149

**Figure 3.52** – Weight loss of (a) 0.8BOMF/1MNA-2-MI0.5-pc180 and (b) 0.8BOMF/1MNA-2-MI0.5-pc230 in inert (Nitrogen) and oxidative (Air) atmosphere ..... 149

**Figure 3.64** – Stress-strain curves for samples post-cured at 180 °C..... 152

**Figure 3.65** – Stress-strain curves for samples post-cured at 230 °C..... 153

<b>Figure 3.66</b> – Stress-strain curves for BOMF/MNA-2-MI <sub>0.5</sub> undergone to different curing treatments .....	155
<b>Figure 3.67</b> – Stress-strain curves for 1BOMF/0.8MNA-2-MI <sub>0.5</sub> undergone to different curing treatments.....	155
<b>Figure 3.68</b> – Stress-strain curves for 0.8BOMF/1MNA-2-MI <sub>0.5</sub> undergone to different curing treatments.....	156
<b>Figure 3.57</b> – Stress-strain curves for DGEBA/MNA-2-MI <sub>0.5</sub> undergone to different curing treatments.....	156
Figure 4.1 – DSC thermograms of cure process for all systems at a heating rate of 10 °C/min.....	181
Figure 4.2 – DSC thermograms of cure process for all systems at 130 °C .....	182
Figure 4.3 – Rheological tests on (a) BOMF/MNA, (b) BOMF/MNA-1TiO <sub>2</sub> , (c) BOMF/MNA-3TiO <sub>2</sub> and (d) BOMF/MNA-5TiO <sub>2</sub> heated at 1.5 °C/min.....	184
Figure 4.4 – Comparison of (a) elastic moduli (G') and (b) complex viscosity ( η* ) between for BOMF/MNA and BOMF/MNA-3TiO <sub>2</sub> heated at 10 °C/min.....	185
Figure 4.5 – Rheological tests on (a) BOMF/MNA, (b) BOMF/MNA-1TiO <sub>2</sub> , (c) BOMF/MNA-3TiO <sub>2</sub> and (d) BOMF/MNA-5TiO <sub>2</sub> at 110 °C/min.....	187
Figure 4.6 – Comparison of (a) elastic moduli (G') and (b) complex viscosity ( η* ) for systems at 110°C.....	187
Figure 4.7 – Conversion (α) of anhydride, ester and epoxy groups of (a) BOMF/MNA, (b) BOMF/MNA-1TiO <sub>2</sub> , (c) BOMF/MNA-3TiO <sub>2</sub> and (d) BOMF/MNA-5TiO <sub>2</sub> cured at 1.5 °C/min heating rate.....	189

Figure 4.8 – Comparison of anhydride groups conversion for all samples cured at 1.5 °C/min.....190

Figure 4.9 – Comparison between conversion of ester groups, evaluated by FTIR-ATR analysis, and rheological properties of (a) BOMF/MNA, (b) BOMF/MNA-1TiO<sub>2</sub>, (c) BOMF/MNA-3TiO<sub>2</sub> and (d) BOMF/MNA-5TiO<sub>2</sub> cured at 1.5 °C/min ..... 191

Figure 4.10 – Relative conversion (α) of characteristic groups in (a) BOMF/MNA, (b) BOMF/MNA-1TiO<sub>2</sub>, (c) BOMF/MNA-3TiO<sub>2</sub> and (d) BOMF/MNA-5TiO<sub>2</sub> cured at 110 °C..... 192

Figure 4.11 – Comparison of characteristic groups conversion between BOMF/MNA and BOMF/MNA-3TiO<sub>2</sub> cured at 110°C..... 193

Figure 4.12 – (a) Weight loss and (b) derivative weight loss in nitrogen atmosphere for samples cured at 180°C.....194

Figure 4.13 – (a) Weight loss and (b) derivative weight loss in air atmosphere for samples cured at 180°C ..... 195

Figure 4.14 – Comparison of weight loss of (a) BOMF/MNA, (b) BOMF/MNA 1TiO<sub>2</sub>, (c) BOMF/MNA 3TiO<sub>2</sub> (d) BOMF/MNA 5TiO<sub>2</sub>and (e) DGEBA/MNA in air and nitrogen .....196

Figure 4.15 – Specimen for tensile test (type V ASTM D638) ..... 197

Figure 4.16 – Stress-strain curves for bulk materials..... 197

Figure 4.17 – Visual appearance of (a) untreated tinplate and (b) treated tinplate, coated with BOMF/MNA resin .....199

Figure 4.18 – SEM micrography of (a) untreated tinplate and (b) treated tinplate ..... 200

Figure 4.19 – Contact angle measurements of BOMF/MNA drops on (a) untreated and (b) treated tinplate ..... 201

Figure 4.20 – Viscosity of studied systems in function of shear rate .....202

Figure 4.21 – Visual appearance of (a) BOMF/MNA-1TiO<sub>2</sub>, (b) BOMF/MNA-3TiO<sub>2</sub> and (c) BOMF/MNA-3TiO<sub>2</sub> coating on a treated tinplate specimen..... 203

Figure 4.22 – Static contact angles (CA) of water on different substrates: BOMF/MNA, BOMF/MNA 1TiO<sub>2</sub>, BOMF/MNA 3TiO<sub>2</sub> and BOMF/MNA 5TiO<sub>2</sub>..... 204

Figure 4.23 – Visual appearance of (a) BOMF/MNA, (b) BOMF/MNA 1TiO<sub>2</sub>, (c) BOMF/MNA 3TiO<sub>2</sub>, (d) BOMF/MNA 5TiO<sub>2</sub> coating after 30 days immersion in ethanol..... 206

Figure 4.24 – Visual appearance of (a) BOMF/MNA, (b) BOMF/MNA 1TiO<sub>2</sub>, (c) BOMF/MNA 3TiO<sub>2</sub>, (d) BOMF/MNA 5TiO<sub>2</sub> coating after 3 days immersion in the acetic acid solution ..... 206

Figure 4.25 – SEM micrographs of (a) BOMF/MNA and (b) BOMF/MNA-3TiO<sub>2</sub> 208

Figure 4.26 – SEM micrographs of (a) BOMF/MNA and (b) BOMF/MNA-3TiO<sub>2</sub> after 3 days of immersion in ethanol ..... 208

Figure 4.27 – SEM micrographs of (a) BOMF/MNA and (c) BOMF/MNA-3TiO<sub>2</sub> after 3 days of immersion in 3 vol.% acetic acid aqueous solution..... 209

Figure 4.28 – SEM micrographs of (a) BOMF/MNA and (b) BOMF/MNA-3TiO<sub>2</sub> after 30 days of immersion in ethanol ..... 210

Figure 4.29 – SEM micrographs at different magnification of (a) BOMF/MNA and (c) BOMF/MNA-3TiO<sub>2</sub> after 30 days of immersion in 3 vol.% acetic acid aqueous solution..... 210



Figure 4.30 – Adhesion test performed on (a) BOMF/MNA, (b) BOMF/MNA-1TiO<sub>2</sub>,  
(c) BOMF/MNA-3TiO<sub>2</sub> and (d) BOMF/MNA-5TiO<sub>2</sub> coating..... 214



## List of Tables

---

<b>Table 2.1</b> – Peak assignments in FTIR spectrum of FDCA and BOFD obtained by FDCA glycidylation .....	62
<b>Table 3.1</b> – Samples denomination and compositions .....	100
<b>Table 3.2</b> – List of reactants and initiators used in the synthesis of bio-based epoxy resins.....	108
<b>Table 3.3</b> - Values of total enthalpy of reaction ( $\Delta H_{tot}$ ), peak temperature ( $T_p$ ) and onset temperature ( $T_{onset}$ ) obtained from dynamic DSC analysis on reacting mixtures containing the same percentages of different initiators.....	111
<b>Table 3.4</b> – Total heat of reaction ( $\Delta H_{tot}$ ) and peak time ( $t_p$ ) of systems with different initiators, cured at 130°C.....	111
<b>Table 3.5</b> – Values of total enthalpy of reaction ( $\Delta H_{tot}$ ), peak temperature ( $T_p$ ) and onset temperature ( $T_{onset}$ ) obtained from dynamic DSC analysis of resins with 2-MI as initiator in different percentages.....	113
<b>Table 3.6</b> – Peak temperature ( $T_p$ ), total enthalpy of reaction ( $\Delta H_{tot}$ ) and glass transition temperature ( $T_g$ ) for mixtures with different epoxy/anhydride ratios, cured at different heating rates.....	117
<b>Table 3.7</b> – Curing kinetics parameters .....	127
<b>Table 3.8</b> – Degradation temperature at 5% weight loss ( $T_{d5}$ ) and at 10% weight loss ( $T_{d10}$ ) of resins with different epoxy/anhydride ratios in both air and nitrogen atmosphere .....	147

<b>Table 3.9</b> – Swelling indexes for bio-based resins and reference samples cured with two different thermal treatments.....	150
<b>Table 3.9</b> – Young’s Modulus, stress and stain at peak of for samples undergone to different curing treatments.....	153
Table 4.1 – Total heat of reaction ( $\Delta H_{tot}$ ), peak temperature ( $T_p$ ), onset temperature ( $T_{onset}$ ) and glass transition temperature ( $T_g$ ) of systems cured at 10°C/min .....	181
Table 4.2 – Total heat of reaction ( $\Delta H_{tot}$ ), peak time ( $T_p$ ) and glass transition temperature ( $T_g$ ) of systems cured at 130°C.....	182
Table 4.3 – Degradation temperature ( $T_{d5}, T_{d10}$ ) and final weight ( $W_f$ ) of samples in both air and nitrogen atmosphere.....	194
Table 4.4 – Young's Modulus, stress and strain at peak of the investigated samples.....	198
Table 4.5 – Elemental EDX analysis of treated and untreated tinplate. ....	200
Table 4.6 – Contact angle (CA) values with standard deviation for water droplets on coatings.....	204
Table 4.7 – Pencil hardness of coatings before and after chemical resistance test .....	212
Table 4.8 – Hardness of coatings before and after chemical resistance test ...	212





## List of abbreviations

---

$\dot{\gamma}$	shear rate
$ \eta^* $	complex viscosity
1-MI	1-methylimidazole
2-MI	2-methylimidazole
$A_t$	absorbance area
ATR	Attenuated Total Reflectance
BDMA	benzyl dimethylamine
BHMF	2,5-bis(hydroxymethyl)furan
BOFD	bis(oxiran-2-yl-methyl)furan-2,5-dicarboxylate
BOMF	2,5-bis[(oxiran-2-ylmethoxy)methyl]furan
BPA	bisphenol A
C	molar concentration
C	molar concentration
$C_0 \alpha$	absolute conversion
CA	static contact angle
$CDCl_3$	deuterated chloroform
COSY	Homonuclear Correlation spectroscopy
DEPT	Distortionless Enhancement by Polarization Transfer
DGEBA	diglycidyl ether of Bisphenol-A
$dH/dt$	heat flow
DM-FDCA	2,5-furandicarboxylate
DSC	Differential Scanning Calorimetry
$d\alpha/dt$	conversion rate

## | List of abbreviations

EA	ethyl acetate
ECH	epichlorohydrin
EDX	energy dispersive X-ray
EEW	Epoxy Equivalent Weight
FDCA	furan-2,5-dicarboxylic acid
FT-IR	Fourier-Transform Infrared Spectroscopy
G'	elastic modulus
G''	viscous modulus
HMBC	Heteronuclear Multiple-Bonds Correlation spectroscopy
HMF	5-hydroxymethylfurfural
HSQC	Heteronuclear Single-Quantum Correlation spectroscopy
HX	hexane
$k$	rate constant
KOCN	potassium cyanate
m-CPBA	m-chloroperoxybenzoic acid
$M_n$	molecular weight
MNA	Methyl-5-norbornene-2,3-dicarboxylic anhydride (methyl nadic anhydride)
$n$	polymerization degree
NMR	Nuclear Magnetic Resonance
PEF	polyethylene furanoate
PET	polyethylene terephthalate
R	epoxy/anhydride ratio
SEM	Scanning electron microscopy
SI	swelling index
$T_{amb}$	room temperature
TBBr	tetrabutylammonium bromide



$T_d$	Degradation temperature
$T_g$	glass transition temperature
TGA	Thermogravimetric Analysis
$T_{gel}$	gelation temperature
THF	tetrahydrofuran
TLC	Thin Layer Chromatography
$T_{onset}$	onset temperature
$T_p$	peak temperature
$t_p$	peak time
$T_{pc}$	post cure temperature
$W_d$	dry weight
$W_s$	swelled weight
$\alpha$	conversion degree
$\gamma$	deformation
$\Delta H_t$	heat of reaction at t time
$\Delta H_{tot}$	enthalpy of the curing process
$\Delta H_{tot}$	total heat of reaction
$\omega$	frequency



# Chapter 1.

---

## Introduction and objectives



## 1.1. General overview on bio-based polymers

---

Polymers are the most tailored and engineered materials and they are commonly associated with the synthetic materials even if widespread in nature. Natural rubber, shellac, amber, cellulose, silk, wool, proteins and DNA are some examples of natural polymers. Some of these, as natural rubber and cellulose have been chemically modified obtaining vulcanized rubber, rayon and nitrocellulose, all materials that have had a major cultural impact as well as technological. One of the first plastics totally synthetic was Bakelite, formed by phenol and formaldehyde. Despite their natural origin polymers synthesis focused mainly on fossil-based chemicals. Production of polymers is grown by 1950 to 2016 from 0,35 to 355 million tons in the world, whereas in Europe it, since 2002, remained quite stable about 57 million tons<sup>1</sup>. Polymers dominate our everyday life and we bump into them in most various aspects of our life but their link with non-renewable fossil resources poses a question for the years to come. Not only the oil reserves come to an end, but the environmental pollution related to the production of materials is becoming an increasingly important problem. The European Directive EU SDS, aims to reduce the overall use of non-renewable natural resources and the related environmental impacts of raw material use<sup>2</sup>.

Already in 1988 Narayan<sup>3</sup> published the first work on synthesis of bio-based polymeric materials, expressing all the problems related to the use of petroleum-based compounds and the benefits that bio-based polymers would bring. One of the most powerful characteristic of bio-based products is the widespread presence of raw materials all over the world meaning there is no exclusive access to feedstocks by some countries as in the case of fossil

## | Introduction and objectives

resources. Moreover, attention must be paid to biological raw materials chosen to use in the production of polymers, and materials in general; more specifically should be avoided the use of natural resources that can be addressed also to the agro-food sector.

Mohanthy et al.<sup>4</sup> communicated in 2002 the need to develop a new generation of environmentally friendly materials taking into account the guidelines of Green Chemistry, the topic of bio-based materials has not been addressed more since, not by chance, the Global financial crisis of 2008, when the related scientific production has seen a remarkable development<sup>5</sup> (**Figure 1.1**).

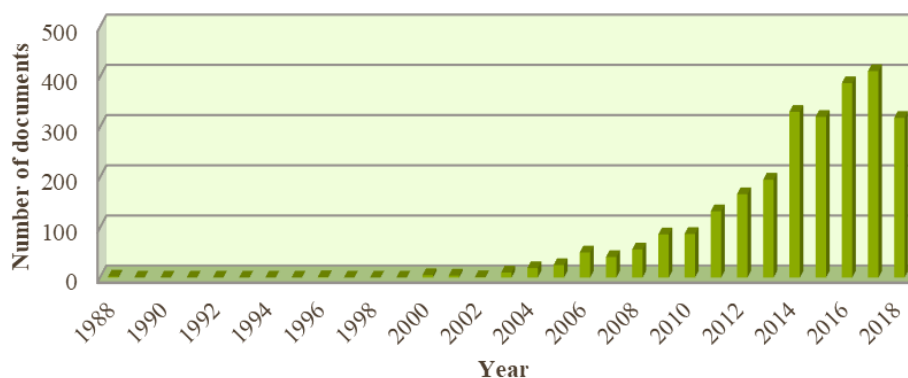


**Figure 1.1** – Number of papers published about “bio-based polymers” from 1988 <sup>5</sup>

Bio based products are wholly or partly derived from materials of biological origin, excluding materials embedded in geological formations and/or fossilized. In industrial processes, by using fermentation and bio-catalysis instead of traditional chemical synthesis, higher process efficiency can be obtained, resulting in a decrease in energy and water consumption, and a reduction of

toxic waste. As they are derived from renewable raw materials such as plants, bio-based products can help reduce CO<sub>2</sub> emissions and offer other advantages such as lower toxicity or novel product characteristics (e.g. biodegradable plastic materials)<sup>6</sup>. Bio-derived does not directly implies that these materials are biodegradable. A material is biodegradable when it can be degraded by means of microbes or enzymes and this is not related to its origin but to its structure and environmental conditions<sup>7</sup>. The ever growing importance of bio-based materials is also reflected in the introduction in 2004 of the ASTM D6866, entitled “*Standard Test Methods for Determining the Bio-based Content of Solid, Liquid, and Gaseous Samples Using Radiocarbon Analysis*”<sup>8</sup>. It defines the bio-based content as the ratio between the amount of bio-based carbon in the material or product and the total organic carbon in the material or product, expressed as fraction weight (mass) or percent weight (mass) (**Equation 1.1**).

$$\% \text{ *BIOBASED content* } = \frac{\text{*BIO (organic) Carbon [mass]*}}{\text{*TOTAL (organic) Carbon [mass]*}} \quad \text{Equation 1.1}$$

This definition is based on the concept that bio-based carbons exists as <sup>14</sup>C radioactive isotope coming from solar irradiation whereas fossil resources, because of their geological lifetime, possess only <sup>12</sup>C isotope, product of the radioactive decay of <sup>14</sup>C<sup>9</sup>. As further evidence of the relevance of this class of materials U.S. Department of Energy compiled in 2004, and revised in 2010, a list of “Top Value-Added Chemicals from Biomass” in which 12 molecules, selected between more than 300 possible building blocks, are proposed as the bio-based molecules with the higher potential, taking account of chemical functionality and potential use<sup>10,11</sup>. These molecules have been selected considering the costs of

## | Introduction and objectives

raw materials, costs and complexity of estimated best available processing pathways, estimated selling price and the market potential for each of them.

Although bio-based polymers are a relatively new class of materials, they have countless potential and are so various that a classification can be made, based on the origin of molecules and production methods<sup>12</sup>:

- Polymers obtained directly by biomass (starch, cellulose)
- Polymers obtained by classical polymerization of bio-based monomers
- Polymers synthesized by microorganisms (PLA, PHA)

Particularly in the second category, we can make a further distinction based on monomers used for the synthesis:

- Bio-derived monomers with the same chemical structure of petrol-derived ones
- Monomers (or oligomers) bearing functional groups that can undergo classical polymerization reactions
- Monomers with innovative structure

In the first of these subcategories are located monomers, like ethylene and propylene, derived from biorefineries which can be polymerized following the conventional optimized chemical route leading to the usual commodities polymers. In the second, instead, lies those molecules, for example vegetable oils, that after some modification can bring functional groups, like hydroxyl or epoxy groups, and be used in synthesis of classical polymers (i.e. polyurethanes or epoxy resins). A fourth subcategory can be imagined, made by composite materials in which the reinforcement (and even matrix) is derived by renewable sources.



A stronger need to synthesize bio-based materials is perceived for specific classes of polymers, such as polyurethanes, epoxy and phenolic resins. Generally used precursors for such polymers, in fact, are proved to be harmful to humans on many levels. It's the case in particular of Bisphenol-A, phenol, formaldehyde, cresols and isocyanates. Good progress have been done in development of bio-based non-isocyanates polyurethanes <sup>13-17</sup> while still very few work have been produced about formaldehyde-free phenolic resins. <sup>18,19</sup> Wide scientific production is instead present about bio-based epoxy resins. Research in this field is strongly pushed by both the great interest in epoxy resins, thanks to their very good properties, and the even more urgent need to find a substitute for Bisphenol-A. This molecule is used in about the 75% of total epoxy resins production and in particular its use in food containers production is in the spotlight. When BPA is present in materials in contact with food it can migrate into food and subsequently ingested; once into the body this molecule is mistaken for some oestrogens by endocrine system and induces several problems.

In this context is placed our research, aimed to the production and development of bio-based epoxy monomers and resins with the final goal of substitution of BPA-based resins in food cans production.

## 1.2. Epoxy resins

---

Epoxy resins are the most versatile thermosetting polymer available. They are extremely resistant to corrosion, moisture and chemicals, have good

## | Introduction and objectives

adhesive strength toward most materials (wettability) and exhibit low shrinkage upon curing, which is a strict requirement for composite industries. Near to full cure they exhibit high glass transition temperatures and excellent mechanical strength.

Because of the aforementioned properties epoxy resins are found in a broad range of applications, from protective coatings, boating materials, but also electronics, structural adhesives, wind turbines, and aerospace composites. In terms of volume the majority of epoxy resin applications are found in coatings<sup>20,21</sup>, composites<sup>22</sup>, and adhesives<sup>23,24</sup>. Since they can exist in the monomeric state as viscous fluid, known as liquid epoxy resins, they are easy to apply under ambient conditions and represents the majority of the epoxy resin industry.

Epoxy resins are a class of thermosetting polymeric materials obtained from monomers containing two or more oxirane groups (epoxides); this functional group allows them a great versatility. The high reactivity of the epoxide ring is a consequence of the  $sp^3$  hybridization of the two carbons, hence the bonded atoms prefer to adopt a  $109^\circ$  orientation from each other, but they are locked into a  $60^\circ$  planar structure which makes the ring highly strained (**Figure 1.2**). Peculiarities in their chemical structure essentially allow the epoxide to react with any strong nucleophile or electrophile.

Thermosetting epoxy resins are obtained starting from a liquid form, which irreversibly solidifies through a cure process. In this way, very rigid materials are generated, in which the motion of the chains is limited due to the high number of cross-links. In fact, the necessary condition for obtaining a thermosetting resin is that the starting monomers have two or more reactive groups per molecule, so as to be able to create a three-dimensional cross-linked

structure which occupies the entire reaction volume <sup>25</sup>. The epoxy resins are available in a large range of molecular structures and they can react with a large range of curing agents; since there is the possibility of using more than a hundred of curing agents, it's obvious that there are a lot of different properties that can be obtained. Therefore, the curing mechanism that promotes crosslinking plays a crucial role for the ending physical properties<sup>26</sup>.

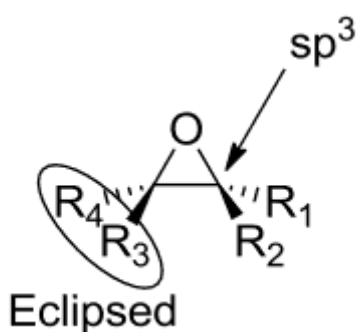


**Figure 1.2** – Epoxide ring structure.

During the first step of the cure epoxy and hardeners react forming somewhat larger molecules. When the cure reaction goes on, molecules size keep increasing since when highly branched molecules are formed. When all branched structures broaden the whole sample it came to a critical point, called gelation point. Before gelation occurs the resin is soluble in suitable solvents but after this point the crosslinked network will not be dissolved but just swells as effect of solvent absorption. The formed gel anyway does not have structural resistance; cure must continue until the quite totality of the resin is connected by a three-dimensional network. As cure proceeds strong changes in the epoxy resins properties are experienced; the most evident is change from a fluid state to a solid material<sup>27</sup>.

## | Introduction and objectives

The cure degree refers to the extent to which epoxy groups and reactive groups of curing agents are consumed. For practical purposes, a system is defined as "cured" when the extension of cross-links is sufficient to guarantee the physical properties required for a given application. Studies on different epoxy resins show that optimization of one physical properties do not necessarily implies optimizations of other properties<sup>26</sup>.

Generally, the epoxy systems provide a first cure made at low temperature, promoting linear polymerization, followed by post-cure at high temperature, promoting reticulation. To cross-link epoxies, amines and carboxylic acid anhydrides are the most commonly used hardeners. Compared with epoxy/amine networks, epoxy/ anhydride products have higher glass transition temperatures as well as less shrinkage.

The invention of epoxy resin is shared by the researcher Castan in Switzerland, which in 1934 produces a low melting resin, amber coloured reticulated with phthalic anhydride, and Greenlee in the United States, who in 1939 explored the synthesis of epichlorohydrin and bisphenol A for the production of resins that can be used as coatings. Epoxy resins were immediately appreciated for their properties: they allow the formation of low viscosity systems, whose curing processes are quick and simple in a very wide range of temperatures<sup>26</sup>.

One of the most important features in the industrial field is the versatility of these compounds, as their properties can be modified by changing the type of resin or the nature of the curing agents, by tailoring the curing conditions and by using specific fillers. Thanks to their versatility, epoxy resins are used in thousands of industrial applications, especially where mechanical, chemical and thermal resistance properties and strong adhesion are required:

- Adhesives for honeycomb structures, for bristles of brushes and for gasket compounds for cement;
- Repairs of plastic and metal parts for vehicles (boats, cars, etc.)
- Production of moulds for prototypes, and tools;
- Gaskets for electrical and electronic devices;
- Laminates for aerospace applications;
- Functional and decorative coating;
- Additives for other plastics, such as vinyl and acrylic resins, and natural and synthetic rubbers.

Starting from 1948, every year a growth of 10% per year has been recorded, on the sale of epoxy resins and this trend is verifiable even today. In the last years, the uncertainty regarding the price and availability of oil, in addition to the direct political and institutional tendencies towards sustainable development, have pushed the chemical industry to turn towards sustainable and renewable resources to synthesize bio-based products.<sup>25</sup> A further boost has been given by the recent discover on BPA that is toxic for human health, especially for the endocrine system. BPA can mimic the hormones of the body and therefore be recognized by the body as such, causing problems related to the immune and reproductive system along with a change in brain chemistry.

Procedures that lead to the obtainment of epoxy monomers can be categorized in

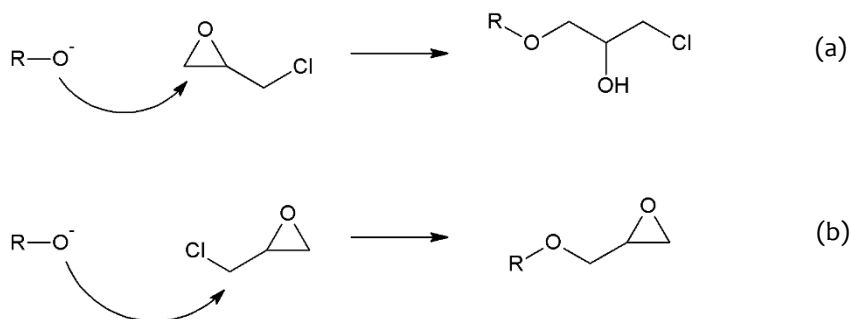
- Conventional glycidylation (with epichlorohydrin);
- Epoxidation with peroxyacids;
- Chemo-enzymatic epoxidation;
- Epoxidation catalysed by metals;

## | Introduction and objectives

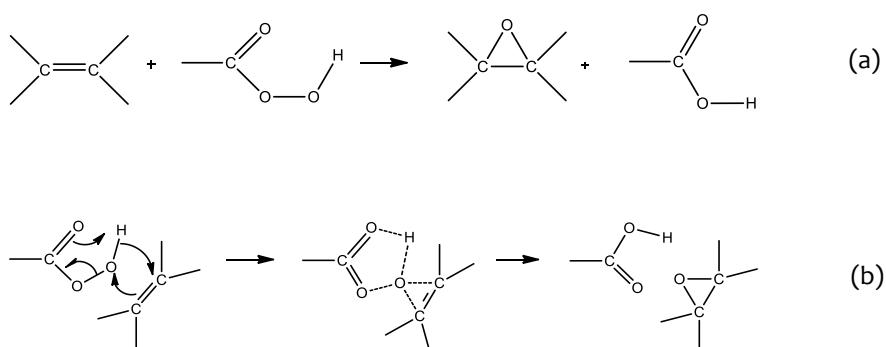
In the first case, a glycidyl moiety is added on hydroxyl groups through the use of epichlorohydrin; the process is not very green and environmentally friendly because of epichlorohydrin toxicity. Conventionally epichlorohydrin (ECH) is synthesized by the chlorohydrination of allyl chloride, which in turn is made by chlorination of propylene. However, the particularly low chlorine atom efficiency and the production of undesired chlorinated organics from the hypochlorination steps make the need to take a view on other, more eco-friendly alternatives for its production. A recent implemented process, Epicerol<sup>®</sup>, allows the production of bio-based epichlorohydrin from glycerol via 1,3-dichloropropanol<sup>28,29</sup>. Moreover, the utilization of glycerol as a by-product from biodiesel production makes the process more sustainable. First step of glycidylation process consists in reaction of alcohols with epichlorohydrin in presence of catalysts. Two possible mechanisms can occur: if hydroxyl oxygen directly attacks chlorine an SN<sub>2</sub> (**Scheme 1.1b**) mechanism is followed while SN<sub>1</sub> mechanism involves the attack of hydroxyl oxygen on the methylene carbon in the oxirane ring. SN<sub>1</sub> mechanism produces an halohydrin intermediate that takes part to the second step of the general glycidylation process (**Scheme 1.1a**). Vicinal halohydrin reacts in presence of a Lewis base which deprotonates the alcohol forming an alkoxide intermediate that has enhanced nucleophilicity. Follows an intramolecular SN<sub>2</sub> reaction where the alkoxide nucleophile attacks the electrophilic C displacing the leaving group (the halide ion). Despite the possibility of using bioderived epichlorohydrin the hazard of this molecule remains.

For this reason are ever more preferred synthetic routes consisting in oxidation with peroxyacids. Even in the event that the selected molecule to be epoxidized do not possess double bonds but only hydroxyl groups, epoxidation

can be carried out by means of a first allylation, that leads to the formation of glycidyl groups, in a second step epoxidized by means of peroxyacids.



**Scheme 1.1** – Competitive mechanisms of nucleophilic attack



**Scheme 1.2** – Mechanism of epoxidation of alkenes with peracids

In the epoxidation of alkenes a single atom of oxygen is added to the double bond through electrophilic addition replacing the  $\pi$  bond with the characteristic three-membered ring (**Scheme 1.2a**). Peroxides are used as source of oxygen; in fact the extra oxygen atom between the carbonyl group and the acidic hydrogen forms the covalent bond O-O is highly polarized and results in an

## | Introduction and objectives

electrophilic character of the hydroxyl oxygen, whose adds to the double bond. Attack at this position by a nucleophile displaces carboxylate, which is a good leaving group.

The reaction proceeds as schematized in **Scheme 1.2b**: first the nucleophilic  $\pi$  bond donates its electrons to the oxygen, breaking the O-O bond to form the new carbonyl bond. The electrons from the peracid O-H bond make up a new C-O bond, and the original carbonyl group uses its electrons to pick up the proton. The transition state for the reaction makes the bond-forming and bond-breaking processes much clearer. The reaction is stereospecific and proceeds via syn addition, as the two new C-O bonds form at the same time from the peracid. A common peracid used for epoxidation of double bonds is meta-chloroperbenzoic acid (MCPBA). However, other reagents may be employed, such as hydrogen peroxide ( $\text{H}_2\text{O}_2$ )<sup>30-33</sup> or potassium hydrogen persulfate ( $\text{KHSO}_5$ ), marketed under the trade name Oxone<sup>®</sup><sup>34</sup>. Methods involving the use of the latter reagents are considered "greener" because the side products (water or sulphate, respectively) are pretty innocuous. These methods are generally slower and are often used with a catalyst. Catalysts used with hydrogen peroxide include Lewis acidic species such as sodium tungstate ( $\text{Na}_2\text{WO}_4$ ) needed to activate the peroxide.

The choice more environmentally friendly however remains that of an enzymatic epoxidation<sup>35-44</sup>, introduced for the first time by Klaas et al.<sup>45</sup> in 1995 using the most common and still largely used enzyme, the immobilized lipase from *Candida Antarctica*.



### 1.2.1. Crosslinking process of epoxy resins

The cross-linking mechanism or curing is commonly referred to all a series of process which involves the conversion of prepolymers into infusible thermoset networks. Epoxy monomers may be reacted either with themselves through anionic or cationic homopolymerization or with a wide range of co-reactants, also referred to as hardeners or curing agents. The hardeners may either initiate the curing reactions through their catalytic activity (initiators) or may react with the epoxy monomer via a polyaddition reaction, the last is particularly favored when there is a labile proton that can be transferred to the oxygen in the epoxide group forming a secondary alcohol and this is typically seen in the reactions with amines, carboxylic acids, and polyphenols. The reactivity of the curing agent depends on its nucleophilic behavior: with strong nucleophiles such as thiols and amines being more reactive, they can even react at room temperature or colder with the process known as “cold curing”. Weak nucleophiles such as carboxylic acids are on the other hand less reactive and thus require higher curing temperature. Anhydrides typically need to be ring opened by a hydroxyl or a catalyst before they can react with epoxy resins and lend themselves to high temperature processing due to being relatively unreactive. Typical catalysts for epoxide ring opening are tertiary amines or hydroxyls with relatively acidic protons such as phenols and they function through intermolecular bonding interactions. The overall goal of a catalyst is to facilitate curing at lower temperatures to reach higher degrees of cure in shorter periods of time and these catalysts are often added in very low amounts when being used with conventional hardeners to minimize potential side reactions such as cationic or anionic homopolymerizations. The use of very strong Lewis acids or bases can also be employed to initiate homopolymerizations. Lewis Bases can

## | Introduction and objectives

also catalyze anionic polymerizations through generation of alkoxides. Strong Brønsted acids will catalyze cationic polymerizations through generation of onium cation. Since Brønsted acids can be generated through an external energy source such as heat or UV light from compounds such as diaryliodonium salts, aryldiazonium salts, and sulfonium salts the catalyst can be stored premixed with the epoxy resin and cured on demand (since the generation of the Brønsted acid is only achieved through UV or thermal initiation). This feature is particularly important in the composite industry. Resins typically used for these types of homopolymerizations are aliphatic in order to reduce absorption of UV light by the resin. During the crosslinking process two main physical transformations occur: gelation and vitrification.

The increase of the molecular weight of the polymer with conversion provokes important evolution of viscosity, from a liquid to solid state. Physical phenomena like gelation and vitrification contribute to the increase of viscosity to a high degree. The consequences could be dramatic for the resulting material because all these transformations especially vitrification could block the ultimate conversion. The identification of these physical transitions is of great importance, because at this stage, the reaction generally changes from a kinetically to a diffusion controlled regime.

The cross-linking process leads, from a liquid initial system, to a 3D solid network. Obvious is that, at some extent of the reaction, a sol-gel transition must occur. At the beginning of the reaction a dispersed phase is present into a dispersion phase; during the crosslink conversion the combination of monomeric precursor increases in molecular weight and polydispersity with the consequent growth of the interactions between the dispersed phases, at some extent of the

conversion a unique giant macromolecular structure that percolates the reaction medium is formed.

As the crosslinking reaction further proceeds, the number of crosslinks rises, and molecular mobility becomes increasingly restricted. The value of glass transition temperature  $T_g$  increases with conversion because of the increase of molar mass in the pre-gel state and of the crosslink density in the post-gel state; if the  $T_g$  is equal or becomes higher than the reaction temperature a phenomenon called vitrification occur. This phenomenon corresponds to a transition from a liquid to a glassy state and provokes a decrease of molecular motions. It can be observed for isothermal or non-isothermal curing processes and can occur before or after gelation. Indeed, it is important to notice that gelation and vitrification are considered as independent events. In term of processability, the knowledge of vitrification temperature is very important because the polymerization kinetic decreases drastically in the glassy state. This effect is very relevant because when the  $(T_g - T)$  difference reaches 20-30°C, the reaction is considered as stopped. <sup>46</sup> The activation energy  $E_a$  as vitrification occur quickly descend to low values, the rate controlling step of reaction shift from kinetic to diffusion regime, it's a direct consequence of the decrease of long range molecular mobility as the epoxy system approaches the glassy state.

Properties of epoxy resins are strictly connected with the used curing agent; for example while amine cured epoxy resins exhibit better mechanical, chemical and solvent resistance than anhydride cured; this last possess higher glass transition temperature, less shrinkage after curing and good insulating and optical properties. By choosing different hardeners rigid or soft materials can be obtained.

## | Introduction and objectives

Curing mechanisms are completely different depending on crosslinking agent nature, that can act as hardeners and also as catalyst. In the latter case they behave as initiator or accelerator, in presence of another hardener that became a comonomer, of an homopolymerization reaction. Hardeners are generally primary and secondary amines, phenols, thiols and carboxylic acids and anhydrides. The epoxy group can react cationically, being opened by an active hydrogen and producing an hydroxyl group, or anionically, coming through an activated specie capable of further reactions.

Tertiary amines takes part to crosslinking reactions as catalysts while primary and secondary amines, bearing active hydrogen, can react with epoxy groups producing hydroxyl groups. Primary amines are much more reactive than secondary and after a first reaction with an epoxy group, being transformed in a secondary amine, can further react with a second oxirane. Tertiary amines produced by reaction of secondary amines can act as catalyst while, when obtained starting by a primary amine are quite ineffective as catalyst.<sup>26</sup> Moreover, the hydroxyl compounds formed can accelerate the reaction with the amines. In fact the hydrogen atom of the hydroxyl group can form an hydrogen bond with the oxygen atom of the epoxy ring carrying the activation of the methylene and to a nucleophilic attack by the amine. Epoxides cross-linked with aromatic amines have a better chemical and thermal resistance compared to those treated with aliphatic or cycloaliphatic amines.

The most common acid curing agents for epoxy resins are carboxylic acid anhydrides and dicarboxylic acids. When crosslinking reaction is carried out with these compounds it results in the production of polyesters. The mechanism of reaction for dicarboxylic acids, generally catalyzed by amines or phosphonium salts, involves the reaction of functionalized acid with the epoxide followed by

esterification of the hydroxyl group of the epoxide with the acid. This ester can further react with another acid molecule and form a diester and the hydroxyl group with a further epoxy molecule.

Anhydrides have successfully replaced many aromatic and toxic aliphatic amines in the preparation of structural composites. However, anhydrides reaction mechanism is more complex because of competitive reactions that can undergo. First of all a Lewis base, like a tertiary amine, imidazole derivatives and mercaptans, is needed to catalyze both opening of epoxy ring and anhydride group. The reaction can proceed by etherification and esterification: the first is the result of reactions between two epoxy groups while, when an epoxy reacts with an anhydride an ester is obtained. Moreover, the hydroxyl groups formed by epoxide can further react with anhydride forming a diester. When catalyzed by Lewis bases both anhydride and epoxy ring are bifunctional.

### 1.2.2. BPA issue

A pinnacle example of a controversial petroleum-based building block and additive utilized in the polymer industry is Bisphenol A (BPA, **Figure 1.3a**). With a global volume consumption of 7.7 million metric tons in 2015, projected to reach 10.6 million metric tons by 2022, BPA exhibits one of the highest production volume of chemicals worldwide.<sup>47</sup>

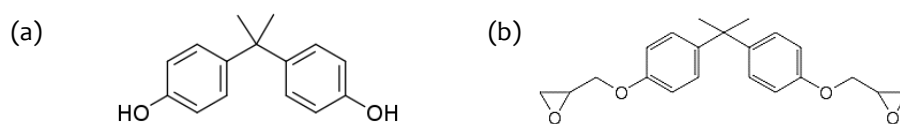


**Figure 1.3** – Chemical structures of (a) BPA and (b) DGEBA

## | Introduction and objectives

About 20% of the BPA produced accounts for the production of epoxy resins, widely employed as protective linings for a variety of canned foods and beverages, as a coating on metal lids for glass jars and bottles, including containers used for infant formula. However, part of the unreacted monomer and some molecules resulting from the break of unstable chemical bonds linking BPA to the polymer backbone, can migrate in foods and the users will inevitably be exposed to BPA via the diet, as consequence of his migration into the food. A recent study shows that BPA has been detected in the urine samples of 93 % of Americans, the biggest consumers of canned food in the world, confirming the link between BPA and food intake

Bisphenol A (BPA) among other bisphenols is part of the common class of endocrine disruptors because of the significant hormonal activity, and according to many lines of evidence it acts as an endocrine disruptor even at low doses.<sup>48,49</sup> The two phenolic and methyl groups of BPA structure have been demonstrated<sup>50</sup> to interact and bind the oestrogen-related receptor- $\gamma$  (ERR $\gamma$ ), hence the organism is induced to believe in a presence of oestrogens.

Considering all the aforementioned mechanism of intake is not surprising that the impact on human health is massive: the role in infertility is alarming, but also precocious puberty, cancer, diabetes, obesity and neurological disorders, are frequently linked to BPA exposure.

BPA exposure lowers levels of vitamin D in the bloodstream, and has also been shown to affect glucose metabolism through insulin resistance, pancreatic  $\beta$ -cell dysfunction, adipogenesis, inflammation and oxidative stress.

The detrimental effects of BPA have led governments to enforce regulations mostly in the European Union and North America in order to limit the

exposition of their citizens to this substance. For example, in 2014, in line with the opinion adopted by the RAC (Risk Assessment Committee), Bisphenol A has been classified in the hazard class reproductive toxicity category 1B “may damage fertility”.

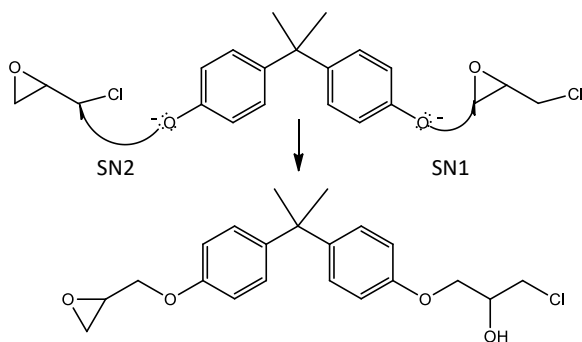
In the frame of the REACH regulation, the French proposition of the restriction of BPA in thermal papers was approved on the 6 July 2016 by the REACH Committee. The BPA European legislation involves different elements such as the restriction of the contact of infants and young people with this substance, through toys, feeding bottles, etc.<sup>51-54</sup> BPA is authorized as additive or monomer in the manufacture of plastic materials and articles in contact with food and water but a specific migration limit value of 0.6 mg/kg of food has been set.<sup>55</sup> Regarding cosmetic products, Bisphenol A is recorded in the list of the prohibited substances.<sup>56</sup> All the products made of BPA can't be eligible for a positive Eco-Label<sup>57</sup> and the indicative limit of occupational exposure<sup>58</sup> to BPA particles is 10 mg/m<sup>3</sup>. Some countries such as France have established even more strict legislations towards BPA,<sup>59</sup> and this country proposed BPA as a REACH Regulation candidate substance of very high concern (SVHC) and confirmed its advert on the 30 August 2016.<sup>60</sup>

The synthesis of epoxy resins from BPA is an efficient process that has been optimized over the years to achieve the lowest cost possible. Challenging this process means mainly to create a simple synthetic route, efficient, that produce a competitive material in mechanical and thermal properties, and ideally have some value added property such as lower viscosity or increased flame retardant property, considering that thermosets that contain the core BPA structure in the polymer network display excellent mechanical properties and provide sturdy materials for use in the construction, transportation, and

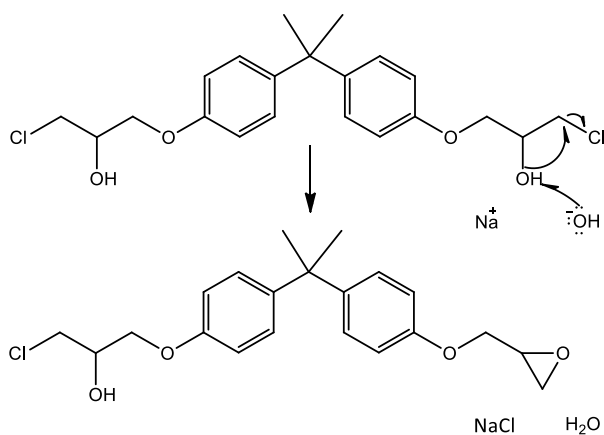
furniture industries and that the raw feedstock from biomass such as cellulose, lignin, vegetable oils and sugars is not readily available because the chemistry and the process still need to be developed and optimized, the challenge is difficult and has attracted a lot of investments.

Diglycidyl ether of Bisphenol A (DGEBA, **Figure 1.3b**) is the monomer mainly used in the epoxy resin industry, filling 75% of the resins used in industrial applications. DGEBA is generally prepared by direct glycidylation between BPA and epichlorohydrin; the reaction occurs in the presence of an alkylammonium halide as a phase transfer catalyst, such as benzyltriethylammonium chloride, tetrabutylammonium bromide or cetyltrimethylammonium chloride, so that the Bisphenol A is deprotonated to the corresponding phenol. The reaction takes place through two different paths, in fact the phenolic oxygen can attach the chlorine atom to directly produce the desired product through a mechanism  $S_N2$  (**Scheme 1.3**) or open the epoxy ring causing the formation of a chlorinated derivative (**Scheme 1.3**) that can be closed by a strong base through a  $S_N1$  mechanism (**Scheme 1.4**). When the synthesis of diglycidyl ether of bisphenol A (DGEBA) takes place in two steps the chlorohydrin intermediate formed is dehydrohalogenated by effect of the addition of caustic solution that acts also neutralizing the hydrochloric acid formed. Theoretically, two moles of epichlorohydrin are required for each mole of bisphenol A to get the monomer. However, to obtain a good yield, an excess of epichlorohydrin is typically employed, and the stoichiometric ratio is doubled or tripled. In this way, yields equal to or greater than 90% are achieved, the purity of diglycidyl ether depending on the excess of epichlorohydrin.<sup>26</sup>





**Scheme 1.3** – Competitive mechanisms of nucleophilic attack on phenolate ion



**Scheme 1.4** – Intramolecular cyclization of chlorohydrin intermediate

## 1.3. Bio-based epoxy resins

The main push for research and development of bio-based epoxy resins lie in the requirement to replace, especially in the field of food packaging, resins based on BPA.

## | Introduction and objectives

Initial attempts to replace this molecule, used in 75% of epoxy resins, concerned the use of epoxidized vegetable oils (EVO), i.e. vegetable oils in which the double bonds have been epoxidized. Such compounds, made up by long aliphatic chains, possess high mobility, especially if compared with the aromatic structure of BPA; it results in terms of poor mechanical properties for the EVO-based resins. For this reason most works involve the replacement, even partial, of the BPA with EVOs, with the intent to mediate the negative effect on the mechanical properties<sup>61-69</sup>. Over the years it has therefore attempt to develop bioderived resins with increasingly better mechanical properties and, at least comparable with those of the DGEBA-based. At this time the development of bio-based epoxy resins has strongly progressed and a first classification of these, depending on the origin of used bio-based molecules, can be done:

- Epoxides derived from vegetable oils
- Epoxides derived from polysaccharides
- Epoxides derived from lignocellulosic compounds

At the pilot plant scale many different bio-derived chemicals are becoming available such as levulinic acid, adipic acid, succinic acid, malonic acid, itaconic acid, vanillin, tannins and polyphenols, cardanol, sugar derivatives, furfural derivatives and unsaturated fatty acids. At the lab scale, exploration of different pyrolysis techniques for valorization of lignin is opening up avenues towards bio-based phenolic molecules such as guaiacols, phenols, eugenol, ferulic acid, and cresols. Thanks to all these feedstock becoming available more molecular architectures can imagined.

### 1.3.1. Epoxides derived from vegetable oils

A good bio-alternative for a wide range of petroleum based molecules is that of triglycerides obtained by plants that are vegetable oils. Triglycerides are fatty acids linked at a glycerol molecule and they differ each other for fatty acids chains, which can be made of 12 to 22 carbons and have different unsaturation degree; some of them also have different functional groups linked, as hydroxyl or epoxy. Each type of oil does not have a well-defined composition, but depending on the kind of plant, its age, the harvesting period, etc. varies the type of fatty acids of which it is made. Vegetable oils have several uses: human nutrition, directly or for cooking food; production of oil paints and colours (drying oils such as linseed); production of soaps; use as a solvent; use as biofuels; and in rural environments also for lighting, environmental heating and other uses.

To ensure as much as possible the sustainability of these resources is necessary to pay attention to edible nature of vegetable oils; in fact if an edible vegetable oil is chosen there will be a competitive use of this resource and is encouraged deforestation to the purpose of cultivation for the production of this raw material. It is therefore desirable to use non-edible plant oils, namely those oils containing toxic substances for humans, such as linseed oil, tung oil and castor oil, rather than the soybean oil. It was also seen that some non-edible oilseed crops not only does not compete with the agricultural resources for the exploitation of land, but also can grow in arid and infertile areas (restoring them) and are easy to propagate.<sup>70</sup> Obviously for use as bio-based source is necessary that this vegetable oils own unsaturation that can undergoes functionalization, in order to tailor their properties and reactivity

Double bonds can undergo manifold modifications; it can be oxidised, halogenated, reduced, epoxidated. As reviewed by Desroches et al.<sup>71</sup> by thiolene

## | Introduction and objectives

reactions vegetable oils can be functionalized in a one or two step synthesis procedures with hydroxyl groups, amines, carbonate or acid groups, becoming suitable monomers for the synthesis of polyurethanes, epoxy resins or polyesters. Among those reactions, epoxidation is a commercially important reaction in organic synthesis since the high reactivity of oxirane rings makes them to be readily transformed into desired functionality. Hence, plenty of researches on the epoxidation of triglyceride oils have been conducted worldwide in order to optimize the conversion rate of epoxidation and increase the epoxy yield. Epoxidized vegetable oils have drawn much attention especially in the polymer industry as they are economical, available, environmentally friendly, non-toxic and renewable. Bio-based epoxidized vegetable oils from renewable natural resources are potential green materials to partially substitute and toughen petrochemical-based polymers<sup>72,73</sup>. Arkema<sup>74</sup> is one of the main industrial producers of epoxidized vegetable oils, with the development of VIKOFLEX® based on epoxidized soybean oil. Moreover the variety of compositions allows to choose molecules that best fit the needs. Unfortunately due to long aliphatic and flexible chains in which there is a relatively low amount of epoxy rings many of which are internal, so with a low reactivity<sup>75</sup>, thermal and mechanical properties of EVO-based epoxy resins are not competitive, especially with DGEBA-based ones. Usual alternatives to go beyond these limits are crosslinking with rigid molecules or use vegetable oils with the maximum amount of functionality.

An example of this strategy was given by Pin et al.<sup>76</sup> which realized highly cross-linked epoxy resins, with high  $T_g$ , improved thermal stability and a good impact strength by anionic living copolymerization of epoxidized linseed oil (ELO) with methylhexahydrophthalic anhydride (MHHPA, a cycloaliphatic

monoanhydride) and benzophenone-3,3',4,4'-tetracarboxylic dianhydride (BTDA, an aromatic dianhydride). ELO possesses low volatility, high resistance to solvents, low migration tendency, high flexibility (due to the aliphatic chains) and an higher content of oxirane rings compared to the other epoxidized vegetable oils (EVO). As hardeners have been chosen those two anhydrides because of their compatibility with the ELO structure in terms of functionality, miscibility and melting point, and of their less toxicity compared to amines. In particular MHHPA was selected for its reactivity, because it is liquid at room temperature, and for its short-chain rigid structure. BTDA was instead chosen because it led to thermosets with high thermal and mechanical properties. (2-methylimidazole (2MI) as an initiator). Curing reactions, carried out with an epoxy excess (1:0.8 ratio for ELO/MHHPA and 1:0.5 for ELO/BTDA) to avoid early gelation during the polymerization process and to allow a good processability of mixtures, was monitored with FTIR spectroscopy, DSC, TOPEM and rheological analysis. In the case of BTDA for a better comprehension of homopolymerization and etherification reactions that can occur, they prepared two samples, one copolymerized, named ELO/BTDA<sub>1</sub>, and another post cured, labelled as ELO/BTDA<sub>2</sub>. FTIR analysis confirmed the completed copolymerization of resins and in case of ELO/BTDA<sub>2</sub> the occurrence of inter-epoxy side reactions but by DSC analysis came to light the different curing behavior depending on hardener. By TOPEM analysis vitrification was evaluated and results happening at 180°C for ELO/MHHPA and at 135°C for ELO/BTDA, that are in good agreement with rheological results. DMA analysis was used to evaluate  $T_{\alpha}$ , related to  $T_g$  and maximum of  $\tan \delta$ , which values are 134°C, 68°C and 127°C for ELO/MHHPA, ELO/BTDA<sub>1</sub> and ELO/BTDA<sub>2</sub> respectively. Values of  $T_{\beta}$  (related to fracture properties of materials) and  $T_{\gamma}$  are also reported, indicating a ductile or semi-ductile behavior of ELO/MHHPA and a not completely crosslinked structure for

## | Introduction and objectives

ELO/BDTA1. Thermal stability of resins, valuated with TGA analysis, is higher than DGEBA based resins; ELO-based resins degradation in air begins at 337°C and follows a complex three step behavior.

Moreover, still in 2015 Pin et al. proposed a novel synthetic route to obtain fully bio-based epoxy resins with improved mechanical properties using ELO, this time copolymerized with polyfurfuryl alcohol (PFA), in presence of boron trifluoride ethylamine complex as catalyst<sup>77</sup>. Furfuryl alcohol (FA) is a bioderived molecule that polymerizes under acid catalysis giving PFA, a polymer with high  $T_g$  and thermal stability but very brittle. The aim of this work was to combine good properties of PFA with flexibility of vegetable oils. Copolymerization was confirmed by FTIR, 1D and 2D NMR and DSC analysis; the last ones was used furthermore to determine the optimal amount of catalyst and the ELO/FA ratio, that were set to 1% of catalyst and 50/50 molar ratio. DMA analysis was conducted and show a complex behavior for the resin resulting in 4 kind of relaxation processes, as highlighted by the presence of  $T_\alpha$ ,  $T_\beta$ ,  $T_{\beta'}$  and  $T_\gamma$ , related to motion of several sections of the chain. Tensile tests, combined with SEM analysis, point out the ductile behavior of ELO50/FA50 resin which has got a modulus of 44MPa, strength at break of 7MPa and deformation at break of 40% (compared with  $E=1\text{GPa}$ ,  $\sigma=40\text{MPa}$  and  $\epsilon=5\%$  of PFA). Finally thermal stability was evaluated and results lower than PFA ones (364°C of ELO/FA versus 402°C of PFA) but still better than DGEBA-based resins. This fully bio-based copolymer in addition presents a complex degradation

ELO was also used by Albarrán-Preza et al.<sup>78</sup> who synthesized a novel xylitol-functionalized epoxidized linseed oil (ELO) polyols. The linseed oil was epoxidized enzymatically using novozyme and hydrogen peroxide. To establish the reaction conditions to synthesize xylitol-functionalized ELO (i.e.

temperature, time and amount of catalyst) for a complete and partial functionalization, the parameters were assessed in a series of five reactions with different temperatures, times and amounts of catalyst. The final monomers obtained are ELO-Xyl-50% and ELO-Xyl-100%; the crosslinking conditions to produce the resins were 180°C for 60 min for ELO-Xyl-50% and 200°C for 120 min for ELO-Xyl-100% + ELO. The NMR analysis confirmed that the desired products were obtained and allowed the evaluation of molecular weight and percentage of epoxidation of the product. The effect of the hydroxylation was reflected in the viscosity property, which was 3 times higher in the 100% functionalized monomer (ELO-Xyl-100%) than in the partially functionalized monomer (ELO-Xyl-50%). Moreover, the hydroxyl groups were highly reactive to the opening of the epoxy rings in the presence of even moderate amounts (an ELO/ZnCl<sub>2</sub> molar ratio of 0.06 mol) of catalyst, due to the increased nucleophilic power of the primary hydroxyls in xylitol, thus increasing the cost-effectiveness of the synthesis procedure.

Pawar et al.<sup>79</sup> first epoxidized Cottonseed oil and algae oil with a yield about 90-94% and then cured them with citric or tartaric acid obtaining 4 kind of totally bio-epoxy resins, whose properties were compared with a petrol based resin made by DGEBA with DETA (diethylenetriamine). More than very good thermal and mechanical properties these resins, characterized for their biodegradability, seed germination and larvicidal activity, showed a complete biodegradability and the ability to kill mosquito larvae, that are the cause of several human diseases like malaria. Moreover these materials resulted as a good substrate to grow black eyed peas in comparison with DGEBA-based materials.

## | Introduction and objectives

Liu et al. in 2016 starting by linoleic acid and hexamethylol melamine (HMM), in presence of some catalysts, obtained through an esterification reaction a six-armed unsaturated molecule, epoxidized with hydrogen peroxide monomer in presence of acetic acid (with a conversion of 97%)<sup>80</sup>. The obtained branched epoxy monomer (EHL) was cured with 4-methyl hexahydrophthalic anhydride (MHHPA) in several ratios and properties of the resulting resins was analyzed in comparison with resins obtained curing two benchmark bio-based epoxides, epoxidized soybean oil (ESO) and epoxidized sucrose soyate.  $T_g$  of EHL resins result higher than ESO (4.6°C) and ESS (50.4°C) but vary with the epoxy/anhydride ratio; the higher value results for sample with higher anhydride content. A similar trend, increasing with the anhydride amount, is shown by cross-linking density. All samples exhibit a one-step degradation profile but temperature at which samples experience a 5% weight loss decreases at increasing anhydride amount; ESO and ESS based show higher degradation temperatures. This behavior is related with the content of the more thermally unstable ester bonds, derived by cross-linking reaction, and the greater thermal stability of glycerol and sucrose than HMM. Tensile tests highlight the fragile behavior of EHL-based resins, that are very brittle, with high modulus and tensile stress, ascribable to intermolecular interactions between HMMs cores, in opposition with the ductile behavior of ESO and ESS (low tensile strength and modulus but markedly higher elongation at break values) A valiant result of this work concerns the biobased content that appears to be rather high despite the HMM core and the hardener are petrol-based. In fact the biobased content is 70.3% for the resin with 1.0:0.4 epoxy/anhydride ratio and decrease to 66.4% and 62.8% increasing the anhydride amount.



In 2015 Carbonell-Verdu et al.<sup>81</sup> used vegetable oils, in particular cotton seed oil (CSO), for the synthesis of epoxy resins. The cotton seed oil epoxidation took place in acid medium with different types of hardeners: a flexible cyclic anhydride, or dodecenyl succinic anhydride (DDSA and on the other hand a rigid cyclic anhydride), or methyl nadic anhydride (MNA). Having different characteristics, the two types of hardeners generated different thermosetting structures: the DDSA generated a flexible resin, whereas MNA produced a more rigid one. Moreover, they required different cure temperatures and underwent diverse polymerization process depending on their length, chain mobility etc. Also the viscosity played a key role: by treating ECSO with DDSA, a structure with Mw greater than that obtained with ECSO and MNA was obtained, due to the minor gelation times: the temperature peak for the system treated with DDSA was close to 179.2 °C, while it was 198.47 °C for the system treated with MNA. These results indicated that ECSO reaction with DDSA occurred in a simpler way than using MNA and these results were consistent with the literature. Furthermore, it was demonstrated that the nature of curing agent affected also the final properties of the cured materials. For example, the flexural modulus of ECSO cross-linked with DDSA was 38.9 MPa, significantly lower than the modulus of ECSO cured with MNA with values of about 151.2 MPa. The use of mixtures of the two anhydrides was also carried out to combine rigidity and flexibility and, depending on the ratio between the two, it was possible to adjust the final properties of the resin according to the required applications. As the amount of DDSA increased in the DDSA:MNA mixture, there was an increase in the flexural modulus.

Boquillon et al.<sup>82</sup> polymerized epoxidized linseed oil with anhydrides, through reactions catalyzed by tertiary amines and imidazole. ELO and

## | Introduction and objectives

tetrahydrophthalic anhydride (THPA), methylhexahydrophthalic anhydride (MHHPA), methyl-endomethylenetetrahydrophthalic anhydride (METH), methyl-tetrahydrophthalic anhydride (MTPHA), were mixed at high temperature in presence of 2-methylimidazole (2MI) as a catalyst. Temperatures were chosen based on the melting points of the precursors. The mechanical tests showed an increase in  $T_g$  with increasing the amount of anhydride (R). In particular, for amounts of anhydride  $R < 1$ , the unreacted epoxy groups moved towards the chain terminals, leading to a decrease of  $T_g$ , while for  $R > 1$  the space between the cross links increased and consequently the  $T_g$  decreased, but an increase in the glass transition temperature ( $T_g$ ) from 34.5°C for R = 0:3 up to 113°C for R = 0:6 is observed. The properties of the resins obtained with the different types of anhydride were also compared: the samples prepared with THPA, MTHPA, MHHPA showed similar bending modules between 1671 and 1726 MPa, and a  $T_g$  ranging from 109°C to 122°C; the samples prepared with PA and METH instead, have a very different flexural modulus between 2000 and 1535 MPa and greater transition temperatures, between 148 and 157°C. THPA was the subject of more in-depth studies as it is the most economical hardener on the market. Furthermore, it was found that by varying the percentages of 2-MI it was possible to play on the final properties of the epoxy resin.

Alsagayar et al. in 2014<sup>83</sup> prepared a mixture of DGEBA epoxy resin and epoxidized palm oil (EPO). The resins were prepared with two different methods: direct mixing, and pre-mixing methods. Mechanical analysis showed that the addition of EPO according to the direct method (10%, 20% and 30% by weight) reduced the tensile strength and the Young's modulus of 13.85% and 16.95% respectively; while there was an increase in elongation at break with an EPO percentage of 10%. The reason lies on the fact that a high percentage of EPO

can generate weak points at the terminals of the chains that nucleate voids under stress and reduce resistance and tension at break. With the pre-mixing method instead, there was an increase in tensile strength with the addition of EPO at 10-20%, while there was a decline of the same with 30% EPO. The explanation is that as the amount of EPO increases, the amount of amine that reacts with the epoxy system is reduced and this leads to a decrease in crosslinking density, which has an effect on the mechanical properties. Furthermore, the tests showed that, using the direct synthesis method, there was a reduction in flexural strength and modulus, as the EPO percentage increased. In particular, passing from 10 to 30% of EPO, a decrease of 37.45% and 30.42% of modulus and flexural strength, respectively, was observed. This is due to the increased flexibility of the chain, which leads the sample to deform before breaking. When EPO and hardener were reacted for 1 hour (pre-mixing synthesis method), an increase in mechanical properties was recorded; when EPO and hardener reacted for two hours, a decline in mechanical properties was then recorded; the improvements are due to an increase in the incorporation of EPO into the crosslinked epoxy network, and therefore a stronger matrix. In conclusion, using EPO with low epoxide content it was possible to obtain a miscible mixture, where the addition of bio resin caused a decrease in the modulus and in the tensile strength due to its low rigidity. On the other hand, the increase of EPO increased the flexibility of the mixture and consequently the toughness, the impact resistance and the tensile stress of the final material.

Abdelwahab et al.<sup>84</sup> explored a new approach to harden a bio-based epoxy with different siloxane types. Three modified siloxanes were used as hardening agents: amine-terminated polydimethylsiloxane (PDMS-amine), polydimethylsiloxane with glycidyl termination (PDMS-glycidyl), polyhedral

## | Introduction and objectives

oligomeric silsesquioxane terminated with glycidyl (POSS-glycidyl). The bio based formulations were obtained by mixing the epoxide with 5% by weight of siloxane compounds at room temperature. DSC analysis showed a single wide exothermic peak due to the reaction between the epoxy groups of the bioepoxy and the amine group of the hardener. Analyzing the reaction kinetics, the effects of siloxanes on gelation time and pot-life were evaluated: all three modified siloxane dioxide showed an increase in viscosity similar to the behavior of the neat resin. The mechanical tests finally helped in comparing the properties of the neat resin with those of the siloxane-modified ones: in general, the bioepoxy had a low impact resistance and elongation at break with high tensile properties , being its tensile modulus and the strength of pure bioepoxy 3.28 GPa and 68.8 MPa, respectively. The incorporation of PDMS-amines or PDMS-epoxy was responsible for a slight decrease in tensile and flexural strength compared to neat resin, suggesting that the incorporation of PDMS elastomeric segments induced a reduction in crosslinking density, which decreased the tensile properties. However, the incorporation of 5% POSS-glycidyl showed a 7% increase in tensile strength. This was due to the reaction between the POSS glycidyl groups with the bioepoxidic system that increased crosslinking density, decreasing the free volume of epoxy backbones. As for the impact resistance and elongation at break, the addition of PDMS-amine had a detrimental effect probably due to the immiscibility and heterogeneity of the elastomeric PDMS, while the addition of PDMS-glycidyl slightly increased the elongation at break of the final product. Finally, the incorporation of POSS-glycidyl improved the elongation at break and impact resistance by 29% and 16% respectively, compared to the neat epoxy resin. This is due to the presence of nanostructured and caged structures of the POSS structure that can absorb impact energy.

Kousaalya et al.<sup>85</sup> studied synthesis of epoxy resins from a vegetable oil, the *Perilla Frutescens*. Epoxidation of Perilla oil (EPeO), carried out using performic acid (HCOOOH). The oil epoxidation occurred in two steps: performic acid formation and, conversion of double bond to epoxy, that occur simultaneously in both oil and aqueous phases. To determinate epoxidation degree, iodine value (IV) is calculated; Iodine value (IV) of perilla oil was estimated to be 196.9 g/100 g (of oil), indicating the double bond concentration to be 0.77 mol per 100 g of oil. Reaction kinetics for epoxidation and ring opening reactions showed activation energy of 20.10 kJ/mol (epoxidation) and 43.11 kJ/mol (ring opening), indicating higher stability of epoxy groups and lower probability of  $\alpha$ -glycol formation. This was further confirmed by results from  $\alpha$ -glycol content test, which showed its molar concentration at less than 20% of epoxy molar concentration.

Hu et al. synthesized castor oil-derived decanediamide (DDA), as a novel flexible epoxy curing agent, by esterification with methanol and successive ammonolysis with ammonia<sup>86</sup>. Then, equimolar amounts of epoxy resin and DDA were mixed and the reaction mixture reacted at high temperature. Dynamic analysis showed that the epoxy cured by castor oil-derived diacid amide exhibited good dynamic mechanical properties even if there's a slight decrease in  $T_g$  value. Moreover, it was demonstrated that thermal stability of epoxy resin cured with DDA was comparable with that of epoxy resin cured by conventional epoxy resin curing agent. The chemical structure of the curing agent, had significant influences on morphology and cross-linking density of its network, therefore, affecting its mechanical properties; the tensile strength of pure epoxy cured by DDA was almost as high as that of the epoxy cured by conventional epoxy curing agent; also the tensile strength reaches its maximum value when 5

## | Introduction and objectives

phr of asphalt was added into this system, enhancing its tensile strength through the physical cross-linking of dispersed asphalt. When asphalt was further added, the tensile strength of this system started to decline. This was attributed to the low distortion temperature and low polarity of asphalt which could not be entirely compatible with epoxy resin when the content of asphalt was excessive.

Cinnamea et al.<sup>87</sup> synthesized a completely bio-based pressure sensitive adhesives (PSA) with tuneable viscoelastic properties from mixtures of epoxidized soybean oil and sebacic acid by a solvent-free one-step reaction, in absence of catalyst. Pressure-sensitive adhesives (PSA) are a special category of polymeric materials that are permanently tacky at the operating temperature and can adhere to any given substrate under slight pressure in a very short time. The behavior of PSA depends on a perfect balance between viscous and elastic properties. The first step was the preparation of the mixture of sebacic acid SA and epoxidized soybean oil ESO, followed by cure treatment. Synthesis was performed by a sustainable and environmentally sound one-pot procedure by reacting ESO and SA in absence of any additional chemicals, such as volatile solvents and catalysts. Curing conditions, pot-life, and gel content were determined. The rheological profile and gel content of the obtained PSA were greatly dependent on the curing conditions (temperature and time). ESO–SA stoichiometric mixtures cured at 170 °C between 65 and 75 min showed the best balance between tack and cohesion.

Sahoo et al.<sup>88</sup> used epoxidized linseed oil (ELO) and bio-based crosslinker to make a toughened bio-based epoxy. Synthesized ELO was blended with DGEBA-epoxy in different ratios (10, 20, and 30 phr) to develop bio-epoxy blends. A transition from non-Newtonian to Newtonian flow was observed as bio-resin content was increased within epoxy, which was attributed to change in

branching and degree of entanglement. So, the epoxidized linseed oil (ELO) was found to be an effective reactive diluent which had the potential to improve the processability of epoxy resin by reducing its viscosity and pseudoplastic behavior. Bio-based phenalkamine (PKA) helped toughen the epoxy matrix significantly. The tensile strength of PKA cured epoxy was found to be similar to epoxy cured with commercial aliphatic amine-based curing agents. The modulus and strength were found to be moderate up to 20 phr ELO loading with significantly higher elongation at break. Both bio-based PKA and ELO bio-resin enhanced the toughness of epoxy and lowered the glass transition temperature because of their flexible long chain molecular structure. Interestingly, no significant change was observed in peak temperature of curing on increasing the concentration of ELO from 20 to 30 phr which indicates that a possible higher bio-resin dilution ( $\approx 30\%$  ELO) may be made without increasing curing efforts.

Same authors<sup>89</sup> also developed a completely bio-based epoxy networks derived from epoxidized linseed oil (LO) and castor oil (CO) cured with citric acid. Linseed and COs were epoxidized through in situ epoxidation in presence of glacial acetic acid and hydrogen peroxide. Then approximately citric acid (CA) was added to form DGEBA-epoxy, ELO, and ECO-based networks, respectively. The shear stress increased with shear rate for all types of resin systems. A nonlinear relationship between shear stress and shear rate (pseudoplastic behavior) was observed in epoxy resin, while ELO exhibited a linear shear stress versus shear rate relation (Newtonian behavior). The viscosity of epoxy was significantly higher than the ELO and ECO at both low and high shear rates. Tensile strength and modulus of epoxy were found to be 49.04 and 1841.41 MPa, respectively, due to the higher crosslink density and aromatic structure in epoxy. The tensile strength and modulus of ELO-based network were 5.25 and 53.58

MPa, which were quite less as compared with those of epoxy. However, the elongation at break of ELO was 300% higher than epoxy, which revealed its much higher toughness. Similarly, ECO exhibited inferior value of tensile strength (258 kPa) and modulus (1490 kPa) but had significantly higher elongation at break (34.1%), which was much higher than cured epoxy and ELO network. Thermal stability of cured epoxy and ELO were almost comparable, while quite inferior stability is noticed in case of ECO. Though multiple transitions were found in DSC thermograms in all the systems, epoxy and ELO displayed major glass transition at 44 and 10°C, respectively, ECO showed glass transitions at -8°C, which was much lower. Finally, it was observed that epoxy exhibited highest  $E'$  value over the investigated range of temperature as compared with epoxidized oil-based network. This superior value of storage modulus of epoxy was ascribed to the rigid bisphenol group and higher degree of crosslinking in DGEBA-based epoxy. On the other hand, despite high oxirane content, ELO-based network exhibited lower  $E'$  value because of flexible aliphatic chain structure and relatively lower degree of crosslinking and high steric hindrance. Similarly, ECO showed lowest storage modulus among all the samples on account of lower epoxy content, higher molecular chain between the crosslinks, and excess polyol groups which resulted in reduced crosslink density as well as enhanced flexibility.

### 1.3.2. Epoxides derived from lignocellulosic compounds

Epoxy resins obtained by EVOs have, as aforementioned, some not desirable features like low  $T_g$ . Because of it, and because the reducing availability



of aromatic petrol based molecules deriving from the shift from oil to shale gas, is rising ever more the idea to develop bio-based aromatic molecules.

The most broad and widespread renewable aromatic source is lignin, a heavy and complex organic polymer consisting mainly of phenolic compounds. Lignin is, for quantity, the second biopolymers on Earth after cellulose; it is found mainly in the cell wall of some plant cells where it's strongly bonded with hemicelluloses and cellulose being, thus, difficult to isolate. The biomass formed by cellulose and lignin represents about 70% of the total biomass. This undesirable feature imposes the need to develop an efficient technique to separate those compounds in order to have the opportunity to use lignin as valiant bio-based material. The molecule of lignin has a high molecular weight, and is obtained by the combination of different acids and phenylpropyl alcohols (coumaryl, coniferyl and synapyl). The random coupling of these radicals gives rise to a three-dimensional, amorphous polymeric structure that has not been completely defined yet (even because chemical composition depends on botanical specie). Lignin has in all the plants the function of binding and cementing the fibers together to give and enhance the compactness and resistance of the plant. Its aromatic structure confers relatively good thermostability and good mechanical properties.<sup>25</sup>

Thanks to the variety of groups and molecules that can be obtained by lignin, included aldehydes, it is also a good candidate to substitute formaldehyde in phenolic resins. In epoxy resins production lignin can be used by directly mixing it with some epoxy resins, or after some modifications, as direct glycidylation. Lignin structure can also be broke down and its constitutive elements can be further functionalized, in particular glycidylated.

Aouf et al.<sup>90</sup> introduced the ability to control the functionalization of gallic acid with a two-step reaction. With a first allylation using allyl bromide followed by the epoxidation, instead of a single step using epichlorohydrin, is possible to achieve higher rate of glycidylation of gallic acid, and obtain a mixture of tri- and tetra-glycidylether derivatives. In this work two routes to epoxidize tetraallylated gallic acid have been tried; a mixture composed by a 60% of tetraglycidylethers and 17% of triglycidylethers can be obtained using an excessive amount of mCPBA (meta-chloroperbenzoic acid), even difficult to eliminate, therefore they proceeded with epoxydation reaction that took place at room temperature by in situ generated dioxirane from 1,1,1-trifluoroacetone and Oxone™. In this case the amount of tri- and tetra-glycidylethers of gallic acid are respectively 30% and 40% and the overall epoxidation yield is only slightly decreased. Curing that glycidyl ether derivative of gallic acid mixtures with IPDA (isophorone diamine) they obtained epoxy resins showing higher cross-linking density, higher  $T_g$ , higher onset temperature of  $E_0$  decrease and a higher char yield than the diglycidyl ether of BPA (DGEBA) network cured in the same conditions.

However, still Aouf<sup>91</sup> proposed a one-step synthetic route for glycidylation of Gallic Acid and tara tannins, with a yield of 60%, using epichlorohydrin.

Fache et al.<sup>92</sup> synthesized three different epoxy monomers, DiGlycidyl Ether of MethoxyHydroquinone (DGEMHY, 5), Diglycidyl Ether of Vanillic Acid (DGEVAC, 6), and DiGlycidyl Ether of Vanillyl Alcohol (DGEVA, 7), starting by vanillin derivatives, successively cross-linked with IPDA (isophorone diamine). The obtained diepoxy monomers, solids at room temperature, were first molten and then IPDA was added, in order to avoid any inhomogeneity or air bubbles in the final material; high processing temperatures required to work in the molten

state limit the industrial relevance of this materials. All materials underwent a post-cure step at a temperature higher than  $T_g$ , to ensure complete reaction. With the epoxy monomers DGEVAC and DGEVA were prepared resins with 2.0/1.0 epoxy/amine functions ratio whereas in the case of DGEMHY, eight materials with varying epoxy/amine ratios ranging from 2.0/0.6 to 2.0/2.0 were produced. Thermo-mechanical properties of the materials obtained were investigated, in particular  $T_g$ ,  $T_\alpha$ ,  $T_{deg}$ , char yield and  $E'$  for the various resins compositions and in comparison with an industrial DGEBA–IPDA, showing comparable results.

Lignin-based epoxy monomers have been synthesized in 2016 by Xin et al.<sup>93</sup> starting by partial depolymerized lignin (PDL) by reacting it directly with epichlorohydrin. PDL used in this work has been obtained from partial hydrogenolysis of enzymolysis lignin and displays three kinds of hydroxyl groups (aliphatic, aromatic and carboxylic) in large amount, increased solubility in organic solvent and narrow molecular weight distribution. During the epoxidation value of aromatic and carboxylic (highly reactive with epichlorohydrin) hydroxyl groups decrease unlike of aliphatic ones. Epoxies such obtained was cross-linked using a bio-based anhydride (which was the Diels–Alder adduct produced from addition of maleic anhydride and methyl ester of eleostearic acid (a major tung oil fatty acid)) as curing agent. Comparative studied carried out through DSC on PDL-based resin and the commercial epoxy resin DER332 demonstrated that the PDL had a higher exothermic peak, due to the more complicated chemical structure responsible for a different reactivity. In particular, the polymerization showed a higher activation energy, evidencing a lower reactivity of the PDL-based resin, probably due to the fact that the PDL is a solid powder that required more energy for the polymerization process. The DMA analysis instead showed that the elastic modulus  $E'$  of the PDL resin was

## | Introduction and objectives

greater than that of the DER332, because of the more rigid structure and an increase of the  $T_g$ , resulting in a greater thermal stability. With the TGA analyzes the decomposition temperatures (5% and 10% by weight) were calculated and results were comparable for the two resins. Based on these properties, PDL resin could be suggested as asphalt modifier.

Asada et al.<sup>94</sup> used low molecular weight lignin obtained from different lignocellulosic biomasses to develop epoxy resins with an high bio-based content. In particular, cedar, bamboo and eucalyptus have been minced and pretreated with steam-explosion mechanism to extract lignin. The solubility of lignin extracted from samples such as cedar was tested in various solvents such as THF, methanol, epichlorohydrin and water and compared with commercial lignin. The results showed that the lignin extracted with steam explosion was soluble in organic solvents, unlike commercial lignin. This feature is mandatory in electrical circuit applications and therefore makes the lignin extracted from cedar a preferable candidate compared to other commercial lignin. The extracted lignin was mixed with epichlorohydrin and methanol; tetramethylammonium chloride (TMAC), a water-soluble phase transfer catalyst. The lignin epoxy resin obtained was further cured with two curing agents: lignin itself, obtaining high bio-based epoxy resins, and a petrol-derived phenol novolac. Thermal analyzes have shown that the increase in the amount of lignin reduces the decomposition temperatures, and despite these temperatures are lower than those of fossil-based epoxy resins, they still meet the parameters of thermal stability for the welding resistance. Among the three samples studied (cedar-, bamboo-, eucalyptus- derived resin), the thermal decomposition temperatures of the cedar-derived resin were higher than the other two; this may be due to the low Mw and the low epoxide equivalent weight of the lignin-

based epoxy monomer. Finally, the insoluble residues of methanol were enzymatically hydrolyzed to produce glucose.

Garrison et al.<sup>95</sup> produced a diepoxy and a diamine starting by p-cymene and produced 4 samples combining these two bio-based monomers with two petrol based monomers, the EPON, a diglycidyl ether of BPA, and methylenedianilin. We can see that totally bio-based material cures at higher temperatures because of the low concentration of functional groups. Really different are enthalpies of reaction too, because of substitution degrees of compounds. An interesting result presented in this work is the moisture up taking of materials that is greatly reduced for bio-based materials. Moreover their  $T_g$  undergoes a lower reduction percentage after the moisture up taking.

Another really interesting work is proposed by Wan et al.<sup>96</sup> They linked two eugenol molecules using p-xylene as bridge, specified and then cured with diaminodiphenyl methane (DDM). The material exhibits a very good increase in young's module, hardness and especially char yield respect DGEBA based resin. An interesting aspect of this work is the high bio-based content of the final resin, that can be further increased using bioderived p-xylene (that can be obtained cellulose-derived furans and bio-isobutanol).

Sasaki et al.<sup>97</sup> used lignin extracted from steam-exploded bamboo, as resource material for the production of cured epoxy resins. Steam explosion was used to break down the lignin structure, and extract lignin from the lignocellulosic material bamboo. Synthesis of epoxy resins is based on a two-step reaction catalyzed by a phase transfer salt, typically tetrabutylammonium bromide (TBAB). The following cured epoxy resin samples were prepared: diglycidyl ether bisphenol A (DGEBA) cured with 1- (2-cyanoethyl)-2-ethyl-4-methylimidazole (2E4MZ-CN), bamboo lignin epoxy resin cured with 2E4MZ-CN,

## | Introduction and objectives

and bamboo lignin epoxy resin cured with bamboo lignin. When using bamboo lignin as a curing agent, the molar ratio of epoxy and hydroxyl groups (OH) was maintained at 1:1 in tetrahydrofuran. It was observed that the use of bamboo lignin as a resource material resulted in decreased transparency compared with the other cured epoxy resins. This is attributed to the heterogeneous character of lignin structure. The thermal analysis show their thermal stability and thermal degradation properties. The decomposition temperature that causes 5% weight loss ( $T_{d5}$ ), and char residues at 800°C. This temperature is lower than the temperature of commercial epoxy resins (DGEBA) but it satisfied the thermal stability requirements for solder-dip resistance.

Chang-Wu and Jau Lee used *Dendrocalamus Latiflorus* Munro (a kind of bamboo) as renewable resource to prepare copolymer epoxy resin<sup>98</sup>. To liquefy the bamboo they employed phenol or PEG/glycerol co-solvent. Copolymer epoxy resins were synthesized by a two-step process: in the first step, epichlorohydrin and bisphenol A was let react in presence of NaOH. Then, other epichlorohydrin and calculated amount of liquefied bamboo were added and copolymerization let proceed. When phenol-liquefied bamboo was employed to prepare copolymer epoxy resins, it was also glycidylated by the epichlorohydrin, so the EEW did change significantly, and the viscosity of copolymer epoxy resin decreased as the ratio of liquefied bamboo increased; on the other hand, when part of bisphenol A was replaced by polyhydric alcohol-liquefied bamboo, both the viscosity and EEW of copolymer epoxy resins raised with increasing the ratio of liquefied bamboo. The curing behavior of copolymer epoxy resins prepared with phenol-liquefied bamboo was similar to that of neat epoxy resin (that could cure at room temperature); however, the rate of temperature increasing and the phenomenon of resin curing were faster than those of the neat epoxy resin.

When polyhydric alcohol-liquefied bamboo was employed to prepare copolymer epoxy resins, the resin with 10% of bisphenol A being substituted by liquefied bamboo released more heat during the cure process that was completed after 9.5 min. However, when the amount of substituted bisphenol A increased to 30 and 50%, the exothermic phenomenon diminished greatly. This result indicated that only a limited amount of polyhydric alcohol-liquefied bamboo could participate in the copolymerization of copolymer epoxy resins due to lack for electron withdrawing aromatic ring. Results gathered by DSC indicated that introducing phenol-liquefied bamboo into the epoxy resin could provide a higher crosslinking density and a more complete net structure. TGA analysis showed that copolymer epoxy resin prepared with phenol-liquefied bamboo had a slower thermal weight loss and higher char content than others samples at temperatures up to 700°C. This is due to the aromatic structure of phenol-liquefied bamboo present in the cured resin that serves as free radical trapper, delaying the thermal degradation.

Yiang et al.<sup>99</sup> synthesized a multi-ring products by using lignin derived phenols such as 4-methylcatechol and carbohydrate-derived furanic molecules such as 5-(hydroxymethylfurfural) (HMF) and furfural as the starting materials. The general strategy of this study was to prepare two mixtures of catechol and furanic compounds obtained from the depolymerization of lignin and carbohydrates. Each catechol and furan mixture was individually reacted in order to understand the reactions and the properties of products. In detail, bisphenol-furan molecules were designed as precursors for polymerization. The synthesis was developed through a basic reaction route. Furfural (FF) and 5-hydroxymethylfurfural (HMF), which can be obtained from carbohydrates, were selected to react with 4-methylcatechol, which is a product of lignin

## | Introduction and objectives

depolymerization. Pure products, 4-methylcatechol–furfural (MF) and 4-methylcatechol–HMF trinuclear compounds (MH), were obtained after recrystallization from ethyl ether and toluene and then epoxidized with epichlorohydrin in presence of tetrabutylammonium bromide (TBAB) to provide the glycidylated products, MFE and MHE, respectively. The so-obtained epoxy monomers were then cured with diethylenetriamine (DETA). The  $T_g$  measured through DMS had a value of 110 °C for MHE-DETA and 100 °C for MFE-DETA. The storage modulus values  $E'$  of MHE-DETA and MFE-DETA at 45 °C were 9.6 GPa and 6.6 GPa, respectively. These results indicated that MHE-DETA had better thermo-mechanical properties compared with MFE-DETA. Degradation temperatures under nitrogen calculated through TGA revealed a good thermal stability of both resins as for both epoxy thermosets the onset degradation temperature (temperature at 5% weight loss,  $T_{d5}$ ) was 174.2 °C for MFE-DETA and 214.0 °C for MHE-DETA. The temperature at 50% weight loss ( $T_{d50}$ ) reached 381 °C for MHE-DETA and 362.4 °C for MFE-DETA, almost comparable to the corresponding BPA-based resins.

Gioia et al. reported a study of the synthesis of thermosetting resins from low molar mass Kraft lignin fractions of high functionality, refined by solvent extraction<sup>100</sup>. The lignin fractionation process developed, involved sequential extraction using organic solvents, ethyl acetate (EtOAc), ethanol (EtOH), methanol (MeOH), and acetone. The sequence of extraction was designed in order to retrieve fractions with low polydispersity and gradually increasing molecular weight. Oxirane moieties were introduced with a glycidylation method through the reaction of epichlorohydrin with the different lignin fractions. In particular, this step was optimized for mild conditions in order to prevent undesired cleavage or aggregation of the lignin backbone structure.



Acetone/water 50:50 was found to be an excellent solvent system for all the fractions at 50 °C. Polyetheramine D2000 was selected as cross-linking agent to cure the epoxidized lignin fractions. This diamine also confers ductility and lowered  $T_g$  to the resin, while lignin promotes high Young's modulus and increased glass transition temperature. The curing procedure consists in a first step where the mixture is heated 1 h at 50 °C in order to remove the solvent, a cure step of 2 h at 100 °C, and post-cure at 150 °C for 2 additional hours. The thermal behavior of the resins was evaluated by DSC analysis and compared with the thermal properties of the corresponding lignin fractions. All the obtained thermosets appear to be homogeneous materials presenting a single  $T_g$ , at about -50 °C. The storage modulus of lignin-based resins was found to follow two different trends, discriminated by their glass transition temperatures: in the glassy state, the resin prepared from the fraction with the lower molecular weight, showed a significantly higher storage modulus compared to the other thermosets. Above the glass transition, an inversion of the trend occurred. Finally, the Young's moduli of the lignin-based soft epoxy resins range from 6 to 100 MPa, and the tensile strength of the resins varied from 1.2 to 5.0 MPa and increases with the molecular weight of the lignin fraction.

Salanti et al.<sup>101</sup> in their work used exploiting epoxidized lignin as both hard segment and cross-linkers to produce bio-based epoxy resins. The epoxidation on lignin allowed the separation of high molecular weight fragments, and thus solely collected the lignin fraction suitable for further wet processing. The thermoset resin was prepared with a co-macromonomer combined with PEG and two different amines. The PEG acted as a soft segment to modulate the polymer characteristics, while the amines were used as chain extender and cross-linkers. By raising the content of PEG and lignin, a ductile gel was obtained.

## | Introduction and objectives

The DSC analyses showed that higher  $T_g$  values were detected at larger lignin concentration, which denoted a higher cross-link degree due to the presence of more reticulation points in the lignin macromolecule.

Yan et al.<sup>102</sup> synthesized lignin-based epoxy acrylate (LBEA) oligomers with various percentages of lignin functionalized with epoxy and acrylic acid groups, to be used as coatings. The synthesis of LBEA was performed through two steps. In the first step, LBE was prepared by etherification reaction between lignin and epoxy with varying percentages of lignin from 5% to 15%; in the second step, LBEA was prepared by esterification reaction between LBE (lignin based epoxy) and acrylate to produce LBEA. As the content of lignin increased, ring opening reaction between the epoxide group on LBE and the acrylic acid was accelerated, and the reaction time was shortened. When lignin content was 25%, the reaction time was only 35 min. Mechanical properties were evaluated: LBEA coatings always had higher hardness than EA coatings. LBEA with 5% and 10% lignin showed the maximum hardness of 3H. The hardness decreased with the cross-linking density of the system. The addition content of lignin to EA resin could significantly increase the adhesion of the coatings due to the abundance of hydroxyl groups on the lignin. Thus, hydroxyl content of LBEA was increased, and the adhesion was improved. Also, the aliphatic side chain in the structure of lignin was responsible for an improved flexibility of coatings, in fact, when lignin content was 5%~25%, the flexibility of film was 4~8 mm, which was much better than that of EA (12 mm). LBEA membranes also possessed good thermal stability according to the TGA analysis.

Jablonskis et al.<sup>103</sup> realized modification of LignoBoost™ softwood Kraft lignin with epichlorohydrin in water-organic solvents media. The acetone soluble fraction of Kraft lignin (KLAF) was isolated by double solid-liquid extraction of 10

g of Kraft Lignin (KF) with 100 mL of acetone in a round flask at room temperature. Two different reaction media were used for KL glycidylation: epichlorohydrin (ECH) and ECH- dimethyl sulfoxide (DMSO). A significantly higher content of epoxy groups in acetone soluble fraction of lignin-based epoxy resin (GLAF) was determined in the products synthesized in the presence of DMSO. However, the yield of the acetone soluble fraction was about twice lower in comparison with that for the GLAF synthesized in ECH. The  $T_g$  of acetone soluble fractions of all glycidylated lignin (GL) samples under study was lower compared to the unmodified acetone soluble fraction of KL, testifying the modification of the lignin matrix by ECH. The lignin-containing cured epoxies demonstrated also a higher charcoal yield and a lower degradation rate at the high temperature impact compared to BPA-based epoxy resin Araldite® LY1564, cured by the amine hardener Aradur®3486, suggesting the lignin epoxies' potential for fabrication of flame resistant epoxides. A drastic increase in the viscosity of commercial epoxy resin due to the incorporation of lignin epoxies therein was observed, which restricted the extent of commercial epoxy resin substitution.

### 1.3.3. Epoxides derived from polysaccharides

Sugars are organic chemical compounds constituted by carbon atoms, hydrogen and oxygen, and are part of the family of carbohydrates or saccharides. From a chemical point of view, carbohydrates are aldehydes or ketones to which various hydroxyl groups have been added, usually one for each carbon atom that is not part of the aldehyde or ketone functional group.

## | Introduction and objectives

There are several classifications of saccharides. Typically, carbohydrates are distinguished in:

- simple carbohydrates: monosaccharides and oligosaccharides;
- complex carbohydrates: polysaccharides.

Monosaccharides and disaccharides are called sugars. Sugars are often used for the production of bio-based epoxy resins. Literature is rich of studies<sup>104</sup> on monomers derived from carbohydrates, such as sucrose, sorbitol, maltitol, and isosorbide, which lead to epoxy networks with interesting properties. Polysaccharides are made by monosaccharides bond together in long chains by glycosidic linkages, to form polymeric carbohydrate molecules. The most important polysaccharide, especially in bio-based materials production, is cellulose, composed by D-glucose units, that constitutes, together with hemicellulose and lignin, the structural component of vegetal cell.

Features that made of carbohydrates an important natural, easily renewable, source of building blocks for the synthesis of biodegradable polymers are the great availability (they may even come from agricultural wastes) as well as the very rich variety of chemical structures, with great stereochemical diversity, that they possess. Carbohydrate-based polycondensates have the great advantage of lower toxicity and higher susceptibility to biodegradation, compared to those coming from petrochemical feedstock; nevertheless they typically show also an increased hydrophilicity.

Epoxidized 1,4:3,6-dianhydrohexitols are the carbohydrate-based monomer most widely employed in the synthesis of epoxy resins thanks to their availability, especially regarding isosorbide, but they show a strong hydrophilicity. Other important categories of sugar-derived molecules are

furans, obtained by dehydration of pentose and hexose sugars, that exhibit great potential as platform chemicals in the biorefinery. Interest of furanic molecules is increasing in the last years leading to ever improved technology for production of furfural and hydroxymethylfurfural (HMF) from C<sub>5</sub> and C<sub>6</sub> sugars or polysaccharides, respectively. These platform molecules can undergo to further transformation resulting in a widespread variety of molecules with all kind of functionality.<sup>105</sup> Nowadays the greatest industrial interest is posed on oxidation of HMF into 2,5-furandicarboxylic acid (FDCA), named one of most promising platform molecules.<sup>10,11,106</sup> FDCA is used in production of the bio-derived polyethylene furanoate (PFA) with improved properties compared with its petrol-derived counterpart, i.e. polyethylene terephthalate (PET) and PEF<sup>106</sup> is already substituting PET in bottles production<sup>107</sup>.

Realization of isosorbide-based epoxy resins was proved by Feng et al. but at the same time the high hydrophilicity of this material was proved<sup>108</sup>. Generally this characteristic is not considered as a good property but Park et al. proved that this feature can be used in proper mode, proving the antifogging behaviour (depending on thickness of films and lasting only for few seconds) of this water-adsorbing kind of material.<sup>109</sup>

An interesting work on a fully isosorbide-based crosslinked material was proposed by Li et al.<sup>110</sup>. They were able to obtain not only the diglycidyl ether of isosorbide (ISE) via the epoxidation of diallyl isosorbide but also, by thiol-ene click reaction in aqueous conditions, an isosorbide diamine (ISA). If cured together this two molecules give a shape-memory fully bio-based epoxy resin (cured resin showed a constant  $R_f$  of about 97% during the three cycles; as for the  $R_r$ , the value was only 81% in the first cycle and it was increased to near 100% in the second and third cycle).

## | Introduction and objectives

Starting by D-glucose and Methyl- $\alpha$ -D-glucofuranoside (obtained by the condensation of D-glucose with methanol in the presence of cation-exchange resin as catalyst), Rapi et al.<sup>11</sup>, synthesized mixtures of tri- and tetra-functionalized epoxy component; in particular have been obtained mixtures of bi-, tri- and tetra-glucofuranoside- based epoxies and a trifunctional glucofuranoside-based epoxy. Synthetic routes set-up to obtain those multifunctional molecules involve specific group protection step, allylation of remained hydroxyl group and the consequent epoxidation; a one-step reaction starting by methyl-4,6-O-benzylidene- $\alpha$ -D-glucofuranoside and letting it to react with epichlorohydrin have been tried under different reaction conditions but the pure compound having two epoxy propyl groups has not been obtained. Moreover a solvent free reaction of protected methyl-D-glucofuranoside resulted in mixtures of mono- and disubstituted products. EEW is lower than BPA's except for the difunctionalized glucofuranoside. Curing enthalpy of reaction between glucofuranoside- and glucofuranoside-based epoxies with 4,4'-diaminodiphenyl methane (DDM) is independent from the molecular structure of the components but the degree of cure between the glucofuranoside-based epoxy components is only 60–80% (because these bioepoxies are solid and it is not possible to obtain a molecular level homogenization by mixing in the mortar; with glucofuranoside-based epoxy instead a curing degree of 90% is obtained. The glass transition temperatures ( $T_g$ ) of the different glucose-based resins are variable and the highest value was reached with the trifunctional glucofuranoside-based component. However this last one shows degradation at lower temperature and a slighter decomposition against the other systems but all of them show high char yield at 800°C. Also hardness of those materials has been analyzed and its values are similar to the DGEBA- based resins.

In 2014 Ma et al. proposed the trifunctional epoxy monomer of itaconic acid (TEIA) as valid substitute of DGEBA<sup>12</sup>. Itaconic acid (IA) is obtained by the fungal fermentation of carbohydrates and has been evaluated as one of the “Top Value Added Chemicals from Biomass” by the U.S. Department of Energy.<sup>10</sup> TEIA has been obtained from IA by allylation and consequent epoxidation and then cured with two different curing agents, poly(propylene glycol) bis(2-aminopropyl ether) (D230) and methyl hexahydrophthalic anhydride (MHHPA). The obtained resins exhibit lower dynamic viscosity than DGEBA-based resins obtained with both the same curing agents and gelation occurs at lower temperature, resulting for itaconic acid-based resins in a better processability and ability to cure at lower temperature or in shorter times compared to the DGEBA-based. DSC analyses of the curing reactions highlighted the presence of two different curing processes, the first at lower temperatures than the curing temperature for DGEBA, related to the ring-opening reaction of glycidyl epoxides, and the second at higher temperature, attributed to the curing reaction of pendant epoxide. This second process happens at temperature similar to the DGEBA-based systems if the curing agent is D230 and at higher temperature if is used MHHPA. It affects also the activation energy for cross-linking reactions: TEIA exhibit a general higher reactivity than DGEBA, but if considered only the  $E_a$  related with the pendant epoxide it's similar for D230 cured and higher for MHHPA cured bio-resins. Regarding thermal properties  $T_g$  varies changing curing agent, ranging from lower (using D230) to higher (using MHHPA)  $T_g$  than DGEBA, and degradation temperature are ever lower, but itaconic acid-based resins exhibit improved mechanical properties, in particular flexural strength, flexural modulus and strain at break.

Darroman et al.<sup>113</sup> used sucrose, isosorbide and sorbitol epoxy derivatives to improve the properties of materials derived from epoxidized cardanol, which is treated with different amines, and studied to potentially replace DGEBA. They prepared mixtures of cardanol diglycidyl ether with different weight percent (75%, 50%, 25%) using sorbitol ether and two commercially available isosorbide epoxy reagents (Denacol GR100 and Denacol GSR102). The cure process was carried out in presence of commercial amines at room temperature, without the use of solvents and the final products obtained were compared with DGEBA-based resins in terms of gel time, glass transition temperature, hardness. Bio-epoxy resins showed reduced gelation times compared to DGEBA-based ones, being the sorbitol the most reactive one. The reactivity of epoxy functionalized sorbitol is due to the presence of six epoxy groups instead of the two characterizing cardanol and isosorbide epoxies. Thermogravimetric analyzes showed that the thermal stability of DGEBA was greater than the other reagents ( $T$  at 30% weight loss = 365°C). However, a good substitute could be epoxidized isosorbide that exhibited a degradation temperature of 362°C. The glass transition temperature was analyzed in discussed taking into account the nature of curing agents and catalysts. DSC analysis demonstrated that the IPDA led to higher  $T_g$  compared to Jeffamine T403. The lowest  $T_g$  recorded was that of the material based on cardanol ( $T_g = 41^\circ\text{C}$  with IPDA and  $T_g = 23^\circ\text{C}$  with Jeffamine T403), while the  $T_g$  of Denacol GSR102 was closer to that of BPA (109°C isosorbide, 121°C BPA ). The same research group prepared epoxy resins based on a mixture of cardanol and sorbitol. Thermogravimetric analyzes showed that with increasing the amount of cardanol, regardless of the type of diamine used, the temperature of thermal degradation decreased. As far as the  $T_g$  is concerned, as the amount of sorbitol increased, the transition temperature increased even if it was not sufficient to replace the DGEBA in all applications. Then, cardanol



and Denacol GSR100 were mixed to get epoxy resins. TGA analysis indicated isosorbide had a detrimental effect on degradation temperature values. However, it had still the potential to replace DGEBA since the derived resins were thermally stable up to 300°C. Moreover, as the quantity of isosorbide increased,  $T_g$  increased, independently of the amine used. The best compromise was obtained cardanol/Denacol GSR100 ratio was 25/75. In both cases, as the sorbitol and isosorbide increased, there is an increase in the hardness of the material.

Nie et al. studied a new corn starch adhesive modified by starch-g-polyvinyl acetate (starch-g-PVAc) and epoxy resin<sup>114</sup>. First oxidized starch latex was prepared by oxidizing starch with sodium hypochlorite and subsequently reacted with epoxy chloropropane to crosslink. The second step was the preparation of starch-g-polyvinyl acetate latex by reacting oxidized starch latex, prepared before, lauryl sodium sulphate, Tween-80, ammonium persulfate (APS) water solution and vinyl acetate. To further improve the resin performances, starch adhesive modified by starch-g-PVAc and epoxy resin were also prepared. The dry shear strength increased with the amount of starch latex when the mass fraction was <30% and decreased markedly when the mass fraction was >30%. The wet shear strength decreased markedly compared with the dry shear strength, and both the dry and the wet shear strength increased with the mass fraction of epoxy resin (the wet shear strength increased more sharply). The water resistance of the new starch adhesive was highly improved. The optimal performance was achieved when the mass fraction of epoxy resin and starch-g-PVAc is 70%, with  $m(\text{Ep}) : m(\text{starch-g-PVAc}) \frac{1}{4} 1:2$ . At this time, the solid content is 48%, and the viscosity is 0.875 Pa·s.

Chrysantos et al.<sup>104</sup> synthesized two isosorbide epoxy prepolymers, using two different synthesis paths: the classical route that involved the direct reaction

## | Introduction and objectives

with epichlorohydrin (DGEDASo), and the epoxidation method developed by Sachinvala et al. (DGEDASn)<sup>115</sup>. This latter method involved the allylation of the isosorbide with allyl bromide. After preparing the allyl, a peracid was added to the solution to obtain the isosorbide diglycidyl ether (DGEDASo). Amines in varying amounts were used as hardening agents. Both the prepolymers and the amines were liquid at room temperature, and could be mixed vigorously to obtain a homogeneous cured material. Three types of compounds are used for the studies: DGEBA (as a reference), DGEDASo and DGEDASn. Size Exclusion Chromatography (SEC) analyses showed that there was a difference on the distribution of the molar mass: in the DGEDASn there is a 30% pure monomer (DGEDASo), and the remaining part of various oligomers. The gel time of the three different reactive systems was determined by rheological measurements. It showed that the DGEDASn system reacted with Isophoron diamine (IPD) with shorter gel time than the traditional DGEBA/IPD, while the DGEDASo/IPD system had almost the same gel time as DGEBA/IPD. The  $T_g$  of the bio-based systems were lower than DGEBA-based one, but the elastic modulus were higher, due to the low molar mass and high functionalization. Isosorbide-based polymeric precursors were thus excellent candidates for BPA replacement except for the disadvantage of requiring a storage in dry environments to avoid damages caused by water.

Cho et al.<sup>116</sup> used carbohydrate biomass to form furan-based compounds with epoxy terminations with a yield of over 70%. The kinetics of the cationic photo-cure of synthetic compounds was studied in terms of total heat flow calculated through photo-DSC analysis. It was shown that the values of the first half time ( $t_{1/2}$ ), which corresponds to the cure rate, varied from 0.54 to 1.15 minutes when irradiated with UV 40 mW/cm<sup>2</sup>. The studies also showed that in

presence of furan rings there was an increase in tensile strength of almost double (4.7 MPa) compared to the functionalization of polycarbonate with phenyl glycidyl ether based on petrochemicals with formation of phenyl rings (2.6 MPa). The bis-epoxy-furan compound, followed a synthesis path very similar to the one for the mono-furan-diepoxy, but it showed a lower resistance due to its hydrophobic and stiffness properties.

Ma et al. synthesized a bio-based epoxy resin trifunctional epoxy resins from itaconic acid (TEIA) with high epoxy value (1.16) and low viscosity (0.92 Pas, 25 °C), using itaconic acid<sup>112</sup>. The trifunctionalized epoxy resin was synthesized in two steps: allylation of itaconic acid, through dehydrobromuration between itaconic acid and allyl bromide, generating AIA (allylated itaconic acid) and epoxidation of the AIA. By comparing the viscosity of the TEIA with that of the DGEBA it was clearly visible that in the first case a much lower viscosity could be measured, and this affected the final thermal and mechanical properties. The lower viscosity was responsible for a minor gelation time, which could therefore allow faster treatment and better processability. The curing agents used were D230 (polypropylene glycol bis 2-aminopropyl ether) and hexahydrophthalic methyl anhydride (MHHPA). DSC analysis showed that while for DGEBA there was a single exothermic peak generated by the opening of the epoxy ring, regardless of the used agent, in the case of TEIA there were two peaks. The lower peak corresponded to the opening of the ring, while the higher peak corresponded to the cure of the hanging epoxides with D230 and MHHPA indicating a greater reactivity. DGEBA and TEIA exhibited a similar reactivity to D230, while with MHHPA TEIA had a lower reactivity. These results were confirmed by the calculation of the activation energy. The  $T_g$  of TEIA/D230 was lower than that of the DGEBA/D230, otherwise for TEIA/MHHPA that shows a

higher  $T_g$ . The reasons may be that in the fact that TEIA has a higher epoxy index, the amount of required healing agents must be greater than the DGEBA. TGA analysis showed that thermal degradation occurs first for TEIA/D230 and TEIA/MHHPA systems rather than for systems with DGEBA. Finally, regards mechanical properties, studying the stress-strain curve it was observed that, while the DGEBA systems exhibit a typical fragile fracture behavior, TEIA systems show a ductile behavior curve. Bending modules, bending strength, breaking stress, breaking strain of TEIA systems are greater or similar to those of DGEBA systems.

Pan et al. used novel highly functional bio-based epoxy compounds, epoxidized sucrose esters of fatty acids (ESEFAs), cross-linked with a liquid cycloaliphatic anhydride to prepare polyester thermosets<sup>6</sup>. ESEFAs were epoxidized by peracetic acid generated in situ from hydrogen peroxide and acetic acid in presence of a catalyst based on an acidic ion-exchange. In particular, four different ESEFAs were employed: epoxidized sucrose linseedate (ESL), epoxidized sucrose safflowerate (ESSF), epoxidized sucrose soyate (ESS), and epoxidized sucrose soyate B6 (ESSB6). Epoxidized soybean oil (ESO) is used for comparison. The tensile properties of the ESEFA materials were significantly different than that of the ESO thermoset, with the ESEFA materials having a significantly higher modulus and tensile strength. The ESL thermoset was a brittle material; ESSF and ESSB6 thermosets were more flexible than the ESL thermoset because each of them showed a well-defined yield point after the linear elastic portion and failed in plastic deformation. The ESS thermoset was more plastic and had a lower modulus than both ESSB6 and ESSF thermosets. The ESO thermoset exhibits rubbery behavior with the lowest modulus and tensile strength, and an extremely high elongation at break. For the fully

substituted ESEFAs, the glass-transition temperatures were in a range from 48 to almost 104°C ( $T_g(\text{ESL}) > T_g(\text{ESSF}) > T_g(\text{ESS})$ ). For the fully substituted ESEFAs, the epoxide equivalent weight (EEW) values were in the order  $\text{EEW}(\text{ESL}) < \text{EEW}(\text{ESSF}) < \text{EEW}(\text{ESS})$ , and thus the concentrations of epoxides are  $[\text{e}](\text{ESL}) > [\text{e}](\text{ESSF}) > [\text{e}](\text{ESS})$ . The storage moduli are  $E'(\text{ESL}) > E'(\text{ESSF}) > E'(\text{ESS})$ . Whereas ESSB6 had the lowest epoxide content, it showed a higher  $T_g$  and storage modulus than the ESSF and ESS thermosets. Epoxidized sucrose esters showed much better performance than ESO in epoxy/anhydride curing. The thermosets using epoxidized sucrose esters are hard and ductile with high modulus and exhibit excellent coating performance. However, thermosets using ESO were highly flexible and rubbery with low modulus and exhibited poor coating performance. The compact structure of ESEFAs contributed to the hardness of the thermoset. The high epoxide functionality leads to a rapid gelation and cross-linking upon curing.

Yu et al.<sup>117</sup>. synthesized bio-based thermosets from dimethacrylated epoxidized sucrose soyate (DMESS). The synthesis of DMESS was achieved via ring-opening reaction of epoxidized sucrose soyate (ESS) with methacrylic acid followed by methacrylic anhydride addition. For the curing process formulations of DMESS alone and with 10, 20, and 30 percent by weight styrene as the reactive diluent were prepared. The thermoset was compared with methacrylated epoxidized sucrose soyate MESS studied by Yan and Webster<sup>118</sup>. Compared with MESS, DMESS had lower viscosity, which made it more processible. DMESS required a much lower amount of styrene to achieve a similar formulation viscosity than that of MESS, enabling the reduction of styrene content. The crosslink densities of the resulting thermosets were much higher than the thermosets based from MESS and, consequently, higher  $T_g$ s. Tensile strength

## | Introduction and objectives

and Young's moduli showed direct proportionality with the degree of methacrylation.

Esmaeli et al.<sup>119</sup> synthesized a bio-resourced thermosetting epoxy foam through a two-step strategy involving the glycidylation of tannic acid (TA) to get the epoxidized product (ETA) and the successive simultaneously curing and foaming process to achieve the foamy product with a high yield (~98%). The thermal stability of ETA foam was high enough to be considered for using in building industry. Moreover, the bio-based ETA foam was thermally stable until 245 °C, and thus potentially suitable for building industries.

Qi et al.<sup>120</sup> used epoxidized soybean oil (ESO) cured with tannic acid (TA) for fully bio-based epoxy resin. TA was formulated with ESO at different mass ratios of TA/ESO (20%, 23%, 26% and 29%) via a solvent blending method to achieve homogeneous mixtures. It was found that the relaxation temperature ( $T_{\alpha}$ ) and storage modulus values at 25 °C of the cured thermosets increased with increasing TA content up to a threshold value after which, they decreased. A similar trend was observed for  $T_g$  values of the thermosets cured with different TA contents that firstly increased to a maximum (63 °C for H1/TA26), then decreased due to the lower crosslinking density. Thermal stabilities of the cured samples under nitrogen were investigated via thermogravimetric analysis (TGA). The degradation temperatures at 5 wt% weight loss were around 300 °C.  $T_{5\%}$  of the thermosets generally decreased with increasing TA content. The thermal stability at high temperatures was enhanced by introducing the TA component. Moreover, the high tensile strength lap-shear strength were measured.

Shibata et al. prepared new bio-based epoxy resin systems, the glycerol polyglycidyl ether (GPE) and the sorbitol polyglycidyl ether (SPE) with tannic acid (TA) at various conditions<sup>121</sup>. DMA and TMA results for GPE/TA with

epoxy/hydroxyl ratio 1.0/0.6–1.0/1.4 cured at 160 °C for 3 h, showed that both peak temperature and  $T_g$  increased with increasing amount of TA. A similar trend was observed for the SPE/TA cured at 160 °C for 2 h. The SPE/TA cured materials showed higher  $T_g$  than the corresponding GPE/TA cured materials due to the higher functionality of SPE. Composites based on GPE-TA1.0 with microfibrillated cellulose (MFC) and SPE-TA1.0 with MFC were also prepared. The tensile strength at 25 °C for GPE-TA/MFC10 was 76% higher than that of GPE-TA1.0, while the tensile modulus was only slightly improved. The tensile strength and modulus of SPE-TA1.0/MFC10 were 30 and 55% higher than those of SPE-TA1.0, respectively.

#### 1.3.4. Bio-based curing agents

Since the weight ratio of curing agents can go up as high as 50 wt% in the epoxy formulations, they can determine the ultimate properties of the cured resin in large extent. An overview of the main bio-based curing agents is therefore introduced.

Warth et al.<sup>122</sup> synthesized maleated soybean oil (MSO) and maleated linseed oil (MLO) through the reaction of maleic anhydride (MA) with a double bond of the triglyceride section, the reaction known as maleinization is a common method to introduce an anhydride group into a triglyceride, generating flexible anhydride curing agents.

B.P.Patel et al.<sup>123</sup> synthesized three different types of amino functionalized castor oil (ACO) making reacting the brominated castor oil (BCO) with excess of ethylene diamine, 1,3-propane diamine and 1,6-hexane diamine; castor oil, is derived from beans of the castor plant (*Recinus communis*), it mainly contains ricinoleic acid, which has unique characteristic due its 18-carbon

backbone with one hydroxyl group on the 12th carbon atoms and a cis double bond between the 9th and 10th carbon atoms.

Yang X. et al.<sup>124</sup> cured a commercial epoxy resin (E-51) with a Diels-Alder adduct of myrcene and maleic anhydride (MMY), with a castor oil modified adduct of myrcene and maleic anhydride (CMMY), and mixed composition of those in order to evaluate the effect of castor oil on the mechanical properties, result shows that the elongation at break is increased and the tensile strength and glass transition temperature are decreased with increasing weight ratio of CMMY, while the impact strength is increased gradually.

Rosin based curing agents due to their large hydrogenated phenanthrene ring structure are similar in rigidity to petroleum-based cycloaliphatic or aromatic compounds. In fact the hydrogenated phenanthrene ring led to higher  $T_g$  and modulus but slightly lower thermal stability. Rosin, obtained directly from pine and conifer exudates or as a by-product from the pulping process is a complex mixture of naturally occurring high molecular weight organic acids (~90%, generally named rosin acids) and related neutral materials (~10%), rosin acids are mainly composed of isomeric abietic-type acids and pimaric-type acids. Maleopimaric acid (MPA), obtained via Diels-Alder reaction between levopimaric acid and maleic anhydride (MA), is probably one of the most important and abundantly available rosin derivatives. MPA itself can be used as curing agent or easily modified with acids and amines to form new types of curing agents. Zhang et al.<sup>125</sup> have synthesized several epoxy curing agents derived from rosin, namely, MPA, methyl maleopimarate (MMP), rosin maleic anhydride imidodicarboxylic acid (RMID), di-RMID (D-RMID), and MPA-terminated polycaprolactones (MPA-PCL). Maleopimaric acid (MPA) and methyl maleopimarate (MMP) resemble 1,2,4-benzenetricarboxylic anhydride (BTCA)



and 1,2-cyclohexanedicarboxylic anhydride (CHDB) in structure and functionality, which are both important (petroleum-based) epoxy curing agents in encapsulation packaging of electronic products.

## 1.4. Coatings

---

Coatings are layers deposited in substrates with functional or decorative purpose.

The application of organic coating on metallic substrates is a well consolidate technique that meets both protective and decorative needs. Decorative function responds to the needs of imprint logos and information on branded products and is demanded to coatings applied generally on external surfaces of containers. The inner side of those containers must, instead, possess protective properties ensuring protection of metal substrate from chemical attack by products contained, and vice versa, for the long storage periods. In any case also the coatings of external surfaces must own protective properties to guarantee resistance to environmental conditions<sup>20</sup>.

Basic coating systems consist generally of two layers for the inner covering and up to six layers when applied for decorative purpose (e.g. in automotive industries)<sup>126</sup>.

Coating formulation are generally solutions or dispersions of resinous materials made liquid by addition of appropriate solvents. Coating process needs

## | Introduction and objectives

so a step following the application of the resinous layer, in which it is dried by solvent removal, oxidation and/or polymerization. When further coating layers are needed, each coat will be dried/heated before the application of the subsequent (except in cases in which the application “wet on wet” is specifically required)<sup>20</sup>.

For the specific application in food can coating, precise properties are required: resistance to scratching, steam processes and fabrication conditions (e.g. welding). Moreover, they have to guarantee that no substance is extracted, above all toxic-ones, during cans lifecycle and does not have to affect flavor of products in them contained<sup>20</sup>. Canning food and beverages has the function of protect and preserve them taste and nutritional values for months to year<sup>127</sup>.

To can coatings are requested a variety of different technical and legal requirements<sup>127</sup>:

- ideally, they should be flexible enough to avoid defections during fabrication, which would result in acid attack on exposed metal,
- be universally applicable to all different food types,
- resist a wide temperature and pressure range deriving by food processing,
- do not transfer constituents to food in quantities that can affect human health
- do not peel off during can production, shelf-life and after non- intentional deformation of the cans
- resist to the chemistry of aggressive food types (e.g. acidic foods) and protect the metal of the can from corrosion
- preserve the flavor and appearance of food and maintain its organoleptic properties
- be stable over several years

Basic methods used for the application coating on metallic surfaces are roller coating and spraying<sup>20</sup>. The majority of food and beverage cans, coatings are applied to both sides of planar metal sheets or coils by roller coating before the cans are formed. Spray coating are mainly applied in the inner side of cans<sup>127</sup>. Resins are generally applied as suspensions in organic or aqueous solvents, dried by solvent removal, oxidation or heat polymerization, which is usually achieved by heating and/or UV radiation. In some cases powder coatings are applied under the direction of an electrostatic field and cured by heat<sup>127</sup>.

Coating composition depends also by food that will be contained in those. When acid colored food are wrapped more attention is posed on chemical resistance of coating that must protect the metallic substrate from reaction with food pigments (inducing both substrate corrosion and food color changes), more than resist to high mechanical and thermal treatments. Vegetables, instead, are generally made of sulphur-containing proteins that can migrate from food during hot packaging: sulphur reacts with substrate generating tin sulphide or iron sulphide layer, not toxic but affecting the appearance of the container. Opposite are operating conditions of meat-containers: strong sterilization processes are required so that coating must possess great thermal resistance<sup>20</sup>. In specific cases tin cans can be also produced without an internal organic layer; it is the case of tin cans containing light colored, acidic juices and fruits. Tin is more easily oxidized than the food, thus preventing darkening and flavor changes caused by oxidation of the food<sup>127</sup>.

Early coatings were made oleoresins, basically blends of natural resins and gums with drying oils. Their use largely stopped with the invention of epoxy coatings but oleoresins were rediscovered as BPA-free alternatives even if their

## | Introduction and objectives

properties are not competitive. In fact, they do not adhere well to metallic substrates and even if they can be easily applied, need long curing time, do not guarantee a good protection to metal corrosion and can change organoleptic properties of food<sup>127</sup>.

Over years, new coating materials have been developed, with improved properties (but not ever suitable for food cans lining applications), differing for their main chemical composition, production processes, costs and properties.

Epoxy-based resins are the most commonly used class of coatings for aluminum and steel cans and 55% of epoxy resins production is intended for coating application. They protect the metal from corrosion, withstand a wide range of foods, resist to heat and acidic conditions, have good flexibility and adhesion properties.<sup>127</sup> Epoxy resins are usually more expensive than competing resins but show improved properties both in processing and as final cured resin. Processing epoxy resins is convenient since it is possible to formulate compositions with the required rheological properties (such as low viscosity), that can be cured at room temperature as well as at elevated temperature, thanks to the wide range of possible hardeners. Moreover, no volatiles are produced during cure and resins show a low shrinkage<sup>128</sup>

Vinyl coating, made by vinyl chloride and vinyl acetate, are really flexible but do not adhere on metals and are commonly utilized as “top coat” that is a second coating layer. Generally mixed with oleoresins, need the addition of stabilizers and plasticizers. They can endure to acidic environments but not to high temperatures

Alkyds are widely used for decorative applications thanks to low price and the easy modification for specific purposes; however they cannot be used in

contact with food possessing themselves a taste that can interfere with food taste.<sup>20</sup>

Phenolic and acrylic resins are really good in corrosion protection but possess very low adhesion properties, low flexibility and in contact with food can adulterate their organoleptic properties. Polyesters resins, obtained by condensation of polyacids with polyalcohol or epoxides, have, instead, good adhesion properties but do not resist to acidic conditions and have low resistance to corrosion.

Organic coating composition may be a complex formulation of a variety of components, each of them having a specific function. Generally each formulation is composed by three components, with a specific function, that are binders, particles and pigments. Binders are basically the resinous material, have the task of stick pigments and impart the chemical and physical properties of the coating. Additives modify the properties of coating in fluid states while pigments contribute to the color of the resin and can accomplish to further functions.<sup>126</sup>

## 1.5. Objectives

---

In the light of the above, the general aim of this Ph.D. project was the development of new bio-based epoxy resins coatings for food containers applications, starting from the obtainment of epoxy monomer from bio-based precursors.

Precursors were chosen from carbohydrate derivatives, in particular 2,5-furandicarboxylic acid (FDCA) and 2,5-bis(hydroxymethyl)furan (BHMF), as

replacement of BPA. These molecules were selected because possess a rigid aromatic moiety (i.e. furan); in fact keeping the aromaticity is a necessary condition to achieve comparable mechanical properties. Aromatic compounds are widely used in organic materials for their stability, their toughness, and above all their ability to structure the matter by  $\pi$ -stacking, thus allowing to confer good thermal and mechanical properties to the epoxy thermosets. Moreover, FDCA is widely used in production of polyesters with great properties<sup>129-132</sup> but very few work are produced about its application in epoxy resins production<sup>133,134</sup>.

The project was developed to study the complete life cycle (production and application) of the proposed epoxy resins proceeding with the following step:

- Development and optimization of synthetic procedure for the obtainment of furan-based epoxides from BHMF and FDCA.
- Optimization of formulation for the production of epoxy thermosets employing the furanic diglycidyl ester and furanic diglycidyl ester previously synthesized.
- Kinetic study of crosslinking reaction that lead to the obtainment of furan-based epoxy thermosets, also in function of reacting mixture composition.
- Evaluation of thermal and mechanical properties of furan-based epoxy resins.
- Obtainment of bio-based epoxy nanocomposites and application of these resins as coating for metallic substrates.
- Test of physical properties and chemical resistance of coating

The experimental work presented is structured in three chapter; in Chapter 2 new synthetic procedures for the obtainment of a diglycidyl ester of

furan starting from FDCA and the synthesis of diglycidyl ether of furan will be presented. The latter epoxy monomer was utilized for production of bio-based epoxy resins. Curing process was studied in the work presented in Chapter 3, by a thermodynamic and chemo-rheologic point of view as effect of different formulation composition. Also mechanical and thermal properties were tested. In Chapter 4 the application of the obtained bio-based epoxy resins as lining for metallic cans is presented. The effect of addition of fillers was monitored and, in addition to chemo-rheological analysis, characteristic properties of coatings were tested.

## 1.6. Bibliography

---

1. No Title. <https://www.statista.com/statistics/282732/global-production-of-plastics-since-1950/>.
2. Eurostat. *Sustainable Development in the European Union 2015.*; 2015.
3. Narayan R. Preparation of bio-based polymers for materials applications. *Appl Biochem Biotechnol.* 1988;17(1-3):7-22. doi:10.1007/BF02779142
4. Mohanty AK, Misra M, Drzal LT. Sustainable Bio-Composites from renewable resources: Opportunities and challenges in the green materials world. *J Polym Environ.* 2002;10(1-2):19-26. doi:10.1023/A:1021013921916
5. Scopus. Research keywords: "bio-based polymers". [www.scopus.com](http://www.scopus.com).
6. Pan X, Sengupta P, Webster DC. High biobased content epoxy-anhydride thermosets from epoxidized sucrose esters of fatty acids. *Biomacromolecules.* 2011;12(6):2416-2428. doi:10.1021/bm200549c
7. Witt U, Yamamoto M, Seeliger U, Müller R-J, Warzelhan V. Biodegradable Polymeric Materials-Not the Origin but the Chemical Structure Determines Biodegradability. *Angew Chemie Int Ed.* 1999;30(10):1438-1442. doi:10.1002/(SICI)1521-3773(19990517)38:10<1438::AID-ANIE1438>3.0.CO;2-U
8. ASTM-D6866 -18, Standard Test Methods for Determining the Biobased Content of Solid, Liquid, and Gaseous Samples Using Radiocarbon Analysis, ASTM International, West Conshohocken, PA, 2018, [www.astm.org](http://www.astm.org).



9. Society of the Plastics Industry Bioplastics Council. *Understanding Biobased Carbon Content.*; 2012.
10. Werpy T, Petersen G. Top Value Added Chemicals from Biomass. *US Dep energy.* 2004;1:76. doi:10.2172/926125
11. Bozell JJ, Petersen GR. Technology development for the production of biobased products from biorefinery carbohydrates—the US Department of Energy’s “Top 10” revisited. *Green Chem.* 2010;12(4):539-554. doi:10.1039/b922014c
12. Pawar P a, Purwar AH. Biodergradable Polymers in Food Packaging. *Am J Eng Res.* 2013;(05):151-164.
13. Carré C, Zoccheddu H, Delalande S, Pichon P, Avérous L. Synthesis and characterization of advanced biobased thermoplastic nonisocyanate polyurethanes, with controlled aromatic-aliphatic architectures. *Eur Polym J.* 2016. doi:10.1016/j.eurpolymj.2016.05.030
14. Poussard L, Mariage J, Grignard B, et al. Non-Isocyanate Polyurethanes from Carbonated Soybean Oil Using Monomeric or Oligomeric Diamines To Achieve Thermosets or Thermoplastics. *Macromolecules.* 2016;49(6):2162-2171. doi:10.1021/acs.macromol.5b02467
15. Cheng C, Zhang X, Huang Q, et al. Preparation of Fully Bio-Based UV-Cured Non-Isocyanate Polyurethanes From Ricinoleic Acid. *J Macromol Sci Part A.* 2015;52(6):485-491. doi:10.1080/10601325.2015.1029374
16. Rokicki G, Parzuchowski PG, Mazurek M. Non-isocyanate polyurethanes: Synthesis, properties, and applications. *Polym Adv Technol.* 2015;26(7):707-761. doi:10.1002/pat.3522

## | Introduction and objectives

17. Nohra B, Candy L, Blanco JF, Guerin C, Raoul Y, Mouloungui Z. From petrochemical polyurethanes to biobased polyhydroxyurethanes. *Macromolecules*. 2013;46(10):3771-3792. doi:10.1021/ma400197c
18. Foyer G, Chanfi BH, Boutevin B, Caillol S, David G. New method for the synthesis of formaldehyde-free phenolic resins from lignin-based aldehyde precursors. *Eur Polym J*. 2016;74:296-309. doi:10.1016/j.eurpolymj.2015.11.036
19. Foyer G, Chanfi B-H, Virieux D, David G, Caillol S. Aromatic dialdehyde precursors from lignin derivatives for the synthesis of formaldehyde-free and high char yield phenolic resins. *Eur Polym J*. 2016;77:65-74. doi:10.1016/j.eurpolymj.2016.02.018
20. MORGAN E. Protective and Decorative Coating Systems. *Tinpl Mod Canmak Technol*. 1985:194-223. doi:10.1016/B978-0-08-028680-8.50013-8
21. Sørensen PA, Kiil S, Dam-Johansen K, Weinell CE. Anticorrosive coatings: a review. *J Coat Technol Res*. 2009;6(2):135-176. doi:10.1007/s11998-008-9144-2
22. Jacob GC, Hoevel B, Pham HQ, et al. TECHNICAL ADVANCES IN EPOXY TECHNOLOGY FOR WIND TURBINE BLADE COMPOSITE FABRICATION.
23. Wright CD, Muggie JM. Epoxy Structural Adhesives. In: *Structural Adhesives*. Boston, MA: Springer US; 1986:113-179. doi:10.1007/978-1-4684-7781-8\_4
24. Kinloch AJ. *Adhesion and Adhesives*. Springer-S.; 1987. doi:10.1179/sic.1984.29.Supplement-1.5
25. Auvergne R, Caillol S, David G, Boutevin B, Pascault JP. Biobased

- thermosetting epoxy: Present and future. *Chem Rev.* 2014;114(2):1082-1115. doi:10.1021/cr3001274
26. Lee H, Neville K. *Handbook of Epoxy Resins*. Mc-Crow-Hill Book; 1982.
  27. Ellis B. Introduction to the chemistry, synthesis, manufacture and characterization of epoxy resins. *Chem Technol Epoxy Resins*. 1993:1-36. doi:10.1007/978-94-011-2932-9\_1
  28. Bell BM, Briggs JR, Campbell RM, et al. Glycerin as a renewable feedstock for epichlorohydrin production. The GTE process. *Clean - Soil, Air, Water*. 2008;36(8):657-661. doi:10.1002/clen.200800067
  29. Solvay. Epicerol. <https://www.solvay.us/en/markets-and-products/featured-products/epicerol.html>.
  30. Asutaka Ishii Y, Yamawaki K, Ura T, Yamada H, Yoshida T, Ogawa M. Hydrogen Peroxide Oxidation Catalyzed by Heteropoly Acids Combined with Cetylpyridinium Chloride: Epoxidation of Olefins and Allylic Alcohols, Ketonization of Alcohols and Diols, and Oxidative Cleavage of 1,2-Diols and Olefins. *J Org Chem*. 1988;53:3581-3593.
  31. Goud V V., Patwardhan A V., Pradhan NC. Studies on the epoxidation of mahua oil (*Madhumica indica*) by hydrogen peroxide. *Bioresour Technol*. 2006. doi:10.1016/j.biortech.2005.07.004
  32. Coud V V., Pradhan NC, Patwardhan A V. Epoxidation of karanja (*Pongamia glabra*) oil by H<sub>2</sub>O<sub>2</sub>. *JAACS, J Am Oil Chem Soc*. 2006. doi:10.1007/s11746-006-1250-7
  33. Dinda S, Patwardhan A V., Goud V V., Pradhan NC. Epoxidation of cottonseed oil by aqueous hydrogen peroxide catalysed by liquid

- inorganic acids. *Bioresour Technol.* 2008.  
doi:10.1016/j.biortech.2007.07.015
34. François C, Pourchet S, Boni G, et al. Diglycidylether of iso-eugenol: a suitable lignin-derived synthon for epoxy thermoset applications. *RSC Adv.* 2016;6(73):68732-68738. doi:10.1039/C6RA15200G
35. Hilker I, Bothe D, Prüss J, Warnecke HJ. Chemo-enzymatic epoxidation of unsaturated plant oils. *Chem Eng Sci.* 2001;56(2):427-432. doi:10.1016/S0009-2509(00)00245-1
36. Orellana-Coca C, Törnvall U, Adlercreutz D, Mattiasson B, Hatti-Kaul R. Chemo-enzymatic epoxidation of oleic acid and methyl oleate in solvent-free medium. *Biocatal Biotransformation.* 2005;23(6):431-437. doi:10.1080/10242420500389488
37. Törnvall U, Orellana-Coca C, Hatti-Kaul R, Adlercreutz D. Stability of immobilized *Candida antarctica* lipase B during chemo-enzymatic epoxidation of fatty acids. *Enzyme Microb Technol.* 2007;40(3):447-451. doi:10.1016/j.enzmictec.2006.07.019
38. Miao S, Zhang S, Su Z, Wang P. Chemoenzymatic Synthesis of Oleic Acid-Based Polyesters for Use as Highly Stable Biomaterials. *J Polym Sci Part A Polym Chem.* 2008;46:4243-4248. doi:10.1002/pola
39. Aouf C, Lecomte J, Villeneuve P, Dubreucq E, Fulcrand H. Chemo-enzymatic functionalization of gallic and vanillic acids: synthesis of bio-based epoxy resins prepolymers. *Green Chem.* 2012;14(8):2328. doi:10.1039/c2gc35558b
40. Pion F, Reano AF, Ducrot P-H, Allais F. Chemo-enzymatic preparation of

- new bio-based bis- and trisphenols: new versatile building blocks for polymer chemistry. *RSC Adv.* 2013;3(23):8988. doi:10.1039/c3ra41247d
41. Zanette AF, Zampakidi I, Sotiroudis GT, et al. Chemo-enzymatic epoxidation catalyzed by *C. antarctica* lipase immobilized in microemulsion-based organogels. *J Mol Catal B Enzym.* 2014;107:89-94. doi:10.1016/j.molcatb.2014.05.013
  42. Milchert E, Malarczyk K, Kłos M. Technological Aspects of Chemoenzymatic Epoxidation of Fatty Acids, Fatty Acid Esters and Vegetable Oils: A Review. *Molecules.* 2015;20(12):21481-21493. doi:10.3390/molecules201219778
  43. Cecchini MM, De Angelis F, Iacobucci C, Reale S, Crucianelli M. Mild catalytic oxidations of unsaturated fatty acid methyl esters (FAMES) by oxovanadium complexes. *Appl Catal A Gen.* 2016;517:120-128. doi:10.1016/j.apcata.2016.01.045
  44. Llevot A, Grau E, Carlotti S, Grelier S, Cramail H. Selective laccase-catalyzed dimerization of phenolic compounds derived from lignin: Towards original symmetrical bio-based (bis) aromatic monomers. *J Mol Catal B Enzym.* 2016;125:34-41. doi:10.1016/j.molcatb.2015.12.006
  45. Warwel S, Klaas MR. Chemo-enzymatic epoxidation of unsaturated carboxylic acids. *J Mol Catal B Enzym.* 1995;1(1):29-35. doi:10.1016/1381-1177(95)00004-6
  46. Pascault JP, Williams RJJ. General Concepts about Epoxy Polymers. *Epoxy Polym New Mater Innov.* 2010:1-12. doi:10.1002/9783527628704.ch1
  47. Bisphenol-A - A Global Market Overview - Research and Markets.

[https://www.researchandmarkets.com/research/4xx8j9/bisphenola\\_a](https://www.researchandmarkets.com/research/4xx8j9/bisphenola_a).  
Accessed October 14, 2018.

48. Vandenberg LN, Ehrlich S, Belcher SM, et al. Low dose effects of bisphenol A. *Endocr Disruptors*. 2013;1(1):e26490. doi:10.4161/endo.26490
49. Vandenberg LN, Hauser R, Marcus M, Olea N, Welshons W V. Human exposure to bisphenol A (BPA). *Reprod Toxicol*. 2007;24(2):139-177. doi:10.1016/j.reprotox.2007.07.010
50. Okada H, Tokunaga T, Liu X, Takayanagi S, Matsushima A, Shimohigashi Y. Direct Evidence Revealing Structural Elements Essential for the High Binding Ability of Bisphenol A to Human Estrogen-Related Receptor- $\gamma$ . *Environ Health Perspect*. 2008;116(1):32-38. doi:10.1289/ehp.10587
51. REGULATIONS COMMISSION IMPLEMENTING REGULATION (EU) No 321/2011 of 1 April 2011 amending Regulation (EU) No 10/2011 as regards the restriction of use of Bisphenol A in plastic infant feeding bottles. 2011.
52. COUNCIL DIRECTIVE 94/33/EC of 22 June 1994 on the protection of young people at work. 1994.
53. DIRECTIVE 2009/48/EC OF THE EUROPEAN PARLIAMENT AND OF THE COUNCIL of 18 June 2009 on the safety of toys (Text with EEA relevance). 2009.
54. COMMISSION DIRECTIVE 2014/81/EU of 23 June 2014 amending Appendix C of Annex II to Directive 2009/48/EC of the European Parliament and of the Council on the safety of toys, as regards bisphenol A (Text with EEA relevance).
55. COMMISSION REGULATION (EU) No 10/2011 of 14 January 2011 on plastic

- materials and articles intended to come into contact with food (Text with EEA relevance). 2011.
56. REGULATION (EC) No 1223/2009 OF THE EUROPEAN PARLIAMENT AND OF THE COUNCIL of 30 November 2009 on cosmetic products (recast) (Text with EEA relevance). 2009.
  57. REGULATION (EC) No 1980/2000 OF THE EUROPEAN PARLIAMENT AND OF THE COUNCIL of 17 July 2000 on a revised Community eco-label award scheme. 2000.
  58. COMMISSION DIRECTIVE 2009/161/EU of 17 December 2009 establishing a third list of indicative occupational exposure limit values in implementation of Council Directive 98/24/EC and amending Commission Directive 2000/39/EC (Text with EEA relevance). 2009.
  59. LOI n° 2010-729 du 30 juin 2010 tendant à suspendre la commercialisation de tout conditionnement comportant du bisphénol A et destiné à recevoir des produits alimentaires | Legifrance. <https://www.legifrance.gouv.fr/affichTexte.do?cidTexte=LEGITEXT000026832122&dateTexte=20181008>. Accessed October 14, 2018.
  60. Registry of SVHC intentions - ECHA. <https://echa.europa.eu/registry-of-svhc-intentions>.
  61. Chen Y, Yang L, Wu J, et al. Thermal and mechanical properties of epoxy resin toughened with epoxidized soybean oil. *J Therm Anal Calorim*. 2013;113(2):939-945. doi:10.1007/s10973-012-2859-4
  62. Roudsari GM, Mohanty AK, Misra M. Study of the Curing Kinetics of Biobased Epoxy Resin in the Presence of a Biobased Hardener. *ACS Sustain*

- Eng. 2014;(Epon 828):2111-2118. doi:10.1021/sc500176z
63. Sienkiewicz AM, Czub P. The unique activity of catalyst in the epoxidation of soybean oil and following reaction of epoxidized product with bisphenol A. *Ind Crops Prod.* 2016;83:755-773. doi:10.1016/j.indcrop.2015.11.071
64. Kumar S, Samal SK, Mohanty S, Nayak SK. Epoxidized Soybean Oil-Based Epoxy Blend Cured with Anhydride- Based Cross-Linker: Thermal and Mechanical Characterization. *Ind Eng Chem Res.* 2017;56:687-698. doi:10.1021/acs.iecr.6b03879
65. Miyagawa H, Misra M, Drzal LT, Mohanty AK. Fracture toughness and impact strength of anhydride-cured biobased epoxy. *Polym Eng Sci.* 2005;45(4):487-495. doi:10.1002/pen.20290
66. Jin F-L, Park S-J. Thermomechanical behavior of epoxy resins modified with epoxidized vegetable oils. *Polym Int.* 2008;57:577-583. doi:10.1002/pi
67. Park S-J, Jin F-L, Lee J-R. Effect of Biodegradable Epoxidized Castor Oil on Physicochemical and Mechanical Properties of Epoxy Resins. *Macromol Chem Phys.* 2004;205(15):2048-2054. doi:10.1002/macp.200400214
68. Miyagawa H, Mohanty AK, Misra M, Drzal LT. Thermo-physical and impact properties of epoxy containing epoxidized linseed oil, 1: Anhydride-cured epoxy. *Macromol Mater Eng.* 2004;289(7):629-635. doi:10.1002/mame.200400004
69. Tan SG, Chow WS. Thermal properties of anhydride-cured bio-based epoxy blends. *J Therm Anal Calorim.* 2010;101(3):1051-1058. doi:10.1007/s10973-010-0751-7



70. Atabani AE, Silitonga AS, Ong HC, et al. Non-edible vegetable oils: A critical evaluation of oil extraction, fatty acid compositions, biodiesel production, characteristics, engine performance and emissions production. *Renew Sustain Energy Rev.* 2013;18:211-245. doi:10.1016/j.rser.2012.10.013
71. Desroches M, Benyahya S, Besse V, Auvergne R, Boutevin B, Caillol S. Synthesis of bio-based building blocks from vegetable oils: A platform chemicals approach. *Lipid Technol.* 2014;26(2):35-38. doi:10.1002/lite.201400014
72. Alam M, Akram D, Sharmin E, Zafar F, Ahmad S. *Vegetable Oil Based Eco-Friendly Coating Materials: A Review Article.* Vol 7.; 2014:469-479. doi:10.1016/j.arabjc.2013.12.023
73. Tan SG, Chow WS. Biobased Epoxidized Vegetable Oils and Its Greener Epoxy Blends: A Review. *Polym - Plast Technol Eng.* 2010;49:1581-1590.
74. Arkema. <https://www.arkema.com/en/>.
75. Radojčić D, Hong J, Ionescu M, Wan X, Javni I, Petrović ZS. Study on the Reaction of Amines with Internal Epoxides. *Eur J Lipid Sci Technol.* 2016;118. doi:10.1002/ejlt.201500490
76. Pin J-M, Sbirrazzuoli N, Mija A. From epoxidized linseed oil to bioresin: An overall approach of epoxy/anhydride cross-linking. *ChemSusChem.* 2015;8(7):1232-1243. doi:10.1002/cssc.201403262
77. Pin J-M, Guigo N, Vincent L, Sbirrazzuoli N, Mija A. Copolymerization as a Strategy to Combine Epoxidized Linseed Oil and Furfuryl Alcohol: The Design of a Fully Bio-Based Thermoset. *ChemSusChem.* 2015;8:4149-4161. doi:10.1002/cssc.201501566

78. Albarrán-Preza E, Corona-Becerril D, Viguera-Santiago E, Hernández-López S. Sweet polymers: Synthesis and characterization of xylitol-based epoxidized linseed oil resins. *Eur Polym J.* 2016;75:539-551. doi:10.1016/j.eurpolymj.2015.12.025
79. Pawar M, Kadam A, Yemul O, Thamke V, Kodam K. Biodegradable bioepoxy resins based on epoxidized natural oil (cottonseed & algae) cured with citric and tartaric acids through solution polymerization: A renewable approach. *Ind Crops Prod.* 2016;89:434-447. doi:10.1016/j.indcrop.2016.05.025
80. Liu R, Zhang X, Gao S, Liu X, Wang Z, Yan J. Bio-based epoxy-anhydride thermosets from six-armed linoleic acid-derived epoxy resin. *RSC Adv.* 2016;6:52549-52555. doi:10.1039/c2ra23270g
81. Carbonell-Verdu A, Bernardi L, Garcia-Garcia D, Sanchez-Nacher L, Balart R. Development of environmentally friendly composite matrices from epoxidized cottonseed oil. *Eur Polym J.* 2015;63:1-10. doi:10.1016/j.eurpolymj.2014.11.043
82. Boquillon N, Fringant C. Polymer networks derived from curing of epoxidised linseed oil: influence of different catalysts and anhydride hardeners. *Polymer (Guildf).* 2000;41:8603-8613. doi:http://dx.doi.org/10.1016/S0032-3861(00)00256-1
83. Alsagayar ZS, Rahmat AR, Arsad A, Fakhari A, binti Wan Tajulruddin WN. Mechanical Properties of Epoxidized Palm Oil/Epoxy Resin Blend. *Appl Mech Mater.* 2014;695(July):655-658. doi:10.4028/www.scientific.net/AMM.695.655
84. Abdelwahab MA, Misra M, Mohanty AK. Epoxidized pine oil-siloxane:

- Crosslinking kinetic study and thermomechanical properties. *J Appl Polym Sci.* 2015;132(37):1-12. doi:10.1002/app.42451
85. Kousaalya AB, Beyene SD, Gopal V, Ayalew B, Pilla S. Green epoxy synthesized from *Perilla frutescens*: A study on epoxidation and oxirane cleavage kinetics of high-linolenic oil. *Ind Crops Prod.* 2018;123(May):25-34. doi:10.1016/j.indcrop.2018.06.047
86. Hu K, Bao L, Chen X, Xiao Y, Lei J. Synthesis of Castor Oil-Derived Decanediamide as a Novel Flexible Asphalt-Modified Epoxy Resin Curing Agent. *Adv Polym Technol.* 2018;37(4):1092-1098. doi:10.1002/adv.21760
87. Ciannamea EM, Ruseckaite RA. Pressure Sensitive Adhesives Based on Epoxidized Soybean Oil: Correlation Between Curing Conditions and Rheological Properties. *J Am Oil Chem Soc.* 2018;95(4):525-532. doi:10.1002/aocs.12046
88. Sahoo SK, Khandelwal V, Manik G. Development of toughened bio-based epoxy with epoxidized linseed oil as reactive diluent and cured with bio-renewable crosslinker. *Polym Adv Technol.* 2018;29(1):565-574. doi:10.1002/pat.4166
89. Sahoo SK, Khandelwal V, Manik G. Development of completely bio-based epoxy networks derived from epoxidized linseed and castor oil cured with citric acid. *Polym Adv Technol.* 2018;29(7):2080-2090. doi:10.1002/pat.4316
90. Aouf C, Nouailhas H, Fache M, Caillol S, Boutevin B, Fulcrand H. Multi-functionalization of gallic acid. Synthesis of a novel bio-based epoxy resin. *Eur Polym J.* 2013;49(6):1185-1195. doi:10.1016/j.eurpolymj.2012.11.025
91. Aouf C, Benyahya S, Esnouf A, Caillol S, Boutevin B, Fulcrand H. Tara

- tannins as phenolic precursors of thermosetting epoxy resins. *Eur Polym J.* 2014;55:186-198. doi:10.1016/j.eurpolymj.2014.03.034
92. Fache M, Auvergne R, Boutevin B, Caillol S. New vanillin-derived diepoxy monomers for the synthesis of biobased thermosets. *Eur Polym J.* 2015;67:527-538. doi:10.1016/j.eurpolymj.2014.10.011
93. Xin J, Li M, Li R, Wolcott MP, Zhang J. A green epoxy resin system based on lignin and tung oil and its application in epoxy asphalt. *ACS Sustain Chem Eng.* 2016;acssuschemeng.6b00256. doi:10.1021/acssuschemeng.6b00256
94. Asada C, Basnet S, Otsuka M, Sasaki C, Nakamura Y. Epoxy resin synthesis using low molecular weight lignin separated from various lignocellulosic materials. *Int J Biol Macromol.* 2015;74:413-419. doi:10.1016/j.ijbiomac.2014.12.039
95. Garrison MD, Harvey BG. Bio-based hydrophobic epoxy-amine networks derived from renewable terpenoids. *J Appl Polym Sci.* 2016;43621:1-12. doi:10.1002/app.43621
96. Wan J, Gan B, Li C, et al. A sustainable, eugenol-derived epoxy resin with high biobased content, modulus, hardness and low flammability: Synthesis, curing kinetics and structure-property relationship. *Chem Eng J.* 2016;284:1080-1093. doi:10.1016/j.cej.2015.09.031
97. Sasaki C, Wanaka M, Takagi H, Tamura S, Asada C, Nakamura Y. Evaluation of epoxy resins synthesized from steam-exploded bamboo lignin. *Ind Crops Prod.* 2013;43(1):757-761. doi:10.1016/j.indcrop.2012.08.018
98. Wu C-C, Lee W-J. Synthesis and properties of copolymer epoxy resins prepared from copolymerization of bisphenol A, epichlorohydrin, and

- liquefied *Dendrocalamus latiflorus*. *J Appl Polym Sci*. 2010;116(4):NA-NA. doi:10.1002/app.31703
99. Jiang Y, Ding D, Zhao S, Zhu H, Kenttämäa HI, Abu-Omar MM. Renewable thermoset polymers based on lignin and carbohydrate derived monomers. *Green Chem*. 2018;20(5):1131-1138. doi:10.1039/C7GC03552G
100. Gioia C, Re G Lo, Lawoko M, Berglund L. Tunable Thermosetting Epoxies Based on Fractionated and Well-Characterized Lignins. 2018. doi:10.1021/jacs.7b13620
101. Salanti A, Zoia L, Simonutti R, Orlandi M. Epoxidized Lignin Derivatives as Bio-based Cross-linkers Used in the Preparation of Epoxy Resins. *BioResources*. 2018;13(2):2374-2396. doi:10.15376/biores.13.2.2374-2396
102. Yan R, Yang D, Zhang N, et al. Performance of UV curable lignin based epoxy acrylate coatings. *Prog Org Coatings*. 2018;116(January):83-89. doi:10.1016/j.porgcoat.2017.11.011
103. Jablonskis A, Arshanitsa A, Arnautov A, Telysheva G, Evtugin D. Evaluation of Ligno Boost™ softwood kraft lignin epoxidation as an approach for its application in cured epoxy resins. *Ind Crops Prod*. 2018;112:225-235. doi:10.1016/J.INDCROP.2017.12.003
104. Chrysanthos M, Galy J, Pascault JP. Preparation and properties of bio-based epoxy networks derived from isosorbide diglycidyl ether. *Polymer (Guildf)*. 2011;52(16):3611-3620. doi:10.1016/j.polymer.2011.06.001
105. Lewkowski J. Synthesis, chemistry and applications of 5-hydroxymethylfurfural and its derivatives. *Arkivoc*. 2005;2001(1):17-54. doi:10.3998/ark.5550190.0002.102

## | Introduction and objectives

106. Synvina - Products. <https://www.synvina.com/products/fdca/>.
107. Avantium. <https://www.avantium.com/press-releases/alpla-joins-coca-cola-company-danone-avantiums-pef-bottle-development/>.
108. Feng X, East AJ, Hammond WB, Zhang Y, Jaffe M. Overview of advances in sugar-based polymers. *Polym Adv Technol.* 2011;22(1):139-150. doi:10.1002/pat.1859
109. Park S, Park S, Jang DH, Lee HS, Park CH. Anti-fogging behavior of water-absorbing polymer films derived from isosorbide-based epoxy resin. *Mater Lett.* 2016;180:81-84. doi:10.1016/j.matlet.2016.05.114
110. Li C, Dai J, Liu X, Jiang Y, Ma S, Zhu J. Green Synthesis of a Bio-Based Epoxy Curing Agent from Isosorbide in Aqueous Condition and Shape Memory Properties Investigation of the Cured Resin. *Macromol Chem Phys.* 2016;217(13):1439-1447. doi:10.1002/macp.201600055
111. Rapi Z, Szolnoki B, Bakó P, et al. Synthesis and characterization of biobased epoxy monomers derived from d-glucose. *Eur Polym J.* 2015;67:375-382. doi:10.1016/j.eurpolymj.2014.09.025
112. Ma S, Liu X, Fan L, et al. Synthesis and properties of a bio-based epoxy resin with high epoxy value and low viscosity. *ChemSusChem.* 2014;7(2):555-562. doi:10.1002/cssc.201300749
113. Darroman E, Durand N, Boutevin B, Caillol S. New cardanol/sucrose epoxy blends for biobased coatings. *Prog Org Coatings.* 2015;83:47-54. doi:10.1016/j.porgcoat.2015.02.002
114. Nie Y, Tian X, Liu Y, Wu K, Wang J. Research on starch-g-polyvinyl acetate and epoxy resin-modified corn starch adhesive. *Polym Compos.*

- 2013;34(1):77-87. doi:10.1002/pc.22379
115. Sachinvala ND, Winsor DL, Menescal RK, Ganjian I, Niemczura WP, Litt MH. Sucrose-based epoxy monomers and their reactions with diethylenetriamine. *J Polym Sci Part A Polym Chem*. 1998;36(13):2397-2413. doi:10.1002/(SICI)1099-0518(19980930)36:13<2397::AID-POLA27>3.0.CO;2-4
  116. Cho JK, Lee J, Jeong J, Kim B. Synthesis of carbohydrate biomass-based furanic compounds bearing epoxide end group (s) and evaluation of their feasibility as adhesives. *J Adhes Sci Technol*. 2013;27(18-19):2127-2138. doi:10.1080/01694243.2012.697700
  117. Yu AZ, Rahimi A, Webster DC. High performance bio-based thermosets from dimethacrylated epoxidized sucrose soyate (DMESS). *Eur Polym J*. 2018;99:202-211. doi:10.1016/J.EURPOLYMJ.2017.12.023
  118. Yan J, Webster DC. Thermosets from highly functional methacrylated epoxidized sucrose soyate. *Green Mater*. 2014;2(3):132-143. doi:10.1680/gmat.14.00002
  119. Esmaeili N, Salimi A, Zohuriaan-Mehr MJ, Vafayan M, Meyer W. Bio-based thermosetting epoxy foam: Tannic acid valorization toward dye-decontaminating and thermo-protecting applications. *J Hazard Mater*. 2018;357:30-39. doi:10.1016/J.JHAZMAT.2018.05.045
  120. Qi M, Xu Y-J, Rao W-H, Luo X, Chen L, Wang Y-Z. Epoxidized soybean oil cured with tannic acid for fully bio-based epoxy resin. *RSC Adv*. 2018;8(47):26948-26958. doi:10.1039/C8RA03874K
  121. Shibata M, Nakai K. Preparation and properties of biocomposites

## | Introduction and objectives

- composed of bio-based epoxy resin, tannic acid, and microfibrillated cellulose. *J Polym Sci Part B Polym Phys*. 2010;48(4):425-433. doi:10.1002/polb.21903
122. Warth H, Mülhaupt R, Hoffmann B, Lawson S. Polyester networks based upon epoxidized and maleinated natural oils. *Angew Makromol Chemie*. 1997;249(1):79-92. doi:10.1002/apmc.1997.052490106
123. Patel BP, Patel HS, Patel SR. Modified Castor Oil as an Epoxy Resin Curing Agent. *E-Journal Chem*. 2004;1(1):11-16. doi:10.1155/2004/412906
124. Yang X, Wang C, Li S, et al. Study on the synthesis of bio-based epoxy curing agent derived from myrcene and castor oil and the properties of the cured products. *RSC Adv*. 2017;7(1):238-247. doi:10.1039/C6RA24818G
125. Liu X, Xin W, Zhang J, et al. Rosin-based acid anhydrides as alternatives to petrochemical curing agents. *Green Chem*. 2009;11(7):1018. doi:10.1039/b903955d
126. Mathiazhagan A, Rani J. Nanotechnology-A New Prospective in Organic Coating - Review. *Int J Chem Eng Appl*. 2011;2(4):225-237.
127. Geueke B. *Dossier-Can Coatings*.; 2016. doi:10.5281/zenodo.200633
128. Ashcroft WR, Cantwell WJ, Chen XM, et al. *Chemistry and Technology of Epoxy Resins*. (Ellis B, ed.). Springer Science+Business Media, B.V.; 1993. doi:10.1007/978-94-011-2932-9
129. Tsanaktsis V, Terzopoulou Z, Exarhopoulos S, et al. Sustainable, eco-friendly polyesters synthesized from renewable resources: preparation and thermal characteristics of poly(dimethyl-propylene furanoate). *Polym Chem*. 2015;6. doi:10.1039/c5py01367d



130. Wu H, Wen B, Zhou H, et al. Synthesis and degradability of copolyesters of 2, 5-furandicarboxylic acid, lactic acid, and ethylene glycol. *Polym Degrad Stab.* 2015. doi:10.1016/j.polymdegradstab.2015.08.009
131. Morales-Huerta JC, Martínez De Ilarduya A, Muñ Oz-Guerra S. Sustainable Aromatic Copolyesters via Ring Opening Polymerization: Poly(butylene 2,5-furandicarboxylate-co-terephthalate)s. *ACS Sustain Chem Eng.* 2016;4:4965-4973. doi:10.1021/acssuschemeng.6b01302
132. de Jong E, Dam MA, Sipos L, Gruter G-JM. Furandicarboxylic Acid ( FDCA ), A Versatile Building Block for a VeryInteresting Class of Polyesters. In: *Biobased Monomers, Polymers, and Materials.* ; 2012:1-13. doi:10.1021/bk-2012-1105.ch001
133. Deng J, Liu X, Li C, Jiang Y, Zhu J. Synthesis and properties of a bio-based epoxy resin from 2,5-furandicarboxylic acid (FDCA). *RSC Adv.* 2015;5:15930-15939. doi:10.1007/s11426-013-5025-3
134. Miao JT, Yuan L, Guan Q, Liang G, Gu A. Biobased Heat Resistant Epoxy Resin with Extremely High Biomass Content from 2,5-Furandicarboxylic Acid and Eugenol. *ACS Sustain Chem Eng.* 2017;5(8):7003-7011. doi:10.1021/acssuschemeng.7b01222



# Chapter 2.

---

## Synthesis of furan-based epoxy monomers



## 2.1. Introduction

---

The necessity to find non-toxic and sustainable building blocks to replace BPA in the production of epoxy resins was a key objective of this experimental work. The decreasing availability of oil-derived feedstock was also considered, so the research of new molecules was logically focused on bio-derived chemicals.

In order to further improve chemical, thermal and mechanical properties of epoxy resins, the presence of significant content of aromatic moieties is required. In this frame, lignin derivatives appear to be the natural substitutes of BPA. However, time- and energy-consuming extraction processes make lignin-based epoxies expensive and barely available.

On the other hand, furanic molecules combine aromatic structure and easily available resources, such as carbohydrate biomass. Among furanic molecules, furan-2,5-dicarboxylic acid (FDCA) has been labelled in 2004 as "top value added chemical from biomass" from U.S. Department of Energy and it has been confirmed being a valuable chemical in 2010<sup>1,2</sup>. FDCA is a commercially available compound obtained by dehydration of hexose polysaccharides and consequent oxidation of the 5-hydroxymethylfurfural (HMF) intermediate<sup>3-9</sup>, also by effect of enzymes<sup>10</sup>. As a matter of fact, FDCA already results to be an excellent substitute of terephthalic acid in the production of polyesters. Polyethylene furanoate (PEF), obtained from polycondensation of FDCA and ethylene glycol, showed up to be a perfect substitute of PET thanks also to the improved barrier properties. Some big companies, indeed nowadays commercialize bottles made of PEF<sup>11</sup>.

When, instead, HMF is reduced, 2,5-bis(hydroxymethyl)furan (BHMF), a furanic diol, is obtained. Bearing two hydroxyl groups, this molecule can be imagined as clear replace for BPA, also in the already optimized industrial processes for its glycidylation into DGEBA.

In a pioneering work Cho et al.<sup>12</sup> obtained different mono- and di-furanic diglycidyl ethers, starting from furanic diols and acid, and demonstrated their feasibility as adhesives. Some years later, the synthesis and cure of furanyl- and phenyl-based diepoxy monomers was described and properties of obtained epoxy resins were analyzed. Epoxy monomers were obtained by reacting BHMF with epichlorohydrin and cured with both commercial hardeners<sup>13</sup> and a furfuryl amine<sup>14</sup>. In a more recent work, starting from the same precursor and epichlorohydrin, Shen et al.<sup>15</sup> synthesized a bio-based epoxy monomer and once obtained the Diels–Alder adduct, resulted by the cycloaddition reaction between the furan ring and maleimide moieties, was cured in presence of a commercial toughening agent. Mechanical and morphological properties of the reinforced systems were evaluated. The use of furan-based Diels–Alder adduct as a curing agent for diglycidyl ether of Bisphenol-A (DGEBA) has been also proposed by Tachibana et al.<sup>16</sup>.

Scientific papers reporting FDCA as a building block for the production of epoxy resins are still lacking. In a recent work<sup>17</sup> FDCA has been used as linker between two eugenol molecules, which were then epoxidized leading to materials with good thermal resistance properties. Only Deng et al. used FDCA to obtain the corresponding diglycidyl ester, with a two-steps procedure involving first allylation on the acidic groups with allyl bromide and consequent epoxidation with *m*-chloroperoxybenzoic acid (*m*-CPBA)<sup>18</sup>. The long reaction time, reagents and solvents used and the hazardous by-products, especially from

an environmental point of view, make this process still complex and only moderately safe. Therefore, the obtainment of epoxy resins from FDCA monomers through simple, scalable and low environmental and human health impact protocols represents still a challenge.

In this experimental work, bis(oxiran-2-yl-methyl)furan-2,5-dicarboxylate (BOFD) was synthesized according to two new different procedures, involving in the first case the glycidylation of FDCA with ECH, and in the second case the transesterification of DM-FDCA in the presence of glycidol, as described in details in the experimental part. Also 2,5-bis[(oxiran-2-ylmethoxy)methyl]furan (BOMF) synthesis is proposed and the obtained epoxide fully characterized.

## 2.2. Experimental section

---

### 2.2.1. Materials

The commercially available bio-based epoxy precursors, namely Furan-2,5-dicarboxylic acid (FDCA, 98%) was purchased from Carbosynth Ltd (Compton, United Kingdom), 2,5-bis(hydroxymethyl)furan (BHMF, 97%) and 2,5-furandicarboxylate (DM-FDCA, 99%) were purchased from Apollo Scientific Ltd (Whitefield Rd, United Kingdom). Epichlorohydrin (ECH, > 99%), glycidol (96%), tetrabutylammonium bromide (TBBr, ≥99%), p-xylene (anhydrous, ≥99%), silica gel (60Å, 70-230 mesh), potassium cyanate (KOCN) were purchased from Sigma-Aldrich. Anhydrous sodium hydroxide pellets (NaOH, ≥97%), ethyl acetate (EA, 99%), hexane (HX, 99%) tetrahydrofuran (THF, 99.9%) and magnesium sulfate

(MgSO<sub>4</sub>) were purchased from Carlo Erba. All chemical products were used as received, without further purification

## 2.2.2. Synthesis of bis(oxiran-2-yl-methyl)furan-2,5-dicarboxylate (BOFD)

### *Glycidylation of FDCA with ECH*

Two different and innovative single-step routes for the synthesis of BOFD have been set-up. The first route involves the reaction of FDCA with ECH, according to the following procedure. A round bottomed flask equipped with a mechanical stirrer and a condenser was charged with ECH (0.26 mol) and the atmosphere was saturated with nitrogen. TBBr (0.40 mmol) and FDCA (13 mmol) were then added and the temperature set at 90 °C. The mixture was kept under stirring and the pH of the solution was steadily monitored. After 2 hours, the pH became neutral and the solution limpid yellow. Therefore, the temperature was decreased to 40 °C and the flask equipped with a vacuum system. A vacuum of 0.7 bar was applied and a 50 wt.% NaOH (26 mmol) aqueous solution was added dropwise over a period of 2 hours; then the reaction was allowed to react for additional 4 hours. The reaction mixture was filtered and the recovered liquid phase washed two times with distilled water. The organic phase was then dried with MgSO<sub>4</sub>, and the remaining ECH stripped off using a rotatory evaporator. The solid white product was obtained after purification by a silica gel chromatographic column using hexane/ethyl acetate (1/1 by volume) as eluent. The obtained yield was 3.4%.



$^1\text{H}$  NMR (400 MHz,  $\text{CDCl}_3$ )  $\delta$  7.27 (s, 1H), 4.65 (dd,  $J = 12.2, 3.2$  Hz, 1H), 4.20 (dd,  $J = 12.2, 6.3$  Hz, 1H), 3.34 (td,  $J = 6.3, 3.1$  Hz, 1H), 2.93 – 2.86 (m, 1H), 2.73 (dd,  $J = 4.8, 2.6$  Hz, 1H).

$^{13}\text{C}$  NMR (101 MHz,  $\text{CDCl}_3$ )  $\delta$  157.73, 146.65, 119.16, 66.16, 49.23, 44.95.

### *Transesterification of DM-FDCA and glycidol*

The second route is based on the transesterification of DM-FDCA with glycidol. In a round bottomed flask, DM-FDCA (15 mmol), glycidol (45 mmol), KOCN (0.90 mmol) and xylene (13 mL) were introduced. A vacuum of 30 mbar was operated. The solution was vigorously stirred and reacted for 6 hours at 60 °C. Once the mixture was cooled to room temperature, 50/50 v/v mixture of ethyl acetate and distilled water was added. The two phases were separated through separatory funnel. Successively, the organic phase was dried with  $\text{MgSO}_4$  and the solvent evaporated at atmospheric pressure. The solid white product was purified by adsorption chromatography on silica gel using hexane/ethyl acetate (1/1 by volume) as eluent and the final yield was 5.3%.

$^1\text{H}$  NMR (400 MHz,  $\text{CDCl}_3$ )  $\delta$  7.27 (s, 2H), 4.65 (dd,  $J = 12.2, 3.2$  Hz, 2H), 4.19 (dd,  $J = 12.2, 6.3$  Hz, 2H), 3.34 (td,  $J = 6.4, 3.1$  Hz, 2H), 2.90 (t,  $J = 4.5$  Hz, 2H), 2.73 (dd,  $J = 4.8, 2.6$  Hz, 2H).

$^{13}\text{C}$  NMR (101 MHz,  $\text{CDCl}_3$ )  $\delta$  157.72, 146.65, 119.16, 66.16, 49.23, 44.95.

### 2.2.3. Synthesis of 2,5-bis[(oxiran-2-ylmethoxy)methyl]furan (BOMF)

BOMF was synthesized according to a modified procedure described by Cho et al.<sup>12</sup> A 50 wt.% aqueous solution of NaOH (1.44 mol, 115 g), TBBr (1.68 mol, 3.86 g) and ECH (1.68 mol, 132 mL) were added to a double-necked round-bottomed flask equipped with a magnetic stirrer and a condenser. The reaction system was saturated with Argon and put under vigorous stirring for 30 minutes at room temperature. The flask was then placed in a bath at 50 °C and a solution of BHMf (0.120 mol, 15.4g) in THF (120 mL, 128 g/L) was added dropwise. The reaction mixture was let react for 2 hours and subsequently poured into 600mL of ice/water. The so-obtained reaction mixture was extracted two times with 600 mL of ethyl acetate and the organic phase anhydriified with MgSO<sub>4</sub>, filtered and dried with a rotatory evaporator. To remove the ECH excess the crude product was washed three times with hexane and dried again. The total yield of the synthesis was 85%. The obtained product was an amber-colored viscous liquid at room temperature.

<sup>1</sup>H NMR (400 MHz, CDCl<sub>3</sub>) 6.27 (s, 2H), 4.48 (q, J = 12.8 Hz, 4H), 3.74 (dd, J = 11.5, 3.1 Hz, 1H), 3.40 (dd, J = 11.5, 5.9 Hz, 1H), 3.13 (td, J = 6.2, 2.9 Hz, 2H), 2.76 (dd, J = 6.8, 2.3 Hz, 1H), 2.58 (dd, J = 5.0, 2.7 Hz, 1H).

<sup>13</sup>C NMR (101 MHz, CDCl<sub>3</sub>) δ 151.84, 110.36, 70.75, 65.21, 50.75, 44.33.

Viscosity (η) at 30 °C = 0.03 Pa\*s.

## 2.2.4. Methods

FT-IR analysis was performed in ATR mode using a PerkinElmer Spectrum One FTIR spectrophotometer equipped with a universal ATR sampling accessory (Wellesley, MA, USA). Spectra were acquired in the range of 4000-600  $\text{cm}^{-1}$  with a resolution of 4  $\text{cm}^{-1}$  and 32 scans. Data were processed using the PerkinElmer Spectrum software.

Mono- and multi-dimensional NMR spectra were recorded using a Bruker Advance 400 MHz spectrometer, and processed with MestreNova software.

Epoxy equivalent weight (EEW) was evaluated using  $^1\text{H}$ -NMR spectra by the method described by Garcia et al.<sup>19</sup> When BOFD spectra were analysed, first an accurate peak deconvolution process through Global Spectral Deconvolution (GSD) with 20 fitting cycles was carried out in order to break down the peak at 7.25 ppm, and fail to take account of the solvent peak in numerical evaluations of EEW.

A TA Instrument TGA 500 was used for the thermogravimetric analysis (TGA) of the obtained compounds. Each test was carried out from 25°C to 650 °C at 10 °C  $\text{min}^{-1}$ , under a 60  $\text{mL min}^{-1}$  nitrogen flux.

A TA Instrument DSC Q2000, equipped with Refrigerator Cooling System (RCS), was used for calorimetric analysis (DSC), using nitrogen as purge gas (50  $\text{mL min}^{-1}$ ). A first heating scan at 2 °C  $\text{min}^{-1}$  was performed from -30 to 150 °C, followed by a cooling step to -30 °C and a second heating scan to 150 °C, at 2 °C  $\text{min}^{-1}$ .

## Epoxy equivalent weight (EEW) evaluation

The EEW is the weight, in grams, of resin containing one gram of epoxy equivalent, and it is related to molecular weight of the epoxide. In case of BOFD, whose general formula is reported in **Figure 2.1**, the molecular weight of monomer (for  $n = 0$ ) is 268.16, while the repetitive unit weight is 212.10; this results in a theoretical expression ( $M_n = 212.10 n + 268.16$  Equation 2.1) of the molecular weight  $M_n$  as a function of the polymerization degree  $n$ :

$$M_n = 212.10 n + 268.16 \quad \text{Equation 2.1}$$

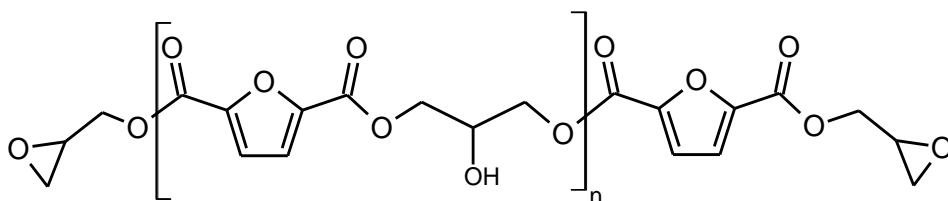


**Figure 2.1** – General formula of oligomeric epoxy resins based on BOFD

Consequently, the EEW formula as a function of polymerization degree is:

$$EEW = 106.05 n + 134.08 \quad \text{Equation 2.2}$$

In an aromatic epoxy resin the relation between aromatic and epoxy protons can be defined as:

$$R_p = \frac{l_2}{l_1} \quad \text{Equation 2.3}$$

where  $l_2$  is the intensity of peak associated to the aromatic protons, and  $l_1$  is the sum of intensities of peaks given by the epoxide terminal protons.

Theoretically, considering a monomeric epoxy resin with  $n = 0$ , the relation between aromatic and epoxy resins can be expressed as :

$$R_t = \frac{I_{2,t}}{I_{1,t}} \quad \text{Equation 2.4}$$

where  $I_{2,t}$  represents the number of aromatic protons, i.e. 2, and  $I_{1,t}$  is the number of oxirane protons, i.e. 6 (due to BOMF bifunctionality). The value of polymerization degree can now be determined taking in account that:

$$n = \frac{(R_p - R_t)}{R_t} \quad \text{Equation 2.5}$$

## 2.3. Results and discussion

---

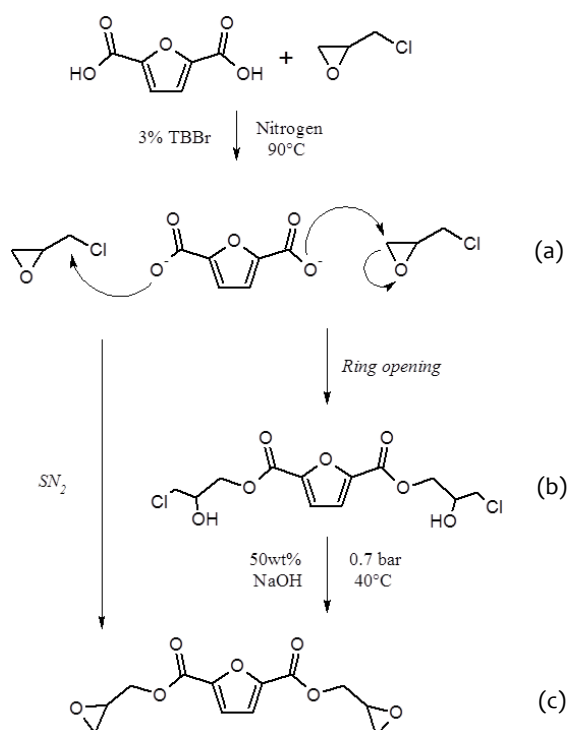
### 2.3.1. Synthesis and characterization of bis(oxiran-2-yl-methyl)furan-2,5-dicarboxylate (BOFD)

#### *Glycidylation of FDCA with ECH*

As above-mentioned, FDCA is a commercially available compound obtained by dehydration of hexose polysaccharides and consequent oxidation of the 5-hydroxymethylfurfural (HMF) intermediate. The reaction between acidic groups of FDCA and ECH to form the glycidyl ester proceeds through a mechanism, reported in *Errore. L'origine riferimento non è stata trovata.*, similar to that recently reported by other authors for the acid moieties of vanillic and gallic acids<sup>20-22</sup>.

The reaction proceeds through the addition of the carboxylate group of FDCA to the epoxy ring of epichlorohydrin. As a first step of this procedure, FDCA is mixed with epichlorohydrin in inert atmosphere in presence of the charge transfer catalyst TBBr. The catalyst allows the furan-2,5-dicarboxylate oxyanion to coexist with epichlorohydrin, used also as solvent (Errore. L'origine riferimento non è stata trovata.). Once the oxyanion and epichlorohydrin are in contact, the reaction proceeds directly with an SN2 mechanism or with a mechanism involving the opening of the epoxy ring that binds to the ion, resulting in the formation of the chlorohydrin intermediate represented in Errore. L'origine riferimento non è stata trovata.**b**. Subsequently, cyclization of the chlorohydrin yields the glycidyl product (Errore. L'origine riferimento non è stata trovata.Errore. L'origine riferimento non è stata trovata.**c**). Initially, the mixture had an almost neutral pH, being a white opaque suspension of FDCA. When heated up to 90 °C, the pH decreased to a value of 5.25, suggesting the dissociation of FDCA. The reaction was left to proceed until the pH of the mixture got back to neutrality, indicating the complete transformation of the carboxylate ion into the halohydrin intermediate; as a further evidence, the solution became a limpid yellow liquid and the insoluble portion of FDCA dissolved. Temperature was then lowered, a slight vacuum applied, and the second synthetic step was started adding dropwise the alkaline solution; the latter is needed to allow the ring closure, resulting in the formation of NaCl as by-product. As soon as NaOH was added, a white solid precipitated instantaneously. As the alkaline solution addition started, the reaction was left to proceed for a total of 6 hours, then it was stopped. The reacting mixture was filtered, the organic phase washed with water, separated, anhydridified with magnesium sulphate and dried with a rotary evaporator. The crude product, pale yellow viscous, obtained after the synthesis results impure as can be noticed by the <sup>1</sup>H-NMR spectra reported in **Figure 2.2**,

where it is compared with the spectra of BOFD after purification. A preliminary TLC (hexane/ethyl acetate 1:1) performed on the yellow viscous product showed the presence of at least six different compounds. Among them, oligomers and unreacted halohydrins could be detected by NMR analysis of the fractions obtained upon purification through column chromatography that resulted mandatory. In particular, several yellow and highly viscous fractions were obtained, except for BOFD, which was a white crystalline solid.



**Scheme 2.1** – Reaction mechanism in the glycidylation of FDCA

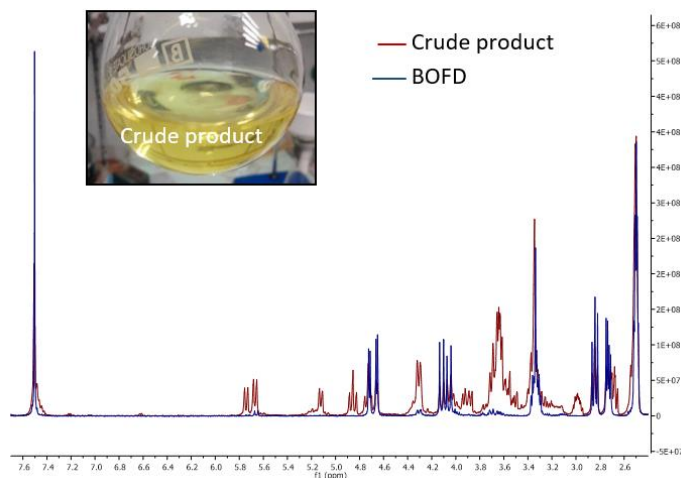


**Figure 2.2** – <sup>1</sup>H-NMR spectra for the crude product of FDCA glycidylation (red line) and BOFD (blue line)

To prove the occurrence of the condensation reaction between glycidyl group and FDCA, first FTIR-ATR and mono- and multi-dimensional <sup>1</sup>H and <sup>13</sup>C-NMR analyses were carried out.

FTIR-ATR spectra of FDCA and the purified BOFD are shown in **Figure 2.3**. The disappearance of the broad adsorption band due to –OH from carboxylic groups between 3200 and 2300 cm<sup>-1</sup> correlated with the appearance of the strong ester band at 1709 cm<sup>-1</sup> confirmed the conversion of carboxylic acids into ester moieties. The formation of the glycidyl group was confirmed by the appearance of the characteristic epoxy C-O-C absorption band at 902 cm<sup>-1</sup> as well as of a peak at 1342 cm<sup>-1</sup> related to the glycidyl methylene (See **Table 2.1**).

In **Table 2.1** are listed the characteristic FTIR bands of FDCA and BOFD, respectively.



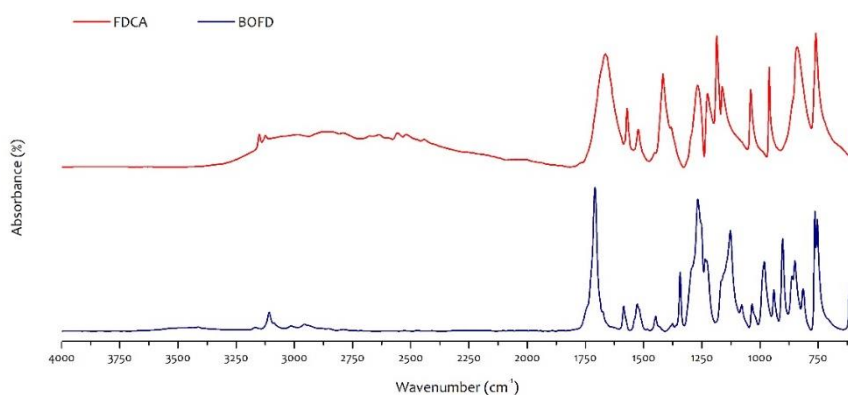


**Figure 2.3** – FTIR spectra of FDCA and BOFD

**Table 2.1** – Peak assignments in FTIR spectrum of FDCA and BOFD obtained by FDCA glycidylation

WAVENUMBER (CM <sup>-1</sup> )	ASSIGNMENT
<b>FDCA</b>	
3151 TO 2520	Stretching O-H Carboxylic acid
1665	Stretching C=O Carbonyls
1570 TO 1416	Stretching C=C Aromatics (furan)
1267 TO 1039	Stretching C-O Carboxylic acid
960	Stretching C=O, C-C-C bending 2,5 sub-furan ring
840 TO 760	Bending C-H Alkene (furan)
<b>BOFD OBTAINED BY FDCA GLYCIDYLATION</b>	
3165 TO 2955	Stretching C-H Aromatics (furan)
1708	Stretching C=O Ester
1585 TO 1448	Stretching C=C Aromatics (furan)
1375 – 1343	Bending C-H, CH <sub>2</sub> of Glycidyl
1267 TO 1235	Stretching C-O Ester and Epoxy ring
1127 – 1077	Stretching C-O Aromatic (furan)
1034 TO 902	Stretching C-O Epoxy ring

862 TO 815

Stretching C-C Epoxy ring

764 – 753

Rocking C-H Glycidyl

To get a further insight on the effective addition of the glycidyl group to FDCA, NMR analysis was performed through monodimensional  $^1\text{H}$  and  $^{13}\text{C}$  NMR spectroscopy to check the presence of the predicted structure and its purity.

**Figure 2.4** displays the  $^1\text{H}$ -NMR spectra of BOFD. The characteristic peaks of furanic proton at 7.27 ppm, overlapped with the signal of  $\text{CDCl}_3$ , is visible in the figure inset; two double doublets at 4.65 and 4.20, due to protons of methylene linked to the ester group, a sextet at 3.34 ppm from methyne proton of oxirane ring, a triplet at 2.93 – 2.86 and a double doublet 2.73 due to protons of methylene on oxirane ring are also visible. These signals are in agreement with those reported in literature for the BOFD molecule obtained with a two-step procedure involving first the allylation of FDCA and the subsequent epoxidation of the double bond.<sup>18</sup>

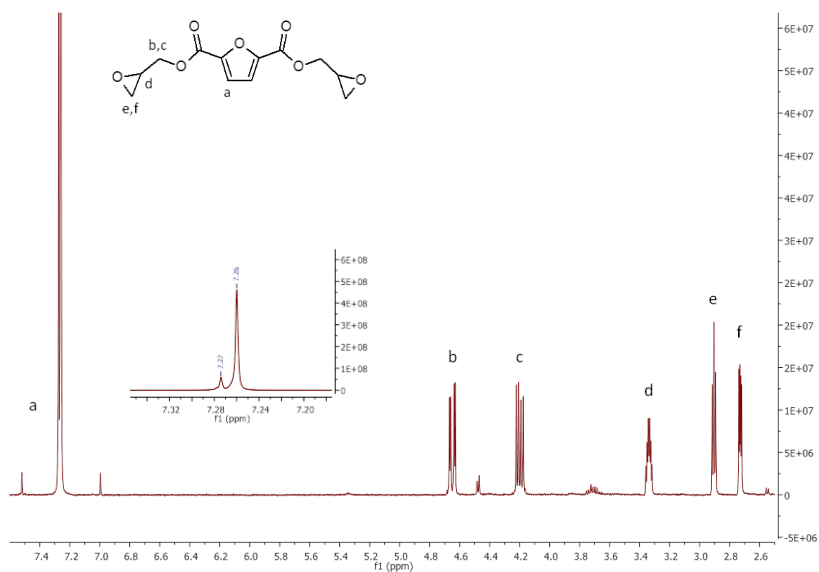


**Figure 2.4** –  $^1\text{H}$ -NMR spectra of BOFD obtained by FDCA glycidylation

$^{13}\text{C}$ -NMR spectra of BOFD (**Figure 2.5**) shows the peak at 157.73 ppm corresponding to the ester carbon, the quaternary furanic carbon peak at 146.65 ppm, the CH furanic peak of 119.16 ppm, the glycidyl  $\text{CH}_2$  carbon peak at 66.16 ppm, and the peaks related to the CH and  $\text{CH}_2$  carbons of oxirane ring at 49.23 and 44.95 ppm, respectively. This spectrum is in agreement with that reported by Deng et al.<sup>18</sup>

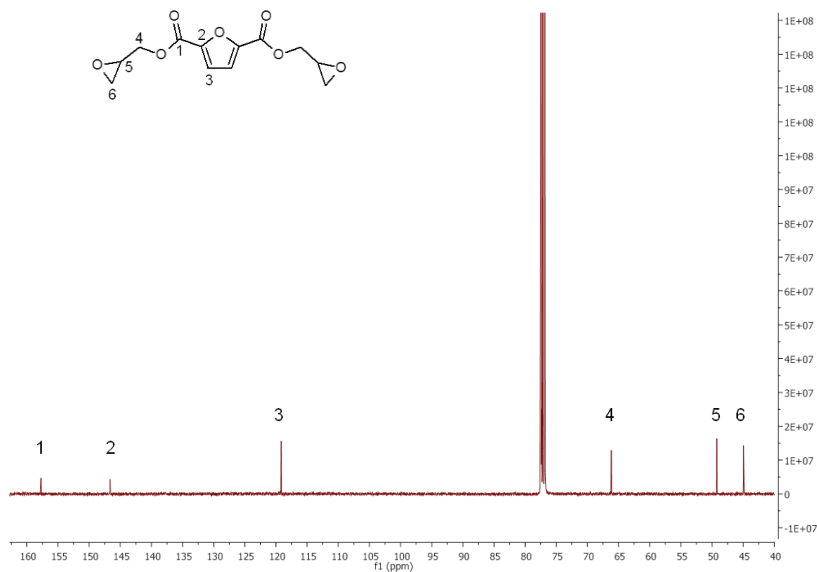


**Figure 2.5** –  $^{13}\text{C}$ -NMR spectra of BOFD obtained by glycidylation

Once characterized the BOFD by monodimensional  $^1\text{H}$ -NMR and  $^{13}\text{C}$ -NMR the structure was elucidated by performing further mono- and multi-dimensional NMR spectroscopy. Distortionless Enhancement by Polarization Transfer at  $90^\circ$  (DEPT 90) and Distortionless Enhancement by Polarization Transfer at  $135^\circ$  (DEPT 135) spectroscopy were performed while, as for multidimensional analysis, homonuclear correlation spectroscopy (COSY), heteronuclear single-quantum correlation spectroscopy (HSQC) and heteronuclear multiple-bonds correlation spectroscopy (HMBC) were carried out. DEPT 90 gives signals only from tertiary carbons and DEPT 135 gives primary and tertiary carbons signals as positive peaks while secondary carbons are represented as negative peaks. In DEPT 90 and DEPT 135 spectra for BOFD obtained by glycidylation, reported in **Figure 2.6**, are present two positive peaks at 119.16 ppm and 49.24 ppm confirming the previous assignments of these respectively to furanic and oxirane CH. Peaks at 66.16 ppm

and 44.95 are then confirmed to be secondary carbons, the first from glycidyl and the second on the oxirane ring.

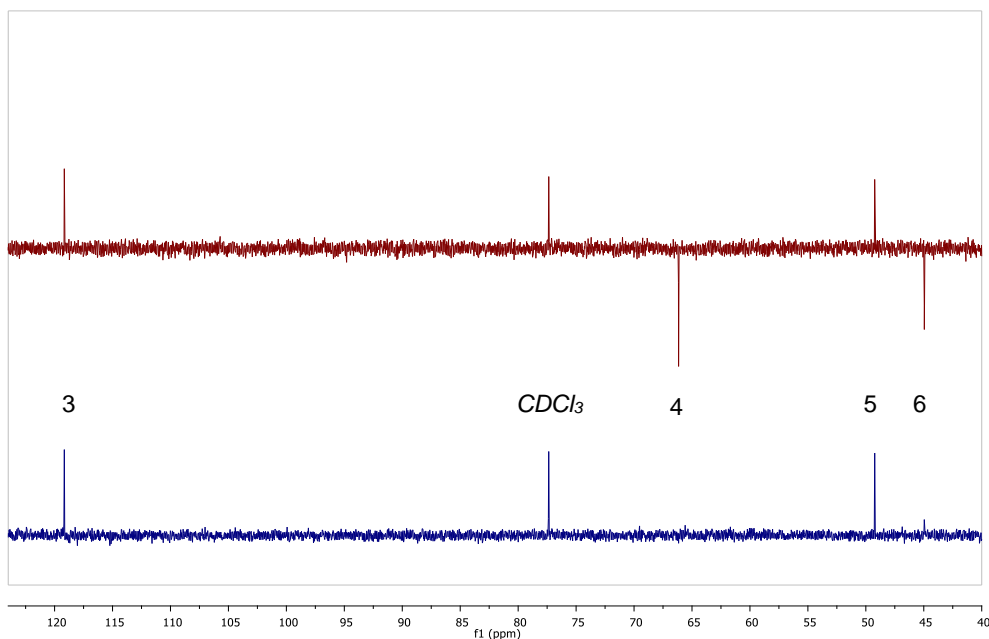


**Figure 2.6** – DEPT 90 (blue line) and DEPT 135 (red line) NMR analysis for BOFD obtained by glycidylation

COSY spectroscopy shows the homonuclear interactions between hydrogens and thanks to this analysis is possible to identify the protons linked to carbons separated by a single bond. Heteronuclear HSQC and HMBC spectroscopy relate in different ways  $^1\text{H}$ -NMR and  $^{13}\text{C}$ -NMR spectra. Single quantum correlation (HSQC) gives strong information about heteronuclear atoms directly connected by a single bond helping to assign at each carbon the chemical shift of the hydrogens bonded. HSQC spectroscopy, reporting only the correlation between carbons and hydrogens directly linked, is usually represented in function of DEPT 135; quaternary carbons in fact do not give signal in this kind of spectroscopy because not linked to any hydrogen. Complementary

to this analysis is the multiple-bond correlation (HMBC) that relates nuclei separated by about 2 to 4 bonds. This analysis gives the last information about the molecular structure, especially to assign definitely the chemical shifts related to quaternary carbons. In fact, peaks related to this kind of carbons are present only in the HMBC multidimensional analysis, reported in function of  $^{13}\text{C}$ -NMR as  $f_1$ . It has to be reminded also that in HMBC spectroscopy are present signals related to  $^1\text{J}_{\text{CH}}$  correlations too, but they appear as doublets.

The COSY spectroscopy, reported in **Figure 2.7**, shows the interactions between adjacent protons and in both axes are reported  $^1\text{H}$  spectra. In this case the cross-peaks highlighted by green circles confirm the relation between protons of methylene linked at the ester group (b,c) and methyne protons on oxirane ring (d), while the cross-peaks highlighted by blue circles prove the correlation between this last proton (d) and methylene protons on oxirane ring (e,f). However the two types of methylene protons (b,c and e,f) were not directly related to each other, as expected.

HSQC spectroscopy investigates on  $^1\text{J}_{\text{CH}}$  correlations and gives information about nuclei of two different species connected by a bond. Results of HSQC spectroscopy for BOFD are reported in **Figure 2.8** as function of DEPT 135 and  $^1\text{H}$ -NMR analysis. Through this analysis the  $\text{CH}_2$  glycidyl carbons (4), represented by a negative peak at 66.16 ppm on  $f_1$ , can be directly correlated to protons of methylene linked to the ester group (b,c; purple circle). Analogously the CH carbons at 49.19 ppm (5, positive on  $f_1$ ) result bonded with the methyne protons of the oxirane ring (d; green circle) and the  $\text{CH}_2$  carbons on oxirane ring (6, negative peak at 44.95 ppm on  $f_1$ ) are bonded to the external methylene protons of the oxirane ring (e,f; orange circle). Also the in the furanic moiety of

the molecule the bond between the CH carbons (3, positive peak at 119,16 ppm on f<sub>1</sub>) and hydrogens (a) are shown by a peak highlighted with a red circle.

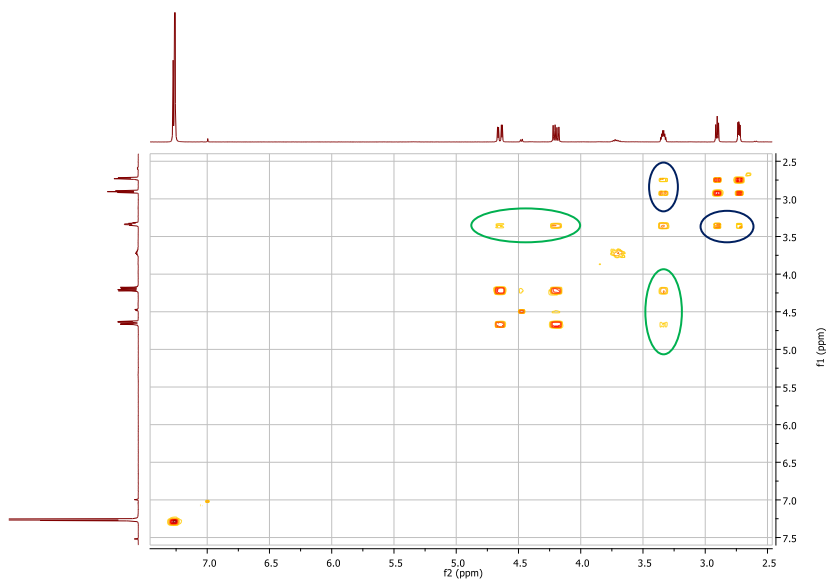


Figure 2.7 – COSY analysis of BOFD obtained by glycidylation

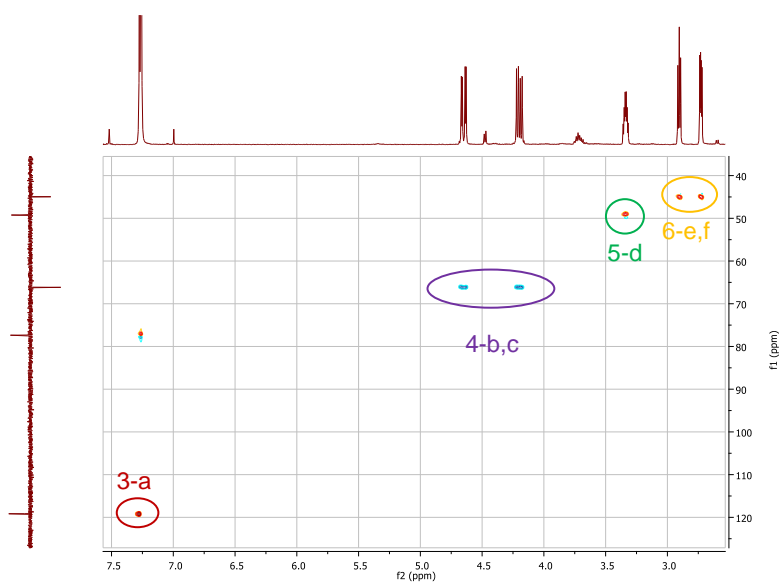
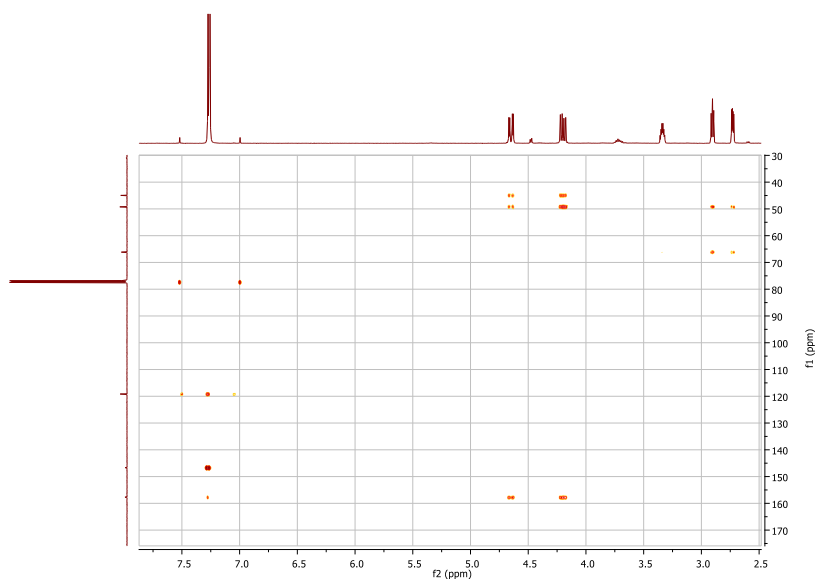


Figure 2.8 – HSQC analysis of BOFD obtained by glycidylation

**Figure 2.9** reports the HMBC spectroscopy for BOFD sample. In the graph a correlation of the C=O carbon (1) with the furanic (a) and the glycidyl (b,c) protons are evidenced. The furanic protons result correlated also to the furanic quaternary carbon, while glycidyl protons are also correlated to the carbons on the oxirane ring. Methylene protons of the oxirane ring are correlated to the tertiary carbon of oxirane ring and the glycidyl carbon directly linked with the ester group.

Epoxy Equivalent Weight (EEW) was evaluated according to an alternative method proposed by Garcia et al and Garea et al, which relates the ratio between the peak intensity of epoxy and furanic ring protons in the  $^1\text{H-NMR}$  spectra, with the polymerization degree  $n$ .<sup>19,23</sup>



**Figure 2.9** – HMBC analysis of BOFD obtained by glycidylation



In the specific case of BOFD, according to **Equation 2.3** and **Equation 2.4** reported in Experimental section,  $R_p = 0.39$  and  $R_t = 0.33$ . Consequently, the degree of polymerization  $n$ , evaluated by **Equation 2.5** is 0.17, that according to **Equation 2.2** results in  $EEW = 152.41$ .

### *Transesterification of dimethyl 2,5-furandicarboxylate and glycidol*

According to this procedure, BOFD was obtained through a transesterification reaction involving DM-FDCA, the dimethyl ester of furan 2,5-dicarboxylic acid, and glycidol, the simplest molecule bearing both an hydroxyl and an epoxy group.

Transesterification of DM-FDCA with diols is part of an industrially optimized two-step procedure for the production of *furanic/furanoate* polyesters (followed by a polycondensation).<sup>24,25</sup> This procedure requires high temperature (190-200 °C) and the use of potentially toxic catalysts<sup>26</sup>.

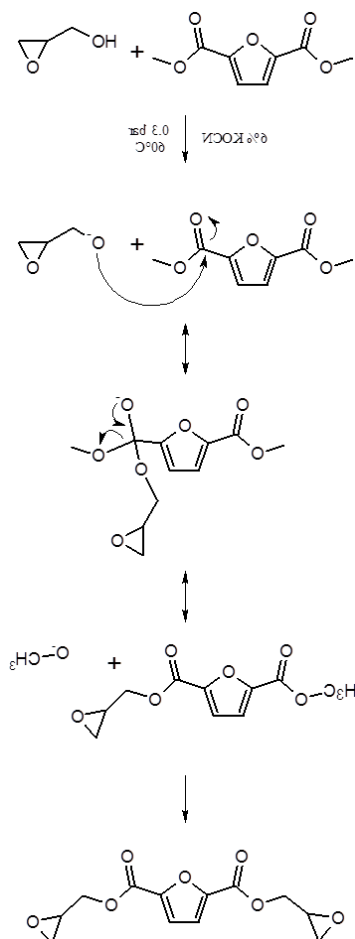
In this paper, the synthesis is carried out at relatively low temperature (60 °C). This is the maximum temperature that can be reached due to the high reactivity of glycidol, which easily polymerize, already at room temperature. An excess of glycidol was used in order to avoid as much as possible the formation of oligomers and a slight vacuum was used in order to allow stripping of methanol produced during the reaction, yet hindering the volatile solvent evaporation. An improvement introduced by the proposed procedure is the use of a cheap, non-toxic catalyst.

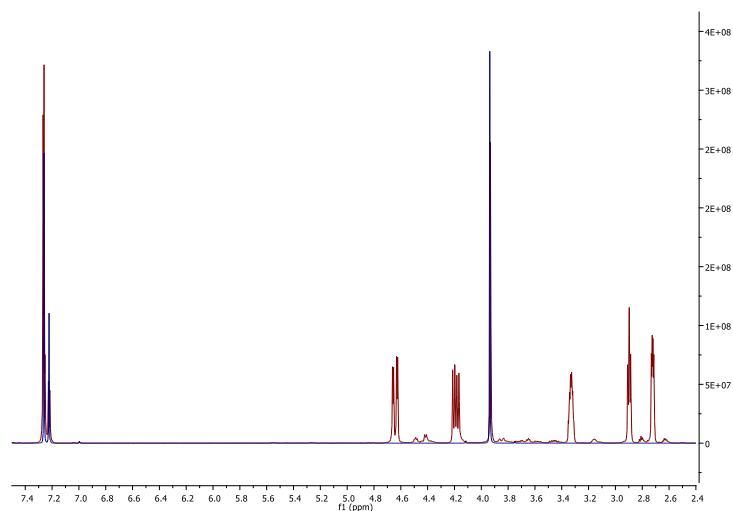
The procedure proposed for the production of BOFD by transesterification of DM-FDCA and glycidol results much more convenient than

## | Synthesis of furan-based epoxy monomers

the glycidylation process both in terms of synthetic conditions and in terms of yield. Transesterification indeed does not need a large excess of reagents and is performed at lower temperature and for shorter time than glycidylation. The crude product obtained in this case is a white crystalline product and the main impurity is easily identified by  $^1\text{H-NMR}$  analysis (**Figure 2.10**) being unreacted DMFDCA.

The transesterification proceeded in a single-step reaction schematized in **Scheme 2.2**.



**Scheme 2.2** – Mechanism of transesterification of DM-FDCA with glycidol

**Figure 2.10** –  $^1\text{H-NMR}$  spectra for the crude product of transesterification (red line) and DM-FDCA (blue line)

At room temperature, DM-FDCA and the catalyst were insoluble in the reaction mixture. However, heating resulted in a clear and transparent solution. The successful progress of the reaction was confirmed by the appearance of the mixture cooled down after 6 hours of reaction, which was viscous and transparent, with no evidence of precipitates. The so-obtained reaction mixture was washed with a mixture of ethyl acetate and distilled water; in this way, the undesired by-products were dissolved in the aqueous phase, while the diglycidyl ester product was recovered in the organic. The two phases were immiscible and thus it was possible to separate them, and recover the product soluble in the organic phase through evaporation of the solvent. A further chromatographic

purification was then performed to remove the residual unreacted DM-FDCA in the product.

The conversion of DM-FDCA into BOFD was confirmed by FTIR-ATR and mono- and multi-dimensional  $^1\text{H}$  and  $^{13}\text{C}$ -NMR analyses. The FTIR-ATR spectrum of BOFD obtained by transesterification presents the same peaks as the one performed on BOFD obtained by glycidylation. FTIR spectra for DM-FDCA and purified BOFD obtained by transesterification, are reported in **Figure 2.11**.

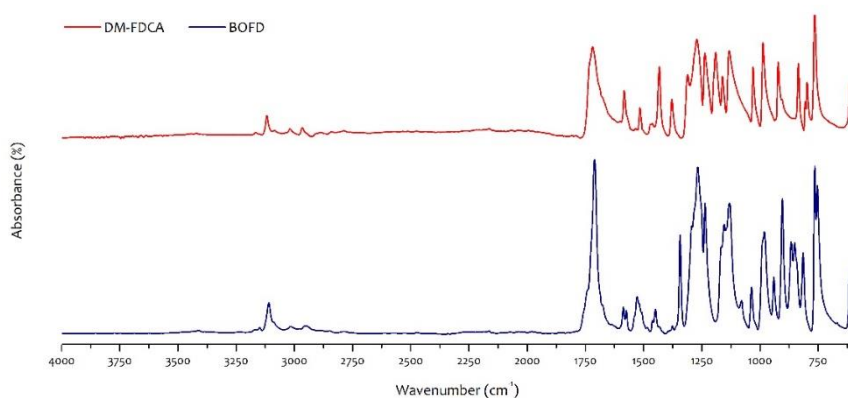


**Figure 2.11** – FTIR spectra for DM-FDCA and BOFD obtained by transesterification

Also in this case, the  $^1\text{H}$ -NMR spectrum of BOFD obtained by transesterification of DM-FDCA (**Figure 2.12**) displays the characteristic peaks of furanic proton at 7.27 ppm, the two double doublets at 4.65 ppm and 4.19 ppm due to the protons of methylene linked to the ester group, a sextet at 3.34 from methyne protons on oxirane ring, a triplet at 2.90 and a double doublet 2.73 due to protons of methylene on oxirane ring. These signals are in agreement with those reported for BOFD obtained by glycidylation, and in this case can be

noticed also a decrease of the intensity of signals given by oligomeric impurities at 4.47 and 3.70 ppm.

A further confirmation of transesterification effectiveness is given by  $^{13}\text{C}$ -NMR analysis (**Figure 2.13**) which gives the same results of the spectra previously shown for BOFD obtained by glycidylation

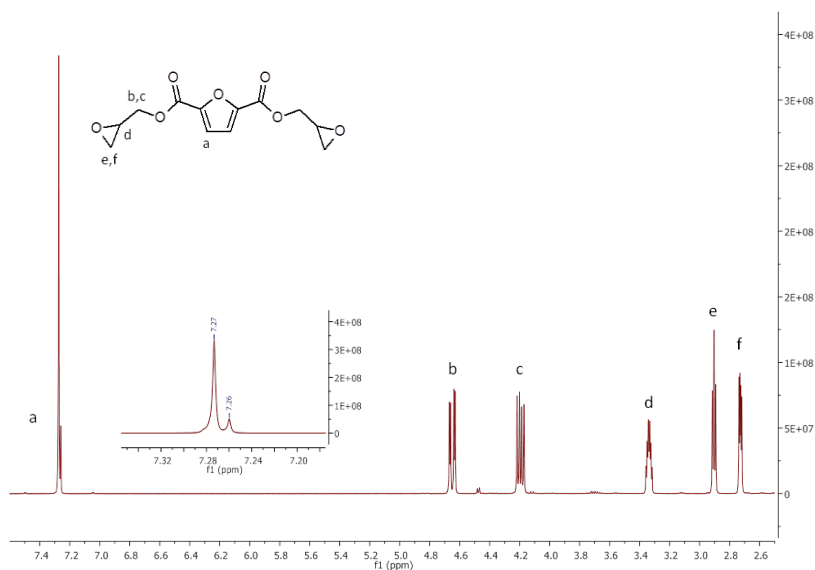


**Figure 2.12** –  $^1\text{H}$ -NMR spectra of BOFD obtained by transesterification of DM-FDCA

As for the EEW calculation, in the case of BOFD obtained by transesterification, the degree of polymerization  $n$ , was 0.011, providing also in this case a pure, low-molecular weight diepoxy compound, with EEW = 135.30.

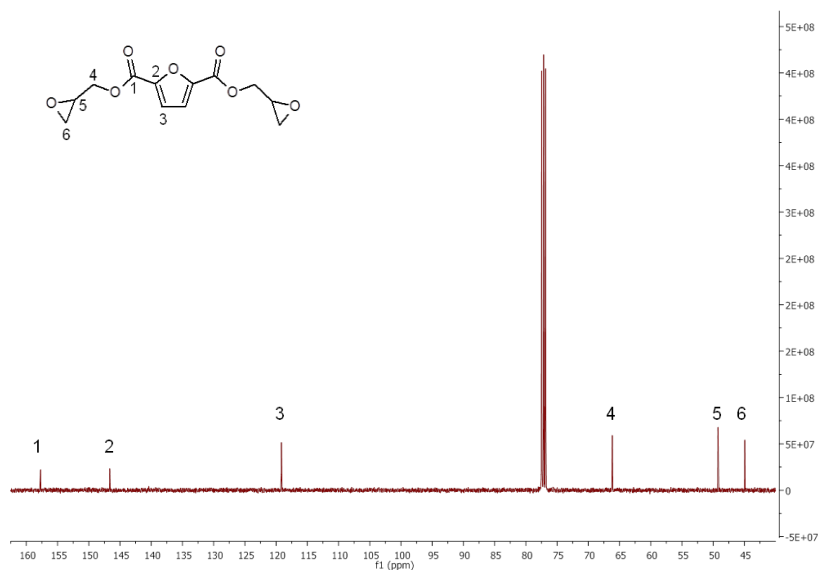


**Figure 2.13** – <sup>13</sup>C-NMR spectra of BOFD obtained by transesterification of DM-FDCA

Once we proved the structure of the monomeric diglycidyl ester of furan, an accurate thermal characterization was carried out by thermogravimetric analysis (TGA) and differential scanning calorimetry (DSC), to determine the thermal stability, as well as melting and crystallization temperatures of the compounds.

As can be noticed in TGA thermogram (**Figure 2.14**), BOFD resulted thermally stable up to 185 °C. At the end of this step a total weight loss of 95% was measured that could be attributed to the vaporization of the monomer. A second mass loss step is visible at temperatures above 300 °C, after which the residue at 650°C was 1%.

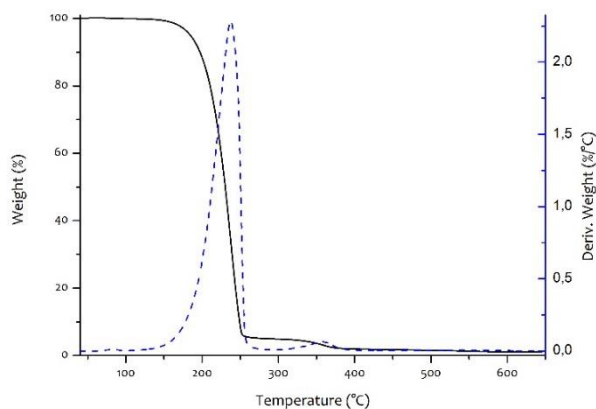


**Figure 2.14** –TGA analysis (10 °C/min, under nitrogen) of BOFD obtained by transesterification

DSC analysis (**Figure 2.15**) showed a sharp endothermic peak associated to the melting process of BOFD at 88 °C ( $\Delta H = 112 \text{ J/g}$ ). During the cooling scan the occurrence of crystallization was evidenced by the presence of an exothermic peak having a maximum at 47 °C (91 J/g). The second heating scan overlapped the first scan. The sharpness of the endothermic melting peak was a further evidence of the compound purity. Analogously the crystallization peak exhibit a shape that reminds of BOFD high purity, even if broader than the melting one; crystallization process is, indeed, more complex than melting and results in broader peaks also for pure compounds. The thermogram represented have been obtained at low heating (and cooling) rate; when faster analysis are performed no crystallization is detected during the cooling scan but the sample experience a cold crystallization during the second heating scan, in the same temperature range of crystallization detected by slower analyses.

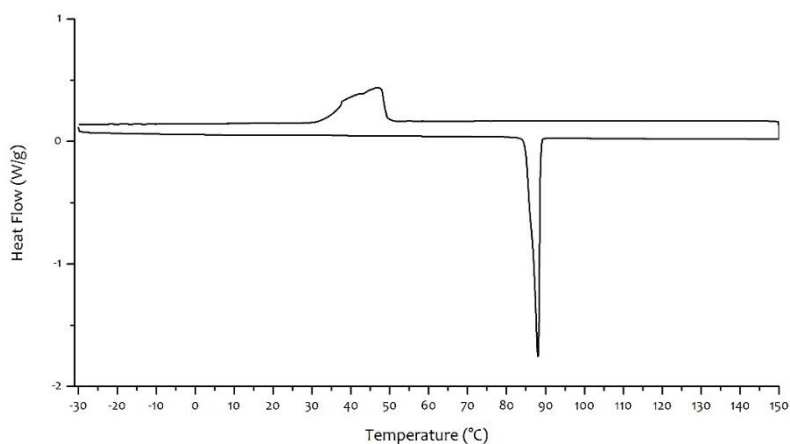


**Figure 2.15** – Dynamic DSC analysis (heating – cooling cycle) of BOFD obtained by transesterification

### 2.3.2. Synthesis and characterization of 2,5-bis[(oxiran-2-ylmethoxy)methyl]furan (BOMF)

With the aim of obtaining the 2,5-bis[(oxiran-2-ylmethoxy)methyl]furan (BOMF) epoxy monomer in good yield two synthetic routes already present in literature were experimented. The synthesis of BOMF was proposed by Hu et al. following a procedure very similar to BPA glycidylation. This procedure is based on the reaction of BHMf with epichlorohydrin followed by the addition of an alkaline solution to dehydrohalogenate the chlorohydrin intermediate formed<sup>27</sup> The chlorohydrin intermediate is produced thanks to the presence of tetrabutylammonium hydrogen sulfate, allowing the etherification reaction between epichlorohydrin oxirane ring and hydroxyl groups of BHMf. By our experience the procedure proposed by Hu et al., where a quite stoichiometric



amount of epichlorohydrin is used, leads to a resinous product from which it is impossible to extract the diglycidyl monomer.

As a consequence, an optimization of this process was attempted. First, a large excess of epichlorohydrin was used (20 times BHMf moles) that, in presence of a quaternary ammonium salt as catalyst, should improve reaction yield<sup>28</sup>. Moreover, other reaction conditions, such as temperature, time, catalyst were varied to get an optimized protocol. The pure monomer was anyway obtained only at low yield and the main products of these synthetic pathways were BOMf oligomers.

Cho et al.<sup>12</sup>, in a work where adhesive properties of several furan-based photo-cured epoxy resins were analyzed, proposed a different synthetic route for the obtainment of the diglycidyl ether of furan. A key difference in the process for the obtainment of BOMf relies in the reaction between epichlorohydrin and sodium hydroxide. While generally glycidylation reactions proceed through the formation of an halohydrin of the platform molecule (e.g. BPA for DGEBA, BHMf for BOMf) as intermediate, in the process proposed by Cho the intermediate was given by reaction between epichlorohydrin and sodium hydroxide in presence of the quaternary ammonium salt, at room temperature. This intermediate successively was reacted with BHMf previously dissolved in THF. The creation of this intermediate was used also by Yao et al.<sup>29</sup> two years later, to produce a diglycidyl divinyl ether by the reaction of only ECH and NaOH. The second step reaction, in which BHMf was finally glycidylated, was carried out in mild conditions ( $T = 50\text{ }^{\circ}\text{C}$ ) for short time (2 hours), under argon. The reaction product was then washed with water (in which dissolves the NaOH excess, the NaCl by-product and the catalyst) and extracted in ethyl acetate.

According to the procedure proposed by Cho to obtain the pure diglycidyl ether a further purification by flash chromatography was required.

The procedure described above was applied in our experimental work. By analyzing NMR spectra performed on crude products, after that an appropriate extraction with water an ethyl acetate was performed, no by-products were noticed. In some cases, only the presence of some residual epichlorohydrin, remained entrapped in the viscous BOMF and that could not be extracted with rotatory evaporator, was detected. Thus the purification by chromatography resulted unnecessary and was replaced by a repeated extraction with hexane. Hexane, being mixable with ECH insoluble with BOMF, when vigorously mixed with the reaction product was able to extract efficiently all the ECH excess. The absence of a chromatography purification step was of great advantage, allowing the use of reduced amounts of solvent and reaction time, keeping a high yield of reaction.

The so-obtained BOMF was fully characterized by FTIR-ATR analysis and mono and multi-dimensional NMR analysis.

The successful addition of glycidyl moieties was first confirmed by infrared spectroscopy by comparing the spectrum of BHMF with that of BOMF. As evidenced in **Figure 2.16**, the band at  $3500 - 3000 \text{ cm}^{-1}$  characteristic of BHMF disappeared, due to the formation of a new ester bond, associated to C-O stretching band at  $1075 \text{ cm}^{-1}$ , and the epoxy band between  $900$  and  $700 \text{ cm}^{-1}$  appeared in BOMF spectrum.

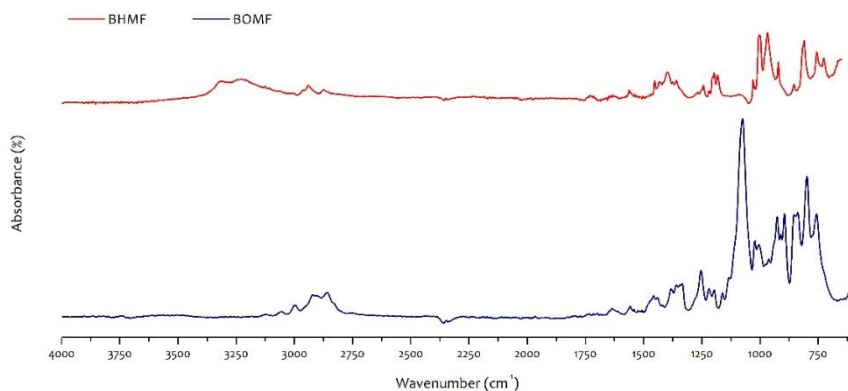


**Figure 2.16** – FTIR spectra of BOMF and BHMF

By  $^1\text{H}$  NMR analysis it was possible to detect the characteristic peaks of furanic proton at 6.27 ppm, a quartet at 4.48 ppm associated to the two methylene protons on the ether carbon bonded with the furan moiety. Peaks of glycidyl moieties are present as the two double doublets at 3.74 and 3.40, due to protons of methylene linked to the ether group, a sextet at 3.13 ppm due to methyne proton of oxirane ring and two double doublets, at 2.76 and 2.58 ppm, due to protons of methylene on oxirane. The spectrum reported in **Figure 2.17** is in agreement with the one reported by Hu et al. <sup>27</sup>.

In **Figure 2.18** is represented the  $^{13}\text{C}$ -NMR spectrum of BOMF where it can be noticed at 151.84 ppm the quaternary furanic carbon peak, at 110.30 ppm the CH furanic peak and at 65.21 the peak related to the ester  $\text{CH}_2$  linked with the furan. Regarding the glycidyl,  $\text{CH}_2$  ester carbon peak is present at 70.75 ppm while oxirane CH is present at 50.75 ppm and oxirane  $\text{CH}_2$  at 44.33 ppm.

## | Synthesis of furan-based epoxy monomers

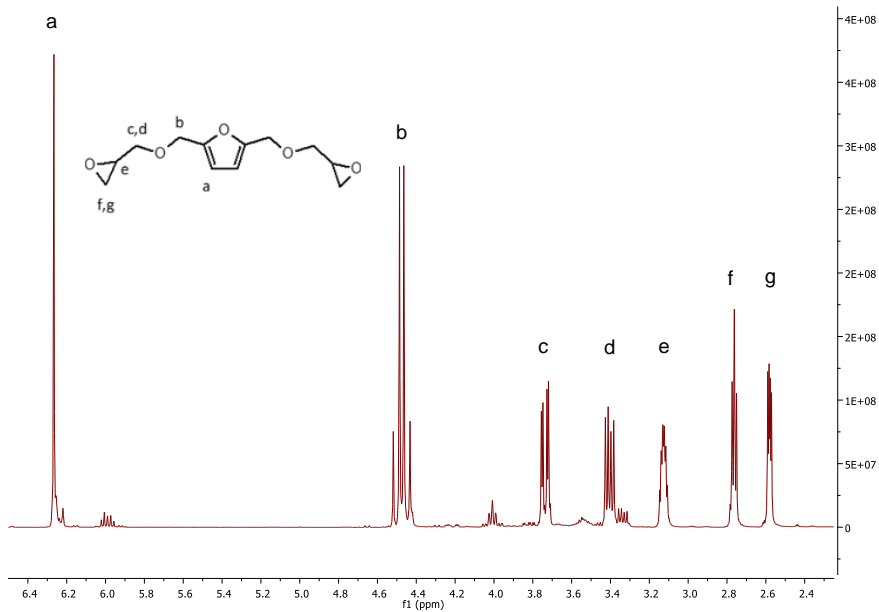


Figure 2.17 – <sup>1</sup>H-NMR spectrum of BOMF

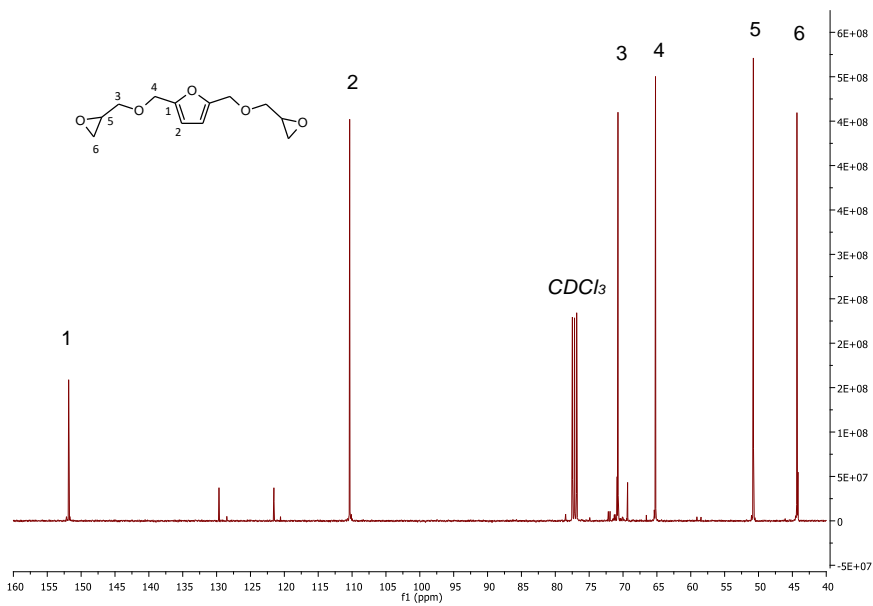
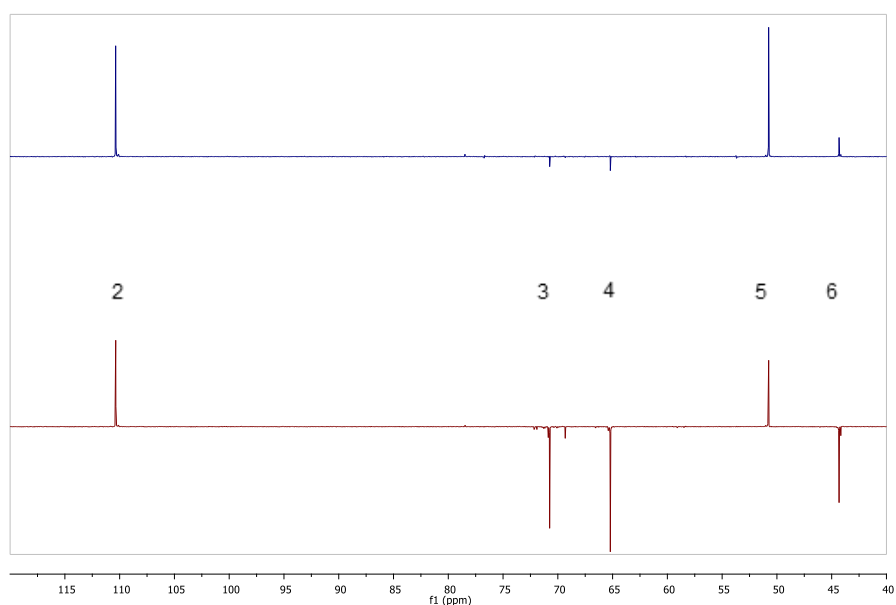


Figure 2.18 – <sup>13</sup>C-NMR spectrum of BOMF

Assignment of chemical shifts was made with the help of multi-dimensional analysis reported following. In **Figure 2.19** DEPT 90 (blue line) and DEPT 135 (red line) are compared. The two positive peaks at 110.30 and 50.75 ppm can be attributed to furanic and glycidyl CH respectively. Thanks to negative peaks present in DEPT 135 spectra, the signal at 70.75, 65.21 and 44.33 can be attributed to CH<sub>2</sub> carbons of glycidyl, oxirane and ester respectively. The absence of peaks at 151.84 ppm implies that it is related to the quaternary furanic carbon.



**Figure 2.19** – DEPT 90 (blue line) and DEPT 135 (red line) NMR analysis for BOMF

Interactions between adjacent protons are shown in the COSY spectra reported in **Figure 2.20**. Peaks highlighted by red square prove that both protons f and g are present on the same carbon forming the methylene on oxirane ring. Analogously, in the purple square c and d peaks are highlighted, and correlated in the glycidyl methylene. Cross-peaks highlighted by green and blue circles,

instead, show the relation between methyne protons on oxirane ring (e) with protons of glycidyl methylene (c,d), and methylene protons on oxirane ring (f,g), respectively. No correlation, as expected, is shown for furanic protons and methylene linked to furan.

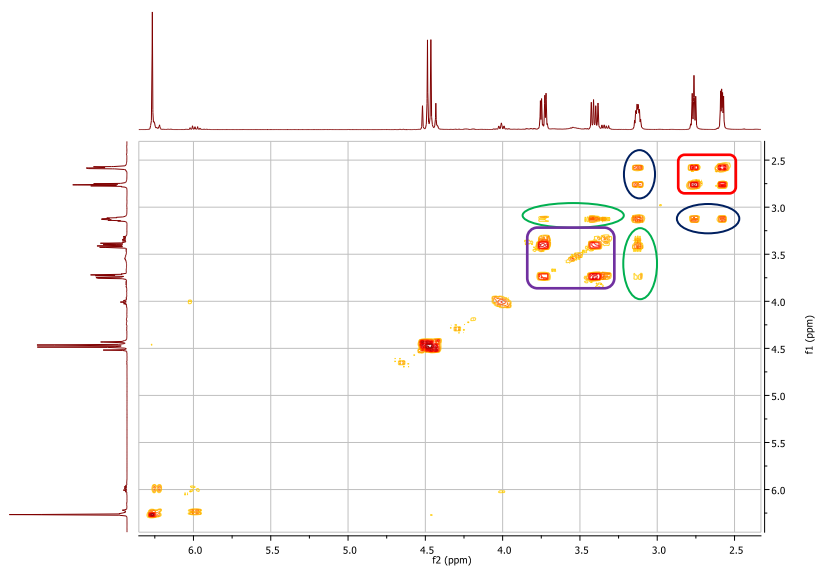


**Figure 2.20** – COSY analysis of BOMF

<sup>1</sup>J<sub>CH</sub> correlation between carbons and proton directly linked are expressed in HSQC spectra reported in **Figure 2.21**. Furanic hydrogens (a) and CH carbons (2) are directly correlated by the peak highlighted by the orange circle, while correlation between methylene carbon near to furan (4) with its own protons (b) is expressed in peak highlighted in light blue. Glycidyl methylene carbon (3) is instead correlated with both double doublets presents at 3.70 and 3.40 ppm (c,d) (red circle). Finally also correlation of oxirane methyne (5) and methylene

(6) carbons with protons at 3.13 (e) and 2.74 – 2.58 ppm (f,g) are expressed and highlighted by purple and green circles, respectively.

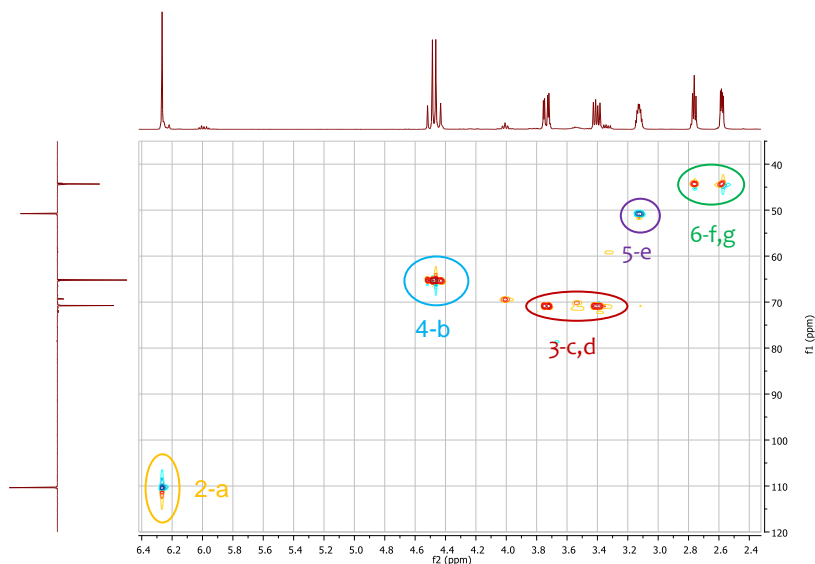


**Figure 2.21** – HSQC analysis of BOMF

In **Figure 2.22** is reported the HMBC spectroscopy for BOMF sample. Results obtained by HSQC analysis are confirmed and further information about disposition of groups within the molecule can be obtained. Proximity of quaternary furanic carbon (1) with protons previously assigned to furanic methyn (a) and methylene protons (b) is confirmed.

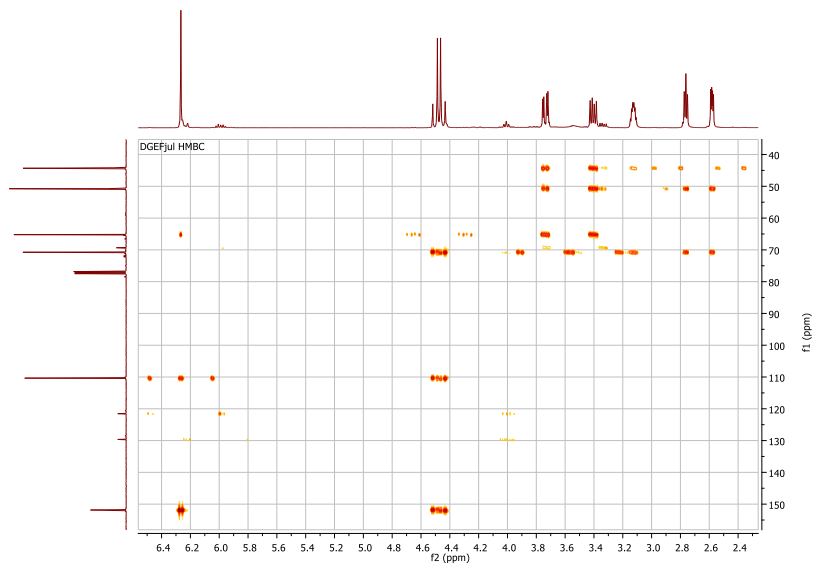


**Figure 2.22** – HSQC analysis of BOMF

BOMF was obtained in liquid form and when cooled up to  $-50^{\circ}\text{C}$  no crystallization was detected by thermal analysis. Viscosity of BOMF at  $30^{\circ}\text{C}$  was evaluated by rheological shear stress analysis and resulted being  $\eta = 0.03 \text{ Pa}\cdot\text{s}$ .

Thermal degradation was evaluated by thermogravimetric analysis under nitrogen flux. Thermogram is reported in **Figure 2.23**. A first evaporation step was detected before  $100^{\circ}\text{C}$  and protracted until  $120^{\circ}\text{C}$ , where 10 wt.% of sample was lost. It could be related to evaporation of water adsorbed. The main degradation process started just following the previous and in a range of  $140^{\circ}\text{C}$  (between  $120$  and  $260^{\circ}\text{C}$ ), leaving only a 20 wt.% residue with respect to the initial weight of the sample. Complete degradation was reached after a third degradation process occurring starting from  $230^{\circ}\text{C}$ .



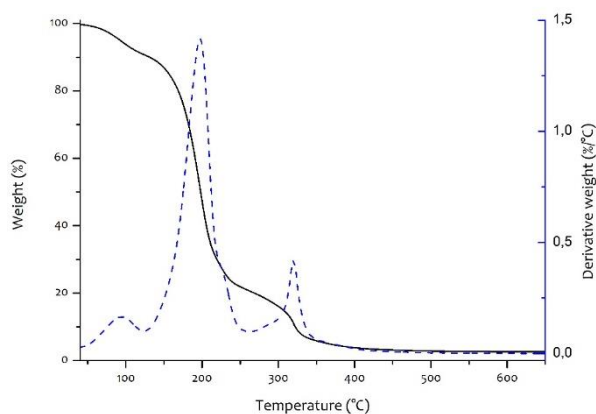


**Figure 2.23** – (a) Weight percent and (b) derivative weight percent of BOMF

## 2.4. Conclusions

---

In the present chapter, two new single-step synthetic routes are reported for the production of BOFD. Both approaches are of remarkable importance, as they combine the use of safer reagents, low temperatures and short reaction times, with the easiness of the procedures based on fast, single-step procedures.

FTIR-ATR, mono- and multi-dimensional analysis confirmed the theoretical structure for BOFD and evidenced a highly pure compound. Thermal properties of BOFD were determined through TGA and DSC analyses, which indirectly confirmed the purity of the compounds. In the present work, a proof of concept demonstrating the feasibility of simple and scalable routes to the synthesis of BOFD.

Further optimization of the presented synthesis protocols is needed to get higher reaction yields and consider BOFD obtained by these new procedures in applications for epoxy resins production. BOMF, instead, is obtainable in very good yield and with a very easy procedure being a valuable candidate for the obtainment of epoxy thermosets, as those that will be presented in following chapter.

## 2.5. Bibliography

---

1. Werpy T, Petersen G. Top Value Added Chemicals from Biomass. *US Dep energy*. 2004;1:76. doi:10.2172/926125
2. Bozell JJ, Petersen GR. Technology development for the production of biobased products from biorefinery carbohydrates—the US Department of Energy’s “Top 10” revisited. *Green Chem*. 2010;12(4):539-554. doi:10.1039/b922014c
3. Yang C, Huang C. Biotransformation of 5-hydroxy-methylfurfural into 2,5-furandicarboxylic acid by bacterial isolate using thermal acid algal hydrolysate. *Bioresour Technol*. 2016;214:311-318. doi:10.1016/j.biortech.2016.04.122
4. Boisen A, Christensen TB, Fu W, et al. Process integration for the conversion of glucose to 2,5-furandicarboxylic acid. *Chem Eng Res Des*. 2009;87:1318-1327. doi:10.1016/j.cherd.2009.06.010
5. Han X, Geng L, Guo Y, Jia R, Liu X. Base-free aerobic oxidation of 5-hydroxymethylfurfural to 2,5-furandicarboxylic acid over a Pt/C–O–Mg catalyst. *Green Chem*. 2016;18:1597-1604. doi:10.1039/c5gc02114f
6. Jiang N, You B, Boonstra R, Terrero Rodriguez IM, Sun Y. Integrating Electrocatalytic 5-Hydroxymethylfurfural Oxidation and Hydrogen Production via Co–P-Derived Electrocatalysts. *ACS Energy Lett*. 2016;1(2):386-390. doi:10.1021/acsenergylett.6b00214
7. Koopman F, Wierckx N, de Winde JH, Ruijsenaars HJ. Efficient whole-cell biotransformation of 5-(hydroxymethyl) furfural into FDCA, 2,5-furandicarboxylic acid. *Bioresour Technol*. 2010;101(16):6291-6296. doi:10.1016/j.biortech.2010.03.050
8. Yi G, Teong SP, Zhang Y. Base-free conversion of 5-hydroxymethylfurfural to 2,5-furandicarboxylic acid over a Ru/C catalyst. *Green Chem*. 2016;18:979-983. doi:10.1039/c5gc02114f
9. Kucherov FA, Romashov L V, Galkin KI, Ananikov VP. Chemical Transformations of Biomass-Derived C6-Furanic Platform Chemicals for Sustainable Energy Research,

## | Synthesis of furan-based epoxy monomers

- Materials Science, and Synthetic Building Blocks. *ACS Sustain Chem Eng.* 2018;6:8064-8092. doi:10.1021/acssuschemeng.8b00971
10. Yuan H, Li J, Shin H, et al. Improved production of 2,5-furandicarboxylic acid by overexpression of 5-hydroxymethylfurfural oxidase and 5-hydroxymethylfurfural/furfural oxidoreductase in *Raoultella ornithinolytica* BF60. *Bioresour Technol.* 2018;247:1184-1188. doi:10.1016/j.biortech.2017.08.166
  11. Avantium. <https://www.avantium.com/press-releases/alpla-joins-coca-cola-company-danone-avantiums-pef-bottle-development/>.
  12. Cho JK, Lee J, Jeong J, Kim B. Synthesis of carbohydrate biomass- based furanic compounds bearing epoxide end group (s) and evaluation of their feasibility as adhesives. *J Adhes Sci Technol.* 2013;27(18-19):2127-2138. doi:10.1080/01694243.2012.697700
  13. Hu F, La Scala JJ, Sadler JM, Palmese GR. Synthesis and characterization of thermosetting furan-based epoxy systems. *Macromolecules.* 2014;47(10):3332-3342. doi:10.1021/ma500687t
  14. Hu F, Yadav SK, La Scala JJ, Sadler JM, Palmese GR. Preparation and Characterization of Fully Furan-Based Renewable Thermosetting Epoxy-Amine Systems. *Macromol Chem Phys.* 2015;216(13):1441-1446. doi:10.1002/macp.201500142
  15. Shen X, Liu X, Wang J, Dai J, Zhu J. Synthesis of an Epoxy Monomer from Bio-Based 2,5-Furandimethanol and Its Toughening via Diels-Alder Reaction. *Ind Eng Chem Res.* 2017;56(30):8508-8516. doi:10.1021/acs.iecr.7b01624
  16. Tachibana Y, Torii J, Kasuya K, Funabashi M, Kunioka M. Hardening process and properties of an epoxy resin with bio-based hardener derived from furfural. *RSC Adv.* 2014;4:55723-55731. doi:10.1039/C4RA11636D
  17. Miao JT, Yuan L, Guan Q, Liang G, Gu A. Biobased Heat Resistant Epoxy Resin with Extremely High Biomass Content from 2,5-Furandicarboxylic Acid and Eugenol. *ACS Sustain Chem Eng.* 2017;5(8):7003-7011. doi:10.1021/acssuschemeng.7b01222
  18. Deng J, Liu X, Li C, Jiang Y, Zhu J. Synthesis and properties of a bio-based epoxy resin from

- 2,5-furandicarboxylic acid (FDCA). *RSC Adv.* 2015;5:15930-15939. doi:10.1007/s11426-013-5025-3
19. Garcia FG, Soares BG. Determination of the epoxide equivalent weight of epoxy resins based on diglycidyl ether of bisphenol A (DGEBA) by proton nuclear magnetic resonance. *Polym Test.* 2003;22(1):51-56. doi:10.1016/S0142-9418(02)00048-X
  20. Fache M, Viola A, Auvergne R, Boutevin B, Caillol S. Biobased epoxy thermosets from vanillin-derived oligomers. *Eur Polym J.* 2015;68:526-535. doi:10.1016/j.eurpolymj.2015.03.048
  21. Aouf C, Benyahya S, Esnouf A, Caillol S, Boutevin B, Fulcrand H. Tara tannins as phenolic precursors of thermosetting epoxy resins. *Eur Polym J.* 2014;55:186-198. doi:10.1016/j.eurpolymj.2014.03.034
  22. Aouf C, Le Guernevé C, Caillol S, Fulcrand H. Study of the O-glycidylation of natural phenolic compounds. The relationship between the phenolic structure and the reaction mechanism. *Tetrahedron.* 2013;69:1345-1353. doi:10.1016/j.tet.2012.11.079
  23. Garea SA, Corbu AC, Deleanu C, Iovu H. Determination of the epoxide equivalent weight (EEW) of epoxy resins with different chemical structure and functionality using GPC and <sup>1</sup>H-NMR. *Polym Test.* 2006;25(1):107-113. doi:10.1016/j.polymertesting.2005.09.003
  24. Papageorgiou GZ, Tsanaktis V, Bikiaris DN. Synthesis of poly(ethylene furandicarboxylate) polyester using monomers derived from renewable resources: thermal behavior comparison with PET and PEN. *Phys Chem Chem Phys.* 2014;16(17):7946-7958. doi:10.1039/C4CP00518J
  25. Carlos Morales-Huerta J, Martínez De Ilarduya A, Muñoz-Guerra S. Poly(alkylene 2,5-furandicarboxylate)s (PEF and PBF) by ring opening polymerization. *Polymer (Guildf).* 2016;87:148-158. doi:10.1016/j.polymer.2016.02.003
  26. Wang J, Liu X, Zhang Y, Liu F, Zhu J. Modification of poly(ethylene 2,5-furandicarboxylate) with 1,4-cyclohexanedimethylene: Influence of composition on mechanical and barrier properties. *Polym (United Kingdom).* 2016;103:1-8. doi:10.1016/j.polymer.2016.09.030
  27. Hu F, La Scala JJ, Sadler JM, Palmese GR. Synthesis and characterization of thermosetting

## | Synthesis of furan-based epoxy monomers

- furan-based epoxy systems. *Macromolecules*. 2014;47(10):3332-3342. doi:10.1021/ma500687t
28. Serra A, Cádiz V, Mantecón A, Martínez PA. New glycidyl ester compounds containing a preformed imide ring-I. *Tetrahedron*. 1985;41(4):763-768. doi:10.1016/S0040-4020(01)96454-3
29. Yao Y, Li Z, Qiu Y, et al. Unprecedented reactions: From epichlorohydrin to epoxyglycidyl substituted divinyl ether and its conversion into epoxyglycidyl propargyl ether. *Sci Rep*. 2015;5(September):1-6. doi:10.1038/srep14231







# Chapter 3.

---

Epoxy thermosets  
based on  
furan-diglycidyl  
ether



## 3.1. Introduction

---

Epoxy resins are among the most used thermosets in a wide range of applications, going from structural materials in aerospace or automotive industries, to insulation or electronics. Concerns about resource consumption, as well as about toxicity of materials for people and environment, are growing in last decades. This concern strongly pushed research on new building blocks and materials as valuable and more sustainable substitutes of currently produced materials.

Relevant replacement to petrol-derived molecules can be obtained by natural feedstocks. Biorefinery is an ascending technology in production of chemicals that allows the production also of substances with chemical structures different from petrol-derived ones<sup>1</sup>. The kind of molecules that can be obtained depends on biomass sources. The most exploited resources are plant oils and constituents of vegetal cells walls, i.e. cellulose, hemicellulose and lignin. Vegetable oils have been widely studied for epoxy resins production and, even if their chemical structure is made of long flexible chains that negatively affect mechanical properties of materials, research is leading to the obtainment of materials with good properties<sup>2-7</sup>. From lignin is instead possible to extract molecules composed by at least one aromatic moiety that can ensure good mechanical and thermal properties to the final material<sup>8-17</sup>. Anyway the extraction of small molecules from lignin is a very difficult and energy-consuming process, that make lignin not yet suitable as an efficient replacement of petrol-derived molecules.

A valuable feedstock for polymers can be cellulose, from which a variety of molecules with different chemical structures and properties can be easily produced. Among cellulose and carbohydrate derivatives, furanic molecules are nowadays already efficiently used in the production of bio-derived polyesters with improved properties compared to petrol-derived ones (i.e. polyethylene furanoate, PEF).

Despite the good properties shown from furanic molecules, comprehensive scientific studies on the production on furan-based epoxy resins are still lacking. Furanic epoxies from furandimethanol have been synthesized in 2013 by Cho et al<sup>18</sup>. and in 2014 by Hu et al<sup>19</sup>. The former work proposes different furan-based epoxy resins as adhesives while in the latter epoxy resins obtained from furan diglycidyl ether and benzene diglycidyl ether were compared. A further work by Hu aimed to the obtainment of fully furan based epoxy resins, by mean of a furanic amine as hardener<sup>20</sup>. Recently Shen et al.<sup>21</sup> starting from the furan diglycidyl ether obtained through a Diels–Alder cycloaddition reaction between the furan ring and maleimide moiety of N-hexyl maleimide, a toughening agent, obtained epoxy resins successively cured with isophoronediamine. The use of furan-based Diels-Alder adduct as curing agent for DGEBA has been proposed by Tachibaha et al.<sup>22</sup> However, very few works are present in literature in which other furanic molecules are used in epoxy resins production<sup>23,24</sup>.

In the work presented in this chapter, the carbohydrate derived compound 2,5-bis(hydroxymethyl)furan (BHMF) has been used as precursor for the synthesis of a bio-based epoxy monomer. In particular, from BHMF the 2,5-bis[(oxiran-2-ylmethoxy)methyl]furan (BOMF) was synthesized and employed for the realization of thermosetting resins using methyl nadic anhydride (MNA)

as a curing agent. Different initiators were tested in order to evaluate the most efficient one, and then a set of resins was obtained by changing the epoxy-to-anhydride ratio.

The aim of this experimental study was to synthesize furan-based systems with physico-chemical as well as mechanical properties comparable to traditional epoxy analogues. Afterward, the structure-to-property relationships were studied for potential coating applications in the field of food and beverage packaging, as discussed in Chapter 4.

## 3.2. Experimental section

---

### 3.2.1. Materials

The bio-based epoxy monomer 2,5-bis[(oxiran-2-ylmethoxy)methyl]furan (BOMF) was synthesized following the synthetic procedure presented in the *Experimental Section of Chapter 2*. Methyl-5-norbornene-2,3-dicarboxylic anhydride (methyl nadic anhydride, MNA, 90%), used as a curing agent, Poly(Bisphenol A-co-epichlorohydrin), glycidyl end-capped (DGEBA, average Mn ~377), used as reference epoxide, N,N-dimethylbenzylamine (BDMA, ≥99%) and 1-methylimidazole (1-MI, 99%) were purchased from Sigma-Aldrich. 2-methylimidazole (2-MI, 99%), was purchased from Acros Organics. All chemicals were used as received.

### 3.2.2. Preparation of epoxy/anhydride thermosets

Epoxy/anhydride reaction mixtures were prepared assuming that both BOMF epoxy monomer and MNA curing agent were bifunctional. In particular, the following formulations of reacting mixtures reported in **Table 3.1** were prepared.

**Table 3.1** – Samples denomination and compositions

<b>SAMPLE DENOMINATION</b>	<b>EPOXY/ANHYDRIDE MOLAR RATIO</b>	<b>INITIATOR</b>	<b>INITIATOR wt.%*</b>
<b>BOMF/MNA-BDMA0.5</b>	1:1	BDMA	0.5
<b>BOMF/MNA-1-MI0.5</b>	1:1	1-MI	0.5
<b>BOMF/MNA-2-MI0.5</b>	1:1	2-MI	0.5
<b>BOMF/MNA-2-MI1.5</b>	1:1	2-MI	1.5
<b>BOMF/MNA-2-MI3.0</b>	1:1	2-MI	3.0
<b>1BOMF/0.8MNA-2-MI0.5</b>	1:0.8	2-MI	0.5
<b>0.8BOMF/1MNA-2-MI0.5</b>	0.8:1	2-MI	0.5

\*of the total amount of epoxy monomer and curing agent

As a general procedure, a mixture containing the proper amounts of epoxy monomer, curing agent and catalyst was prepared by adding all the components at the same time, at room temperature under magnetic stirring to form a homogeneous viscous system. In case of DGEBA containing samples a degassing step using a desiccator was necessary.

For selected formulation two sets of thermosets were obtained by applying two different cure and post-cure programs. More specifically, the thermal treatments applied were the following:

Cure at  $T = 130\text{ }^{\circ}\text{C}$  for  $t = 2\text{ h}$ ; post-cure at  $T = 180\text{ }^{\circ}\text{C}$  for  $t = 1\text{ h}$

Cure at  $T = 130\text{ }^{\circ}\text{C}$  for  $t = 2\text{ h}$ ; post-cure at  $T = 180\text{ }^{\circ}\text{C}$  for  $t = 1\text{ h}$  and  $T = 230\text{ }^{\circ}\text{C}$  for  $t = 1\text{ h}$

### 3.2.3. Methods

A TA Instrument DSC Q2000, equipped with Refrigerator Cooling System (RCS), was used for calorimetric analysis (DSC), under inert nitrogen flux ( $50\text{ mL min}^{-1}$ ). Samples for DSC analysis were prepared immediately after the preparation of mixtures: about 6-8 mg of resin were sealed in aluminum pans and stored at  $-30\text{ }^{\circ}\text{C}$  for a maximum of 2 days. Dynamic measures from 25 to  $200\text{ }^{\circ}\text{C}$  at 1.5 and  $10\text{ }^{\circ}\text{C/min}$  heating rates and isothermal analysis at 90, 100, 110, 120,  $130\text{ }^{\circ}\text{C}$  were performed. A second scan at  $20\text{ }^{\circ}\text{C/min}$  to  $-10\text{ }^{\circ}\text{C}$  and a following heating scan at  $10\text{ }^{\circ}\text{C/min}$  to  $200\text{ }^{\circ}\text{C}$  were performed on all the samples. Numerical analysis was performed using an Origin software.

A Thermo MARS III rheometer interfaced with a iN20 Nicolet FT-IR spectrophotometer by a Rheonaut temperature controller, were used to perform the combined rheological and attenuated total reflectance infrared spectroscopy (ATR FT-IR) analysis. Chemo-rheological tests were performed on plate-plate geometries (20 mm diameter and 0.8 mm gap) at a fixed frequency ( $\omega$ ) of  $10\text{ rad/s}$  and deformation ( $\gamma$ ) in auto-strain mode of  $15\% \pm 15\%$ . Two kinds of measurements were performed: dynamic measurement by varying the

temperature from 50 to 150 °C, at a heating rate of 1.5 °C/min and isothermal analysis at 110 °C. The temperature of crossover of the values of storage ( $G'$ ) and loss ( $G''$ ) moduli was considered as the temperature of gelation ( $T_{gel}$ ). Simultaneous to rheological measurements, ATR FT-IR analysis were carried out on the reacting epoxy/anhydride mixtures. Spectra were acquired as single beam spectra in the range of 4000-400  $\text{cm}^{-1}$  with a resolution of 4  $\text{cm}^{-1}$  and 8 scans; before each analysis different background spectra were collected at different temperatures in the above-mentioned temperature range. Data were first processed with Omnic software to subtract the appropriate background, then spectra were exported to the PerkinElmer TimeBase software to perform the time-dependent analysis.

Thermogravimetric analysis (TGA) was performed by using a TA Instrument TGA 500 thermobalance. Tests were carried out from 25 to 750 °C at a heating rate of 10 °C/min; different measurements were performed under a 60  $\text{mL min}^{-1}$  nitrogen or air flux respectively.

The crosslink density was measured by swelling test in THF. Samples of about 30 – 40 mg were weighed, the weight recorded as  $W_d$ , and immersed in 20 ml of THF. After 24h, the sample were recovered, blotted, weighed, and weight recorded as  $W_s$ . The swelling index  $SI$  was evaluated by the following equation, as mean value on 3 tests for each sample.

$$SI [\%] = \frac{W_s - W_d}{W_d} \quad \text{Equation 3.1}$$

To perform tensile tests on cured samples an INSTRON 4505 dynamometer equipped with a 100 kN load cell was used. 3 specimens for each



composition were tested with 2mm/min crosshead speed in environmental conditions of 20 °C and 50% humidity.

### 3.2.4. Kinetic models

#### Calorimetric models

The kinetic studies on the curing process of BOMF and MNA mixture were carried out by DSC data. In the field of the calorimetric analysis basilar for kinetic studies is the assumption that the heat flow ( $dH/dt$ ) detected during the analysis is directly proportional to the conversion rate ( $d\alpha/dt$ ).<sup>25,26</sup> Explicitly:

$$\frac{d\alpha}{dt} = \frac{1}{\Delta H_{tot}} \frac{dH}{dt} \quad \text{Equation 3.2}$$

where  $\Delta H_{tot}$  is the heat needed to complete the reaction.

It follows from the relation between the degree of conversion  $\alpha$  and the heat  $\Delta H_t$  evolved during the chemical reaction:

$$\alpha = \frac{\Delta H_t}{\Delta H_{tot}} \quad \text{Equation 3.3}$$

In literature<sup>27-30</sup> several kinetic models have been developed to study the extent of cure, the most general expression being

$$\frac{d\alpha}{dt} = k f(\alpha) \quad \text{Equation 3.4}$$

where  $f(\alpha)$  is the reaction model and  $k$  a rate constant generally expressed in the Arrhenius form

$$k = A e^{(-E/RT)} \quad \text{Equation 3.5}$$

where  $A$  is a preexponential factor,  $R$  is the gas constant,  $T$  is the absolute temperature and  $E$  is the activation energy.

The reaction model reflects the reaction mechanism and for epoxy curing reactions takes generally the form of an  $n^{\text{th}}$ -order kinetic model (**Equation 3.5**) or an autocatalytic process (Kamal model, **Equation 3.6**).

$$\frac{d\alpha}{dt} = (1 - \alpha)^n \quad \text{Equation 3.6}$$

$$\frac{d\alpha}{dt} = (k_1 + k_2\alpha^m)(1 - \alpha)^n \quad \text{Equation 3.7}$$

Kamal model describes generally very well systems in which reaction rate is increases due to the catalytic effect of the groups produced during the reaction itself. Anyway, in some cases, when cure completion is not reached, is necessary to take into account that maximum conversion reached is  $\alpha_{\text{max}} \neq 1$ <sup>26,31</sup> and the reaction kinetics can be fitted by the following equation:

$$\frac{d\alpha}{dt} = (k_1 + k_2\alpha^m)(\alpha_{\text{max}} - \alpha)^n \quad \text{Equation 3.8}$$

## Kinetic analysis by FT-IR

FT-IR spectroscopy is often used to identify chemical structures because functional groups give rise to characteristic bands both in terms of intensity and position (frequency). Moreover, time acquired infrared spectra can be used for a quantitative analysis of the monitored functional groups involved in the curing process.

The experimental relative conversion ( $\alpha$ ), for the species consumption, can be expressed as follows:<sup>32</sup>

$$\alpha = \frac{c_0 - c_t}{c_0} = 1 - \frac{c_t}{c_0} \quad \text{Equation 3.9}$$

Considering the Lambert-Beer relation holds true

$$\alpha = 1 - \frac{A_t}{A_0} \quad \text{Equation 3.10}$$

where  $C$  is the species molar concentration and  $A_t$  is the monitored absorbance area, the subscripts  $0$  and  $t$  stand for zero and current time, respectively **Equation 3.9** was used to determine conversion of disappearing groups while **Equation 3.10** was used to evaluate the conversion degree of groups that are formed during the process<sup>33</sup>.

$$\alpha = \frac{A_t - A_0}{A_\infty - A_0} \quad \text{Equation 3.11}$$

The term  $A_\infty$  in the last equation refers to the final absorbance value of the species monitored.

In the specific case of this work, to evaluate the epoxy group reactivity during curing process the band between  $950$  and  $870 \text{ cm}^{-1}$  was monitored. However, in this region characteristic epoxy and anhydride groups absorptions are overlapped so the absorbance area related only to the epoxy group must be evaluated by the following equation:

$$A_{t,epox} = A_t - (1 - \alpha_{anh}) \cdot A_t \cdot F \quad \text{Equation 3.12}$$

where  $A_{t,epox}$  is the effective absorbance of epoxy group,  $A_t$  is absorbance area of the entire  $950 - 870 \text{ cm}^{-1}$  band,  $\alpha_{anh}$  is anhydride conversion previously evaluated following peaks at  $1855$  and  $1776 \text{ cm}^{-1}$  and  $F$  is the contribute given by anhydride to the band<sup>34</sup>.  $F$  value was evaluated operating a deconvolution in the region between  $950$  and  $870 \text{ cm}^{-1}$  to estimate the relative contribution of the epoxy peak at  $913 \text{ cm}^{-1}$  and anhydride at  $895 \text{ cm}^{-1}$ , to the band.

In all mathematical analysis the area of the invariant band between  $3080$  and  $2770 \text{ cm}^{-1}$ , associated to carbon-hydrogen stretching, was used as a reference.

## 3.3. Results and discussion

---

### 3.3.1. Optimization of curing formulations

The process of epoxy crosslinking involves the use of opportune curing agents. There is a variety of curing agents commercially available, mostly including amines, anhydride, dicarboxylic acids. The choice depends on the processing conditions, such as curing time, pot life, viscosity, etc. and the end-use requirements in terms of chemical, mechanical and thermal resistance<sup>35</sup>.

Among anhydrides, methyl nadic anhydride, hexahydrophthalic anhydride, trimellitic anhydride, phthalic anhydride and methyl hexahydrophthalic anhydride are the most extensively employed for curing of epoxy resins<sup>8</sup>. In order to improve the system reactivity the tertiary amines are often used as catalysts to accelerate the gel time and cure achievement at opportune temperature conditions<sup>36</sup>.

Another key factor in the optimization of curing process is the relative anhydride/epoxy ratio, which can affect the performance of the final product. Usually an excess of epoxy is needed, with an anhydride/epoxy equivalent ratio ranging from 0.5–0.9 to avoid competition between etherification and esterification reactions<sup>7,37,38</sup>. However, some literatures exists dealing with the use of an excess of anhydride<sup>36,39</sup>.

In this frame, in the present work MNA was selected as curing agent, since, analogously to BOMF, it is liquid at room temperature. Therefore, the two components were easily mixed achieving a homogeneous material. In order to get a detailed insight on the curing mechanism involved in the formation of the

epoxy network, three different formulations were prepared, by selecting three epoxy-to-anhydride molar ratios (R), and precisely R = 1:1, 1:0.8, and 0.8:1.

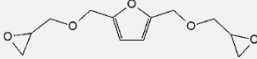
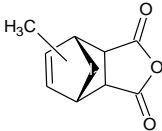
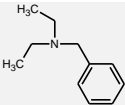
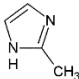
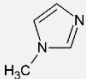
Moreover, the effect of the nature and amount of initiator on the curing behavior were evaluated. More specifically, the reaction mixtures containing the same percentages (0.5 wt.% of initiator with respect to the total weight of epoxy+anhydride) of different initiators, namely BDMA, 1-MI and 2-MI were evaluated. BDMA is a tertiary amine and cannot react by addition with epoxy groups but it works as catalyst for curing reactions of epoxides with acid anhydrides as well as polyamines and polyamide<sup>40</sup>. Imidazoles are good accelerators for anhydride-epoxy resins and if used as curing agents they initiate polymerization via an anionic mechanism. The several derivatives of imidazole, where hydrogen is substituted with the most varied groups, have different physical properties and are used as catalysts in different conditions; among them 2-MI, however, is used only as accelerator and not as curing agent<sup>35</sup>.

Then, the best performing one (2-MI) was selected for further analysis, aimed at determining the proper amount of initiator required to optimize the curing process. To this purpose, three different percentages of 2-MI were analyzed, and precisely 0.5, 1.5 and 3.0 wt.% on the total weight of epoxy+anhydride mixture. Chemical structure of reactants and initiators used for the different formulations are reported in **Table 3.2**

The crosslinking mechanism of epoxy with anhydride is highly complex, due to the large amount of competitive reactions that may occur. The network formation can follow both etherification and esterification reactions by reason of possible inter- and intramolecular reactions<sup>7,41,42</sup>. Catalysts used can be broadly categorised in four classes: bases, onium compounds (phosphonium or aluminium halides), metals and cationic catalysts (Lewis acids). In particular

among bases secondary and, to a higher extent, tertiary amines show good catalytic properties<sup>43</sup>.

**Table 3.2** – List of reactants and initiators used in the synthesis of bio-based epoxy resins

NAME	ACRONYM	STRUCTURE	FUNCTION
<b>2,5-bis[(oxiran-2-ylmethoxy)methyl]furan</b>	BOMF		Epoxy monomer
<b>Methyl-5-norbornene-2,3-dicarboxylic anhydride</b>	MNA		Anhydride curing agent
<b>N,N-dimethylbenzylamine</b>	BDMA		Initiator
<b>2-methylimidazole</b>	2-MI		Initiator
<b>1-methylimidazole</b>	1-MI		Initiator

The reaction proceeds through an initiation step involving the nucleophilic attack of the amine to either the oxirane ring (**Scheme 3.1a**) or the anhydride (**Scheme 3.1b**) that generates a zwitterion intermediate containing a quaternary nitrogen cation and an active oxyanion. The latter reacts with the anhydride or the epoxy group giving rise to a carboxylate (**Scheme 3.1-propagation**) or alkoxide anion, respectively, which initiate the chain-wise polymerization<sup>4,7,41,42,44-46</sup>. The formed anion reacts with the epoxy group and then with the anhydride, propagating the chain growth through an alternating copolymerization anionic mechanism<sup>47</sup>.



BOMF/MNA-BDMA0.5 and BOMF/MNA-1-MI0.5 clearly showed a bimodal behavior, while such feature was not observed in the case of BOMF/MNA-2-MI0.5, suggesting a different mechanism of initiation and propagation of the curing reaction.

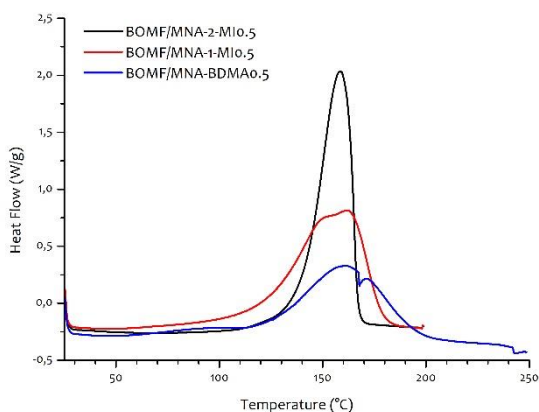


**Figure 3.1** – DSC Dynamic heating scan curves at 10 °C/min heating rate of BOMF/MNA-BDMA0.5, BOMF/MNA-1-MI0.5 and BOMF/MNA-2-MI0.5 mixtures

**Table 3.3** - Values of total enthalpy of reaction ( $\Delta H_{tot}$ ), peak temperature ( $T_p$ ) and onset temperature ( $T_{onset}$ ) obtained from dynamic DSC analysis on reacting mixtures containing the same percentages of different initiators

SAMPLE	$\Delta H_{tot}$ [J/g]	$T_p$ [°C]	$T_{onset}$ [°C]
BOMF/MNA-BDMA0.5	208.8	161.4	120.2
BOMF/MNA-1-MI0.5	257.2	162.2	120.5
BOMF/MNA-2-MI0.5	264.9	158.4	139.4



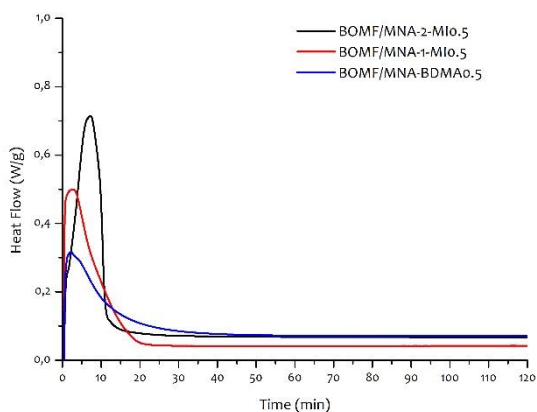


**Figure 3.2** – DSC isothermal curves at  $T = 130\text{ }^{\circ}\text{C}$  of BOMF/MNA-BDMA<sub>0.5</sub>, BOMF/MNA-1-MI<sub>0.5</sub> and BOMF/MNA-2-MI<sub>0.5</sub> mixtures

**Table 3.4** – Total heat of reaction ( $\Delta H_{tot}$ ) and peak time ( $t_p$ ) of systems with different initiators, cured at  $130\text{ }^{\circ}\text{C}$

SAMPLE	$\Delta H_{tot}$ [J/g]	$t_p$ [min]
BOMF/MNA-BDMA <sub>0.5</sub>	425.5	2.2
BOMF/MNA-1-MI <sub>0.5</sub>	396.6	2.7
BOMF/MNA-2-MI <sub>0.5</sub>	538.2	7.2

Isothermal analysis (**Figure 3.2**) showed an interesting overview on the reaction mechanism involved in the curing process. For samples containing 1-MI and BDMA, which are tertiary amines, the reaction proceeded with an  $n^{\text{th}}$ -order reaction mechanism, being the highest conversion rate at zero time (peak time are reported in Table 3.4). On the other hand, when a secondary amine such as 2-MI, was used as initiator, an autocatalytic reaction mechanism occurred, highlighted by the maximum of conversion rate at 7 min.<sup>48</sup> Moreover, a sharp

curve associated to the cure of BOMF/MNA-2-MI<sub>0.5</sub> was evidenced, demonstrating a rapid and more controllable process.

Taking all these considerations into account, 2-MI was chosen as the most suitable initiator for the cure of BOMF/MNA resins. Further calorimetric analyses were performed to choose the right amount of initiator: 0.5, 1.5 and 3.0 wt.% were selected as testing amounts. DSC thermograms for both dynamic and isothermal mode analysis are reported in **Figure 3.3**.

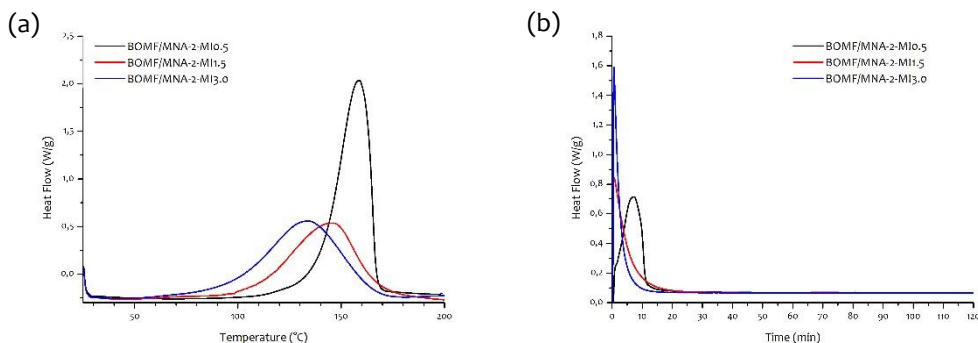


**Figure 3.3** – (a) DSC heating scan at 10 °C/min heating rate and (b) Isothermal curves at T = 130 °C of samples containing different percentages of 2-MI

**Table 3.5** – Values of total enthalpy of reaction ( $\Delta H_{tot}$ ), peak temperature ( $T_p$ ) and onset temperature ( $T_{onset}$ ) obtained from dynamic DSC analysis of resins with 2-MI as initiator in different percentages

SAMPLE	$\Delta H_{tot}$ [J/g]	$T_p$ [°C]	$T_{onset}$ [°C]
<b>BOMF/MNA-2-MI<sub>0.5</sub></b>	264.9	158.4	139.4
<b>BOMF/MNA-2-MI<sub>1.5</sub></b>	224.9	146.1	107.4
<b>BOMF/MNA-2-MI<sub>3.0</sub></b>	219.5	134.1	94.8

The interpretation of these thermograms must be done taking into account the experimental evidences. In facts, during the preparation of samples with 1.5 and 3.0 wt.% of initiators (more remarkably in the latter case), it was possible to notice the quite instantaneous increase in viscosity of the mixture once the initiator was added, suggesting that the cure reaction started immediately, and reached soon the gelation point. For this reason, the decrease in  $\Delta H_{tot}$  on increasing the initiator amount, can be attributed to a partial cure begun before starting calorimetric analysis. Analogously for the isotherm analysis, the maximum conversion rate at the starting time can be attributed to the already ongoing reaction rather than to an  $n^{th}$ -order mechanism. BOMF/MNA-2-MI<sub>3.0</sub> and BOMF/MNA-2-MI<sub>0.5</sub> resulted completely cured after 15 minutes; the latter undergoes complete curing during the isothermal analysis while the sample with much higher amount of 2-MI, already gelled at  $T_{amb}$  during sample preparation. A residual curing reaction is indeed present for BOMF/MNA-2-MI<sub>1.5</sub> protracted for 20 minutes. Delay in completion of the cure reaction may be due to diffusion processes needed to complete the network formation, by reason of partial hinderance of already formed crosslinked structure

Therefore, an amount of 0.5 wt.% of 2-MI was selected for the preparation of BOMF/MNA resins in different epoxy/anhydride ratios. Consequently, calorimetric and chemo-rheological analysis were carried out on BOMF/MNA-2-MI<sub>0.5</sub>, 1BOMF/0.8MNA-2-MI<sub>0.5</sub>, 0.8BOMF/1MNA-2-MI<sub>0.5</sub>, (**Table 3.1**).

### 3.3.2. Thermokinetics study of crosslinking

#### DSC analysis

The study on curing process of epoxy/anhydride reacting mixtures was first performed through differential scanning calorimetry in both dynamic and isothermal mode.

DSC curves collected at different heating rates (1,5 and 10 °C/min) on the three formulations BOMF/MNA-2-MI0.5, 1BOMF/0.8MNA-2-MI0.5, 0.8BOMF/1MNA-2-MI0.5, are reported in **Figure 3.4**, **Figure 3.5** and **Figure 3.6** respectively, and calculated peak temperature ( $T_p$ ), total enthalpy of reaction ( $\Delta H_{tot}$ ) and glass transition temperature ( $T_g$ ) values depicted in **Table 3.6**.

All the systems exhibited a single exothermic peak throughout the experiments at both heating rates. For the higher heating rate the peak temperature ( $T_p$ ) shifted to higher values (**Table 3.6** and **Figure 3.4**, **Figure 3.5** and **Figure 3.6**).  $T_p$  values of 1BOMF/0.8MNA-2-MI0.5 were generally lower than those of BOMF/MNA-2-MI0.5 and 0.8BOMF/1MNA-2-MI0.5, independently of the heating rate. This trend can be related to the low viscosity (0.03 Pa\*s) of the epoxy compound present in molar excess that caused an increase of the curing rate, as the mobility of growing macromolecular units not yet reacted was favoured. However, the excess of epoxy monomer was also responsible for a lower conversion degree due to the under-stoichiometric anhydride. For this reason, in the case of 1BOMF/0.8MNA-2-MI0.5 the heat of reaction was lower with respect to the values calculated for BOMF/MNA-2-MI0.5 and 0.8BOMF/1MNA-2-MI0.5.

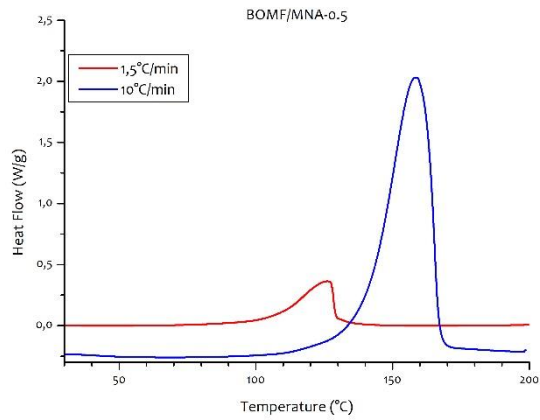


Figure 3.4 – DSC heating scan curves at different heating rates of BOMF/MNA-2-MI0.5

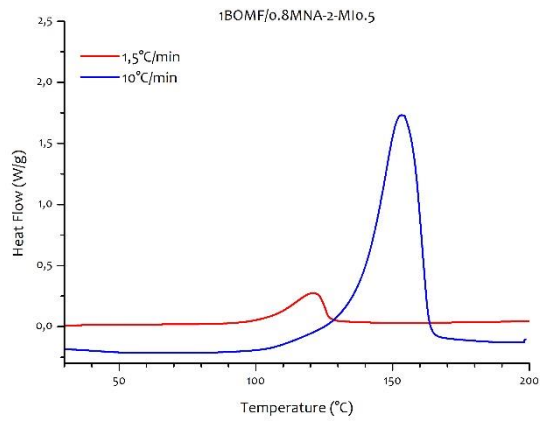
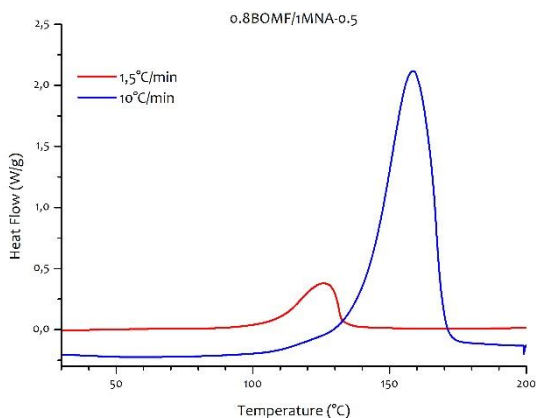


Figure 3.5 – DSC heating scan curves at different heating rates of 1BOMF/0.8MNA-2-MI0.5



**Figure 3.6** – DSC thermograms in dynamic mode at different heating rates of 0.8BOMF/1MNA-2-MI0.5

A second heating ramp was also performed on all samples, to check the occurrence of any residual post-cure reactions and to calculate the  $T_g$  values (reported in **Table 3.6**). BOMF/MNA-2-MI0.5 and 0.8BOMF/1MNA-2-MI0.5 showed higher  $T_g$ s values than those measured for 1BOMF/0.8MNA-2-MI0.5, confirming that the defect of anhydride in 1BOMF/0.8MNA-2-MI0.5 affected the extent of crosslinking also resulting in lower  $T_g$ s. Moreover, the excess of unreacted monomer acts as plasticizers for the cured material.

To get a further insight on the peculiar behavior of 1BOMF/0.8MNA-2-MI0.5, an additional measurement at 10 °C/min heating rate from 25 to 300 °C (**Figure 3.7**) was carried out. In this way it was possible to verify the occurrence of homopolymerization due to the presence of the excess of epoxy monomer. In literature several cases of study are presented where in epoxy/anhydride resins the epoxy monomer is present in excess.<sup>7,39,49</sup> and the cure process analyzed by calorimetric analysis showed a second exothermic peak below 200 °C. In very few cases, instead, homopolymerization process is already present

before temperature of 200 °C is reached.<sup>36,47</sup> As expected, for our system, the heat flow curve started increasing at 200 °C as soon as the homopolymerization occurred. The  $T_g$  value of the cured system, evaluated from the second heating scan, was 60 °C (**Figure 3.8**), thus significantly higher than the  $T_g$  measured before homopolymerization ( $T_g = 3.0$  °C) and comparable with the  $T_g$  of the system with excess anhydride.

**Table 3.6** – Peak temperature ( $T_p$ ), total enthalpy of reaction ( $\Delta H_{tot}$ ) and glass transition temperature ( $T_g$ ) for mixtures with different epoxy/anhydride ratios, cured at different heating rates.

	10 °C/min	1.5 °C/min
	<i>Peak temperature, <math>T_p</math> [°C]</i>	
<b>BOMF/MNA-2-MI0.5</b>	158.4	126.1
<b>1BOMF/0.8MNA-2-MI0.5</b>	153.1	120.9
<b>0.8BOMF/1MNA-2-MI0.5</b>	158.3	125.9
	<i><math>\Delta H_{tot}</math> [J/g]</i>	
<b>BOMF/MNA-2-MI0.5</b>	264.9	270.5
<b>1BOMF/0.8MNA-2-MI0.5</b>	218.1	165.6
<b>0.8BOMF/1MNA-2-MI0.5</b>	298.8	297.3
	<i>Glass transition temperature, <math>T_g</math> [°C]</i>	
<b>BOMF/MNA-2-MI0.5</b>	26.9	34.5
<b>1BOMF/0.8MNA-2-MI0.5</b>	2.9	15.5
<b>0.8BOMF/1MNA-2-MI0.5</b>	66.6	68.1

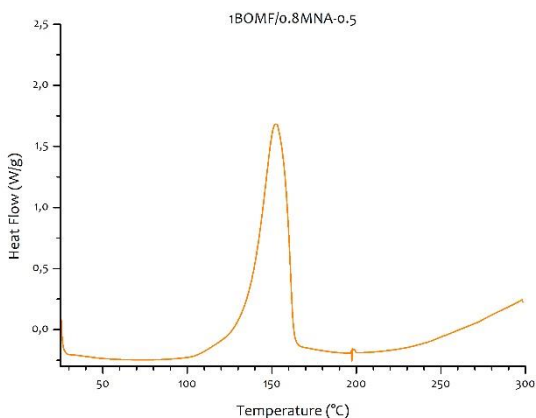


**Figure 3.7** – DSC dynamic heating scan curves at 10 °C/min up to 300 °C of 1BOMF/0.8MNA-2-MI0.5

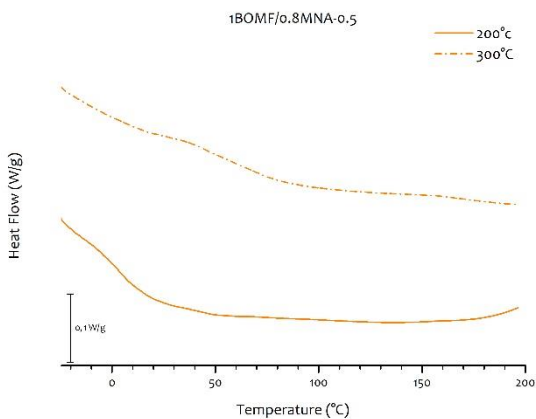


**Figure 3.8** – Comparison of  $T_g$  of 1BOMF/0.8MNA-2-MI0.5 after being heated up to 200 °C (solid curve) and up to 300 °C (dashed curve)

In accordance with thermograms obtained for dynamic analysis, five temperature values were selected to perform isothermal scans. In order to avoid the occurrence of vitrification phenomena, the temperatures selected were below  $T=130$  °C, which corresponded to the onset temperature for BOMF/MNA-



2-MI0.5 in the 10 °C/min dynamic scan. Thermograms reporting isothermal heat flow as a function of time, that is directly related to the rate of conversion according to **Equation 3.1**, are reported in **Figure 3.9**, **Figure 3.10** and **Figure 3.11**, for BOMF/MNA-2-MI0.5, 1BOMF/0.8MNA-2-MI0.5 and 0.8BOMF/1MNA-2-MI0.5, respectively.

As the curing temperature decreased, it took longer for the system to reach the maximum conversion rate and the complete extent of cure. In particular, at 90 °C, the system did not fully react even after two hours, as confirmed by the detection of a residual cure during the second heating scan performed (**Figure 3.12**, **Figure 3.13** and **Figure 3.14**).

On the other hand, increasing the curing temperature resulted in higher values of conversion rate, as well as in lower peak temperatures. This trend is associated to autocatalytic reactions, in which the product formed during the reaction acts as a catalyst, increasing the reaction rate.

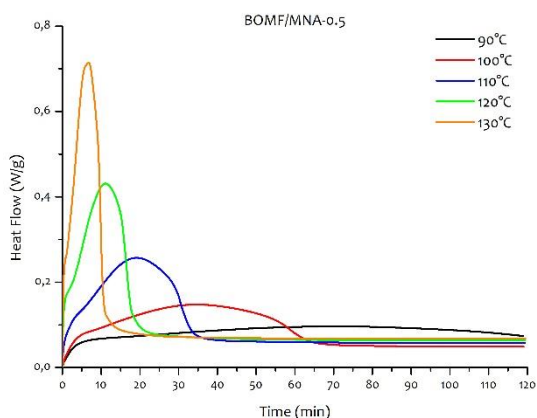


**Figure 3.9** – Isothermal curves obtained at different temperatures for BOMF/MNA-2-MI0.5

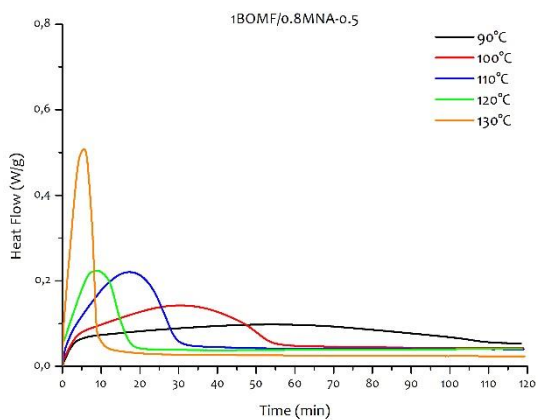


**Figure 3.10** – Isothermal curves obtained at different temperatures for 1BOMF/0.8MNA-2-MI0.5

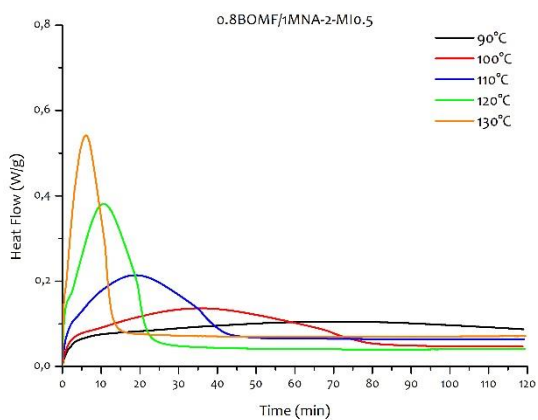


**Figure 3.11** – Isothermal curves obtained at different temperatures for 0.8BOMF/1MNA-2-MI0.5

## Epoxy thermosets based on furan-diglycidyl ether |

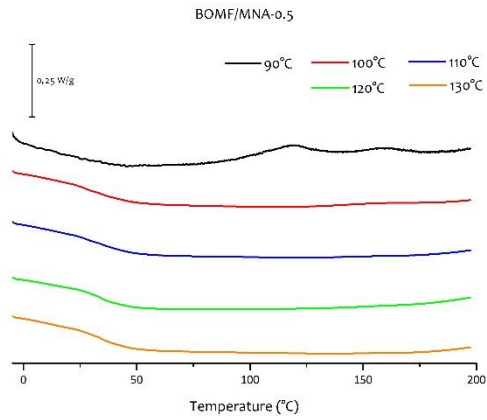


**Figure 3.12** –  $T_g$  of BOMF/MNA-2-MI0.5 cured for 2 h in isothermal method

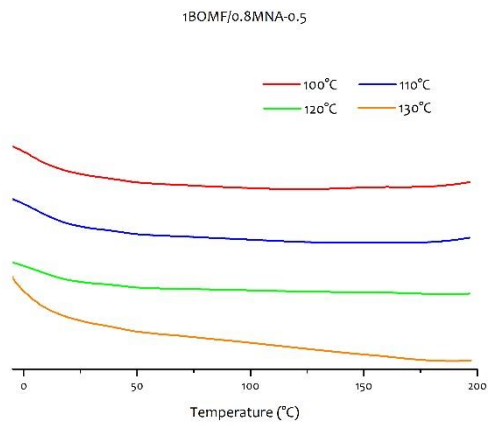


**Figure 3.13** –  $T_g$  of 1BOMF/0.8MNA-2-MI0.5 cured for 2 h in isothermal method

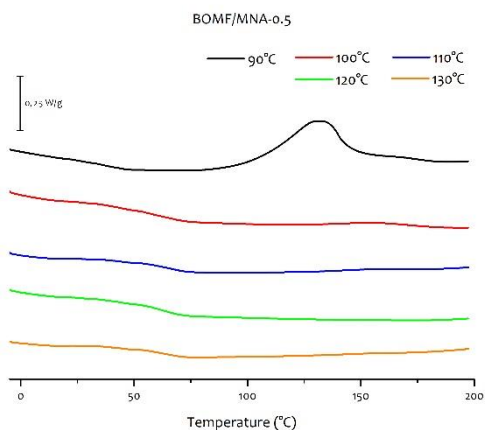


**Figure 3.14** –  $T_g$  of 0.8BOMF/1MNA-2-MI0.5 cured for 2 h in isothermal method

The DSC data obtained from isothermal experiments were then analyzed to calculate kinetic parameters relevant to the curing process. In this respect, the construction of an accurate baseline is necessary for the obtainment of solid quantitative results in the kinetic analysis. To perform isothermal analysis two methods can be used: in the first the sample is placed at room temperature in DSC cell, then rapidly heated to the required temperature, in the second the sample is placed in the furnace already brought at the right temperature. In both cases an initial off-balance signal is detected which can affect the determination of heat flow value, especially at higher temperatures. To mitigate this effect the procedure presented by Barton for baseline detection was performed.<sup>50</sup> Accordingly, a second isothermal scan was performed on post-cured samples, in order to obtain an isotherm scan usable as reference. As collected data (post-cured analysis) were subtracted from each thermogram obtained from the cured sample (before post-cured analysis) and then a clear baseline was taken. From **Equation 3.2**, it was possible to determine the degree of cure as a function of

time for each temperature, using the value obtained from dynamic measurements as  $\Delta H_{tot}$  (**Figure 3.15**, **Figure 3.16** and **Figure 3.17**)

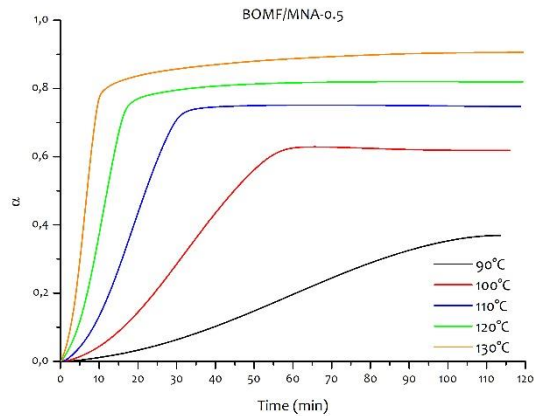


**Figure 3.15** – Degree of conversion ( $\alpha$ ) in function of time for BOMF/MNA-2-MI0.5

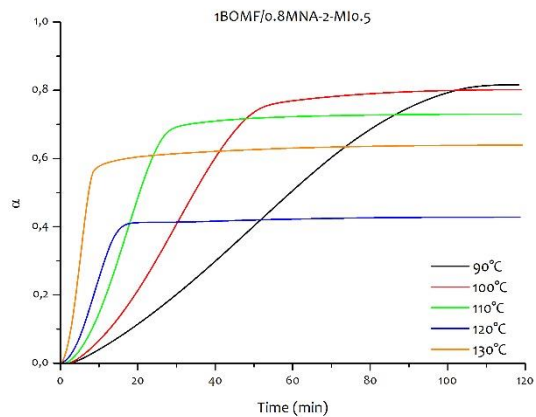


**Figure 3.16** – Degree of conversion ( $\alpha$ ) in function of time for 1BOMF/0.8MNA-2-MI0.5

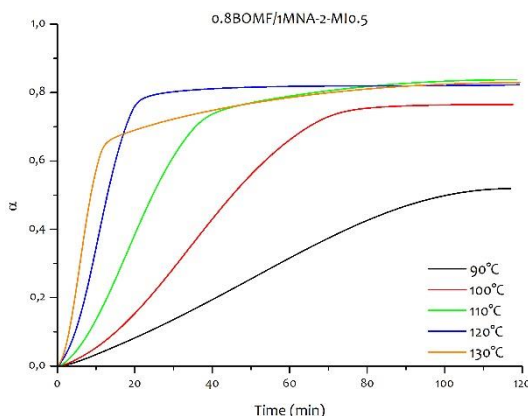


**Figure 3.17** – Degree of conversion ( $\alpha$ ) in function of time for 0.8BOMF/1MNA-2-MI0.5

The “S” shape of curves  $\alpha$ -time, especially for low temperatures, is characteristic of autocatalytic processes: at the beginning of the process, the conversion proceeds slowly then it rapidly increases, and when an high degree of cure is reached it slows down until a plateau is reached. More specifically, at low conversion values, the diffusion of the reacting species is not hindered by big molecules formed, and the reactive groups are still present in high concentrations, so that reaction proceed fast. When high conversions are approached, long chains are formed, viscosity increases and chain mobility is limited; at this point conversion become diffusion controlled and a plateau value for conversion is reached. In this case only an increase in temperature can decrease viscosity, improving chain mobility and subsequently allowing further reaction of unreacted groups.<sup>51</sup> Peculiar is the behavior of 1BOMF/0.8MNA-2-MI0.5 for which strong vitrification is verified for high 120 and 130 °C. As above-mentioned, in dynamic DSC analysis the system with an epoxy excess shows a lower  $T_{\text{onset}}$  compared with other systems and when heated at 10 °C/min at 120 °C the cure reached higher degree of conversion compared with other samples.

This behavior was reflected also in isothermal analysis and in particular in the dependence of conversion with temperature.

Experimental data obtained by isothermal analysis showed that no samples reached full conversion after 2 hours reaction; data were then fitted with **Equation 3.7** model to evaluate  $k_1$ ,  $k_2$ ,  $m$  and  $n$  kinetic parameters. No assumption was made a priori on the total reaction order  $m+n$ . The best-fitting values obtained for kinetic parameters are reported in **Table 3.7**. Fitted data (black lines) are reported, in comparison with experimental data, in **Figure 3.18**, **Figure 3.19** and **Figure 3.20**. The choice of the empirical method is justified by the good agreement between experimental data and fitted curves.

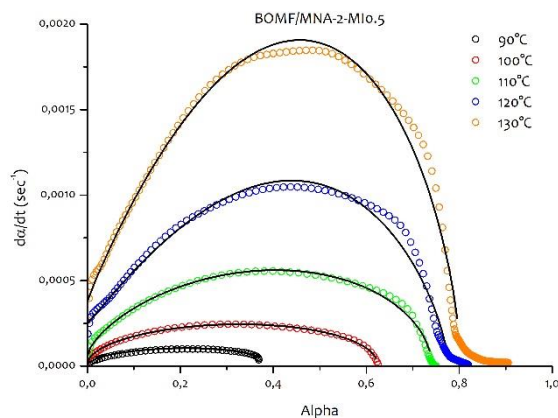


**Figure 3.18** – Isothermal conversion rate at different temperatures as a function of the conversion degree. Open symbols are the experimental values and black line represents the fitting according to Equation 3.11 for BOMF/MNA-2-MI0.5

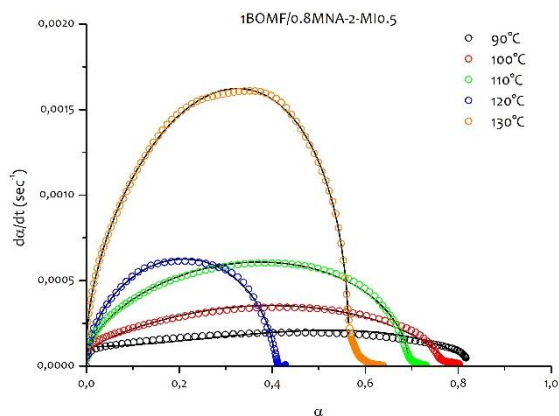


**Figure 3.19** – Isothermal conversion rate at different temperatures as a function of the conversion degree. Open symbols are the experimental values and black line represents the fitting according to Equation 3.11 for 1BOMF/0.8MNA-2-MI0.5

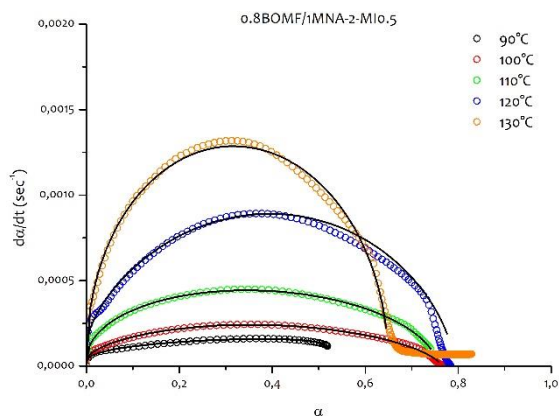


**Figure 3.20** – Isothermal conversion rate at different temperatures as a function of the conversion degree. Open symbols are the experimental values and black line represents the fitting according to Equation 3.11 for 0.8BOMF/1MNA-2-MI0.5

The total reaction order for BOMF/MNA-2-MI0.5 is not constant with temperature and in particular for BOMF/MNA-2-MI0.5 it increases with



temperature while for 1BOMF/0.8MNA-2-MI0.5 the trend is opposite (results in the latter case are more affected by vitrification effects). No trend with the temperature can be detected for 0.8BOMF/1MNA-2-MI0.5.

The influence of the initiator that initiate the polymerization reaction is expressed by the rate constant  $k_1$ , while  $k_2$  reflects the dependence of reaction rate on species formed during first reaction steps that act as catalyst. <sup>52,53</sup>

**Table 3.7** – Curing kinetics parameters

		$k_1$ [sec <sup>-1</sup> ]	$k_2$ [sec <sup>-1</sup> ]	m	n
<b>BOMF/MNA-2-MI0.5</b>	90 °C	$9.71 \cdot 10^{-10}$	$4.63 \cdot 10^{-4}$	0.50	0.40
	100 °C	$1.62 \cdot 10^{-5}$	$7.57 \cdot 10^{-4}$	0.54	0.47
	110 °C	$6.95 \cdot 10^{-5}$	$1.71 \cdot 10^{-3}$	0.68	0.53
	120 °C	$2,96 \cdot 10^{-4}$	$4.74 \cdot 10^{-3}$	1.04	0.70
	130 °C	$4,33 \cdot 10^{-4}$	$7.04 \cdot 10^{-3}$	0.96	0.64
<b>1BOMF/0.8MNA-2-MI0.5</b>	90 °C	$1.30 \cdot 10^{-4}$	$9.73 \cdot 10^{-4}$	1.62	0.68
	100 °C	$1.02 \cdot 10^{-4}$	$1.29 \cdot 10^{-3}$	0.85	0.69
	110 °C	$6.67 \cdot 10^{-5}$	$1.91 \cdot 10^{-3}$	0.64	0.51
	120 °C	$3.05 \cdot 10^{-5}$	$3.64 \cdot 10^{-3}$	0.58	0.53
	130 °C	$1.74 \cdot 10^{-4}$	$5.69 \cdot 10^{-3}$	0.62	0.57
<b>0.8BOMF/1MNA-2-MI0.5</b>	90 °C	$2.15 \cdot 10^{-5}$	$2.81 \cdot 10^{-4}$	0.41	0.15
	100 °C	$4.29 \cdot 10^{-5}$	$7.12 \cdot 10^{-4}$	0.60	0.63
	110 °C	$3.65 \cdot 10^{-5}$	$1.15 \cdot 10^{-3}$	0.49	0.55
	120 °C	$1.49 \cdot 10^{-4}$	$2.64 \cdot 10^{-3}$	0.67	0.61
	130 °C	$3.30 \cdot 10^{-5}$	$3.78 \cdot 10^{-3}$	0.48	0.49

## FT-IR analysis

Combined rheological and infrared analysis were carried out on BOMF/MNA-2-MI<sub>0.5</sub>, 1BOMF/0.8MNA-2-MI<sub>0.5</sub> and 0.8BOMF/1MNA-2-MI<sub>0.5</sub>. In particular, temperature-dependent conversion degree of BOMF crosslinking reaction in presence of MNA and 2-MI as initiator was monitored by collecting FT-IR spectra in ATR mode upon heating the sample at a controlled heating rate (1.5 °C/min) on the rheometer stage. In this way, viscoelastic behavior change could be monitored alongside the chemical evolution of the analyzed system.

**Figure 3.21** shows the IR absorbance spectra of MNA and BOMF; for each compound characteristic peaks are visible. Characteristics peaks for furan ring in BOMF are between 3165–2955 cm<sup>-1</sup> (stretching vibrations of C–H in furan ring and alkyl chains), in the 1585 to 1448 cm<sup>-1</sup> range for the aromatic C=C stretching, and from 1127 to 1077 cm<sup>-1</sup> (stretching of aliphatic and aromatic C–O). Additionally, the presence of epoxide groups is characterized by the appearance of typical bands at 1250, 911, and 830 cm<sup>-1</sup> corresponding to the C-O-C stretching of oxirane groups. In the case of MNA spectrum, the characteristic peaks of antisymmetric and symmetrical stretching vibrations of C=O bond of carbonyl group in anhydride, at 1850 and 1770 cm<sup>-1</sup> respectively, can be clearly identified. C-O stretching is present at 1218 cm<sup>-1</sup> and peaks at 1076, 909 and 894 cm<sup>-1</sup> are correlated to the anhydride ring. CH<sub>3</sub> and CH<sub>2</sub> symmetrical and antisymmetric stretching peaks are present between 2976 and 2877 cm<sup>-1</sup> as well as peaks related to deformation of the same group between 1463 and 1324 cm<sup>-1</sup>.<sup>54</sup>

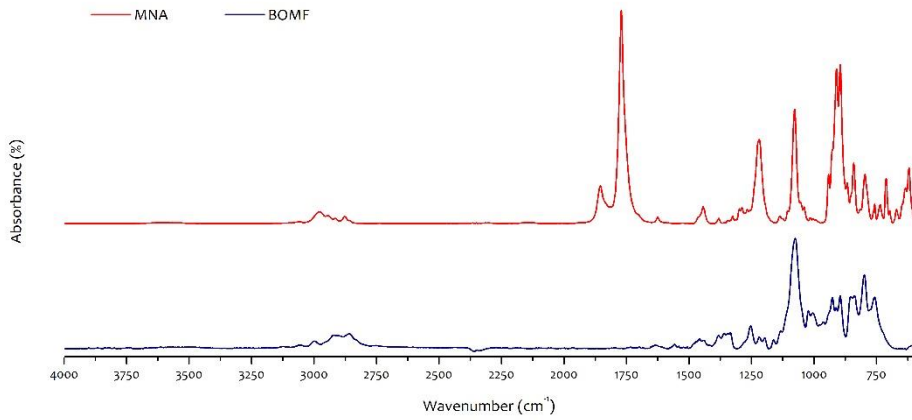


**Figure 3.21** – ATR FT-IR spectra of the epoxy monomer (BOMF) and curing agent (MNA)

In **Figure 3.22** are reported two representative spectra of BOMF/MNA-2-MI0.5 system before and after curing.

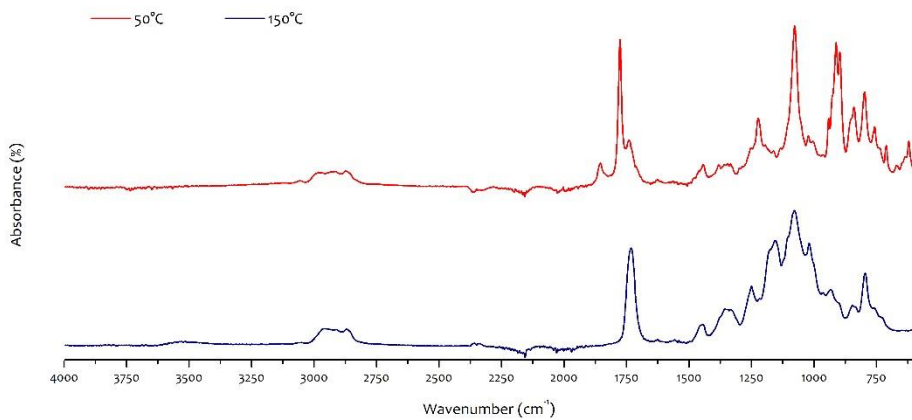


**Figure 3.22** – ATR FT-IR spectra of BOMF/MNA-2-MI0.5

The complete disappearance of the peaks characteristic of the reacting functional groups, as well as the appearance of the characteristic peak of the C=O stretching of ester carbonyl at  $1730\text{ cm}^{-1}$  at  $150\text{ }^{\circ}\text{C}$ , confirmed the occurrence of cure. In particular, the peaks at  $1850$  and  $1770\text{ cm}^{-1}$  were used to follow the curing reaction as they gradually disappeared over the reaction time, due to the opening of the anhydride group and the formation of new C-O-C bonds of the cured resin. Unfortunately, a direct monitoring of peak characteristic of the epoxy ring was not possible due to the overlapping of both the epoxy and anhydride characteristic vibrations in the  $954 - 875\text{ cm}^{-1}$  region. The epoxy conversion was then monitored by analyzing the absorbance of peaks in the region between  $950 - 870\text{ cm}^{-1}$  (from now on labelled as 910) by the use of **Equation 3.9**, **Equation 3.10**, taking also into account **Equation 3.11**. As forming species, the ester characteristic groups are present both in region  $1210 - 1160\text{ cm}^{-1}$  (ether C-O-C=O stretching) and  $1735 - 1750\text{ cm}^{-1}$  (carbonyl C=O stretching). Carbonyl ester stretching at  $1735\text{ cm}^{-1}$  was monitored to determine the kinetics of ester group formation because of fewer overlap in the region analyzed and the consequent construction of a more solid baseline. The band between about  $2770 - 3080\text{ cm}^{-1}$ , given by stretching of carbon-hydrogen bonds that does not take part to crosslinking reactions, was used to normalize all absorbance areas before the evaluation of the degree of conversion.

**Figure 3.23** shows the three-dimensional (absorbance-wavenumber-temperature) FT-IR spectra relative to the curing of the BOMF/MNA-2-MI0.5 system and the details in the wavenumber range  $1900 - 1650\text{ cm}^{-1}$  (**Figure 3.24**) and  $1150 - 750\text{ cm}^{-1}$  (**Figure 3.25**) collected during rheological dynamic measurements.

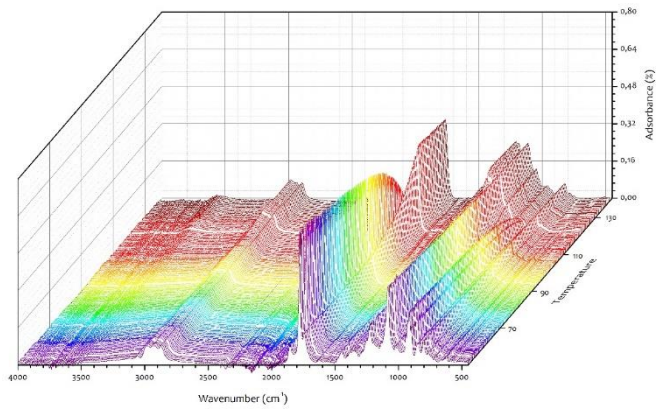


**Figure 3.23** – 3D plot of spectra collected upon heating during rheological measurements on BOMF/MNA-2-MI<sub>0.5</sub>

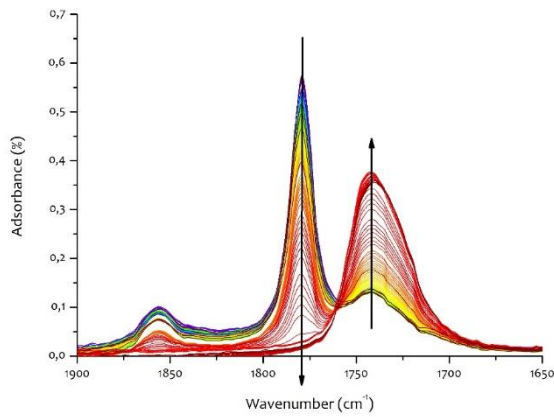


**Figure 3.24** – Time evolution of ATR FT-IR spectra of BOMF/MNA-2-MI<sub>0.5</sub> reacting system in the wavenumber region between 1900 – 1650 cm<sup>-1</sup>

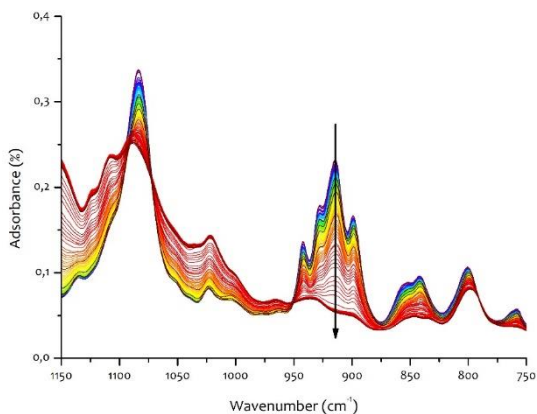


**Figure 3.25** – Time evolution of ATR FT-IR spectra of BOMF/MNA-2-MI0.5 reacting system in the wavenumber region between 1150 – 750  $\text{cm}^{-1}$

Functional groups conversion monitoring was carried out analyzing the spectra collected during the rheological measurements at 1.5  $^{\circ}\text{C}/\text{min}$  heating rate.

Comparison between results obtained for stoichiometric and non-stoichiometric mixtures is possible considering the absolute conversion  $C_0\alpha$ , as a function of temperature<sup>55</sup>. Values of absolute conversion of characteristic groups involved in the cure reaction, evaluated from ATR FT-IR spectra for the three reference systems are reported in **Figure 3.26**, **Figure 3.27** and **Figure 3.28**.

The curves relative to the functional groups conversion of the equimolar mixture show that epoxy groups conversion in the first reaction stage is slightly favoured while the conversion of anhydride groups and the ester formation are almost null up to 100  $^{\circ}\text{C}$ . Afterwards all curves slope rapidly increases until almost complete conversion was achieved at about 130  $^{\circ}\text{C}$ . The curves of the stoichiometrically unbalanced mixtures showed different trends. When epoxy is used in molar excess its conversion at temperature above 70  $^{\circ}\text{C}$  is significantly

higher than anhydride conversion but this trend is inverted when  $T = 110\text{ }^{\circ}\text{C}$  are reached, until completion of crosslink reaction. For 0.8BOMF/1MNA-2-MIo.5, instead, anhydride and epoxy consumption are comparable before  $T = 110\text{ }^{\circ}\text{C}$ , where no significant changes in peaks area are recorded, indicating no consumption of functional groups.

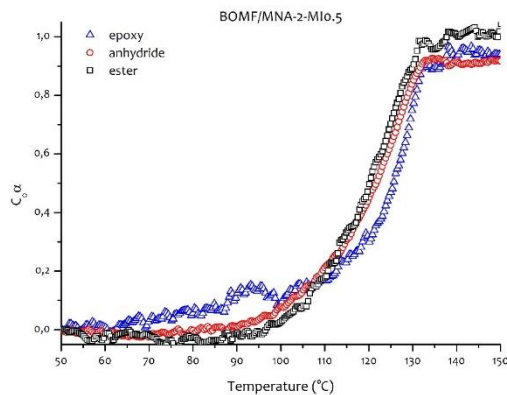


**Figure 3.26** – Absolute conversion of characteristic groups, evaluated from ATR FT-IR spectra collected during the rheological measurements at  $1.5\text{ }^{\circ}\text{C}/\text{min}$  heating rate on BOMF/MNA-2-MIo.5.

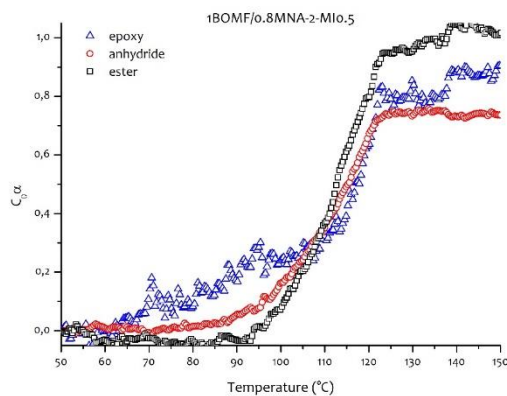


**Figure 3.27** – Absolute conversion of characteristic groups, evaluated from ATR FT-IR spectra collected during the rheological measurements at  $1.5\text{ }^{\circ}\text{C}/\text{min}$  heating rate on 1BOMF/0.8MNA-2-MIo.5.

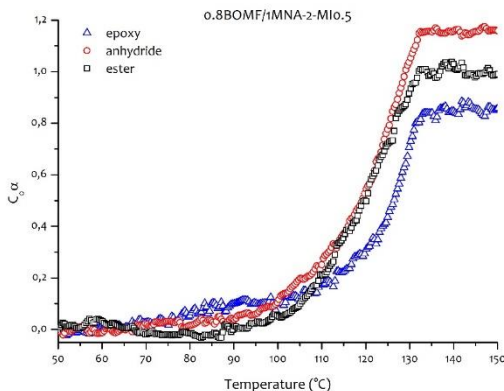


**Figure 3.28** – Absolute conversion of characteristic groups, evaluated from ATR FT-IR spectra collected during the rheological measurements at 1.5 °C/min heating rate on 0.8BOMF/1MNA-2MI-0.5.

In presence of an anhydride excess and for equimolar epoxy/anhydride ratio the reaction proceeded exactly with the same kinetics of formation of the crosslinked structure as can be noticed by **Figure 3.29** where conversion of ester groups for all the three systems are compared. By this comparison it is also possible to notice that the system with epoxy excess reached completion of cure process at lower temperatures respect to other systems studied. Analogous behaviour was present in DSC dynamic analysis conducted at the same heating rate (1.5 °C/min) (**Figure 3.4**, **Figure 3.5** and **Figure 3.6**). For all systems, at temperature below 90 °C no significant changes in heat flow were detected; the cure occurs at about 130 °C and the heat flow reached again the baseline value, sign of cure completion. Increasing the temperature, an increase in conversion rate was experienced by all reactive groups.



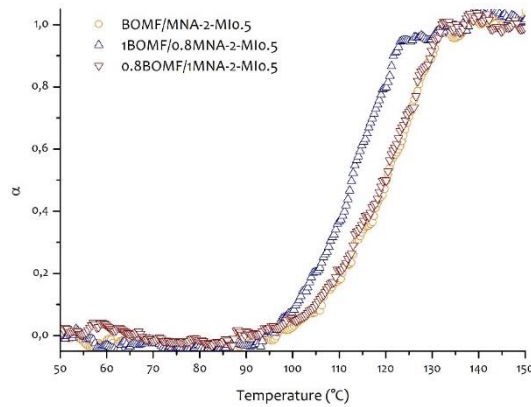


**Figure 3.29** – Absolute conversion of ester groups for BOMF/MNA-2-MI0.5, 1BOMF/0.8MNA-2-MI-0.5 AND 0.8BOMF/1MNA-2-MI0.5

## Rheological analysis

The formation of the viscous polymer network during the conversion of the functional groups was simultaneously monitored through dynamic rheological tests. **Figure 3.30**, **Figure 3.31** and **Figure 3.32** show the  $G'$ ,  $G''$  and  $\eta^*$  variation with the temperature, along with the ester conversion (evaluated by **Equation 3.10**) for the reacting systems characterized by an epoxy/anhydride ratio of 1:1, 1:0.8 and 0.8:1, respectively. Moreover the comparison of the  $G'$  and  $|\eta^*|$  data evolution vs. temperature of the three reacting mixtures is displayed in **Figure 3.33**.

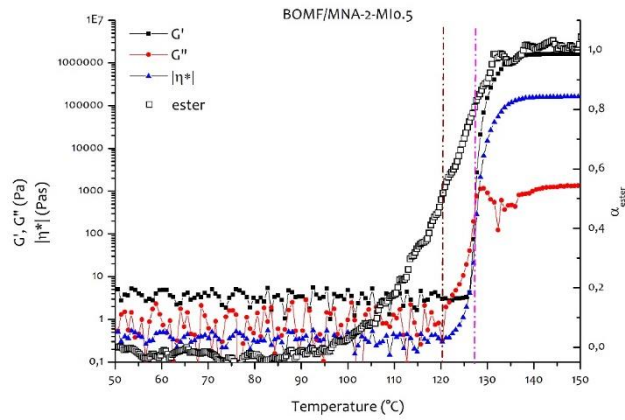


**Figure 3.30** – Elastic modulus ( $G'$ ), viscous modulus ( $G''$ ) and complex viscosity ( $|\eta^*|$ ) compared with ester conversion of BOMF/MNA-2-MI0.5 heated at 1.5 °C/min.

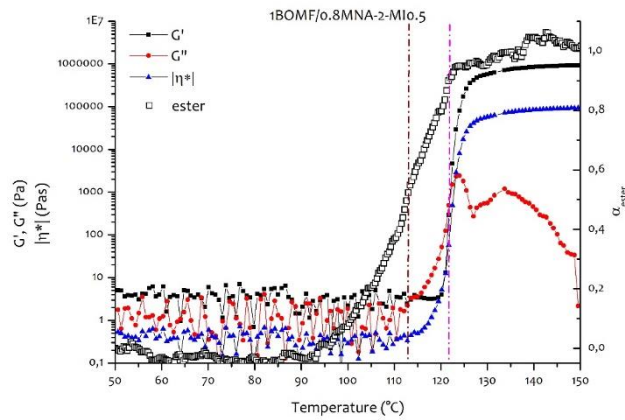


**Figure 3.31** – Elastic modulus ( $G'$ ), viscous modulus ( $G''$ ) and complex viscosity ( $|\eta^*|$ ) compared with ester conversion of 1BOMF/0.8MNA-2-MI0.5 heated at 1.5 °C/min.

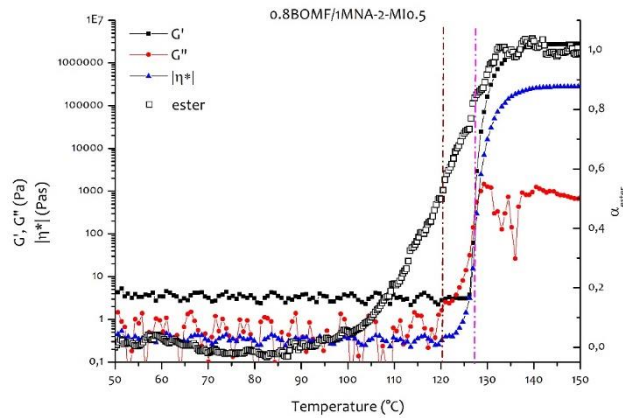


**Figure 3.32** – Elastic modulus ( $G'$ ), viscous modulus ( $G''$ ) and complex viscosity ( $|\eta^*|$ ) compared with ester conversion of o.8BOMF/1MNA-2-MIo.5 heated at 1.5 °C/min.

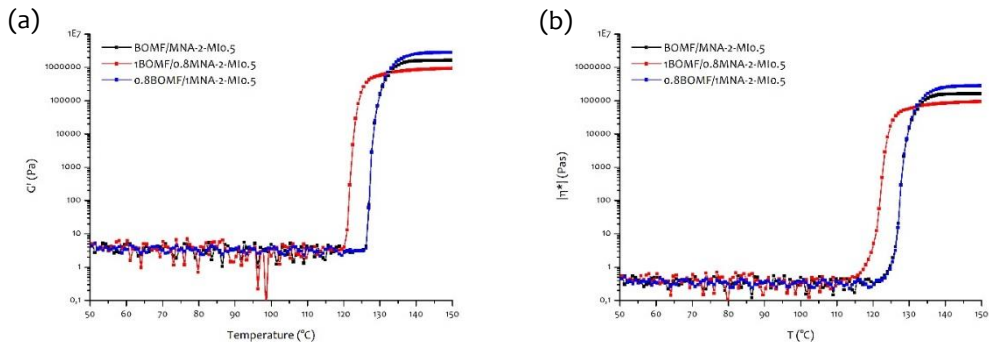


**Figure 3.33** – Comparison of (a) elastic moduli ( $G'$ ) and (b) complex viscosity ( $|\eta^*|$ ) of BOMF/MNA-2-MIo.5, 1BOMF/o.8MNA-2-MIo.5, and o.8BOMF/1MNA-2-MIo.5 heated at 1.5 °C/min

For all three systems, the initial moduli and viscosity values were low and constant up to temperatures of around 110 °C; in this range of low temperature, the elastic modulus  $G'$  is higher than the viscous modulus  $G''$ . This step was followed by a trend reversal, with higher values of  $G''$  with respect to  $G'$ , due to the increase in viscosity of the reacting mixture. The viscous modulus  $G''$

remained higher than  $G'$  until the occurrence of the crossover of the two curves, associated to the gelling process, at 123 °C for 1BOMF/0.8MNA-2-MI0.5 and 127 °C for the remaining systems. After the gel point the elastic modulus grew considerably, becoming significantly higher than the viscous modulus. Later, the curing reaction progressed, and  $G'$  approached its maximum values whereas  $G''$  reached a peak and then started to decrease. In this zone vitrification occurred.

Comparing the different systems, it is noticed that increasing the anhydride amount in the mixture results in higher  $G'$  and  $\eta^*$  ultimate values. Complex viscosity, for all the samples, was low and constant until the ester group formation, evaluated from infrared analysis, reached the value of about 0.4 (**Figure 3.30**, **Figure 3.31** and **Figure 3.32**). It is interesting also to notice that gelation occurred when the ester formation achieved a value of  $\alpha=0.7$  for the formulations with stoichiometric ratio and excess anhydride. For the system with an epoxy excess, gelation was achieved when cure reaction was almost complete ( $\alpha=0.8$ ); this difference was reflected also in the properties of 1BOMF/0.8MNA-2-MI0.5 cured samples, that have lower  $T_g$ s and elastic modulus, in comparison with the other two formulations. The comparison between the three formulations (**Figure 3.33**) shows that the increase in  $G'$  and  $\eta^*$  of 1BOMF/0.8MNA-2-MI0.5 occurred at about 120 °C, that is more than 5 °C lower than the temperatures measured for BOMF/MNA-2-MI0.5 and 0.8BOMF/1MNA-2-MI0.5. This evidence can be due to the lower viscosity of the mixture containing an epoxy excess, which facilitates the monomer diffusion leading to the network formation.

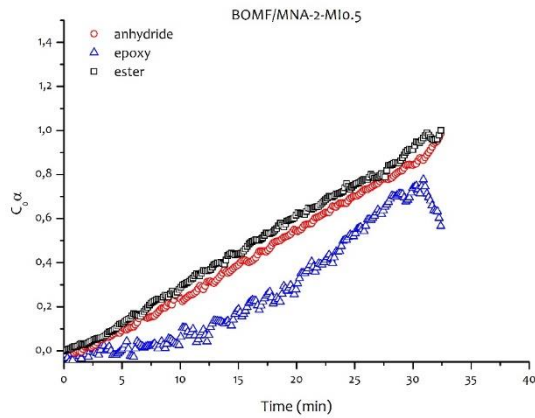


**Figure 3.34** – Absolute conversion ( $C_{0\alpha}$ ) evaluated from ATR FT-IR spectra collected during the rheological measurements at 110 °C on BOMF/MNA-2-MI0.5.

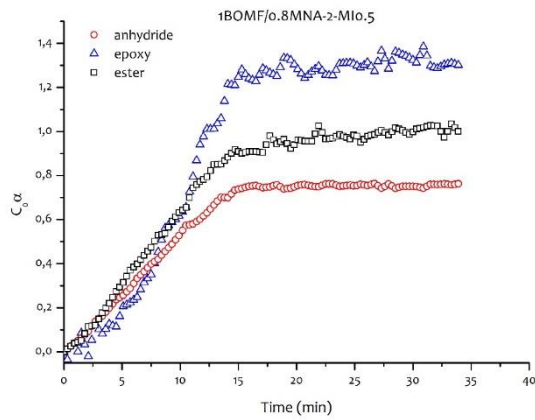


**Figure 3.35** – Absolute conversion ( $C_{0\alpha}$ ) evaluated from ATR FT-IR spectra collected during the rheological measurements at 110 °C on 1BOMF/0.8MNA-2-MI0.5.

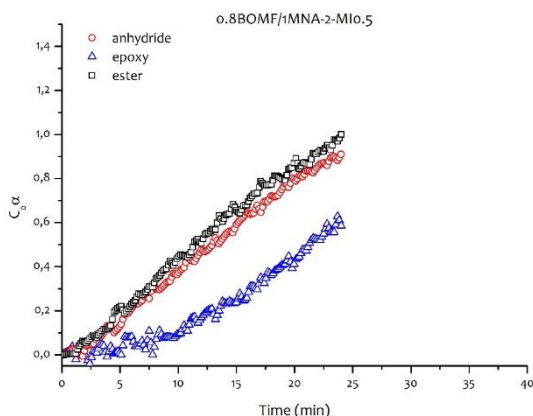


**Figure 3.36** – Absolute conversion ( $C_0 \alpha$ ) evaluated from ATR FT-IR spectra collected during the rheological measurements at 110 °C on 0.8BOMF/1MNA-2-MI 0.5.

In **Figure 3.34**, **Figure 3.35** and **Figure 3.36** the absolute conversions  $C_0 \alpha$  are represented for the three formulations during isothermal curing at 110 °C. This temperature value was chosen from DSC and FT-IR analysis, as being low enough to allow monitoring the curing process during the time needed to set up the measurement, yet high enough to allow reaching a high conversion degree in less than one hour.

Only for the system 1BOMF/0.8MNA-2-MI0.5 was possible to hold the measurement for 60 min; for remaining systems technical limitation related with the rheological analysis caused the interruption of the experiments and of the related collection of IR spectra. The incomplete process of cure was confirmed by DSC analysis, as a post-cure enthalpy was detected.

The consumption of anhydride groups was faster in comparison to that of epoxy rings, suggesting that each epoxy group reacts with two anhydrides: first the epoxy reacts with the anhydride oxygen forming an ester group and

following, the epoxy oxirane reacts with a second anhydride group to form a further ester link. This can be noticed mainly for 0.8BOMF/1MNA-2-MI0.5 where, being an anhydride excess the epoxy conversion rate is even slower.

A comparison of the three systems (**Figure 3.37**) confirms that the formulation with excess epoxy converted with a significantly higher rate with respect to the other ones, as after 15 minutes the reaction reached its limiting value due to the reduced monomer diffusion. In comparison, after the same reaction time, BOMF/MNA-2-MI0.5 and 1BOMF/0.8MNA-2-MI0.5 showed an increasing reaction rate for both anhydride and epoxy groups, being far from their ultimate conversion.

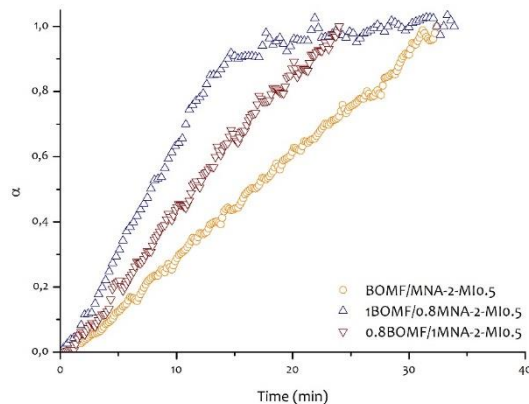


**Figure 3.37** – Comparison between absolute conversions of ester groups for BOMF/MNA-2-MI0.5, 1 BOMF/0.8MNA-2-MI0.5 and 0.8 BOMF/1MNA-2-MI0.5

Isothermal rheological measurements are reported in **Figure 3.38**, **Figure 3.39** and **Figure 3.40**; except for the system with epoxy excess was not possible

to complete the measurement because the maximum stress acceptable for the rheometer was reached.

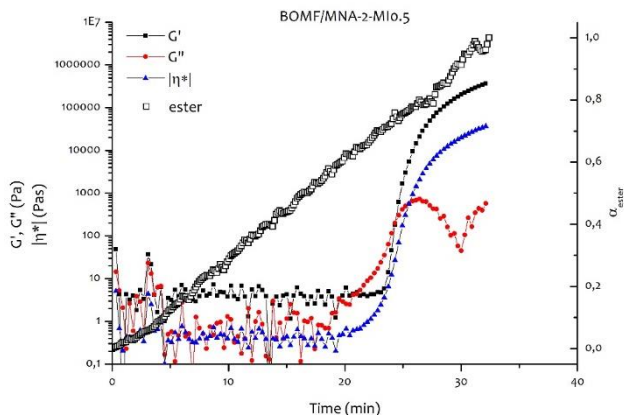


**Figure 3.38** – Elastic modulus ( $G'$ ), viscous modulus ( $G''$ ) and complex viscosity ( $|\eta^*|$ ) compared with ester conversion of BOMF/MNA-2-MI0.5 at 110 °C, in time

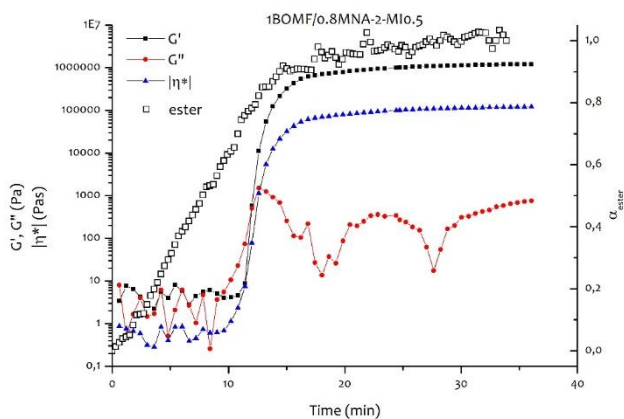


**Figure 3.39** – Elastic modulus ( $G'$ ), viscous modulus ( $G''$ ) and complex viscosity ( $|\eta^*|$ ) compared with ester conversion of 1BOMF/0.8MNA-2-MI0.5 at 110 °C, in time



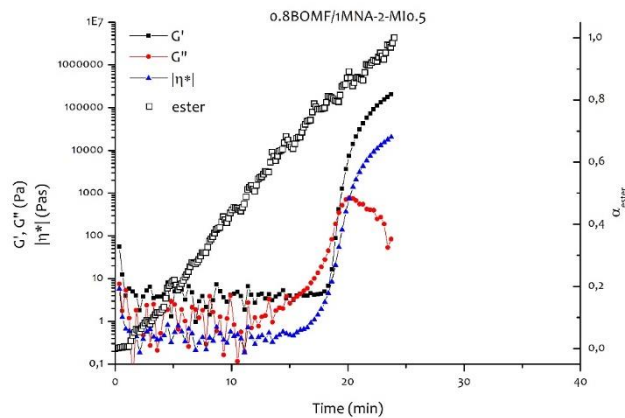


**Figure 3.40** – Elastic modulus ( $G'$ ), viscous modulus ( $G''$ ) and complex viscosity ( $|\eta^*|$ ) compared with ester conversion of 0.8BOMF/1MNA-2-MI0.5 at 110 °C, in time

Comparing the three measurement (**Figure 3.41**) is possible to notice the increase in curing time increasing for, in order, 1BOMF/0.8MNA-2-MI0.5, 0.8BOMF/1MNA-2-MI0.5 and BOMF/MNA-2-MI0.5.

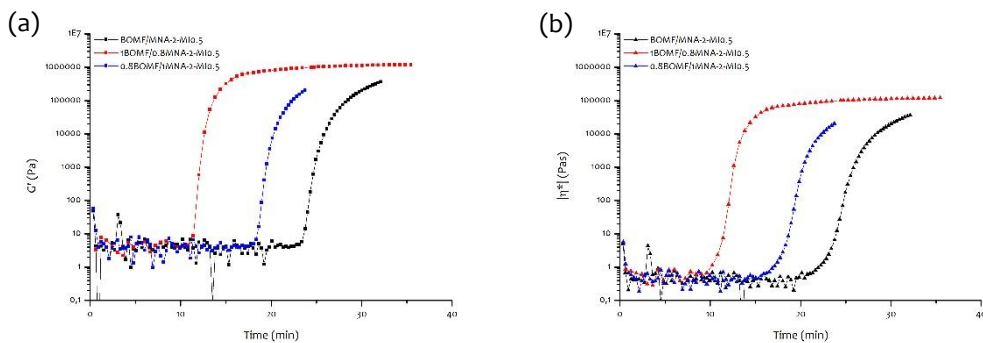


**Figure 3.41** – Comparison between (a) elastic moduli ( $G'$ ) and (b) complex viscosity ( $|\eta^*|$ ) of selected samples at 110 °C

It is interesting to notice that drastic changes in values of rheological parameters (i.e. viscosity, elastic and viscous moduli) are not reflected in conversion rate changes. The formation of ester linkages progress with a constant rate until completion of cure process

### 3.3.3. Study of cured epoxies

In order to choose the optimal curing procedure for the obtainment of epoxy resins samples preliminary test were made by DSC analysis. Curing processes were simulated by imposing different isothermal scan for different times and evaluating  $T_g$ . The optimal thermal treatment was found to be 2 hours at 130 °C and a post-cure for 1 hour at 180 °C. After this treatment samples 0.8BOMF/1MNA-2-MI0.5 and BOMF/MNA-2-MI0.5 were rigid, suggesting the obtainment of a completely cured system, while 1BOMF/0.8MNA-2-MI0.5 was rubbery. A second set of samples was than obtained applying a thermal treatment including a second post-cure step at 230 °C; in this case also samples with epoxy excess resulted rigid thanks to the homopolymerization of epoxy groups in excess <sup>36,47</sup>. The same treatment was applied to obtain reference samples using a commercial DGEBA cured with MNA in molar ratio 1:1, in presence of 0.5 wt% of 2-MI as initiator

Summarizing, two sets of sample for each composition were obtained according to the following treatments:

Cure at  $T = 130\text{ °C}$  for  $t = 2\text{ h}$  and post-cure at  $T = 180\text{ °C}$  for  $t = 1\text{ h}$

Cure at  $T = 130\text{ °C}$  for  $t = 2\text{ h}$  and post-cure at  $T = 180\text{ °C}$  for  $t = 1\text{ h}$  and at  $T = 230\text{ °C}$  for  $t = 1\text{ h}$ .

Hereafter samples obtained with the first treatment will be labelled with a further indication “pc180” (indicating the maximum temperature reached during the cure process) while samples cured following the latter treatment will be labelled with “pc230”.

On cured samples thermogravimetric analysis and tensile tests were performed.

## Thermogravimetric (TGA) analysis

Thermal and thermo-oxidative behavior of bio-furan-based epoxy resins were evaluated by thermogravimetric analysis performed on cured systems under both inert ( $N_2$ ) and oxidative (air) atmosphere. The weight, and derivative weight, vs. temperature curves for the three selected systems (**Figure 3.42**, **Figure 3.43**, **Figure 3.44** and **Figure 3.45**) and in both atmosphere conditions (**Figure 3.46**, **Figure 3.47** and **Figure 3.48**) were compared.

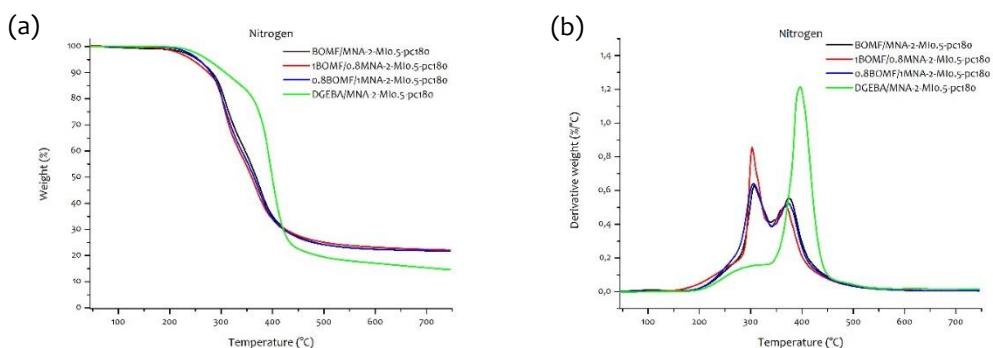


**Figure 3.42** – (a) Weight loss and (b) derivative weight loss in nitrogen atmosphere for samples cured at 180°C

## | Epoxy thermosets based on furan-diglycidyl ether

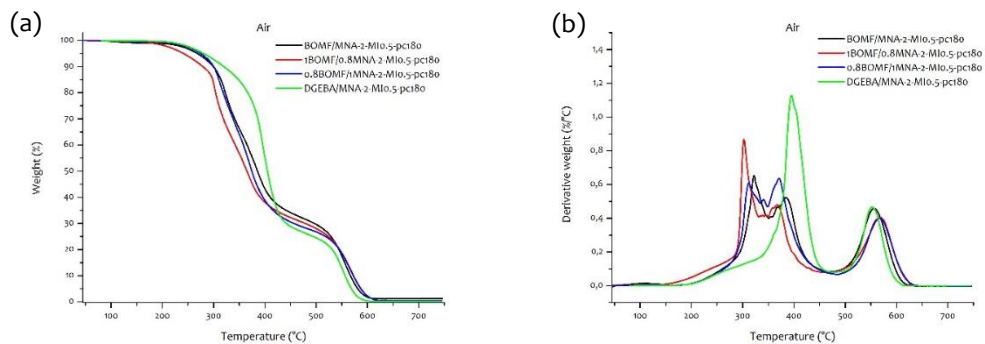


**Figure 3.43** – (a) Weight loss and (b) derivative weight loss in air atmosphere for samples cured at 180 °C

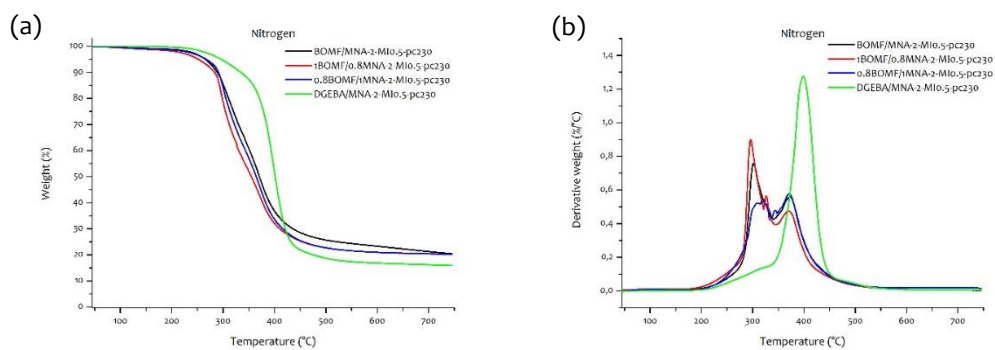


**Figure 3.44** – (a) Weight loss and (b) derivative weight loss in nitrogen atmosphere for samples cured at 230 °C

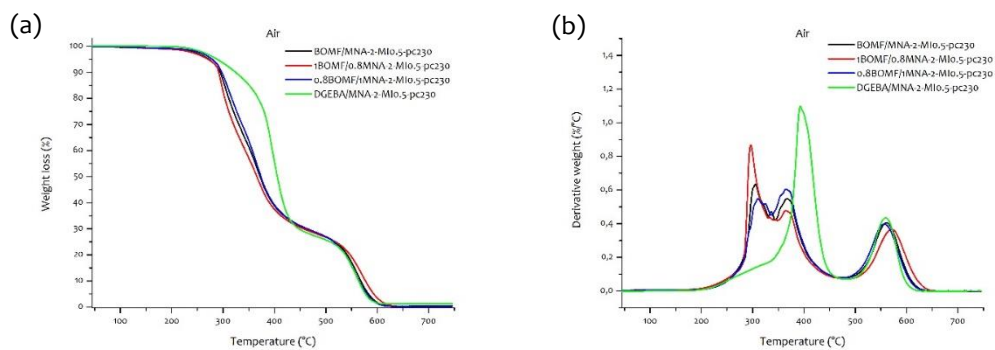


**Figure 3.45** – (a) Weight loss and (b) derivative weight loss in air atmosphere for samples cured at 230 °C

**Table 3.8** – Degradation temperature at 5% weight loss ( $T_{d5}$ ) and at 10% weight loss ( $T_{d10}$ ) of resins with different epoxy/anhydride ratios in both air and nitrogen atmosphere

	$T_{D5}$ [°C]	$T_{D10}$ [°C]
	Nitrogen atmosphere	
<b>BOMF/MNA-2-MI0.5-PC180</b>	254.6	282.7
<b>1BOMF/0.8MNA-2-MI0.5-PC180</b>	241.6	274.2
<b>0.8BOMF/1MNA-2-MI0.5-PC180</b>	256.4	279.1
<b>DGEBA/MNA-2-MI0.5-PC180</b>	274.0	308.5
<b>BOMF/MNA-2-MI0.5-PC230</b>	286.5	292.2
<b>1BOMF/0.8MNA-2-MI0.5-PC230</b>	252.2	283.6
<b>0.8BOMF/1MNA-2-MI0.5-PC230</b>	265.6	288.7
<b>DGEBA/MNA-2-MI0.5-PC230</b>	296.6	334.7
	Air atmosphere	
<b>BOMF/MNA-2-MI0.5-PC180</b>	268.4	299.5
<b>1BOMF/0.8MNA-2-MI0.5-PC180</b>	241.5	279.2
<b>0.8BOMF/1MNA-2-MI0.5-PC180</b>	274.8	300.0
<b>DGEBA/MNA-2-MI0.5-PC180</b>	280.8	320.1
<b>BOMF/MNA-2-MI0.5-PC230</b>	273.0	294.5
<b>1BOMF/0.8MNA-2-MI0.5-PC230</b>	271.1	291.5
<b>0.8BOMF/1MNA-2-MI0.5-PC230</b>	279.1	297.7
<b>DGEBA/MNA-2-MI0.5-PC230</b>	289.1	324.7

Degradation took place in two steps in nitrogen and in three steps in air atmosphere, with total volatilization in air and a 20% residue in  $N_2$ . On heating

epoxy resins above 380°C, a pyrolysis phenomenon occurs and a carbonaceous residue, resistant to inert atmosphere is formed<sup>55</sup>. In a thermooxidative atmosphere, instead, combust and this second degradation process, that leads the material to a complete degradation, is detected by TGA.

Different is the behaviour for DGEBA/MNA resin: only one degradation step was noticed in inert atmosphere, at a temperature about 100 °C higher than that at which the second degradation step of bio-based resins occurred. DGEBA/MNA yielded a residue of 15 wt.%.

For bio-based samples under air atmosphere, degradation took place later than in nitrogen. This was due to the formation in presence of air of an oxide layer, which protected the bulk of the sample increasing the thermal resistance up to high temperatures<sup>56</sup>. Moreover, samples cured until 230 °C exhibited an higher thermo-oxidative resistance.

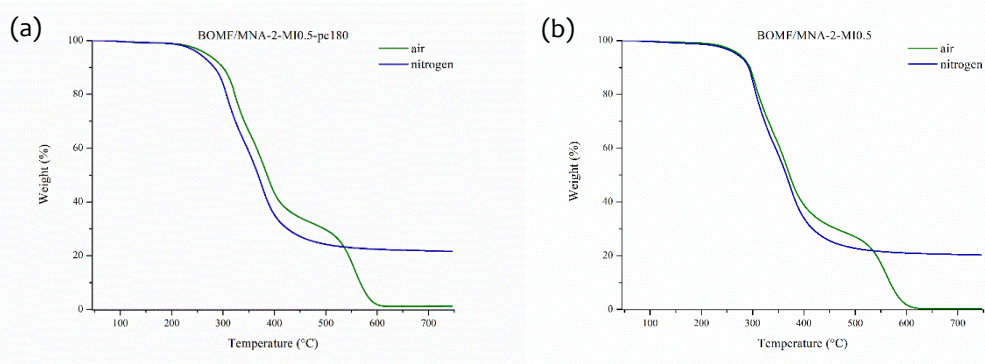


**Figure 3.46** – Weight loss of (a) BOMF/MNA-2-MI0.5-pc180 and (b) BOMF/MNA-2-MI0.5-pc230 under inert (nitrogen) and oxidative (air) atmosphere

## Epoxy thermosets based on furan-diglycidyl ether |

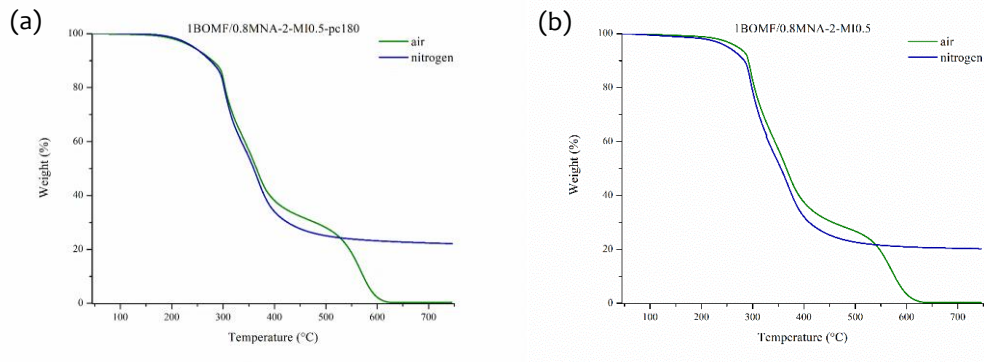


**Figure 3.47** – Weight loss of (a) 1BOMF/0.8MNA-2-MI0.5-pc180 and (b) 1BOMF/0.8MNA-2-MI0.5-pc230 under inert (nitrogen) and oxidative (air) atmosphere

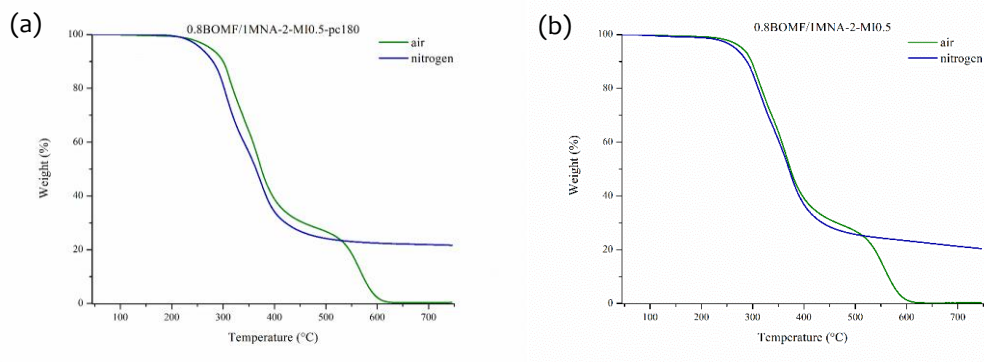


**Figure 3.48** – Weight loss of (a) 0.8BOMF/1MNA-2-MI0.5-pc180 and (b) 0.8BOMF/1MNA-2-MI0.5-pc230 in inert (Nitrogen) and oxidative (Air) atmosphere

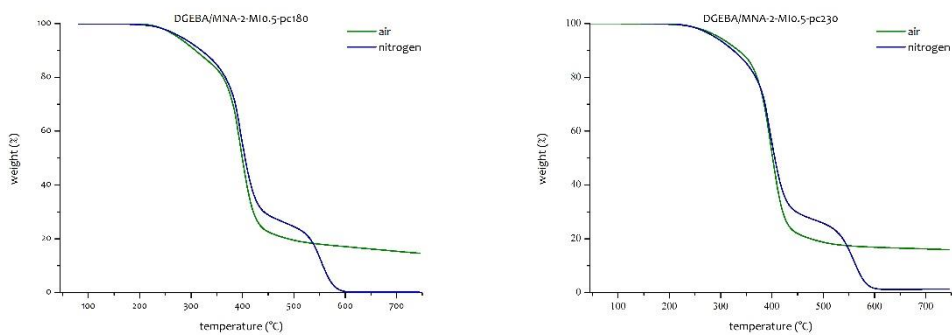


**Figure 3.49** – Weight loss of (a) 0.8BOMF/1MNA-2-MI0.5-pc180 and (b) 0.8BOMF/1MNA-2-MI0.5-pc230 in inert (Nitrogen) and oxidative (Air) atmosphere



Thermal stability of bio-based systems proposed results comparable with data reported in literature for DGEBA/anhydride resins<sup>57,58</sup>.

## Swelling measurements

The swelling index is directly influenced by crosslinking density; in fact, the higher the crosslinking density, the lower the amount of solvent that can be absorbed by the sample. Results obtained for all samples are reported in **Table 3.9**

**Table 3.9** – Swelling indexes for bio-based resins and reference samples cured with two different thermal treatments

	$T_{pc} = 180\text{ }^{\circ}\text{C}$	$T_{pc} = 230\text{ }^{\circ}\text{C}$
<b>BOMF/MNA-2-MI0.5</b>	45.2 ± 8.6	57.3 ± 7.6
<b>1BOMF/0.8MNA-2-MI0.5</b>	91.9 ± 10.7	55.9 ± 4.3
<b>0.8 BOMF/1MNA-2-MI0.5</b>	47.1 ± 8.9	45.9 ± 3.4
<b>DGEBA/MNA-2-MI0.5</b>	45.5 ± 11.6	24.0 ± 12.3

Samples 1BOMF/0.8MNA-2-MI0.5 and 0.8BOMF/1MNA-2-MI0.5 underwent to a second post-cure at higher temperature (namely 230 °C) show a lower swelling index, as could be predicted. The change in SI with different thermal treatment is significant when an epoxy excess is used, confirming that a post-cure happened. The slight change in SI for samples with anhydride excess, instead, suggests that a good crosslinking degree is obtained also with low temperature treatments and is mainly related to the presence of more rigid anhydride units. An unpredictable behavior, instead, is shown by BOMF/MNA-2-



MI0.5: increasing the cure temperature the SI increases. It could be related to a partial degradation of low molecular weight chains.

Comparing samples with different compositions obtained with the same thermal treatment, it is noticed that when  $T_{pc} = 180\text{ }^{\circ}\text{C}$  the highest crosslinking density is obtained when stoichiometric epoxy/anhydride ratio is used while, when of one of the two reactants is used in excess, the lack of the other reactant leads to a low crosslinking degree. Moreover, for 1BOMF/0.8MNA-2-MI0.5, the relatively low post-cure temperature, that does not activates the homopolymerization process, induces a very high SI. Increasing the post-cure temperature a completely different trend is shown by samples with different epoxy/anhydride ratio: the highest crosslinking density is shown by 0.8BOMF/1MNA-2-MI0.5 followed by 1BOMF/0.8MNA-2-MI0.5 and BOMF/MNA-2-MI0.5. DGEBA-based resins show, for  $T_{pc} = 180\text{ }^{\circ}\text{C}$  an SI similar to those of furan-based resins (except 1BOMF/0.8MNA-2-MI0.5) while, when  $T_{pc} = 230\text{ }^{\circ}\text{C}$  the SI is very low, indicating an high crosslinking degree.

## Mechanical tests

Mechanical properties of epoxy resins prepared with different epoxy/anhydride ratio were evaluated by means of tensile tests. The stress-strain curves for all resins are reported in **Figure 3.50** and **Figure 3.51**, while Young's modulus, stress at peak and strain at peak are reported in **Table 3.10**. Comparisons between the different thermal treatment for each system are reported in **Figure 3.52**, **Figure 3.53** and **Figure 3.54**.

By comparing samples post-cured at  $180\text{ }^{\circ}\text{C}$  and samples post-cured at  $230\text{ }^{\circ}\text{C}$ , we can see that in the first case, the bio-based resins prepared with higher

amounts of MNA showed higher Young's Modulus, related to the increase in percentage of rigid moieties in the final structure of the epoxy resins, even if the degree of crosslinking with an MNA excess is lower than that of the stoichiometric sample. As for systems post cured at 230 °C, a decrease of the Young's Modulus was recorded for the resin prepared with an excess of anhydride, while the stoichiometric resin (epoxy/anhydride ratio 1:1) showed the higher modulus (about 1700 MPa). For both the curing processes, the system 0.8BOMF/1MNA-2-MI0.5 showed the highest stress at peak (50.6 MPa and 51.9 MPa for the post-cure at 180 and 230 °C, respectively). If compared with DGEBA/MNA-2-MI0.5, BOMF/MNA-2-MI0.5 shows always higher Young's Modulus and stress at peak. DGEBA-based resins are very fragile and less rigid than furan-based resins.

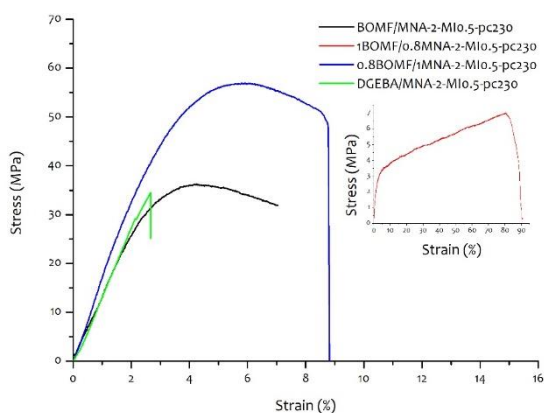


Figure 3.50 – Stress-strain curves for samples post-cured at 180 °C

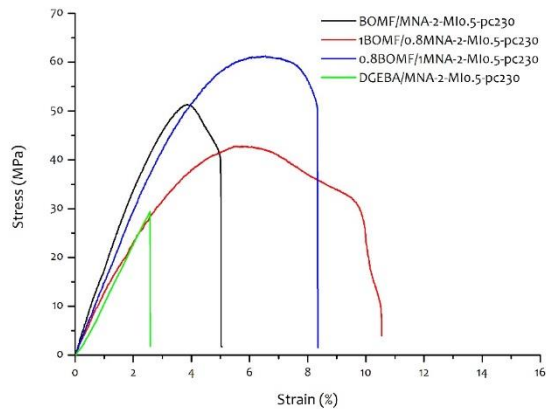


Figure 3.51 – Stress-strain curves for samples post-cured at 230 °C

Table 3.10 – Young's Modulus, stress and stain at peak of for samples undergone to different curing treatments

	YOUNG'S MODULUS [MPa]	STRESS AT PEAK [MPa]	STRAIN AT PEAK [%]
<b>BOMF/MNA-2-MI0.5-pc180</b>	1467 ± 46	32.8 ± 3,6	4.0 ± 0,2
<b>1BOMF/0.8MNA-2-MI0.5-pc180</b>	292.8 ± 72	5.9 ± 1.6	65.7 ± 20.7
<b>0.8BOMF/1MNA-2-MI0.5-pc180</b>	1724 ± 77	48.9 ± 7,0	4.5 ± 1,2
<b>DGEBA/MNA-2-MI0.5-pc180</b>	1326 ± 159	20.43 ± 12	2.6 ± 0.6
<b>BOMF/MNA-2-MI0.5-pc230</b>	1703 ± 254	48,7 ± 3,0	3,8 ± 0,4
<b>1BOMF/0.8MNA-2-MI0.5-pc230</b>	1201 ± 111	44,3 ± 1,7	6,4 ± 0,6
<b>0.8BOMF/1MNA-2-MI0.5-pc230</b>	1325 ± 195	58,5 ± 2,0	6,9 ± 0,9

DGEBA/MNA-2-MI0.5-PC230	1361 ± 163	29.8 ± 2.8	2.5 ± 0.5
-------------------------	------------	------------	-----------

From the image in **Figure 3.43** it is evident that the mechanical behavior of the BOMF/MNA-2-MI0.5 resin changes radically with the curing process. In fact, samples post-cured at 230 °C are more fragile and have higher Young's Modulus than the ones that cure until 180 °C. This can be attributed to a higher cross-linking density achieved with the treatment at 230 °C.

In the case of 0.8BOMF/1MNA-2-MI0.5 resin, the mechanical behaviour did not change significantly, and the curves exhibited a similar trend. The interesting difference is that the sample post-cured at T = 230 °C had lower Young modulus but a higher stress and strain at peak than the one post-cured at 180 °C.

Peculiar is the behaviour of the system prepared with an epoxy excess: as above-mentioned it was rubbery when post-cured at 180 °C, as evident by the stress-strain curve. When post-cured at 230 °C a significant increase in both Young's modulus and stress at break was evidenced. Strain at peak decreases, indicating the fragile behaviour of the samples post-cures at higher temperatures. The bio-based epoxy resins proposed exhibit good mechanical properties

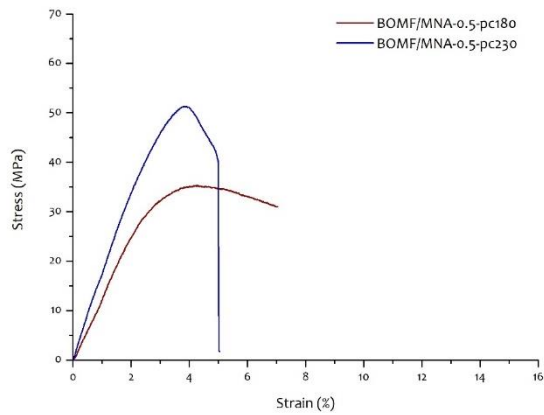


Figure 3.52 – Stress-strain curves for BOMF/MNA-2-MI0.5 undergone to different curing treatments

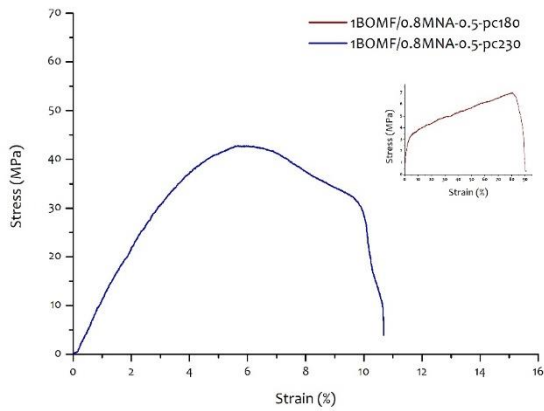
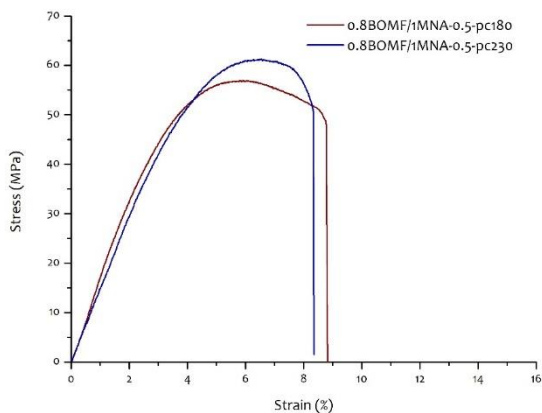
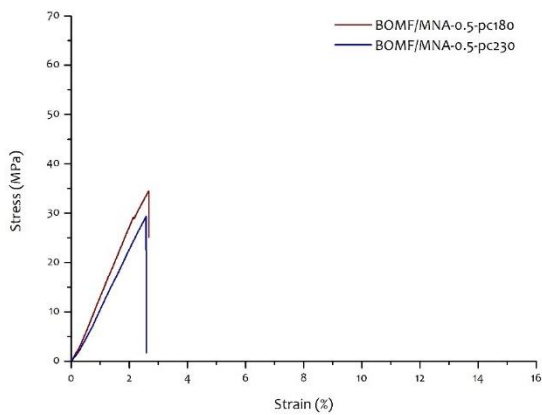


Figure 3.53 – Stress-strain curves for 1BOMF/0.8MNA-2-MI0.5 undergone to different curing treatments



**Figure 3.54** – Stress-strain curves for 0.8BOMF/1MNA-2-MI0.5 undergone to different curing treatments



**Figure 3.55** – Stress-strain curves for DGEBA/MNA-2-MI0.5 undergone to different curing treatments

## 3.4. Conclusions

---

In the experimental work presented in the present chapter, a furan-based epoxy resin starting from 2,5-bis(hydroxymethyl)furan (BHMF) was synthesized. BHMF was obtained from reduction of hydroxyl methyl furfural, in turn, obtained from dehydration of glucose, and therefore it was completely bio-based. BHMF was reacted with epichlorohydrin (ECH), to obtain the starting monomer, the 2,5-bis[(oxyran-2-ylmethoxy)methyl]furan (BOF).

Methyl nadic anhydride (MNA) was used as a curing agent and mixed with epoxy monomer in different epoxy/anhydride ratios (1:1, 1:1.2, 1:0.8). The curing reaction was carried out in presence of 2-methyl imidazole (2-MI), chosen as initiator after the action of other initiators was analyzed.

The reaction kinetics was studied through calorimetric, spectroscopic and rheological methods. DSC analysis was performed in both isothermal and dynamic mode and was used to determine the degree of conversion and get the optimal curing conditions in terms of temperatures and times for the resins.

FT-IR tests showed the effective consumption of anhydride and epoxy groups upon curing, by following the disappearance of characteristic peaks of each one, as well as the formation of carbonyl peaks characteristic of the ester group formation of cured resin. The degree of cure was then evaluated monitoring the relative area of these peaks.

Rheological tests were also carried out to calculate viscoelastic properties of resins undergoing the cure process.

The thermal stability of cured resins was tested by thermogravimetric analysis both in air and nitrogen. The curves showed that the blends exhibited the same trend, and the degradation was higher in nitrogen because of the formation in air of oxide layer that protect the samples. However, the weight loss was full in air, while a 20% of residual weight was registered under nitrogen.

Two sets of samples of this bio-based epoxy resins in different components ratios were obtained following two different curing procedures. On these samples, mechanical tests were carried out. The Young's modulus resulted higher for the resin containing the excess of anhydride (i.e. 0.8BOMF/1MNA-2-MI0.5), when cured until 180 °C, while in the case of the stoichiometric one (BOMF/MNA-2-MI0.5), it was higher when cured until 230 °C. For the epoxy excess resin (1BOMF/0,8MNA-0.5), the modulus was very low when cured until 180 °C, and slightly higher upon post-curing at 230 °C.

Overall results demonstrated that the synthesized furan-based resins have good chemical-physical properties and can be proposed as effective alternatives to traditional, bisphenol A-based resins. Moreover, by changing the relative formulations and the thermal conditions used to cure the systems, the features of the final materials can be modulated depending on the characteristics required for the specific application.



## 3.5. Bibliography

---

1. Pandey, A., Höfer, R., Larroche, C., Taherzadeh, M. & Nampoothiri, K. M. *Industrial Biorefineries and White Biotechnology*. (2015).
2. Stemmelen, M., Lapinte, V., Habas, J. P. & Robin, J. J. Plant oil-based epoxy resins from fatty diamines and epoxidized vegetable oil. *Eur. Polym. J.* **68**, 536–545 (2015).
3. Zhang, C., Garrison, T. F., Madbouly, S. A. & Kessler, M. R. Recent advances in vegetable oil-based polymers and their composites. *Prog. Polym. Sci.* **71**, 91–143 (2017).
4. Kumar, S., Samal, S. K., Mohanty, S. & Nayak, S. K. Epoxidized Soybean Oil-Based Epoxy Blend Cured with Anhydride- Based Cross-Linker: Thermal and Mechanical Characterization. *Ind. Eng. Chem. Res.* **56**, 687–698 (2017).
5. Wang, R. & Schuman, T. P. Vegetable oil-derived epoxy monomers and polymer blends: A comparative study with review. *Express Polym. Lett.* **7**, 272–292 (2012).
6. Pin, J.-M., Guigo, N., Vincent, L., Sbirrazzuoli, N. & Mija, A. Copolymerization as a Strategy to Combine Epoxidized Linseed Oil and Furfuryl Alcohol: The Design of a Fully Bio-Based Thermoset. *ChemSusChem* **8**, 4149–4161 (2015).
7. Pin, J.-M., Sbirrazzuoli, N. & Mija, A. From epoxidized linseed oil to bioresin: An overall approach of epoxy/anhydride cross-linking. *ChemSusChem* **8**, 1232–1243 (2015).
8. François, C. *et al.* Diglycidylether of iso-eugenol: a suitable lignin-derived

- synthon for epoxy thermoset applications. *RSC Adv.* **6**, 68732–68738 (2016).
9. Xin, J., Li, M., Li, R., Wolcott, M. P. & Zhang, J. A green epoxy resin system based on lignin and tung oil and its application in epoxy asphalt. *ACS Sustain. Chem. Eng.* acssuschemeng.6b00256 (2016). doi:10.1021/acssuschemeng.6b00256
  10. Ferdosian, F., Yuan, Z., Anderson, M. & Xu, C. Sustainable lignin-based epoxy resins cured with aromatic and aliphatic amine curing agents: Curing kinetics and thermal properties. *Thermochim. Acta* **618**, 48–55 (2015).
  11. Asada, C., Basnet, S., Otsuka, M., Sasaki, C. & Nakamura, Y. Epoxy resin synthesis using low molecular weight lignin separated from various lignocellulosic materials. *Int. J. Biol. Macromol.* **74**, 413–419 (2015).
  12. Upton, B. M. & Kasko, A. M. Strategies for the Conversion of Lignin to High-Value Polymeric Materials: Review and Perspective. *Chem. Rev.* **116**, 2277 (2015).
  13. Sasaki, C. *et al.* Evaluation of epoxy resins synthesized from steam-exploded bamboo lignin. *Ind. Crops Prod.* **43**, 757–761 (2013).
  14. Kosbar, L. L., Gelorme, J. D., Japp, R. M. & Fotorny, W. T. Introducing Biobased Materials into the Electronics Industry: Developing a Lignin-based Resin for Printed Wiring Boards. *J. Ind. Ecol.* **4**, 93–105 (2000).
  15. Zhao, S. & Abu-Omar, M. M. Biobased Epoxy Nanocomposites Derived from Lignin-Based Monomers. *Biomacromolecules* 150702075936002 (2015). doi:10.1021/acs.biomac.5b00670

16. Jiang, Y. *et al.* Renewable thermoset polymers based on lignin and carbohydrate derived monomers. *Green Chem.* **20**, 1131–1138 (2018).
17. Salanti, A., Zoia, L., Simonutti, R. & Orlandi, M. Epoxidized Lignin Derivatives as Bio-based Cross-linkers Used in the Preparation of Epoxy Resins. *BioResources* **13**, 2374–2396 (2018).
18. Cho, J. K., Lee, J., Jeong, J. & Kim, B. Synthesis of carbohydrate biomass-based furanic compounds bearing epoxide end group (s) and evaluation of their feasibility as adhesives. *J. Adhes. Sci. Technol.* **27**, 2127–2138 (2013).
19. Hu, F., La Scala, J. J., Sadler, J. M. & Palmese, G. R. Synthesis and characterization of thermosetting furan-based epoxy systems. *Macromolecules* **47**, 3332–3342 (2014).
20. Hu, F., Yadav, S. K., La Scala, J. J., Sadler, J. M. & Palmese, G. R. Preparation and Characterization of Fully Furan-Based Renewable Thermosetting Epoxy-Amine Systems. *Macromol. Chem. Phys.* **216**, 1441–1446 (2015).
21. Shen, X., Liu, X., Wang, J., Dai, J. & Zhu, J. Synthesis of an Epoxy Monomer from Bio-Based 2,5-Furandimethanol and Its Toughening via Diels-Alder Reaction. *Ind. Eng. Chem. Res.* **56**, 8508–8516 (2017).
22. Tachibana, Y., Torii, J., Kasuya, K., Funabashi, M. & Kunioka, M. Hardening process and properties of an epoxy resin with bio-based hardener derived from furfural. *RSC Adv.* **4**, 55723–55731 (2014).
23. Deng, J., Liu, X., Li, C., Jiang, Y. & Zhu, J. Synthesis and properties of a bio-based epoxy resin from 2,5-furandicarboxylic acid (FDCA). *RSC Adv.* **5**, 15930–15939 (2015).
24. Miao, J. T., Yuan, L., Guan, Q., Liang, G. & Gu, A. Biobased Heat Resistant

- Epoxy Resin with Extremely High Biomass Content from 2,5-Furandicarboxylic Acid and Eugenol. *ACS Sustain. Chem. Eng.* **5**, 7003–7011 (2017).
25. Vyazovkin, S. et al. ICTAC Kinetics Committee recommendations for collecting experimental thermal analysis data for kinetic computations. *Thermochim. Acta* **590**, 1–23 (2014).
  26. Ivankovic, M., Incarnato, L., Kenny, J. M. & Nicolais, L. Curing Kinetics and Chemorheology of Epoxy / Anhydride System. *J. Appl. Polym. Sci.* **90**, 3012–3019 (2003).
  27. Vyazovkin, S. & Sbirrazzuoli, N. Kinetic methods to study isothermal and nonisothermal epoxy-anhydride cure. *Macromol. Chem. Phys.* **200**, 2294–2303 (1999).
  28. Van Assche, G., Swier, S. & Van Mele, B. Modeling and experimental verification of the kinetics of reacting polymer systems. *Thermochim. Acta* **388**, 327–341 (2002).
  29. Vyazovkin, S. & Sbirrazzuoli, N. Mechanism and kinetics of epoxy-amine cure studied by differential scanning calorimetry. *Macromolecules* **29**, 1867–1873 (1996).
  30. Garschke, C., Parlevliet, P. P., Weimer, C. & Fox, B. L. Cure kinetics and viscosity modelling of a high-performance epoxy resin film. *Polym. Test.* **32**, 150–157 (2013).
  31. Atarsia, A. & Boukhili, R. Relationship between isothermal and dynamic cure of thermosets via the isoconversion representation. *Polym. Eng. Sci.* **40**, 607–620 (2000).

32. Musto, P., Martuscelli, E., Ragosta, G., Russo, P. & Villano, P. Tetrafunctional epoxy resins: Modeling the curing kinetics based on FTIR spectroscopy data. *J. Appl. Polym. Sci.* **74**, 532–540 (1999).
33. Flores, M., Fernández-Francos, X., Ramis, X. & Serra, A. Novel epoxy-anhydride thermosets modified with a hyperbranched polyester as toughness enhancer. I. Kinetics study. *Thermochim. Acta* **544**, 17–26 (2012).
34. Fernández, X. et al. Modification of epoxy-anhydride thermosets using a hyperbranched poly(ester-amide): I. Kinetic study. *Polym Int* **61**, 1710–1725 (2012).
35. Ashcroft, W. R. et al. *Chemistry and Technology of Epoxy Resins*. (Springer Science+Business Media, B.V., 1993). doi:10.1007/978-94-011-2932-9
36. Bouillon, N., Pascault, J.-P. & Tighzert, L. Influence of different imidazole catalysts on epoxy-anhydride copolymerization and on their network properties. *J. Appl. Polym. Sci.* **38**, 2103–2113 (1989).
37. Guerrero, P., De la Caba, K., Valea, A., Corcuera, M. A. & Mondragon, I. Influence of cure schedule and stoichiometry on the dynamic mechanical behaviour of tetrafunctional epoxy resins cured with anhydrides. *Polymer (Guildf)*. **37**, 2195–2200 (1996).
38. Baroncini, E. A., Kumar Yadav, S., Palmese, G. R. & Stanzione, J. F. Recent advances in bio-based epoxy resins and bio-based epoxy curing agents. *J. Appl. Polym. Sci.* **133**, 1–19 (2016).
39. Boquillon, N. & Fringant, C. Polymer networks derived from curing of epoxidised linseed oil: influence of different catalysts and anhydride hardeners. *Polymer (Guildf)*. **41**, 8603–8613 (2000).

40. No Title. Available at: <https://www.threebond.co.jp/en/technical/technicalnews/pdf/tech32.pdf>.
41. Kumar, S., Samal, S. K., Mohanty, S. & Nayak, S. K. Study of curing kinetics of anhydride cured petroleum-based (DGEBA) epoxy resin and renewable resource based epoxidized soybean oil (ESO) systems catalyzed by 2-methylimidazole. *Thermochim. Acta* **654**, 112–120 (2017).
42. Fernández-Francos, X., Ramis, X. & Serra, À. From curing kinetics to network structure: A novel approach to the modeling of the network buildup of epoxy-anhydride thermosets. *J. Polym. Sci. Part A Polym. Chem.* **52**, 61–75 (2014).
43. Supanchaiyamat, N., Shuttleworth, P. S., Hunt, A. J., Clark, J. H. & Matharu, A. S. Thermosetting resin based on epoxidised linseed oil and bio-derived crosslinker. *Green Chem.* **14**, 1759–1765 (2012).
44. Paramarta, A. & Webster, D. C. Bio-based high performance epoxy-anhydride thermosets for structural composites: The effect of composition variables. *React* **105**, 140–149 (2016).
45. Pan, X., Sengupta, P. & Webster, D. C. High biobased content epoxy-anhydride thermosets from epoxidized sucrose esters of fatty acids. *Biomacromolecules* **12**, 2416–2428 (2011).
46. Mahendran, A. R., Wuzella, G., Kandelbauer, A. & Aust, N. Thermal cure kinetics of epoxidized linseed oil with anhydride hardener. *J. Therm. Anal. Calorim.* **107**, 989–998 (2012).
47. Mauri, A. N. & Riccardi, C. C. The effect of epoxy excess on the kinetics of an epoxy-anhydride system. *J. Appl. Polym. Sci.* **85**, 2342–2349 (2002).

48. E2070 – 13 Standard Test Method for Kinetic Parameters by Differential Scanning Calorimetry Using Isothermal Methods 1. 1–12 (2017). doi:10.1520/E2070-13.2
49. Paramarta, A. & Webster, D. C. Curing kinetics of bio-based epoxy-anhydride thermosets with zinc catalyst. *J. Therm. Anal. Calorim.* **130**, 2133–2144 (2017).
50. Barton, J. The application of differential scanning calorimetry (DSC) to the study of epoxy resin curing reactions. *Epoxy Resins Compos. I* **72**, 111–154 (1985).
51. Zhao, L. & Hu, X. Autocatalytic curing kinetics of thermosetting polymers: A new model based on temperature dependent reaction orders. *Polymer (Guildf)*. **51**, 3814–3820 (2010).
52. Kenny, J. M. Determination of Autocatalytic Kinetic Model Parameters Describing Thermoset Cure. *J. Appl. Polym. Sci.* **51**, 761–764 (1994).
53. Barghamadi, M. Kinetics and Thermodynamics of Isothermal Curing Reaction of Epoxy-4, 40-Diaminoazobenzene Reinforced with Nanosilica and Nanoclay Particles. *Polym. Compos.* **31**, 1442–1448 (2010).
54. Mertz, E. & Koenig, J. Application of FT-IR and NMR to Epoxy Resins. *Epoxy Resins Compos. II* 73–112 (1986). doi:10.1007/BFb0017915
55. Musto, P., Martuscelli, E., Ragosta, G., Russo, P. & Scarinzi, G. An Interpenetrated System Based on a Tetrafunctional Epoxy Resin and a Thermosetting Bismaleimide: Structure– Properties Correlation. *J. Appl. Polym. Sci.* **69**, 1029–1042 (1998).
56. Rose, N., Le Bras, M., Delobel, R., Costes, B. & Henry, Y. Thermal oxidative

- degradation of an epoxy resin. *Polym. Degrad. Stab.* **42**, 307–316 (1993).
57. Su, W.-F., Lee, Y.-C. & Pan, W.-P. *Thermal properties of phthalic anhydride- and phenolic resin-cured rigid rod epoxy resins.*
58. François, C. *et al.* Design and synthesis of biobased epoxy thermosets from biorenewable resources. *Comptes Rendus Chim.* **20**, 1006–1016 (2017).







# Chapter 4.

---

Furan-based  
bio-epoxy  
resins and  
nanocomposites  
as tinplate  
coatings



## 4.1. Introduction

---

Thanks to their good properties of mechanical strength, chemical resistance and good adhesion to several substrates, epoxy resins perfectly fit for coating applications. However some of their characteristics as shrinkage upon cure and fragility that can cause affect their use as coating. Not less important is the environmental problem linked to both the nature of the components constituting the resins and the presence of final materials in the environment not being thermosets easily recyclable. To face this problem renewable resources has been used for the synthesis of new platform chemicals to avoid anticipated depletion of fossil oil reserves, that is causing also a rise in oil price. Moreover, the quite majority of epoxy resins are nowadays made by DGEBA, the diglycidyl ether of BPA, banned from production of materials in contact with food<sup>1-5</sup>. Development of new bio-based epoxy resins for can coatings application is consequently of main interest nowadays.

Nevertheless scientific production lacks in bio-based epoxy coatings. Some papers propose cardanol as only partial substitute to DGEBA<sup>6-8</sup>; Its properties are insufficient to substitute DGEBA so that mixtures with other bio-based epoxides from isosorbide or flavonoids were proposed to obtain a coating with good enough properties. Also lignin was bounded to DGEBA moieties and employed to produce coatings with improved properties<sup>9</sup>. Hard coating were obtained with epoxy resins obtained from rosin acid and proposed as corrosion protective coatings<sup>10</sup>. Other bio-based coatings proposed are polyesters, polyurethanes or acrylates<sup>11-14</sup>; anyway to guarantee required properties for a

coating, as mechanical and chemical resistance, aromatic epoxy resins are needed.

Good properties in terms of thermal and mechanical properties exhibited by the bio-based BOMF/MNA resin synthesized and characterized in Chapter 3 suggested that they are valuable substitute for DGEBA-based protective coating for metal cans. In this Chapter, BOMF/MNA resins and nanocomposites obtained by addition of titanium dioxide nanoparticles were tested as tinplate coating.

Coating layers were obtained on a tinplate substrate, previously treated to improve the adhesion. Chemo-rheological, thermal, chemical resistance and morphological tests were used to optimize the processing conditions and to evaluate the overall performance of the bio-based coatings. The effect of TiO<sub>2</sub> nanoparticles on the resin behavior was also studied. Results demonstrated bio-derived epoxy resin and nanocomposite coatings had properties comparable with those of DGEBA-based systems and thus can be proposed as an alternative material for metal can coating industry, highlighting the importance of renewable polymers towards a successful bioeconomy.

## 4.2. Experimental section

---

### 4.2.1. Materials

2,5-bis[(oxiran-2-ylmethoxy)methyl]furan (BOMF) was synthesized following the synthetic procedure presented in the *Experimental Section* of

Chapter 3. Methyl-5-norbornene-2,3-dicarboxylic anhydride (methyl nadic anhydride, MNA, 90%) was provided by Sigma Aldrich and used as a curing agent. 2-methylimidazole (2-MI, 99%) purchased from Acros Organics was used as initiator. Fumed titanium dioxide particles with a specific surface area of  $50 \pm 15 \text{ m}^2/\text{g}$  (AEROXIDE<sup>®</sup> TiO<sub>2</sub> P 25). Ethanol (96%) was purchased by Acros Organics and acetic acid (glacial) from Romil.

#### 4.2.2. Tinplate treatment

The wettability of the substrate by the resin is a key factor to ensure good application and successful curing; a poor wettability can cause defects such as dewetting, holes and poor adhesion properties<sup>15</sup> Improvements in wettability can be obtained by the application of different chemical or physical treatments on the metallic surface aimed at increasing the surface roughness. To get a modification of the surface conditions, a treatment was applied to the previously degreased tinplate, consisting in a thermal treatment for 1 hour at 250°C, followed by mechanical polishing with P 320 sandpaper.

#### 4.2.3. Preparation of coatings

Epoxy/anhydride reaction mixtures were prepared by mixing BOMF epoxy monomer and MNA in stoichiometric ratio  $R = 1$  with 2-MI, used as initiator (0.5 wt.% with respect to the epoxy+anhydride). The reaction mixture was labelled as BOMF/MNA. Three more formulations were obtained by adding 1, 3 and 5 wt.% of TiO<sub>2</sub> to BOMF/MNA; this sample was labelled BOMF/MNA-1TiO<sub>2</sub>, BOMF/MNA-3TiO<sub>2</sub> and BOMF/MNA-5TiO<sub>2</sub> respectively.

To achieve a good dispersion of titanium dioxide nanoparticles in the epoxy resin mixture, the  $\text{TiO}_2$  powder was first mixed with the suitable amount of MNA. The mixture was then sonicated with an ultrasound tip processor. Sonication was held for a total of 15 minutes, at an amplitude of 25%, alternating 30 sec ON/30 sec OFF pulses. Subsequently, the resulting mixture was mechanically mixed with the proper amount of BOMF and 2-MI.

A further formulation, used to obtain reference sample, was prepared by mixing DGEBA and MNA in stoichiometric ratio and 0.5 wt.% of 2-MI as initiator.

Samples of bulk material were obtained to perform mechanical tests and thermal analysis. In order to obtain samples of dimensions indicated in the ASTM638 as type V, silicon mold with the desired shape were produced and following used to cast epoxy samples. A cure program consisting in 1 hour of cure at  $160^\circ\text{C}$  and 1 hour of post-cure at  $180^\circ\text{C}$  was applied and thermosetting samples obtained.

The epoxy mixtures were applied on treated tinplate specimens (50 x 100 mm) with the aid of a K101 n<sup>o</sup>2 K Hand Coater (RK Print Coat Instrument), with a fixed thickness of 12  $\mu\text{m}$ , then cured in oven for 1 hour at  $160^\circ\text{C}$  and post-cured for 1 hour at  $180^\circ\text{C}$ .

#### 4.2.4. Methods

Rheometer MARS III, interfaced with a iN20 Nicolet FT-IR spectrophotometer by a Rheonaut temperature controller, was used to performed combined rheological and infrared analysis. Chemo-rheological tests were performed on plate–plate geometries (20 mm diameter and 0,8 mm gap) at a fixed frequency ( $\omega$ ) of 10 rad/s and deformation ( $\gamma$ ) in auto-strain mode of



15% ± 15%. Two kinds of measurements were performed: dynamic measurements, by varying the temperature from 50 to 150 °C, at a heating rate of 1.5°C/min, and isothermal analysis at 110 °C. The temperature of crossover of the values of storage ( $G'$ ) and loss ( $G''$ ) moduli was considered as the temperature of gelation ( $T_{gel}$ ). Also, rotation ramp tests with a shear rate  $\dot{\gamma}$  from 2 to 200 sec<sup>-1</sup> were performed to evaluate viscosity at 30 °C. Simultaneously to the rheological measurements, FT-IR analysis was carried out on the reacting mixtures. Spectroscopic analysis was performed in ATR mode. Spectra were acquired as single beam spectra in the range of 4000-400 cm<sup>-1</sup> with a resolution of 4 cm<sup>-1</sup> and 8 scans; before each analysis, different background spectra were collected at different temperatures in the above-mentioned temperature range. Data were first processed with Omnic software to subtract the appropriate background, then spectra were exported to the PerkinElmer TimeBase software to perform the time-dependent analysis.

A TA Instrument DSC Q2000, equipped with Refrigerator Cooling System (RCS), was used for calorimetric analysis (DSC), under inert nitrogen flux (50 mL min<sup>-1</sup>). Dynamic measurements from 25 to 200°C at 10°C/min heating rates and isothermal analysis 130°C were performed to evaluate the enthalpy of the curing process ( $\Delta H_{tot}$ ). A second scan at 20°C/min to -10°C and a following heating scan at 10°C were performed on all the samples to detect the  $T_g$  of the cured resins and a potential post-cure. Numerical analysis was performed using Origin software.

Thermogravimetric analysis (TGA) was performed by using a TA Instrument TGA 500 thermobalance. Tests were carried out from 25 to 750 °C at a heating rate of 10 °C/min; different measurements were performed under a 60 mL min<sup>-1</sup> nitrogen or air flux respectively.

Tensile tests on bulk materials were performed by using an INSTRON 5564 with 1kN dynamometer. 3 specimens for each composition were tested with 2mm/min crosshead speed in environmental conditions of 20 °C and 50% humidity.

Static contact angles (CA) of water and BOMF/MNA on different substrates were measured by the sessile drop method with the help of FTA 1000B (First Ten Ångstroms) instrument. Measurements were performed at room temperature and evaluations of the contact angle were performed directly with the FTA32 Video 2.1 software. Distilled water drops of 5µL were deposited on the coatings surface; the contact angle values were reported as average value on five measurements.

Chemical resistance of the coatings was tested by immersing the cured coated metal plates into ethanol (96%) and 3 vol.% acetic acid solutions, used as simulants, for 3,7,15 and 30 days at 25°C.

Treated/untreated tinplate and coatings surfaces (before and after immersion to test chemical resistance) were observed through scanning electron microscopy (SEM) by means of a FEI Quanta 200 FEG SEM in high vacuum mode. Before SEM observations, the samples were mounted onto SEM stubs by means of carbon adhesive disks and sputter coated with a 5-10 nm thick Au-Pd layer by means of a Emitech K575X sputter coater. All the samples were observed at 10-30 kV acceleration voltage using a secondary electron detector.

Energy dispersive X-ray (EDX) analysis was performed on the untreated and treated tinplate by means of a FEI Quanta 200 FEG SEM equipped with an Oxford Inca Energy System 250 and an Inca-X-act LN<sub>2</sub>-free analytical silicon drift detector.

The pencil hardness of coating was measured according to ASTM D3363 test using a pencil set with maximum hardness 5H.

The adhesion test of coating was measured according to ASTM D3359 test using pressure sensitive tape INTERTAPE LA-26/NAT160.

## Kinetic analysis by FTIR-ATR spectroscopy

Quantitative analysis of functional groups involved in the curing process was made by IR spectroscopy. Characteristic peaks, identified both in terms of intensity and position (frequency), were monitored and changes in their absorbance area collected as a function of time or temperature.

The experimental relative conversion ( $\alpha$ ), for the species consumption, can be expressed as follows: <sup>16</sup>

$$\alpha = \frac{C_0 - C_t}{C_0} = 1 - \frac{C_t}{C_0} \quad \text{Equation 4.1}$$

Considering the Lambert-Beer relation follows

$$\alpha = 1 - \frac{A_t}{A_0} \quad \text{Equation 4.2}$$

where  $C$  is the species molar concentration and  $A_t$  is the monitored absorbance area, the subscripts  $o$  and  $t$  stand for zero and current time respectively. **Equation 4.2** was used to determine conversion of disappearing groups while **Equation 4.3** was used to evaluate the conversion degree of groups that are formed during the process. <sup>17</sup>

$$\alpha = \frac{A_t - A_0}{A_\infty - A_0} \quad \text{Equation 4.3}$$

The term  $A_\infty$  in the last equation refers to the final absorbance for the species monitored.

In the case of the monitored band between 930 and 860  $\text{cm}^{-1}$ , characteristic epoxy and anhydride groups are overlapped so the absorbance area related to the only epoxy group must be evaluated by the following equation:

$$A_{t,epox} = A_t - (1 - \alpha_{anh}) \cdot A_t \cdot F \quad \text{Equation 4.4}$$

where  $A_{t,epox}$  is the effective absorbance of epoxy group,  $A_t$  is absorbance area of the entire 950 – 870  $\text{cm}^{-1}$  band,  $\alpha_{anh}$  is anhydride conversion previously evaluated following peaks at 1855 and 1776  $\text{cm}^{-1}$  and  $F$  is the contribute given by anhydride to the band.<sup>17</sup>

## 4.3. Results and discussion

---

### 4.3.1. Characterization of bulk epoxy resins and nanocomposites

Epoxy resins are widely used as coating to protect the metallic substrates from corrosion and, for application in food industry, to avoid the direct contact and chemical reactions between food and metallic surface. Currently, almost the totality of cans linings are constituted by DGEBA-based resins that can release relevant amount of BPA during processing or during the shelf-life of the product, thus promoting the possible migration of BPA into food. Awareness of this phenomenon is leading global governments to introduce legislation that bans the use of BPA-based materials in the food industry<sup>1-5</sup>. Therefore, there is an urgent need to find a valuable substitutes to these resins.

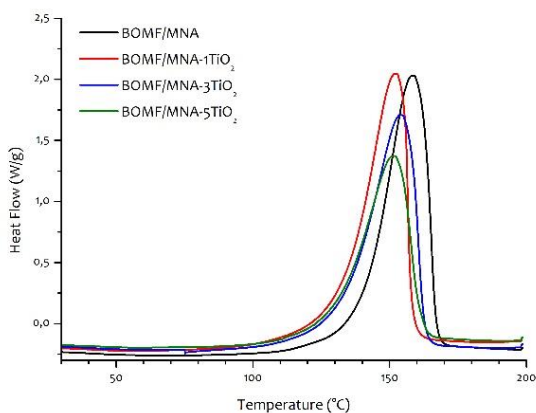
Coatings for food containers must satisfy several technical requirements. Other than being safe for contact with food and beverages by avoiding the migration of dangerous substances and preserving their organoleptic properties, they need to resist to chemical and mechanical stresses. Chemical stresses are first induced by sterilization processes and then by food constituents. Moreover, coatings must guarantee a good adhesion with the metallic substrate both during the metal shaping process and during cans lifecycle, when mechanical deformation can happen accidentally<sup>18</sup>.

Bio-based BOMF/MNA resins presented in the previous Chapter exhibited good properties, especially in terms of thermal resistance. Moreover, they are in liquid form with a relatively low viscosity, that suggest their successful use as coating. In particular, the liquid nature of resins with a low viscosity is a strong technological advantage, as no solvent is needed in the coating process. This application was tested, and the properties of the obtained coating evaluated in terms of mechanical properties and chemical resistance. Nanocomposites have also been obtained adding TiO<sub>2</sub> nanoparticles in different weight percent amounts.

## Thermal analysis of epoxy resins and nanocomposites

One of the effects of filler addition in resins formulations is the variation in thermal characteristics, such as thermal conductivity and exothermal behavior. As can be noticed in **Figure 4.1** the presence of nanosized titanium oxide affects to some extent the curing behavior of the BOMF/MNA system both in terms of curing reaction enthalpy and process kinetics. The exothermic peak associated to the curing process in presence of titanium dioxide is slightly

broader with a comparable peak temperatures. The total heat ( $\Delta H_{tot}$ ) strongly decreases with the amounts of filler (**Table 4.1**), mainly due to the reduction in wt.% of resins on the total weight of the sample analyzed. The broadening of the curing process, starting at lower temperature (onset temperatures are reported in Table 4.1) by effect of nanoparticles addition, is widely reported in literature, and is associated with decrease in reaction enthalpy and peak temperature.<sup>19–22</sup> For BOMF/MNA-5TiO<sub>2</sub> system the broadening effect is noticeable and the curing process ends about 15°C after  $T_p$ ; for the other systems the curing peak ends abruptly after  $T_p$  is reached. Also the glass transition temperature ( $T_g$ ), evaluated by the second heating ramp performed on samples by DSC analysis, is affected by the presence of the filler. When cured through a heating run from room temperature up to 200°C at 10°C/min,  $T_g$  of resins containing nanosized titanium dioxide decreases of about 10–14°C with respect to the plain BOMF/MNA (**Table 4.1**). When filler is added to the epoxy resin it acts as obstacle for the crosslinking reaction between reagents, so the glass transition temperature ( $T_g$ ) undergoes a decrease.

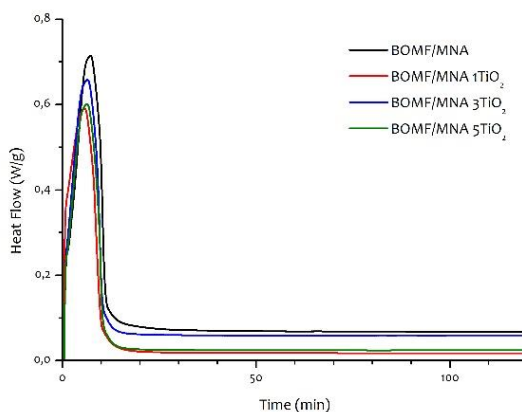


**Figure 4.1** – DSC thermograms of cure process for all systems at a heating rate of 10 °C/min

**Table 4.1** – Total heat of reaction ( $\Delta H_{tot}$ ), peak temperature ( $T_p$ ), onset temperature ( $T_{onset}$ ) and glass transition temperature ( $T_g$ ) of systems cured at 10°C/min

SAMPLE	$\Delta H_{tot}$ [j/g]	$T_p$ [°C]	$T_{onset}$ [°C]	$T_g$ [°C]
BOMF/MNA	264.9	158.4	139.4	26.9
BOMF/MNA-1TiO <sub>2</sub>	259.2	152.1	129.6	25.8
BOMF/MNA-3TiO <sub>2</sub>	253.2	154.0	132.0	24.0
BOMF/MNA-5TiO <sub>2</sub>	204.0	151.4	131.8	28.4

As for the reaction enthalpy, it decreases with the amount of TiO<sub>2</sub>. This is partly due to the reduction in wt.% of resins on the total weight of the sample analyzed. The decrease in reaction enthalpy is much more significant in isothermal analysis carried out at  $T = 130^\circ\text{C}$ , reported in **Figure 4.2** and summarized in **Table 4.2**. Reaction peaks are shifted at higher time but no noticeable influence on  $T_g$  was noticed. In isothermal analysis in facts after the maximum rate of reaction is reached the system has enough time to react and to allow also diffusive processes.

**Figure 4.2** – DSC thermograms of cure process for all systems at 130 °C

**Table 4.2** – Total heat of reaction ( $\Delta H_{tot}$ ), peak time ( $T_p$ ) and glass transition temperature ( $T_g$ ) of systems cured at 130°C

SAMPLE	$\Delta H_{tot}$ [j/g]	$T_p$ [min]	$T_g$ [°C]
BOMF/MNA	538.2	5.7	27.8
BOMF/MNA-1TiO <sub>2</sub>	320.2	5.7	34.6
BOMF/MNA-3TiO <sub>2</sub>	468.9	6.4	24.4
BOMF/MNA-5TiO <sub>2</sub>	338.0	6.3	24.1

## Chemo-rheological analysis of epoxy resins and nanocomposites

To better understand how the presence of the filler affects the curing process of resins, chemo-rheological tests were performed by coupled rheological and FTIR spectroscopic analysis. Rheological measurements, reported in **Figure 4.3**, were performed at 1.5 °C/min heating rate. Particularly interesting is the behavior in pre-gel region, where the elastic modulus is generally higher (or equal) to the viscous modulus.<sup>23</sup> The pristine resin showed two crossover points between elastic and viscous modulus; the first crossover, when  $G''$  passes  $G'$ , corresponded to the increase of viscosity and can be related to the formation of long polymeric chains not yet crosslinked in a tridimensional structure. The second crossover point appeared after less than 10 °C, and it was identified as the gel point. This point is the start of critical region, where a sudden increase in  $G'$  is experienced until a plateau value is reached, corresponding to the final value of elastic modulus for the cures resin.<sup>24</sup> The addition of nanofillers affected the rheological behavior of resin during the curing process. For the system with 1 wt.% of titanium dioxide, the only effect is the reduction of the



distance between the two crossover points, while adding more quantities of filler, viscosity, as well as  $G'$  and  $G''$ , at the beginning of measurement resulted quite constant. Increasing temperature, the resin mixture had low viscosity that vanished the thickening effect of nanoparticles. For the system containing the 3 wt.% of titanium dioxide no overtake of  $G''$  on  $G'$  was observed; at  $120^\circ\text{C}$  the two moduli were equal but afterward elastic modulus started exhibiting a faster growing trend than  $G''$ . The system with 5 wt.% of filler shows a considerable thickening effect; as the temperature increased, the resin becomes fluid until the cure took place. At about  $110^\circ\text{C}$  the values become again constant until the first crossover point (when  $G''$  become bigger than  $G'$ ), that in this case is very close to the second one ( $G' > G''$ ) (Figure 4.3).

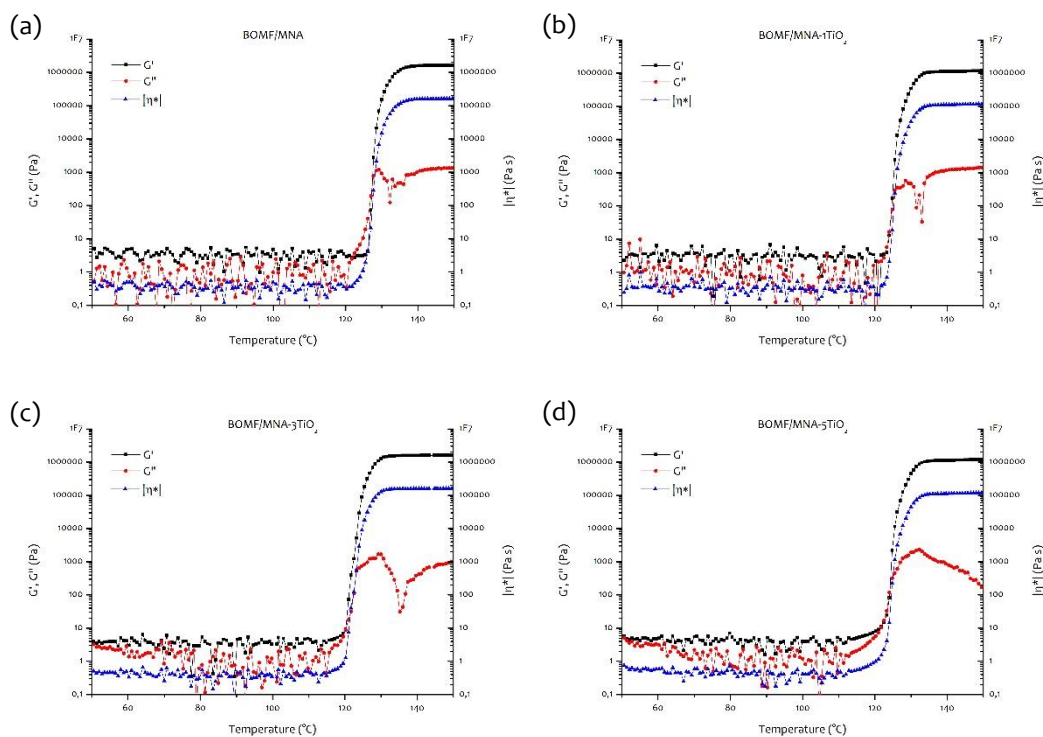


**Figure 4.3** – Rheological tests on (a) BOMF/MNA, (b) BOMF/MNA-1TiO<sub>2</sub>, (c) BOMF/MNA-3TiO<sub>2</sub> and (d) BOMF/MNA-5TiO<sub>2</sub> heated at  $1.5^\circ\text{C}/\text{min}$

As evidenced in **Figure 4.4** and predicted by literature<sup>20</sup>, the addition of nanoparticles induced a decrease in temperature at which the elastic modulus and the complex viscosity strongly increased. These transitions were experimented at different rates depending on presence or not of fillers. When titanium dioxide was added the increase in  $G'$  proceed with a decreased slope. However BOMF/MNA-5TiO<sub>2</sub> showed a different behavior: the cure occurred at higher temperature compared to the system with 3 wt.% of filler, but at lower temperature with respect to BOMF/MNA and BOMF/MNA-1TiO<sub>2</sub>. This behavior is due to the fact that the greater quantity of titanium dioxide has no more an accelerating effect but an hindrance effect on chemical crosslinking reaction.

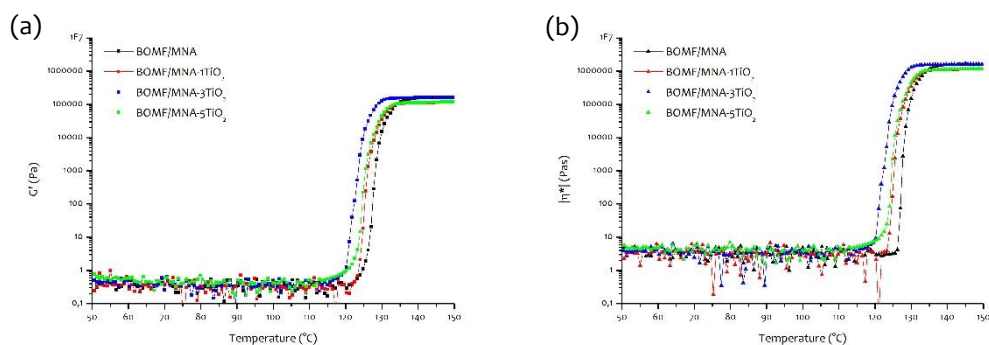


**Figure 4.4** – Comparison of (a) elastic moduli ( $G'$ ) and (b) complex viscosity ( $|\eta^*|$ ) between for BOMF/MNA and BOMF/MNA-3TiO<sub>2</sub> heated at 10 °C/min

Rheological properties were analyzed also as time-dependent behavior at  $T = 110\text{ °C}$  (**Figure 4.5**). In this case, the behavior of BOMF/MNA in the pre-gel region was similar to that exhibited in non-isothermal measurement; in the first 20 minutes of the macromolecular chains formed are not long enough to affect viscoelastic properties of the reacting system. Successively, the first cross

between  $G'$  and  $G''$  was observed, suggesting the occurrence of the crosslinking reaction. Consequently,  $G'$ ,  $G''$  and  $\eta^*$  started growing rapidly. Gel time for the pristine system was reached after about 24 minutes (the technical time related to the start of the test, which depends also on the operator, makes this value not exactly corresponding to reaction times). The measure was interrupted before the completion of crosslinking reaction because the maximum load allowed by the rheometer was reached. In all cases a residual cure was detected by DSC analysis on samples subject to the rheological tests. The rheological behavior of BOMF/MNA-1TiO<sub>2</sub> was similar to the pristine resin in the pre-gel region; however, the start of crosslinking was hastened by the presence of titanium dioxide. The trend of rheological properties for BOMF/MNA-3TiO<sub>2</sub> and BOMF/MNA-5TiO<sub>2</sub> at 110°C was different from that of pristine resin. The presence of higher amounts of filler induced first a thickening effect (even more noticeable with the increasing of filler percentage) in the pre-gel region. In isothermal mode, the analyzed properties showed a quite constant trend in the early 10 minutes, due to the presence of TiO<sub>2</sub> filler. For longer times a thickening phenomenon induced by the increased cross-linking density was observed. A double crossover between  $G'$  and  $G''$  was experienced by all samples but the time between the two crossover point decreased increasing the amount of filler. Therefore, the presence of TiO<sub>2</sub> nanoparticles accelerated the curing reaction in isothermal conditions. Similarly to what observed in the dynamical tests, the presence of titanium dioxide in BOMF/MNA-1TiO<sub>2</sub> and BOMF/MNA-3TiO<sub>2</sub>, accelerates the cure process, while in the system with 5wt.% of filler an hindrance effect was noticed. As TiO<sub>2</sub> increased, the values of rheological properties become stable also before the  $G'$  and  $G''$  crossover. For BOMF/MNA and BOMF/MNA-1TiO<sub>2</sub> the increase of rheological properties values, related to the crosslinking process, is verified in a

narrower range compared to samples filled with 3 and 5 wt.% of titanium dioxide  
(Figure 4.5)

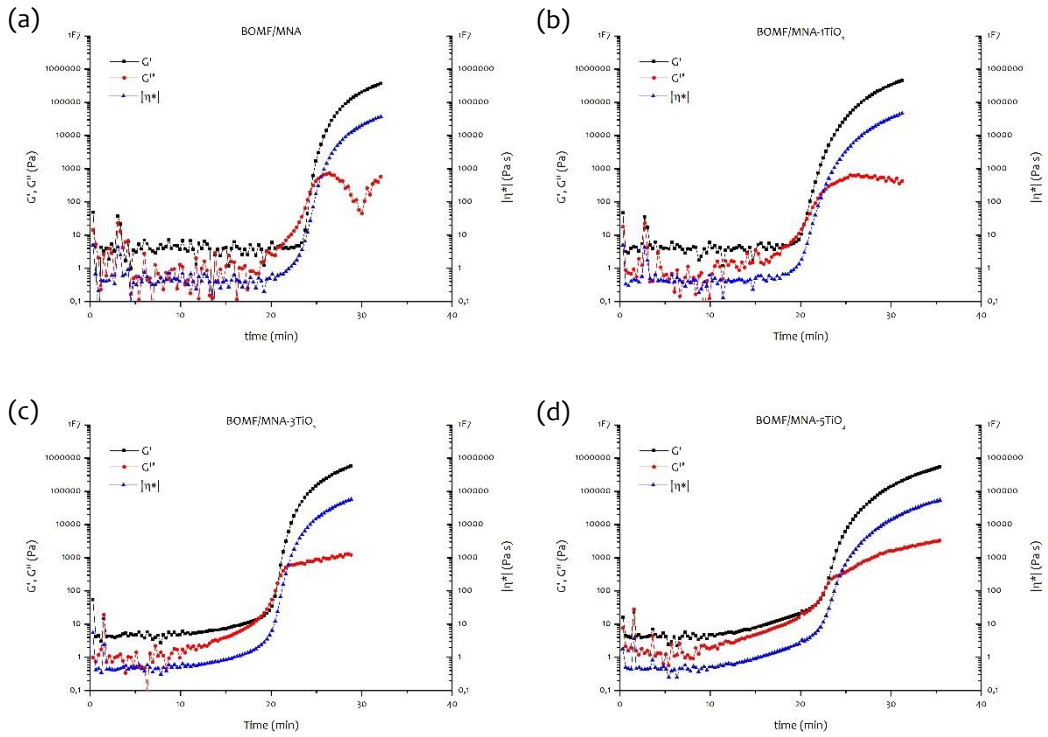


**Figure 4.5** – Rheological tests on (a) BOMF/MNA, (b) BOMF/MNA-1TiO<sub>2</sub>, (c) BOMF/MNA-3TiO<sub>2</sub> and (d) BOMF/MNA-5TiO<sub>2</sub> at 110 °C/min

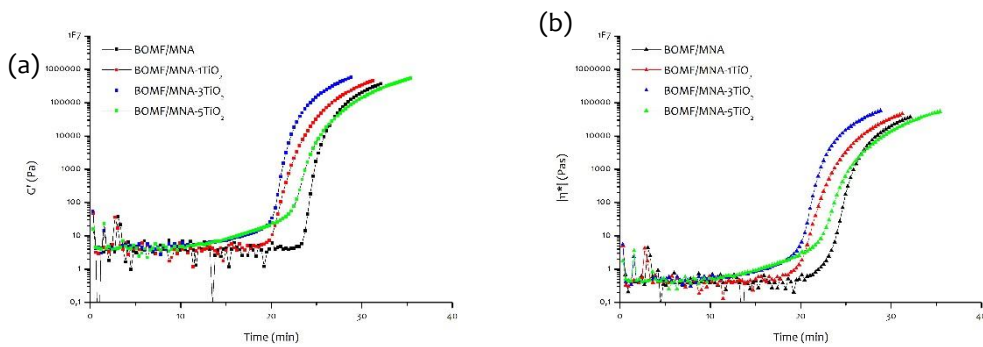


**Figure 4.6** – Comparison of (a) elastic moduli ( $G'$ ) and (b) complex viscosity ( $|\eta^*|$ ) for systems at 110°C

Rheological results were corroborated by the conversion data gained through FTIR-ATR analysis performed on samples undergoing rheological measurements. Characteristic peaks belonging to functional groups taking part at the cure reaction were monitored in their change in absorbance area as a function of time (for isothermal analysis) and temperature (dynamic measurements). Characteristic anhydride carbonyl groups at  $1855$  and  $1776\text{ cm}^{-1}$  and epoxy group at  $913\text{ cm}^{-1}$  were monitored as disappearing groups, while the ester carbonyl group appearing at  $1735\text{ cm}^{-1}$  was monitored as forming group due to the effect of reaction between epoxy and anhydride. Particular attention was paid to the analysis of epoxy group disappearance. Indeed, the characteristic peak is part of a broader band between  $930$  and  $865\text{ cm}^{-1}$ . Therefore the evaluation of the relative contribution of the epoxy peak centered at  $913\text{ cm}^{-1}$  and the anhydride peak, centered at  $895\text{ cm}^{-1}$  was mandatory. The F factor so evaluated was applied in the computation of degree of conversion of the epoxy group following **Equation 4.4**.

Relative conversion of characteristic groups for analyzed systems is reported in **Figure 4.7**. As it can be noticed, at values below 0.4, conversion of epoxy groups is favored compared to anhydride consumption but when the curing rate starts to increase both groups are consumed at the same rate.

By a direct comparison between epoxy characteristic group conversion of all the samples (**Figure 4.8**) it is possible to notice that increasing the titanium dioxide amount the epoxy conversion proceeds faster indicating an interaction phenomenon between filler and epoxy groups. As reported in literature, titanium dioxide can be successfully used in deoxygenation of oxirane rings or conversion in thiiranes<sup>25,26</sup>, suggesting that oxirane rings are really sensible to

TiO<sub>2</sub>. Chemical interaction can so take place between nanoparticles and BOMF promoting the epoxy conversion.

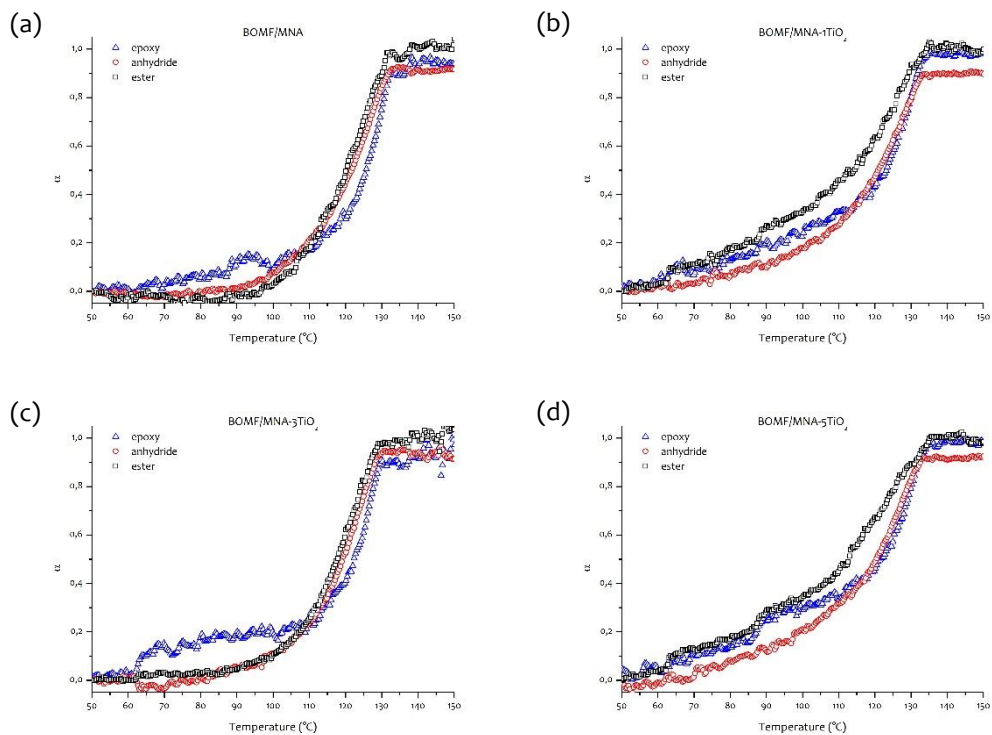


**Figure 4.7** – Conversion (α) of anhydride, ester and epoxy groups of (a) BOMF/MNA, (b) BOMF/MNA-1TiO<sub>2</sub>, (c) BOMF/MNA-3TiO<sub>2</sub> and (d) BOMF/MNA-5TiO<sub>2</sub> cured at 1.5 °C/min heating rate.

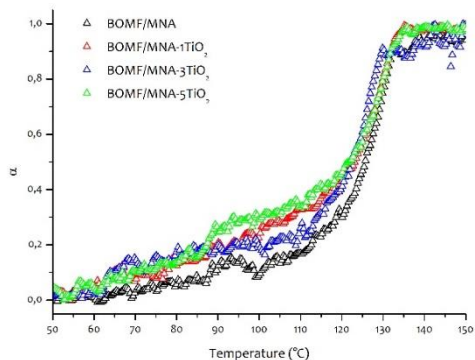


**Figure 4.8** – Comparison of anhydride groups conversion for all samples cured at 1.5 °C/min

As it can be noticed by **Figure 4.9**, where rheological are directly compared with conversion of ester groups evaluated by FTIR analysis, not an unique relation between conversion degree and gelation temperature can be drawn out. Peculiar is the behavior for BOMF/MNA-1TiO<sub>2</sub> which shows an abrupt increase of elastic modulus when conversion degree is 0.7.

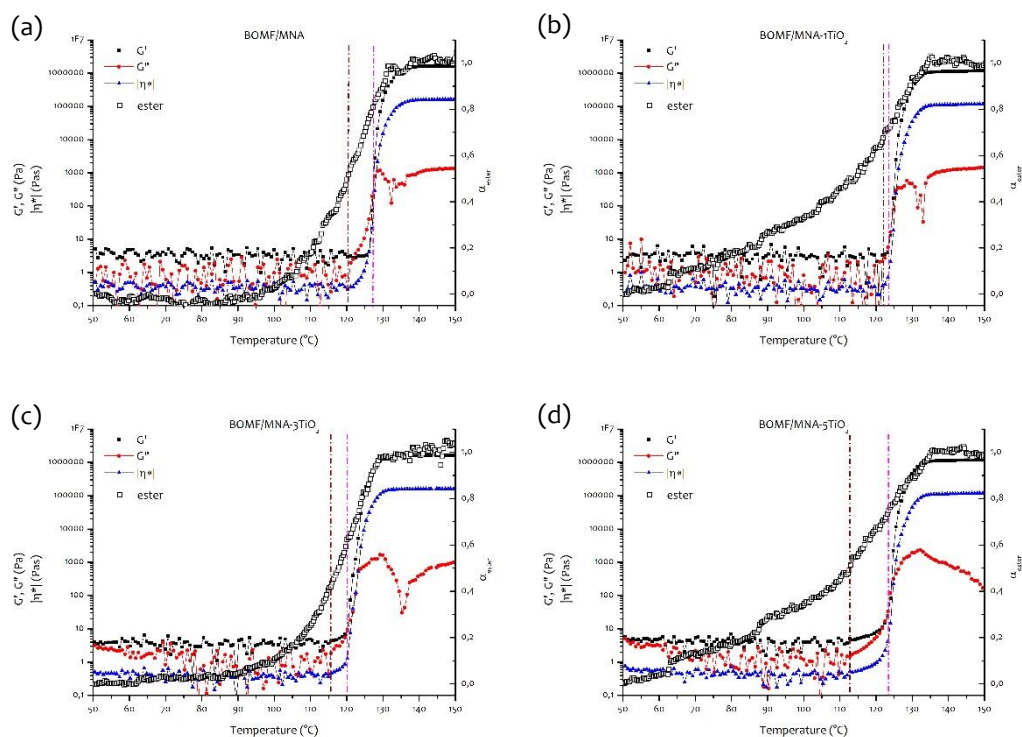


**Figure 4.9** – Comparison between conversion of ester groups, evaluated by FTIR-ATR analysis, and rheological properties of (a) BOMF/MNA, (b) BOMF/MNA-1TiO<sub>2</sub>, (c) BOMF/MNA-3TiO<sub>2</sub> and (d) BOMF/MNA-5TiO<sub>2</sub> cured at 1.5 °C/min

Isothermal relative conversion (α) of epoxy and anhydride groups for all the studied systems, evaluated by FTIR analysis, is reported in **Figure 4.10**. Interestingly can be noticed that, except for BOMF/MNA-5TiO<sub>2</sub>, anhydride



conversion proceeds faster than epoxy. When 5 wt.% of  $\text{TiO}_2$  is added the epoxy consumption is accelerated and proceeds contemporaneously to anhydride.

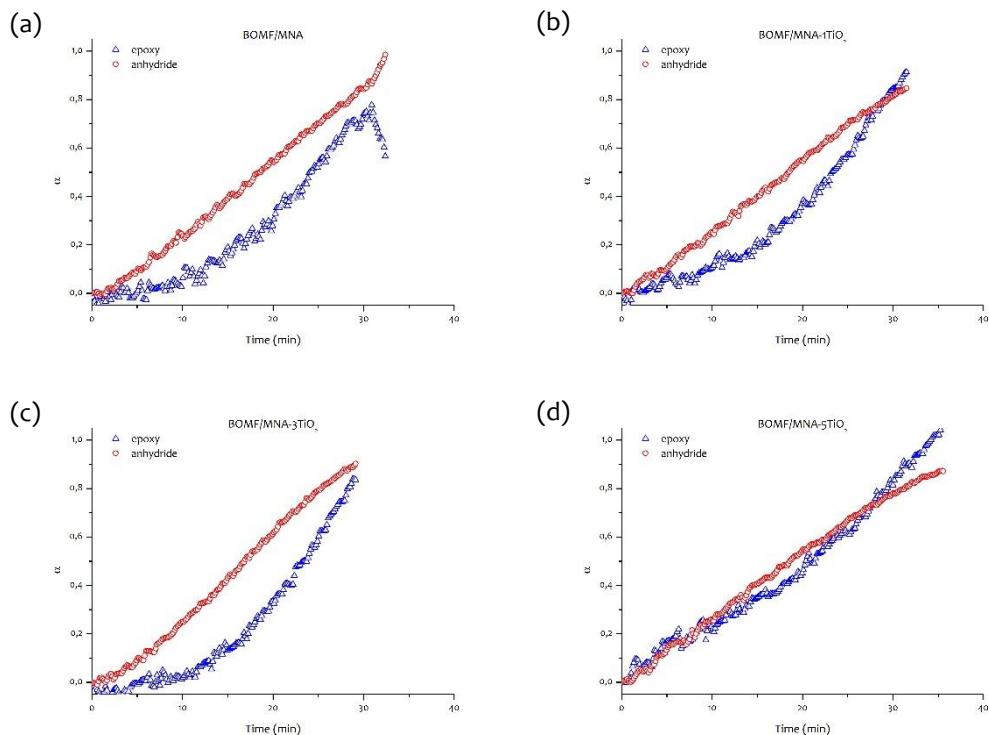


**Figure 4.10** – Relative conversion ( $\alpha$ ) of characteristic groups in (a) BOMF/MNA, (b) BOMF/MNA-1 $\text{TiO}_2$ , (c) BOMF/MNA-3 $\text{TiO}_2$  and (d) BOMF/MNA-5 $\text{TiO}_2$  cured at 110 °C

When absolute conversion are directly compared (**Figure 4.11**) can be noticed that anhydride conversion rate is not affected by filler addition, as well as epoxy conversion rate, exception made for BOMF/MNA-5 $\text{TiO}_2$ . where epoxy conversion proceeds faster than other systems.



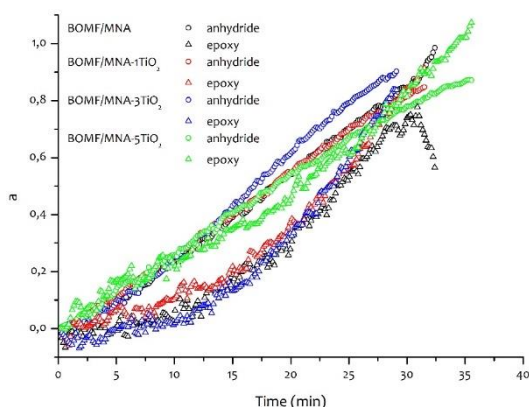


**Figure 4.11** – Comparison of characteristic groups conversion between BOMF/MNA and BOMF/MNA-3TiO<sub>2</sub> cured at 110°C

## Thermal and mechanical properties of epoxy resins and nanocomposites

Thermogravimetric analysis was carried out on cured systems. In particular, samples were subjected to thermogravimetric analysis in both inert (N<sub>2</sub>) and oxidative (air) atmosphere using a heating ramp of 10 °C/min up to a temperature of 750 °C. The weight and derivative weight vs. temperature curves for BOMF nanocomposites and DGEBA/MNA sample, in both atmosphere conditions were compared, as shown in **Figure 4.12**, **Figure 4.13** and in **Table 4.3** are reported the degradation temperatures at 5% (T<sub>d5</sub>) and at 10% (T<sub>d10</sub>) weight loss calculated from TGA curves and the final residue. Moreover comparison for each sample between the two atmospheres are shown in

**Table 4.3** – Degradation temperature ( $T_{d5}$ ,  $T_{d10}$ ) and final weight ( $W_r$ ) of samples in both air and nitrogen atmosphere

	$T_{d5}$ [°C]	$T_{d10}$ [°C]	$W_r$ [%]
	Nitrogen atmosphere		
<b>BOMF/MNA</b>	267.9	293.3	23.9
<b>BOMF/MNA-1TiO<sub>2</sub></b>	265.7	290.2	24.7
<b>BOMF/MNA-3TiO<sub>2</sub></b>	265.2	290.8	26.1
<b>BOMF/MNA-5TiO<sub>2</sub></b>	266.5	293.0	27.9
<b>DGEBA/MNA</b>	274.0	309.8	17.3
	Air atmosphere		
<b>BOMF/MNA</b>	262.0	287.9	0.58
<b>BOMF/MNA-1TiO<sub>2</sub></b>	256.2	280.3	2.43
<b>BOMF/MNA-3TiO<sub>2</sub></b>	255.3	280.6	3.93
<b>BOMF/MNA-5TiO<sub>2</sub></b>	238.8	270.2	5.70
<b>DGEBA/MNA</b>	283.5	320.8	0.45

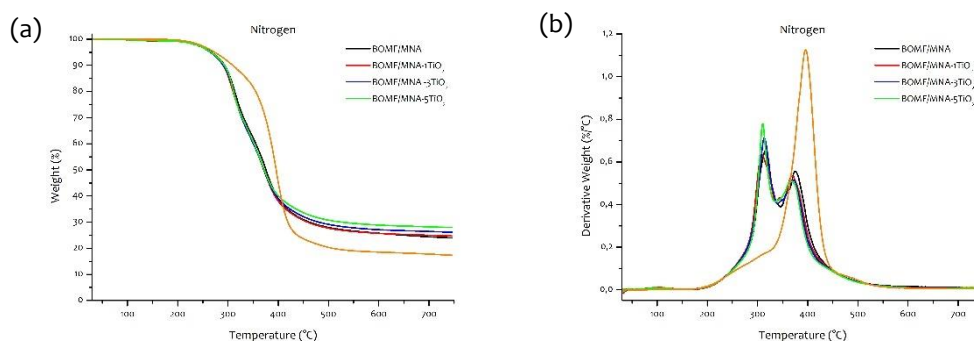


**Figure 4.12** – (a) Weight loss and (b) derivative weight loss in nitrogen atmosphere for samples cured at 180°C

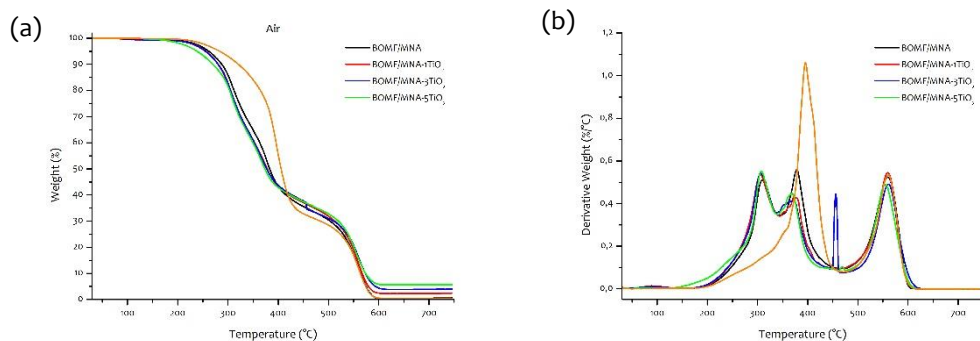


**Figure 4.13** – (a) Weight loss and (b) derivative weight loss in air atmosphere for samples cured at 180°C

For bio-based samples the degradation took place in two steps in nitrogen and in three steps in air atmosphere, with negligible weight residual in air and a final residue in N<sub>2</sub>. DGEBA-based resin, instead, experiences only one degradation phenomenon in nitrogen leaving a residue lighter than residues after degradation in nitrogen of bio-based samples. Residues of nanofilled resins, as could be expected, reflects the amount of titanium dioxide added to the resin.

Interestingly, while for DGEBA under air atmosphere started at higher temperature than under nitrogen flow, this trend is inverted for BOMF- based resins. Moreover, increasing the filler amount present in the resins, increases also the thermal resistance in nitrogen.

To evaluate the mechanical properties, tensile test experiments were carried out on plain BOMF/MNA and on the systems containing nanosized titanium dioxide. These systems were compared with the DGEBA/MNA resin. Samples were obtained in the form indicated by the ASTM D638 type V standard as can be noticed in **Figure 4.15**

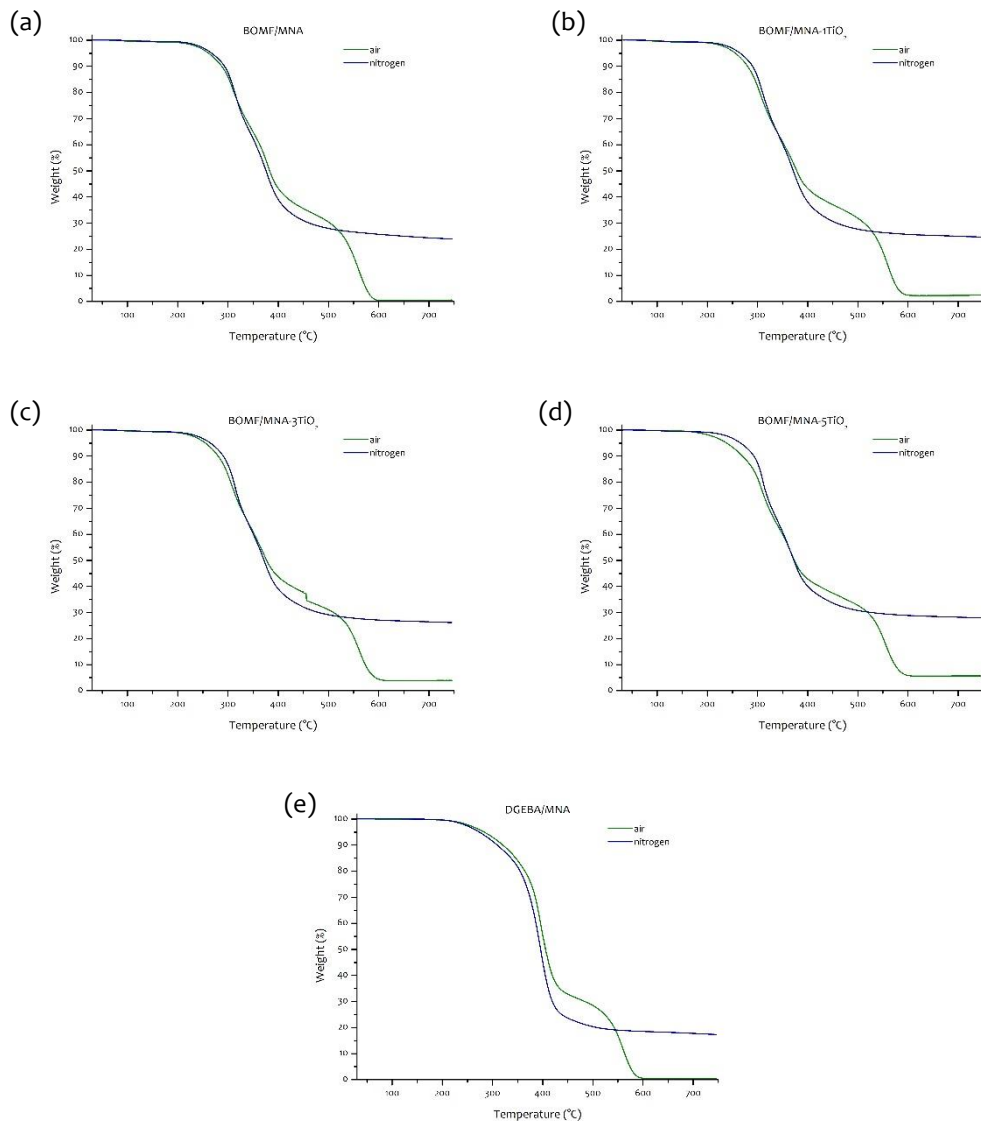


**Figure 4.14** – Comparison of weight loss of (a) BOMF/MNA, (b) BOMF/MNA 1TiO<sub>2</sub>, (c) BOMF/MNA 3TiO<sub>2</sub> (d) BOMF/MNA 5TiO<sub>2</sub> and (e) DGEBA/MNA in air and nitrogen

From the collected stress-strain curves, Young's modulus, stress and strain at peak were determined. Typical stress-strain curves for each resins are reported in **Figure 4.16** and Young's modulus, stress at peak and strain at peak values are reported in **Table 4.4**.

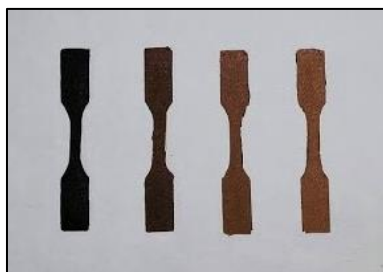


**Figure 4.15** – Specimen for tensile test (type V ASTM D638)

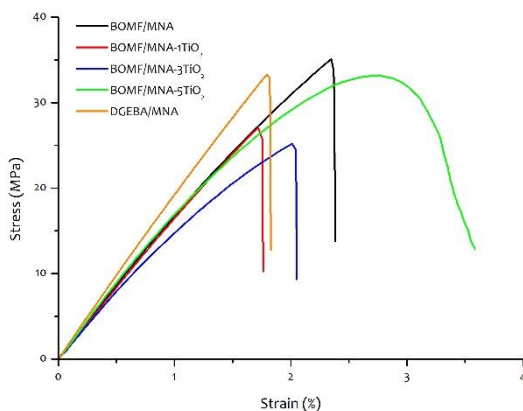


**Figure 4.16** – Stress-strain curves for bulk materials

As it can be noticed, BOMF/MNA has a Young's modulus lower than DGEBA/MNA, and a stress at peak slightly higher.

In the systems BOMF/MNA containing 0, 1 and 5 wt.% of titanium dioxide moduli are almost similar, while in the case of resin with 3 wt.% of  $\text{TiO}_2$  the modulus slightly decreases as expected for nanocomposites<sup>27</sup>. Moreover, it can

be noticed that the resin with 5 wt.% of filler shows no longer a fragile but rather ductile behavior.

**Table 4.4** – Young's Modulus, stress and strain at peak of the investigated samples

Sample	Modulus [Mpa]	Stress at peak [Mpa]	Strain at peak [%]
DGEBA/MNA	20.1 ± 0.8	33.3 ± 5.0	1.7 ± 0.2
BOMF/MNA	17.5 ± 0.1	36.4 ± 1.9	2.3 ± 0.1
BOMF/MNA 1TiO <sub>2</sub>	16.5 ± 0.3	29.8 ± 3.9	1.9 ± 0.2
BOMF/MNA 3TiO <sub>2</sub>	15.3 ± 0.9	25.7 ± 0.7	3.5 ± 0.6
BOMF/MNA 5TiO <sub>2</sub>	17.5 ± 0.8	29.5 ± 5.2	2.7 ± 0.1

### 4.3.2. Optimization of the coating process

The first attempts of coating application of BOMF-based resins revealed that a technological problem was the spreading of the uncured epoxy resins on tinplate, to obtain a uniform coating layer. The poor wettability of the untreated tinplate by the resin induced evident phenomenon of dewetting, as can be noticed in the image in **Figure 4.17a**. The poor wettability issue cannot be attributed uniquely to the substrate or to the resin, so a double strategy was undertaken, in order to modify both resin and tinplate.

Different treatments of tinplate were tackled to improve substrate wettability: first a thermal etching was induced by heating the tinplate at 250°C for 1 hour. Then, since the first process was not as efficient as desired, a mechanical etching was performed, making use of a medium-fine grain sandpaper. Indeed, mechanical treatments of surfaces are a very efficient not

only to improve the compatibility between resins and substrates, but also to optimize the adhesion of the cured resin. Surface roughness increases wettability thanks to capillarity phenomena that are induced even between resins and surfaces that do not wet spontaneously. Moreover, the cavities induced onto the substrate surface improve a mechanical interlock with the resin. <sup>24</sup> The positive effect of the tinplate treatment on final coating are displayed in the images in **Figure 4.17b** where the tinplate was pretreated as previously described: after curing, a uniform layer of transparent amber resin was obtained.

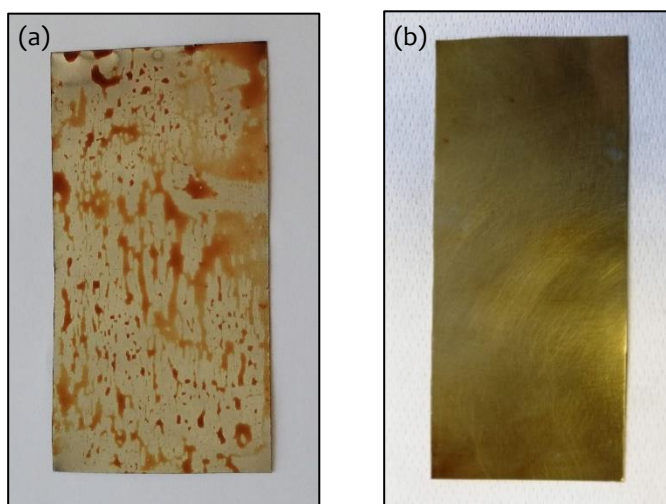


**Figure 4.17** – Visual appearance of (a) untreated tinplate and (b) treated tinplate, coated with BOMF/MNA resin

Morphology and chemical composition of tinplate surface, before and after the treatment, was analyzed by SEM microscopy combined with EDX analysis. As can be noticed in **Figure 4.18** at the micrometric scale magnification, the untreated tinplate has a fairly smooth surface lacking of any kind of defect

and asperity, while after the treatment a rougher morphology is visible on the surface of the tinplate. Grooves of different sizes, ranging from 1 to 5  $\mu\text{m}$  of width, generated by the mechanical treatment can be clearly identified. The effect of the treatment was also investigated by Energy Dispersive X-ray (EDX) analysis and results are reported in **Table 4.5**. Neither oxygen nor other elements resulting from chemical modification of the surface due to the thermal treatment were detected; only a change in the relative ratio between iron and tin occurred, ascribable to the removal of the surface tin layer by the mechanical treatment, was detected.

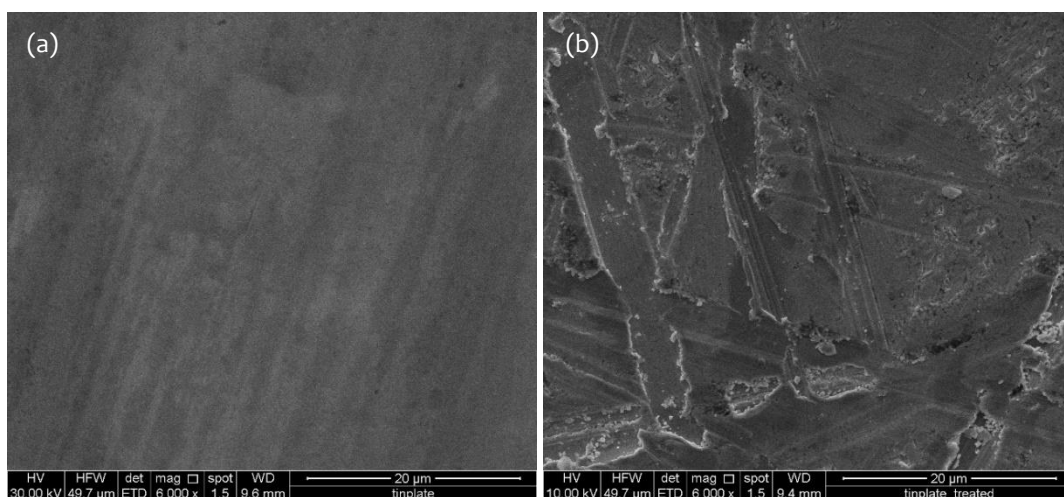


**Figure 4.18** – SEM micrography of (a) untreated tinplate and (b) treated tinplate

**Table 4.5** – Elemental EDX analysis of treated and untreated tinplate.

SAMPLE	Fe [wt.%]	Sn [wt.%]
UNTREATED TINPLATE	69.7 $\pm$ 0.1	30.3 $\pm$ 0.1
TREATED TINPLATE	77.0 $\pm$ 1.1	23.0 $\pm$ 1.1



The effect of tinplate treatment on resin/substrate wettability was proved by static contact angle measurements of BOMF/MNA on untreated and treated tinplate. As it can be noticed by **Figure 4.19**, when tinplate is treated, contact angle decreases to  $17.2^\circ$ , compared with  $41.0^\circ$  BOMF/MNA drop on untreated tinplate. Tinplate treatment does improve wettability between liquid resin and substrate guaranteeing the obtainment of a uniform coating.

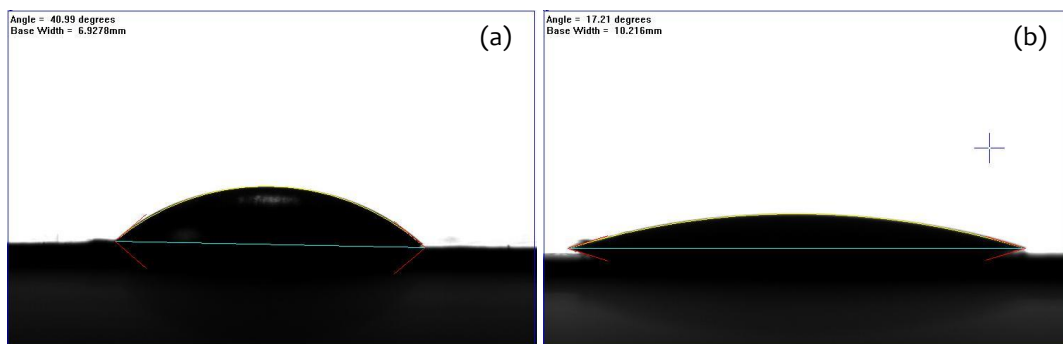


**Figure 4.19** – Contact angle measurements of BOMF/MNA drops on (a) untreated and (b) treated tinplate

Another method to improve tinplate wettability of the resin was based on the modification of the resin viscosity and composition through the addition of titanium dioxide nanoparticles. The use of fillers is widespread in epoxy resins production. They are used to modify characteristics and properties of epoxies, resulting in both advantages and disadvantages. The main advantages are reduced formulation cost, improved toughness, improved abrasion resistance.<sup>28</sup> One of the commonly considered disadvantages, namely the increase in viscosity, could in our case help reducing the dewetting phenomenon

encountered with the pristine resin. In the present case,  $\text{TiO}_2$  was chosen as a filler, as it is largely used in the coating industry. Its use is mainly directed to confer opacity and a white bright color but in case of application in food industry it endows coatings with an added value being antimicrobial.<sup>29</sup>

The addition of a relatively considerable amount of titanium dioxide, namely 1, 3 and 5 wt.% on the total amount of epoxy+hardener, brought about only a slight increase in the viscosity, however it changed the viscoelastic nature of the mixture. Unmodified resin and BOMF/MNA-1 $\text{TiO}_2$  exhibited a Newtonian behavior and a viscosity  $\eta = 0.10 \text{ Pa}\cdot\text{s}$ , while when 3 and 5 wt.% of titanium dioxide was added, the mixture presents a shear thinning behavior increasing with filler percentage ( $\eta = 0.16 \text{ Pa}\cdot\text{s}$ ) (**Figure 4.20**).

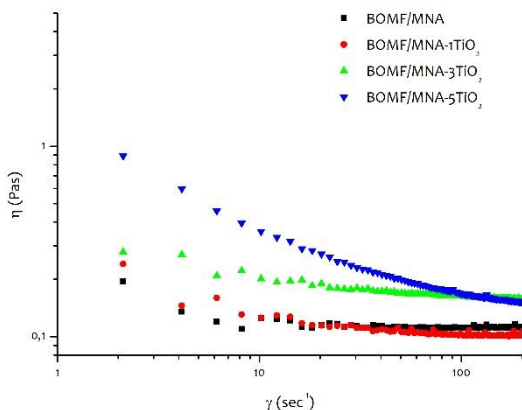


**Figure 4.20** – Viscosity of studied systems in function of shear rate

No evident improvements in wettability was noticed with the addition of titanium oxide nanoparticles when spread on the untreated tinplate. Therefore, also in this case the treatment of tinplate, as described in Methods section, was

required as a technological procedure for the obtainment of uniform coatings with no visible defects as blisters, agglomerates, holes or phase separation. In our case of study, being the epoxy resins amber colored, the addition of titanium dioxide did not result in a white colored resin but in a translucent brown resin, as shown in **Figure 4.21**

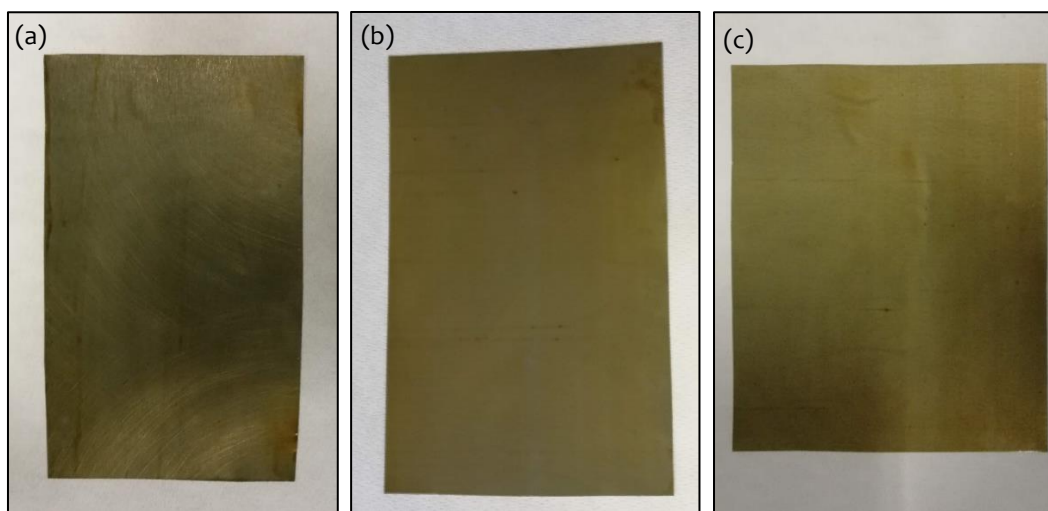


**Figure 4.21** – Visual appearance of (a) BOMF/MNA-1TiO<sub>2</sub>, (b) BOMF/MNA-3TiO<sub>2</sub> and (c) BOMF/MNA-3TiO<sub>2</sub> coating on a treated tinplate specimen.

### 4.3.3. Evaluation of coating properties

#### Contact angle

Contact angle of water usually reflects the hydrophilic/hydrophobic character of the surface. Generally, hydrophobic materials have relatively higher water contact angle. In our case, static contact angles (CA) of water on different

substrates were measured by the sessile drop method and results are shown in **Figure 4.24** and CA values are reported in **Table 4.6**

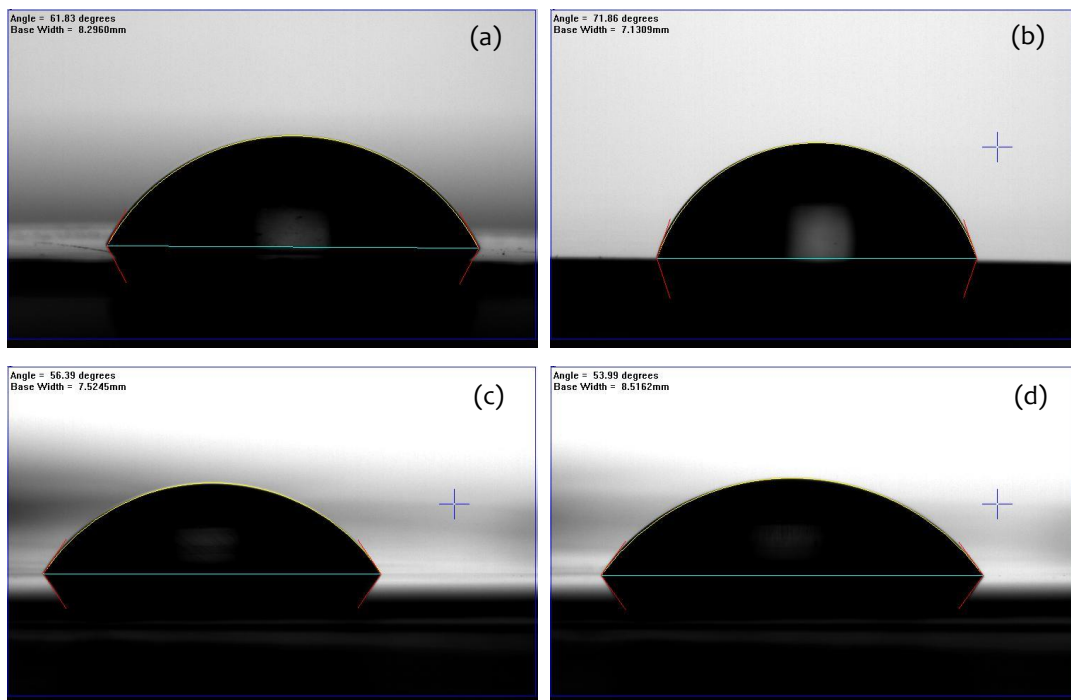


**Figure 4.22** – Static contact angles (CA) of water on different substrates: BOMF/MNA, BOMF/MNA 1TiO<sub>2</sub>, BOMF/MNA 3TiO<sub>2</sub> and BOMF/MNA 5TiO<sub>2</sub>

**Table 4.6** – Contact angle (CA) values with standard deviation for water droplets on coatings.

SAMPLE	CONTACT ANGLE
BOMF/MNA	61.8° ± 3.6°
BOMF/MNA-1TiO <sub>2</sub>	69.6° ± 3.9°
BOMF/MNA-3TiO <sub>2</sub>	56.9° ± 2.6°
BOMF/MNA-5TiO <sub>2</sub>	68.1° ± 4.3°

The values shown in the table are the result of the average of five measurements for each tinplate,.

It can be seen that the angles are all less than  $90^\circ$ , which emphasizes a tendentially hydrophilic nature of the coatings.

## Chemical resistance

For industrial applications, coatings must exhibit properties of chemical resistance, remaining unchanged after exposure to environmental agents. Durability of coatings are related to both chemical and mechanical resistance. In view of their applicability as coating for food containers, in this work we tested the chemical resistance of coatings to solutions simulating foods characteristics. Coated plates were subjected to acid and polar organic solvent environments, and their durability was evaluated on the base of coating failures, cracking and loss of adhesion. Generally, resistance to non-polar solvents is guaranteed in case of non-polar polymers. Polar polymers, instead, even if more prone to establish hydrogen bonds that increase adhesion with the substrate, are more weakened by humidity and polar solvents by effect of interaction between polar groups. Crosslinking density also affects solvent resistance of coatings improving it by effect of decreased chain mobility, hindering diffusion of solvent molecules into the tridimensional structure of the resin. The higher is crosslinking density lower is the ability of any kind of solvent to penetrate the coating.<sup>10</sup>

Two simulating media were prepared. The first was plain ethanol (purity 96%), the second was a water solution of acetic acid (3% vol). Square samples of

metal plates coated with cured BOMF/MNA, BOMF/MNA-1TiO<sub>2</sub>, BOMF/MNA-3TiO<sub>2</sub> and BOMF/MNA-5TiO<sub>2</sub> formulations were immersed in pots containing each of them 100 ml simulating solution. The samples were recovered after 3, 7, 15 and 15 days, let dry and a selection of them analyzed by optical imaging and SEM microscopy. At a first check at naked eye no evident defects were detected for samples immersed in ethanol, even after 30 days (**Figure 4.23**). Remarkable blistering, instead, was noticed for samples immersed in acetic acid after only 3 days (**Figure 4.24**).

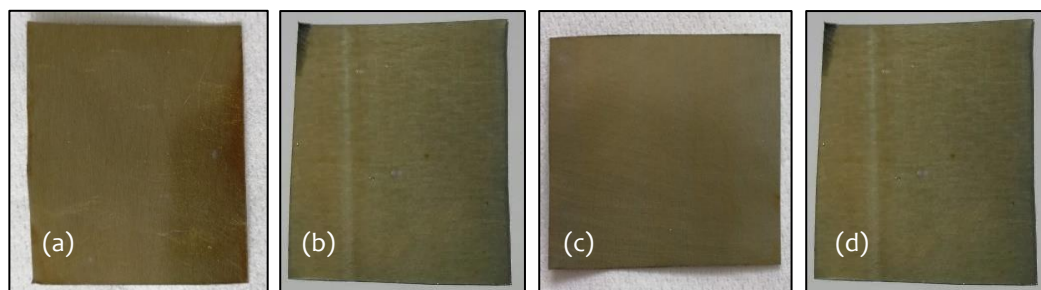


**Figure 4.23** – Visual appearance of (a) BOMF/MNA, (b) BOMF/MNA 1TiO<sub>2</sub>, (c) BOMF/MNA 3TiO<sub>2</sub>, (d) BOMF/MNA 5TiO<sub>2</sub> coating after 30 days immersion in ethanol

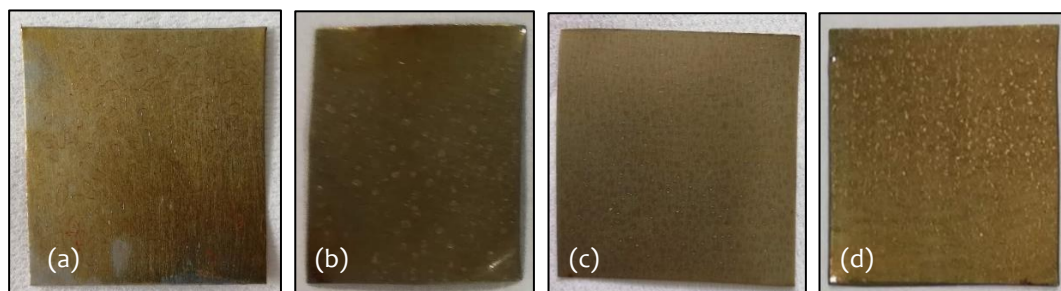


**Figure 4.24** – Visual appearance of (a) BOMF/MNA, (b) BOMF/MNA 1TiO<sub>2</sub>, (c) BOMF/MNA 3TiO<sub>2</sub>, (d) BOMF/MNA 5TiO<sub>2</sub> coating after 3 days immersion in the acetic acid solution

For the latter simulating medium, different bubbles-size distribution was noticed for different compositions of the resins; more precisely the coating containing  $\text{TiO}_2$  nanoparticles presents smaller bubbles than pristine one. This different blister dimension can be attributed to anticorrosion properties of titanium dioxide, typically used in barrier coatings both in acid and alkaline conditions <sup>30</sup>, that inhibited ionic flux through the coating. Anyway, once dried, the center of bubbles became flat and the only surface roughness was given by bubbles boundaries. This suggests that blistering was not provoked by corrosion of the surface, since the oxide residue deposited on the tinplate-resin surface would have induced delamination, but by permeation of the acid solution through the coating. No apparent damages of structural integrity of coating are present.

The surface morphology of the obtained coatings, before and after chemical resistance tests, were studied by SEM analysis.

Hereafter, only BOMF/MNA and BOMF/MNA-3 $\text{TiO}_2$  SEM micrographs are shown. These samples were chosen as the most representative being 1 wt.% of titanium dioxide not enough to affect the resistance properties and 5 wt.% a too high amount, that induced high agglomeration of nanofillers.

As shown in **Figure 4.25**, at low magnifications both BOMF/MNA and BOMF/MNA-3 $\text{TiO}_2$  coatings did not show appreciable surface defects. Coatings were homogeneous at the micrometric scale level, without scratches, pinholes or blisters. Nevertheless, it is possible to appreciate the presence of a percolated structure of titanium dioxide nanoparticles all over the coating<sup>32</sup>



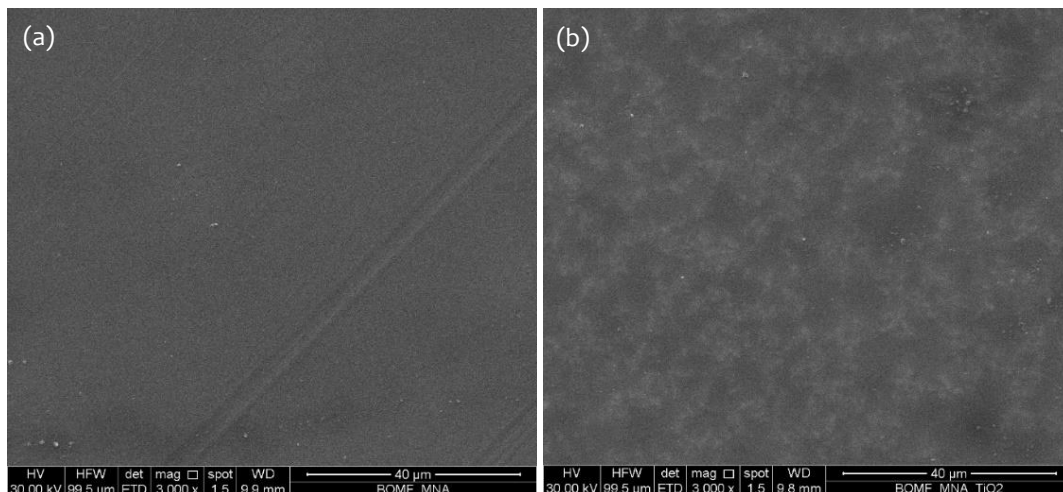


**Figure 4.25** – SEM micrographs of (a) BOMF/MNA and (b) BOMF/MNA-3TiO<sub>2</sub>

SEM micrographs of samples immersed in ethanol for 3 days are reported in **Figure 4.26**. Coating surfaces appear generally smooth with no widespread morphological defects.

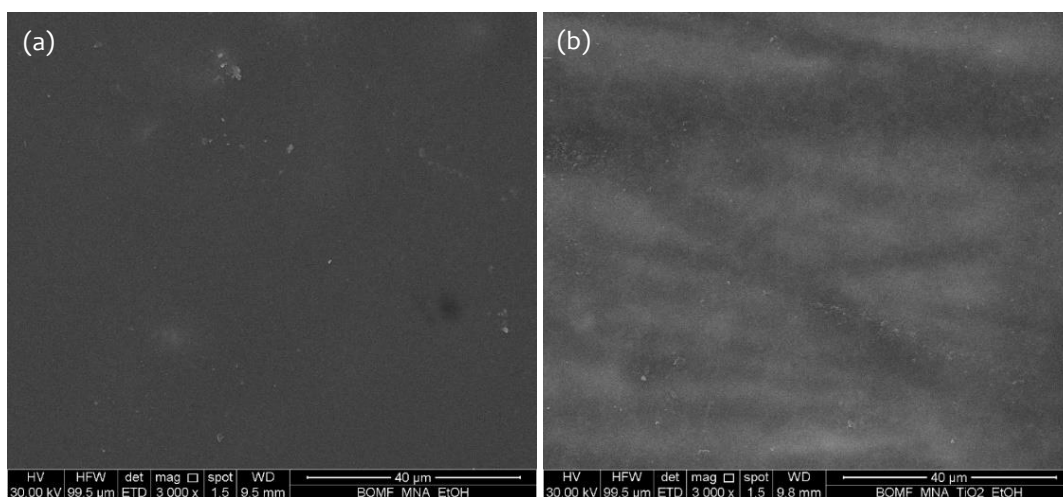


**Figure 4.26** – SEM micrographs of (a) BOMF/MNA and (b) BOMF/MNA-3TiO<sub>2</sub> after 3 days of immersion in ethanol



Samples immersed for 3 days into the acetic acid solution were also analyzed by SEM. **Figure 4.27** reports micrographs for the above-mentioned samples, confirming, on a micrometric scale, the absence of appreciable coating failures in the regions constituting the bubbles surface, where internal stresses were induced as effect of bubbles formation.

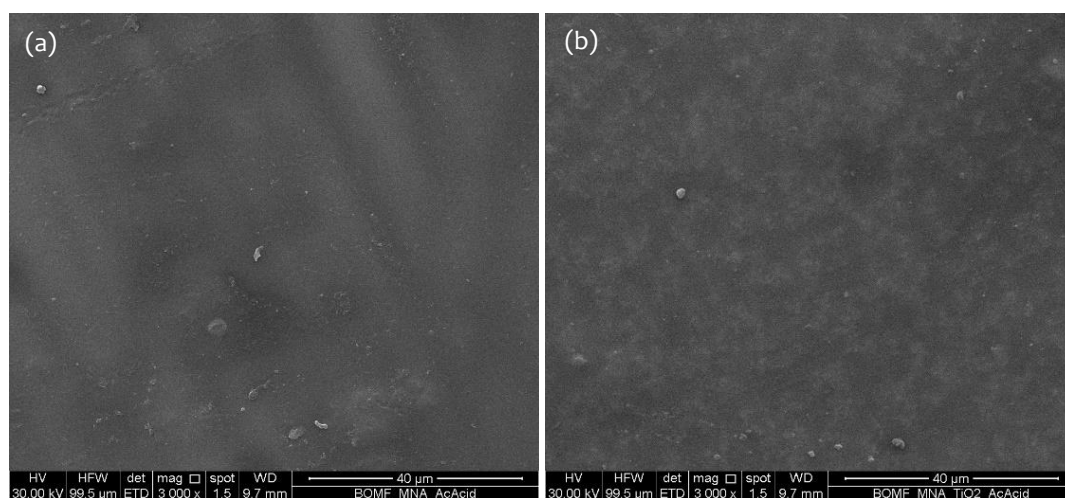


**Figure 4.27** – SEM micrographs of (a) BOMF/MNA and (c) BOMF/MNA-3TiO<sub>2</sub> after 3 days of immersion in 3 vol.% acetic acid aqueous solution.

Samples underwent to chemical resistance tests for 30 days in ethanol and acetic acid solution were also been analysed by SEM and images are reported in **Figure 4.28** and **Figure 4.29**, respectively. As shown, the chemical resistance in ethanol was strongly increased for the sample containing titanium dioxide nanoparticles. Indeed, while the pristine resin shows high degradation possibly due to solvent diffusion within the coating, the coating BOMF/MNA-

$3\text{TiO}_2$  seems only slightly affected by the prolonged exposure to ethanol (**Figure 4.28**).

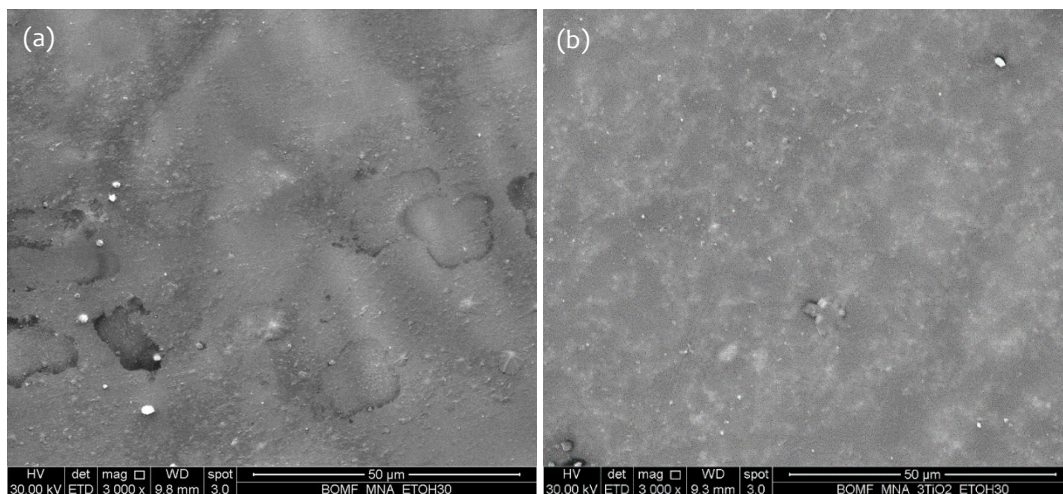


**Figure 4.28** – SEM micrographs of (a) BOMF/MNA and (b) BOMF/MNA- $3\text{TiO}_2$  after 30 days of immersion in ethanol

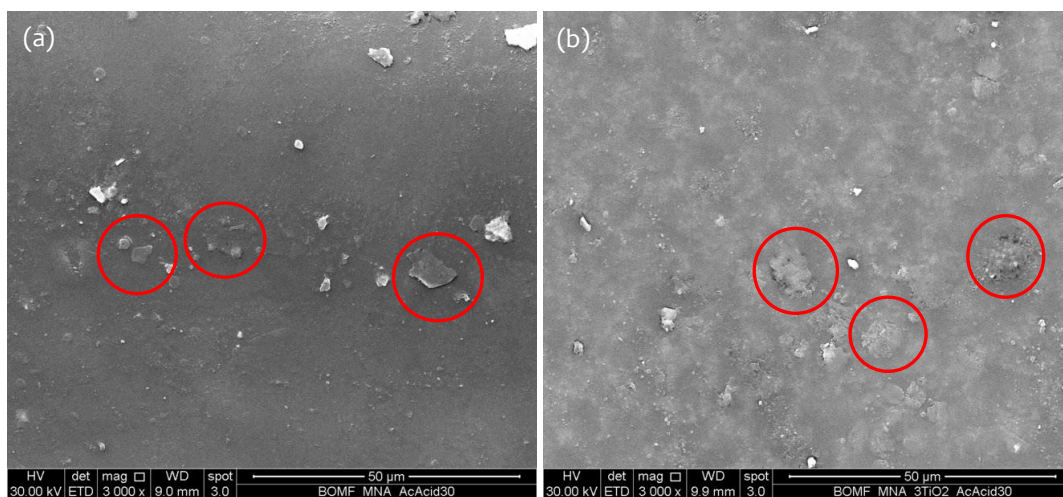


**Figure 4.29** – SEM micrographs at different magnification of (a) BOMF/MNA and (c) BOMF/MNA- $3\text{TiO}_2$  after 30 days of immersion in 3 vol.% acetic acid aqueous solution.

Both the systems, instead, show micrometric crackings after 30 days of immersion in acidic environment. For both samples, the exposure to acetic acid solution does not preserve the structural integrity of the coatings, as evidenced in **Figure 4.29**.

## Pencil hardness of coatings.

An easy way to determine coating hardness is the pencil hardness test described in the ASTM 3363 test method. According to this test, the coating hardness is equated to the highest hardness of the pencil unable to scratch or dig the coating. In this way, two kinds of hardness value are evaluated: pencil hardness and scratch hardness. The first expresses the coating resistance to being cut, while the second expresses a weaker mechanical resistance to scratches. In general, to improve pencil hardness the crosslinking degree has to be maximized.

Pencil hardness test, with a pencil of 5H as highest reference, was performed on untreated BOMF/MNA and BOMF/MNA-3TiO<sub>2</sub> coatings and on samples tested for chemical. Values of both pencil and scratch hardness are reported in **Table 4.7** and **Table 4.8**, respectively. No scratches or gauges were noticed when the maximum hardness pencil (and softer pencils) were used, except for the sample BOMF/MNA-3TiO<sub>2</sub> immersed 3 days in acid environment. In this case, when the pencil tip touched bubbles boundaries, that were tridimensional flaws of the surface, delamination of localized zones, circumscribed by bubbles boundaries itself, was verified. This behavior suggests the occurrence of embrittlement of the epoxy resin filled with titanium dioxide nanoparticles when it is exposed to an acidic environment.

**Table 4.7** – Pencil hardness of coatings before and after chemical resistance test

<b>SIMULANT</b>	<b>DAYS</b>	<b>BOMF/MNA</b>	<b>BOMF/MNA- 1TiO<sub>2</sub></b>	<b>BOMF/MNA- 3TiO<sub>2</sub></b>	<b>BOMF/MNA- 5TiO<sub>2</sub></b>
<b>NONE</b>	/	5H	5H	5H	5H
<b>ETHANOL</b>	3	5H	5H	5H	5H
	7	5H	5H	5H	5H
	15	5H	5H	5H	5H
	30	5H	5H	5H	5H
<b>ACETIC ACID</b>	3	5H	5H	3H	5H
	7	5H	5H	4H	5H
	15	4H	5H	4H	5H
	30	4H	5H	5H	5H

**Table 4.8** – Hardness of coatings before and after chemical resistance test

<b>SIMULANT</b>	<b>DAYS</b>	<b>BOMF/MNA</b>	<b>BOMF/MNA- 1TiO<sub>2</sub></b>	<b>BOMF/MNA- 3TiO<sub>2</sub></b>	<b>BOMF/MNA- 5TiO<sub>2</sub></b>
<b>NONE</b>	/	5H	5H	5H	5H
<b>ETHANOL</b>	3	5H	5H	5H	5H
	7	5H	5H	4H	5H
	15	5H	5H	5H	5H
	30	5H	5H	5H	4H
<b>ACETIC ACID</b>	3	5H	5H	3H	5H
	7	4H	5H	4H	5H
	15	4H	5H	4H	5H
	30	3H	5H	5H	5H

## Adhesion tests

The tape test was applied to determine the adhesion properties of the different coatings on metal substrates. The tape test described in ASTM D3359 consists of pressure sensitive tape that is applied and removed over cuts made in the coating. There are two variants of this test; the X-cut tape test and the cross hatch tape test depending on coating thickness. In our case, being the coating thickness less than 125  $\mu\text{m}$  it was necessary to perform the test method A. Using a scalpel, two cuts were made into the coating with a 30 – 45 degree angle between legs and down to the substrate which intersects to form an “X”. A hard metal straightedge was used to ensure straight cuts. Tape was placed on the center of the intersection of the cuts and some pressure was applied to ensure the correct adhesion of tape on coating, and then removed rapidly. The X-cut area was then inspected for removal of coating from the substrate or previous coating and rated.

The test was carried out on BOMF/MNA plain coatings and coatings containing 1, 3 and 5 wt.% of  $\text{TiO}_2$ .

The results show an optimal adhesion because no peeling or removal happened, as can be noticed in **Figure 4.30** so the adhesion of coating to substrate can be labeled as 5A.

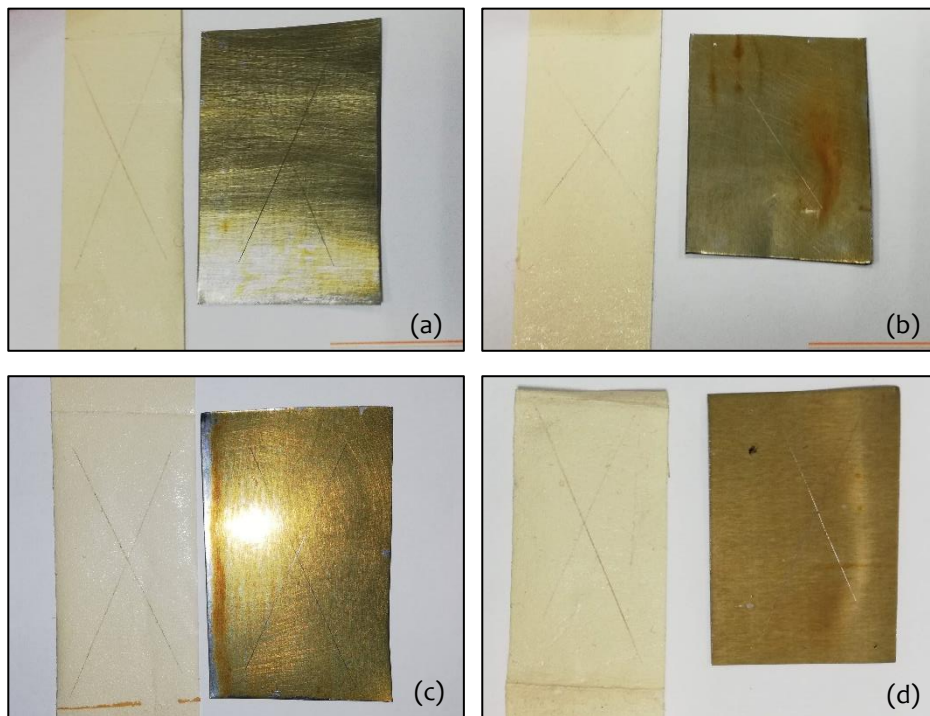


**Figure 4.30** – Adhesion test performed on (a) BOMF/MNA, (b) BOMF/MNA-1TiO<sub>2</sub>, (c) BOMF/MNA-3TiO<sub>2</sub> and (d) BOMF/MNA-5TiO<sub>2</sub> coating

## 4.4. Conclusions

---

In the present work, bio-based epoxy coating based on 2,5-bis[(oxiran-2-ylmethoxy)methyl]furan (BOMF) were obtained and used as a coatings for tinplate for food containers. The effect of addition of titanium dioxide nanoparticles on thermal and chemo-rheological properties of coating was studied. Moreover morphology, chemical resistance and pencil hardness of coatings were analyzed.

Rheological properties were significantly affected by the presence of fillers nanoparticles, in particular viscosity and gel temperature. Also cure kinetic was conditioned by the presence of titanium dioxide, as proved by calorimetric and spectroscopic analysis.

Uniform morphology was obtained regardless of presence of filler nanoparticles. Excellent chemical resistance to polar solvent and good chemical resistance to acid solution was guaranteed. Resins showed excellent values of pencil hardness.

The obtained result indicated that BOMF-based resins has the potential to be a good substitutes for harmful DGEBA-resins. In view of their application as coating for food containers, further analysis have to be carried out to evaluate the appropriate fillers concentration and composition, the chemical resistance and release in food.



## 4.5. Bibliography

---

1. REGULATIONS COMMISSION IMPLEMENTING REGULATION (EU) No 321/2011 of 1 April 2011 amending Regulation (EU) No 10/2011 as regards the restriction of use of Bisphenol A in plastic infant feeding bottles. 2011.
2. COMMISSION DIRECTIVE 2014/81/EU of 23 June 2014 amending Appendix C of Annex II to Directive 2009/48/EC of the European Parliament and of the Council on the safety of toys, as regards bisphenol A (Text with EEA relevance).
3. COMMISSION DIRECTIVE 2009/161/EU of 17 December 2009 establishing a third list of indicative occupational exposure limit values in implementation of Council Directive 98/24/EC and amending Commission Directive 2000/39/EC (Text with EEA relevance). 2009.
4. COMMISSION REGULATION (EU) No 10/2011 of 14 January 2011 on plastic materials and articles intended to come into contact with food (Text with EEA relevance). 2011.
5. LOI n° 2010-729 du 30 juin 2010 tendant à suspendre la commercialisation de tout conditionnement comportant du bisphénol A et destiné à recevoir des produits alimentaires | Legifrance. <https://www.legifrance.gouv.fr/affichTexte.do?cidTexte=LEGITEXT000026832122&dateTexte=20181008>. Accessed October 14, 2018.
6. Darroman E, Durand N, Boutevin B, Caillol S. New cardanol/sucrose epoxy blends for biobased coatings. *Prog Org Coatings*. 2015;83:47-54. doi:10.1016/j.porgcoat.2015.02.002



7. Kathalewar M, Sabnis A. Epoxy resin from cardanol as partial replacement of bisphenol-A-based epoxy for coating application. *J Coatings Technol Res.* 2014;11(4):601-618. doi:10.1007/s11998-014-9570-2
8. Darroman E, Durand N, Boutevin B, Caillol S. Improved cardanol derived epoxy coatings. *Prog Org Coatings.* 2016;91:9-16. doi:10.1016/j.porgcoat.2015.11.012
9. Yan R, Yang D, Zhang N, et al. Performance of UV curable lignin based epoxy acrylate coatings. *Prog Org Coatings.* 2018;116(January):83-89. doi:10.1016/j.porgcoat.2017.11.011
10. Atta AM, Mansour R, Abdou MI, Sayed AM. Epoxy resins from rosin acids: Synthesis and characterization. *Polym Adv Technol.* 2004;15(9):514-522. doi:10.1002/pat.507
11. Narute P, Palanisamy A. Study of the performance of polyurethane coatings derived from cottonseed oil polyol. *J Coatings Technol Res.* 2016;13(1):171-179. doi:10.1007/s11998-015-9741-9
12. Cerit A, Kocaman S, Soydal U. UV-Cured Coatings Based on Acrylated Epoxidized Soybean Oil and Epoxy Carboxylate. *Int Sch Sci Res Innov.* 2016;10(4):464-467.
13. Dai J, Ma S, Liu X, et al. Synthesis of bio-based unsaturated polyester resins and their application in waterborne UV-curable coatings. *Prog Org Coatings.* 2015;78:49-54. doi:10.1016/j.porgcoat.2014.10.007
14. Kathalewar M, Sabnis A, D'Melo D. Polyurethane coatings prepared from CNSL based polyols: Synthesis, characterization and properties. *Prog Org Coatings.* 2014;77(3):616-626. doi:10.1016/j.porgcoat.2013.11.028

15. Ginés MJL, Benítez GJ, Egli W, Giuliani J, Zubimendi JL, Rissone H. Tinplate wettability by organic coatings. In: *15th IAS Rolling Conference, 2004.* ; 2004.
16. Musto P, Martuscelli E, Ragosta G, Russo P, Villano P. Tetrafunctional epoxy resins: Modeling the curing kinetics based on FTIR spectroscopy data. *J Appl Polym Sci.* 1999;74(3):532-540. doi:10.1002/(SICI)1097-4628(19991017)74:3<532::AID-APP8>3.0.CO;2-Q
17. Flores M, Fernández-Francos X, Ramis X, Serra A. Novel epoxy-anhydride thermosets modified with a hyperbranched polyester as toughness enhancer. I. Kinetics study. *Thermochim Acta.* 2012;544:17-26. doi:10.1016/j.tca.2012.06.008
18. Geueke B. *Dossier-Can Coatings.*; 2016. doi:10.5281/zenodo.200633
19. Arbaoui J, Moustabchir H, Vigué JR, Royer F-X. The effects of various nanoparticles on the thermal and mechanical properties of an epoxy resin. *Mater Res Innov.* 2016;20(2):145-150. doi:10.1179/1433075X15Y.0000000026
20. Chen C, Justice RS, Schaefer DW, Baur JW. Highly dispersed nanosilica-epoxy resins with enhanced mechanical properties. *Polymer (Guildf).* 2008;49(17):3805-3815. doi:10.1016/j.polymer.2008.06.023
21. Saeb MR, Nonahal M, Rastin H, et al. Calorimetric analysis and molecular dynamics simulation of cure kinetics of epoxy/chitosan-modified Fe<sub>3</sub>O<sub>4</sub> nanocomposites. *Prog Org Coatings.* 2017;112:176-186. doi:10.1016/J.PORGCOAT.2017.07.015
22. Liu X, Xin W, Zhang J, et al. Rosin-based acid anhydrides as alternatives to petrochemical curing agents. *Green Chem.* 2009;11(7):1018.

doi:10.1039/b903955d

23. Pascault J, Sautereau H, National I, Verdu J, Williams RJJ, Plata M. *Thermosetting Polymers*.
24. Kinloch AJ. *Adhesion and Adhesives*; 1987. doi:10.1179/sic.1984.29.Supplement-1.5
25. Shiraishi Y, Hirakawa H, Togawa Y, Hirai T. Noble-metal-free deoxygenation of epoxides: Titanium dioxide as a photocatalytically regenerable electron-transfer catalyst. *ACS Catal*. 2014;4(6):1642-1649. doi:10.1021/cs500065x
26. Yadollahi B, Tangestaninejad S, Mohammad &, Habibi H. Titanium Dioxide as a Mild and Efficient Catalyst for Conversion of Epoxides to Thiiranes. *Synth Commun*. 2004;34:2823-2827. doi:10.1081/SCC-200026239
27. Pinto D, Bernardo L, Amaro A, Lopes S. Mechanical properties of epoxy nanocomposites using titanium dioxide as reinforcement – A review. *Constr Build Mater*. 2015;95:506-524. doi:10.1016/j.conbuildmat.2015.07.124
28. Ashcroft WR, Cantwell WJ, Chen XM, et al. *Chemistry and Technology of Epoxy Resins*. (Ellis B, ed.). Springer Science+Business Media, B.V.; 1993. doi:10.1007/978-94-011-2932-9
29. Joost U, Juganson K, Visnapuu M, et al. Photocatalytic antibacterial activity of nano-TiO<sub>2</sub> (anatase)-based thin films: Effects on Escherichia coli cells and fatty acids. *J Photochem Photobiol B Biol*. 2015;142:178-185. doi:10.1016/j.jphotobiol.2014.12.010
30. Sørensen PA, Kiil S, Dam-Johansen K, Weinell CE. Anticorrosive coatings: a review. doi:10.1007/s11998-008-9144-2

31. Shi X, Nguyen TA, Suo Z, Liu Y, Avci R. Effect of nanoparticles on the anticorrosion and mechanical properties of epoxy coating. *Surf Coatings Technol.* 2009;204(3):237-245. doi:10.1016/J.SURFCOAT.2009.06.048
32. Uthaman N, Majeed A, Pandurangan. Impact Modification of Polyoxymethylene (POM). *E-Polymers.* 2006:1-9. doi:10.1002/pen





---

# Conclusions

---

The work presented was aimed to the developing of new bio-based epoxy resins, from monomer synthesis to their application as can coatings.

In conclusion:

- New synthetic procedure were developed for the obtainment of bis(oxiran-2-yl-methyl)furan-2,5-dicarboxylate (BOFD), in particular a first procedure mimicking the DGEBA production synthesis consisting in glycidylation of 2,5-furandicarboxylic acid (FDCA) by mean of epichlorohydrin. Furthermore, a greener and more efficient procedure involving transesterification of dimethyl 2,5-furandicarboxylate (DM-FDCA) and glycidol was created. Also 2,5-bis[(oxiran-2-ylmethoxy)methyl]furan (BOMF) was synthesized by a modified procedure presents in literature.
- BOMF, obtained in high yield, was employed with methyl nadic anhydride (MNA), in presence of an initiator, to produce thermosets. Preparatory thermal analysis performed permitted to choose the initiator nature. Mixture with different epoxy/anhydride ratios were prepared to study the effect of resin properties.
- Kinetic study by mean of calorimetric analysis was carried out. The curing reaction was find out being autocatalytic and, by modelling, the values of kinetic constants and reaction order were determined. Chemorheological analysis were also carried out by mean of combined rheological and

## | Conclusions

spectroscopic ATR FT-IR analysis. The latter allowed to verify the mechanism of reaction in function of mixture composition

- Thermal and mechanical analysis of furan-based resins were performed and compared with a DGEBA-based resin. BOMF-based resins exhibited comparable thermal resistance and improved mechanical resistance, both in terms of Young's modulus and Stress at peak.
- Epoxy nanocomposites were obtained by adding titanium dioxide nanoparticles in different percentages; good dispersion of filler was achieved. Nanocomposite mixture were analysed by a thermodynamic and chemorheological, point of view and mechanical and thermal test were performed. After an optimization of the coating process 10 $\mu$ m thick layers of resin and nanocomposites were deposited on tinplates. Bio-based coating were so obtained.
- Properties of coatings were tested. All exhibited perfect adhesion to the substrate, very good hardness an good resistance to acid and polar environments.



